

VIBRATION ANALYSIS OF ROTATING LOW ASPECT RATIO BLADES

VIBRATION ANALYSIS OF ROTATING LOW ASPECT RATIO BLADES  
IDEALIZED AS PRETWISTED CANTILEVER PLATES

by

SUNDER RAWTANI, M.E.

A Thesis

Submitted to the School of Graduate Studies  
in Partial Fulfillment of the Requirements

for the Degree

Doctor of Philosophy

McMaster University

May 1970





### ACKNOWLEDGEMENTS

The author is pleased to record his gratitude to Dr. M. A. Dokainish for suggesting the problem for investigation and for his guidance and encouragement at every stage of the work.

The author is grateful to Dr. D. J. Kenworthy for his assistance in the computer programming and also to Dr. J. H. T. Wade, Dr. G. AE. Oravas, Dr. W. K. Tso and Professor J. N. Siddall for their valuable suggestions.

The constructive criticism of the reviewers of the author's technical papers, based on the present work, deserves special thanks.

Thanks are also due to Mrs. H. Kennelly, who typed the manuscript.

The study leave granted by Maulana Azad College of Technology, Bhopal, India and the fellowship awarded by UNESCO, during the period 1967-69, are gratefully acknowledged.

The investigation was supported by the National Research Council of Canada Grant No. A-2726.

## TABLE OF CONTENTS

	<u>Page</u>
List of Symbols	viii
List of Figures	xiii
<b>CHAPTER</b>	
1 INTRODUCTION	1
2 REVIEW OF ANALYTICAL METHODS FOR VIBRATION ANALYSIS OF TURBOMACHINERY BLADES	5
2.1 Steady State Deformation	7
2.2 Vibration of Nonrotating Blades Without Pretwist	11
2.2.1 Bending Vibrations	11
2.2.2 Torsional Vibrations	13
2.2.3 Shear Centre	15
2.2.4 Coupled Bending-Torsion Vibrations	17
2.3 Vibration of Nonrotating Pretwisted Blades	19
2.3.1 Coupled Bending-Bending Vibrations	20
2.3.2 Torsional Vibrations	29
2.3.3 Coupled Bending-Bending-Torsion Vibrations	31
2.4 Vibration of Rotating Blades Without Pretwist	33
2.5 Vibration of Rotating Pretwisted Blades	42
2.6 Low Aspect Ratio Blades	50
2.7 Effects of Root Flexibility	56
2.8 Effects of Disc Elasticity	59
2.9 Effects of Shrouding	63
2.10 Damping	68



		<u>Page</u>
2.11	Aerodynamic Excitations and Design Considerations	73
2.11.1	Wake Excitation	74
2.11.2	Flutter	76
2.11.3	Rotating Stall Cell Excitation	78
2.11.4	Random Excitations	79
2.11.5	Design Considerations	79
3	THEORY FOR NONROTATING LOW ASPECT RATIO BLADES	83
3.1	Bending Stiffness Matrix for an Element	85
3.2	Complete Stiffness Matrix for an Element	92
3.3	Equivalent Nodal Forces for Distributed Loads	96
3.4	Calculation of Displacements	99
3.5	Bending Mass Matrix for an Element	101
3.6	Complete Mass Matrix for an Element	102
3.7	Natural Frequencies and Mode Shapes	104
4	THEORY FOR ROTATING LOW ASPECT RATIO BLADES	106
4.1	Vibration of Rotating Cantilever Plates	107
4.1.1	Middle Surface Stresses	108
4.1.2	Centrifugal Stiffness Matrix	112
4.1.3	Natural Frequencies and Mode Shapes	114
4.2	Vibration of Rotating Low Aspect Ratio Blades	117
4.2.1	Pseudo-Static Deformation	119
4.2.2	Stiffness Matrix in Deformed Configuration	120

	<u>Page</u>
4.2.3	Centrifugal Mass Matrix 122
4.2.4	Natural Frequencies and Mode Shapes 126
5	CONVERGENCE AND ACCURACY OF THE METHOD 130
5.1	Bending Analysis 132
5.1.1	Simply Supported Plate 132
5.1.2	Clamped Hyperbolic Paraboloid Shell 133
5.1.3	Pretwisted Cantilever Plate 136
5.2	Vibration Analysis 138
5.2.1	Nonrotating Cantilever Plates 138
5.2.2	Nonrotating Pretwisted Cantilever Plates 142
5.2.3	Rotating Cantilever Plates 146
5.2.4	Rotating Pretwisted Cantilever Plates 147
6	RESULTS AND DISCUSSION 151
6.1	Deflection of Pretwisted Cantilever Plate due to Tip Loading 151
6.2	Vibration of Nonrotating Pretwisted Cantilever Plates 154
6.2.1	Mode with Two Longitudinal Nodal Lines 155
6.2.2	Bending Frequencies 156
6.2.3	Torsional Frequencies 161
6.3	Vibration of Rotating Cantilever Plates 164
6.3.1	Southwell Coefficients 166

	<u>Page</u>
6.4 Vibration of Rotating Pretwisted Cantilever Plates	174
6.4.1 Pseudo-Static Deformation	174
6.4.2 Natural Frequencies	176
7 CONCLUDING REMARKS	183
FIGURES	190
REFERENCES	234
APPENDICES	
I D'Almbert Forces for a Rotating Vibrating Blade	247
II Formulation of the Problem of Rotating Blade Including the Coriolis Forces	250
III Computer Programme for Vibration Analysis of Rotating Centilever Plate	253
IV Computer Programme for Vibration Analysis of Rotating Pretwisted Cantilever Plate	278

## LIST OF SYMBOLS

a	Amplitude of vibration
b	Breadth of plate
c	Blade chord
C	Torsional stiffness of untwisted blade
$C_v$	Correction factor for root flexibility
$C_\psi$	Torsional stiffness of pretwisted blade
$C_\omega$	Warping constant
$C_F$	Blade lift coefficient
D	Flexural rigidity corresponding to maximum thickness
e	Energy imparted or taken out from blade by the surrounding air
E	Young's Modulus
f	Frequency of vibration ( $\omega/2\pi$ )
$f_n$	Frequency ratio ( $\omega/\omega_0$ )
$F'_x, F'_y, F'_z$	Forces along $x', y', z'$ axes
g	Acceleration due to gravity
h	Rise of hyperbolic paraboloid shell
I	Moment of inertia about neutral axis of beam
$I_{c.g.}$	Polar moment of inertia per unit length, about centroidal axis
$K_r$	Radius of gyration for the blade section
$l_x, m_x, n_x$	Direction cosines of $x'$ axis
$l_y, m_y, n_y$	Direction cosines of $y'$ axis
$l_z, m_z, n_z$	Direction cosines of $z'$ axis



$l$	Length of blade segment
$L$	Length of plate
$m$	Lengthwise subdivisions
$M$	Bending Moment
$M'_x, M'_y, M'_z$	Moments about $x', y', z'$ axes
$n$	Breadthwise subdivisions
$r$	Disc radius
$\bar{r}$	$r/L$
$r_m$	Shroud mass/blade mass
$R$	Radius of curvature of neutral fibre
$S$	Southwell coefficient
$S_\theta$	Component of Southwell coefficient depending on setting angle
$S_r$	Component of Southwell coefficient depending on disc radius
$S_0$	Component of Southwell coefficient independent of setting angle and disc radius
$t$	Blade thickness
$t_{max}$	Maximum thickness
$u', v', w'$	Displacements along $x', y', z'$ axes
$U$	Strain energy of an element due to bending
$U_1$	Additional strain energy of an element due to initial stresses
$V$	Air velocity relative to blade at inlet
$V_e$	Volume of a triangular element
$W$	Total applied load
$x', y', z'$	Local coordinate axes for an element
$x, y, z$	Global coordinate axes



$\alpha$	Incidence angle of air measured from axial direction
$\alpha_{\omega}$	Variation of angle of incidence
$\alpha_z$	Nondimensional deflection in z direction
$\beta$	Nondimensional frequency of nonrotating blade
$\beta_r$	Nondimensional frequency of rotating blade
$\gamma$	Mass per unit length of blade
$\theta$	Setting angle at the root
$\theta'_x, \theta'_y, \theta'_z$	Rotational displacements about $x', y', z'$ axes
$\lambda$	$L/K_r$
$\mu$	Poisson's ratio
$\rho$	Mass per unit volume of blade material
$\rho_1$	Density of air
$\sigma'_x, \sigma'_y$	Normal stresses in the middle surface of blade along $x', y'$ axes
$\tau'_{xy}$	Shear stress in the middle surface of blade along $x', y'$ axes
$\phi$	Pseudo-static torsional deformation
$\psi$	Total pretwist in the blade
$\omega$	Natural frequency of nonrotating blade
$\omega_1$	Fundamental frequency of nonrotating blade
$\omega_0$	Fundamental frequency of nonrotating blade without pretwist
$\omega_r$	Natural frequency of rotating blade
$\Omega$	Speed of rotation
$\bar{\Omega}$	$\Omega/\omega_1$

## Matrices

$[C'_{ed}]$	Coriolis matrix for an element (18×18)
$[C_d]$	Coriolis matrix for complete blade
$\{F'_p\}, \{\delta'_p\}$	Column vector of 6 in-plane nodal forces (displacements) for an element
$\{F'_b\}, \{\delta'_b\}$	Column vector of 9 bending nodal forces (displacements) for an element
$\{F'_{15}\}, \{\delta'_{15}\}$	Column vector of 15 nodal forces (displacements) for an element
$\{F'_e\}, \{\delta'_e\}$	Column vector of 18 nodal forces (displacements) for an element including moments $M'_z$ (rotations $\theta'_z$ )
$\{F\}, \{\delta\}$	Column vector of nodal forces (displacements) for complete blade
$[I]$	Unit matrix
$[K'_p], [M'_p]$	In-plane stiffness (mass) matrix for an element (6×6)
$[K'_b], [M'_b]$	Bending stiffness (mass) matrix for an element (9×9)
$[K'_e], [M'_e]$	Complete stiffness (mass) matrix for an element (18×18)
$[K'_c]$	Centrifugal stiffness matrix for an element (9×9)
$[K'_{et}]$	Stiffness matrix for an element including centrifugal stiffness matrix (18×18)
$[K], [M]$	Stiffness (mass) matrix for complete blade
$[M'_{ec}]$	Centrifugal mass matrix for an element (18×18)
$[M_c]$	Centrifugal mass matrix for complete blade
$[T_p], [T_b], [T]$	Transformation matrices

### Superscripts

'	The quantity referred to local axes $(x',y',z')$ . When this superscript is dropped, the quantity referred to global axes $(x,y,z)$
*	Virtual displacement along local axes
'	First derivative with respect to time
''	Second derivative with respect to time
-1	Inverse of matrix
T	Transpose of matrix

### Subscripts

eq	Equivalent nodal forces corresponding to distributed loads
$i,j,k$	Value of the quantity at nodes $i,j,k$ .

## LIST OF FIGURES

		<u>Page</u>
Figure 1	Side View of Pretwisted Blade of Rectangular Section Looking Towards Root Section.	191
Figure 2	Sketch of a Blade Without Pretwist Mounted on Rotating Disc at Setting Angle $\theta$ .	192
Figure 3	Lumped Mass Model of a Blade Showing Two Adjacent Segments.	193
Figure 4	Effect of Root Flexibility on Flexural Frequency (Ref. 90).	194
Figure 5	A Simplified Model for Blade-Disc Assembly Suggested by Ellington and McCallion (94).	195
Figure 6	A Simplified Model for Blade-Disc Assembly Suggested by Wagner (97).	196
Figure 7	Natural Frequencies and Mode Shapes of a Packet of Six Shrouded Blades (Ref. 98).	197
Figure 8	A Typical Lift Curve of Compressor Blade in Cascade at Constant Mach Number	198
Figure 9	Effect of Inlet Guide Vane Setting Angle on Flutter Vibration Amplitude (Ref. 115).	199
Figure 10	An Illustration of Campbell Diagram	200
Figure 11	(a) Subdivision of a Blade Into Triangular Elements. (b) Local Coordinate Axes for an Element.	201
Figure 12	An Illustration of the Method of Assembling the Element Stiffness Matrices .	202
Figure 13	(a) Subdivision of a Cantilever Plate Into Triangular Elements	203



		<u>Page</u>
	(b) Local Coordinate Axes for an Element .	
Figure 14	Sketch of a Blade Mounted on Rotating Disc at Setting Angle $\theta$ .	204
Figure 15	An Illustration of the Method of Lumping the Centrifugal Forces at the Nodes.	205
Figure 16	Subdivision of Simply Supported Plate Into Triangular Elements (Mesh $8 \times 8$ ).	206
Figure 17	Central Deflection of Square Simply Supported Plate Under Central Point Load.	207
Figure 18	The Geometry of the Hyperbolic Paraboloid Shell.	208
Figure 19	Deflection Along the Centre Line of Square Clamped Hyperbolic Paraboloid Shell Under Uniformly Distributed Load.	209
Figure 20	(a) Pretwisted Cantilever Plate Loaded at Free Corners. (b) Side View of the Pretwisted Plate Looking Towards Root Section.	210
Figure 21	Bending Frequencies of a Pretwisted Cantilever Plate; $L=6"$ , $b=1"$ , $t=0.068"$ , $E=30 \times 10^6$ psi, $\mu=0.3$ , Density= $0.284$ lbs/in <sup>3</sup> , Mesh( $10 \times 2$ ).	211
Figure 22	Natural Frequencies of a Tapered Pretwisted Cantilever Plate; $L/b=2$ , Mesh ( $7 \times 3$ ).	212
Figure 23	Deflection ( $w$ ) along the Line FD of Pretwisted Cantilever Plate Loaded at Free Corners; $L/b=1$ , $b/t=48$ , Mesh ( $6 \times 6$ ).	213
Figure 24	Deflection ( $w$ ) along the Line CD of Pretwisted Cantilever Plate Loaded at Free Corners; $L/b=1$ , $b/t=48$ , Mesh ( $6 \times 6$ ).	214
Figure 25	Variation of Natural Frequencies with Pretwist for a Nonrotating Plate; $L/b=1$ , $b/t=16$ , Mesh ( $5 \times 5$ ).	215

		<u>Page</u>
Figure 26	Variation of Natural Frequencies With Pretwist for Nonrotating Plate; $L/b=2$ , $b/t=16$ , Mesh (7×3).	216
Figure 27	Variation of Natural Frequencies With Pretwist for a Nonrotating Plate; $L/b=3$ , $b/t=16$ , Mesh (7×3).	217
Figure 28	Variation of the First Two Bending Frequencies with Pretwist for Different Aspect Ratios; $b/t=16$ .	218
Figure 29	Mode Shapes of a Nonrotating Pretwisted Cantilever Plate; $L/b=1$ , $b/t=16$ , Mesh (5×5).	219
Figure 30	Variation of Natural Frequencies With Pretwist for a Nonrotating Plate; $L/b=1$ , $b/t=48$ , Mesh (5×5).	220
Figure 31	Mode Shapes of a Nonrotating Pretwisted Cantilever Plate; $L/b=1$ , $b/t=48$ , Mesh (5×5).	221
Figure 32	Variation of Natural Frequencies With Speed of Rotation for a Cantilever Plate; $L/b=1$ , $r=0$ , Mesh (5×5).	222
Figure 33	Variation of Natural Frequencies With Speed of Rotation for a Cantilever Plate; $L/b=2$ , $r=0$ , mesh (8×4).	223
Figure 34	Variation of Natural Frequencies With Speed of Rotation for a Cantilever Plate; $L/b=3$ , $r=0$ , Mesh (10×3).	224
Figure 35	Variation of Natural Frequencies With Disc Radius for a Rotating Cantilever Plate; $L/b=1$ , $\theta=0^\circ$ , $\bar{\Omega}=1$ , Mesh (5×5).	225
Figure 36	Variation of Natural Frequencies With Disc Radius for a Rotating Cantilever Plate; $L/b=2$ , $\theta=0^\circ$ , $\bar{\Omega}=1$ , Mesh (8×4).	226
Figure 37	Variation of Natural Frequencies With Disc Radius for a Rotating Cantilever Plate; $L/b=3$ , $\theta=0^\circ$ , $\bar{\Omega}=1$ , Mesh (10×3).	227

		<u>Page</u>
Figure 38	Mode Shapes of a Rotating Cantilever Plate; $L/b=1$ , $\bar{r}=0$ , $\theta=0^\circ$ , (Mesh $5 \times 5$ ).	228
Figure 39	An Illustration for Positive Directions for $\psi$ , $\theta$ and $\phi$ in a rotating Pretwisted Cantilever Plate.	229
Figure 40	Pseudo-Static Deformation of a Rotating Pretwisted Cantilever Plate; $L/b=2$ , $b/t=16$ , $\bar{r}=2$ , Mesh ( $8 \times 4$ ).	230
Figure 41	Variation of Natural Frequencies With Pretwist for a Rotating Cantilever Plate; $L/b=2$ , $b/t=16$ , $\bar{r}=2$ , $\theta=90^\circ$ , $\bar{\Omega}=1$ , Mesh ( $7 \times 3$ ).	231
Figure 42	Variation of Natural Frequencies With Speed of Rotation for a Pretwisted Cantilever Plate; $L/b=2$ , $b/t=16$ , $\bar{r}=2$ , $\psi=30^\circ$ , $\theta=90^\circ$ , Mesh ( $7 \times 3$ ).	232
Figure 43	Position Vectors of a Point on the Blade Referred to Fixed and Moving Coordinate Axes.	233



## CHAPTER 1

### INTRODUCTION

Ever increasing demands of high performance together with reliability of operation, long life and light weight, necessitate a constant development of almost every part of a gas turbine. Blades form a vital part of a turbomachine. Apart from their shape and geometry, on which the performance characteristics of the engine largely depend, their dynamic strength is of considerable importance as far as the reliability of operation and the life of the engine are concerned. In an axial engine there may be about 2000 fixed and rotating blades accounting for approximately 30 percent of the cost of the engine. Failure of even one of the blades can cause the shut down of the machine.

The main cause of failure of compressor blades and the blades of lower temperature stages of a turbine is fatigue. Such failures are, naturally, a result of mechanical vibrations resulting in high alternating stresses. These cyclic stresses, superimposed upon the mean steady stresses in the blades, cause fatigue failure. While an evaluation of the steady state stresses due to the aerodynamic and the centrifugal forces is also necessary, the major task, however, is to estimate accurately the vibration characteristics



of the blades.

The most important modes of vibration, from practical considerations, are known to be the first three flapwise bending modes, the first chordwise bending mode and the first two torsional modes. The presence of initial twist in the blade causes a coupling between the flapwise and the chordwise bending motions. The noncoincidence of the shear centre and the centroid in an aerofoil cross-section couples the bending and the torsional vibrations.

In the last twenty years a large number of technical papers have appeared, describing the different approaches for the vibration analysis of turbomachinery blades. The first objective of the present investigation is to review and make a systematic presentation of most of the significant methods.

For vibration analysis, the blades are generally idealized as pretwisted cantilever beams. This beam type of analysis, although good enough for long blades, cannot be expected to give accurate results for low aspect ratio blades. Such blades ought to be treated as shells. For a complex structure like a twisted, tapered, cambered blade of aerofoil cross-section, the exact analysis based on shallow shell theory is rather a formidable task. However, the recent advances in the finite element technique make such an analysis feasible. The second objective

of the present investigation is to develop a method, based on the finite element technique, for the bending and the vibration analysis of rotating and nonrotating low aspect ratio blades.

The finite element method of treating the shell as an assembly of a large number of flat triangular elements, introduces several physical and mathematical approximations. It is, therefore, necessary to test the rate of convergence and the accuracy of the method. This is achieved by applying the method to obtain solutions to several problems for which analytical or experimental results are available.

The third objective of the present investigation is to carry out the numerical computations in order to study,

- (i) the effect of increasing pretwist on the natural frequencies and the mode shapes,
- (ii) the effect of the speed of rotation, the radius of the disc and the setting angle at which the blade is mounted on the disc, on the natural frequencies and the mode shapes, and
- (iii) the manner in which the well known results for long blades based on beam type analysis are approached, with the increase in the aspect ratio.

For the purpose of these computations, the blade is treated as a pretwisted cantilever plate.

The present analysis assumes that the blades are fixed at their roots and there is no damping present in the system. The disc on which the blades are mounted is assumed to be rigid and, therefore, no coupling of the vibratory motion between the blades in the same row takes place.

## CHAPTER 2

### REVIEW OF ANALYTICAL METHODS FOR VIBRATION ANALYSIS OF TURBOMACHINERY BLADES

The blades have an aerofoil cross-section and possess, in addition to camber and longitudinal taper, a pretwist to allow for the variation in tangential velocity along the length. The method of mounting the blades on the disc varies considerably in different types of engines. The root of a blade is neither hinged nor fixed. Also, the root fixidity is considerably altered when the blades are rotating - the centrifugal forces causing additional fixidity at the root. The elasticity of the disc and the shroud couples the vibratory motion of the blades of the same row. A certain amount of damping is also inherently present in the system, arising from material inelasticity, friction at the root, aerodynamic sources etc. An accurate determination of the vibration characteristics of such a system, in centrifugal force field and subjected to aerodynamic excitations, is, no doubt, a challenging task.

Many papers dealing with the analytical and the experimental studies of the problem have appeared in the open literature. The different techniques for the experimental investigation of turbomachinery blade vibrations



have, recently, been reviewed by Dokainish and Jagannath (1)\*.

For the theoretical analysis of blade vibration problem, many simplifying assumptions are generally introduced. In most of the analytical work that has appeared in this field, the blade is idealized as a tapered, pretwisted cantilever beam. The effect of root flexibility, disc elasticity, shrouding and damping have not usually been included in such analysis. However, the effect of these parameters on the vibration characteristics has been studied separately by some investigators. In such investigations several other assumptions are generally made, e.g. neglecting the pretwist, assuming the cross-section to be rectangular, treating the blade as a single degree of freedom system, etc.

The methods of analysis that have been used for blade vibration problems vary considerably - from the exact solution of differential equations of motion on the one extreme to the empirical relations based on experience on the other. The majority of the investigators, however, have used one or the other approximate numerical methods such as the Rayleigh-Ritz energy approach, the Myklestad type lumped mass technique, the Stodola method, the matrix displacement analysis, the numerical solution of differential or integral equations, etc.

For the sake of convenience, this review of the analytical methods is subdivided into several sections;

---

\* Numbers in parantheses designate references at the end.

in such a manner, that in each section a different aspect of the problem is discussed.

### 2.1 Steady State Deformation

The aerodynamic and the centrifugal forces acting on rotating turbomachinery blades produce steady state deformation and stresses. In the case of compressor blades, these stresses may be small as compared to large alternating stresses set up by the vibratory motion. However, the blades of the initial stages of a turbine operate in a creep regime and the steady stresses play an important role under these conditions.

The basic theory of Euler-Bernoulli and the Timoshenko beam theory, wherein the shear effects are also included, form the basis for the bending analysis of the blades. However, due to the presence of initial twist, the deformation along both principal axes of inertia of cross-section of a blade occurs simultaneously. This results in a system of coupled equations for deflections.

The differential equations for bending of a pre-twisted beam are derived by Zickel (2,3) by assuming it to consist of a large number of longitudinal fibres. The expressions for fibre stress, after linearization, are shown to consist of five components resulting from compression, bending along each principal direction, warping of the cross-

section and interaction of the initial and the additional twist. The shear stresses are those given by the Saint Venant's theory of torsion and those which are developed as a result of the variation of fibre stress along the length of the beam. Stress couples and stress resultants are calculated from these stresses by integrating over the cross-section and the equilibrium equations are obtained. The equations are solved for a beam with symmetric cruciform cross-section subjected to bending couples. This particular cross-section has symmetry not only about the principal axes, but also about the lines at  $45^\circ$  to the principal axes. For other types of cross-section, including other doubly symmetric cross-sections such as rectangular, the equations do not permit an easy analytical solution. Mainly the effect of large pretwists (up to  $10\pi$ ) is investigated. It is shown that the beams with equal flexibility in all directions simply become more flexible with the initial twist, a fact that corresponds with earlier observations made by Den Hartog (4).

An important effect of the inclination of longitudinal fibres to the axis of a beam, due to initial twist, is pointed out. Not only does this inclination have the effect of producing a smaller strain due to a given curvature, but in addition the fibre stress is concentrated more towards the centre than in an untwisted beam. The resisting



moment is thus decreased considerably for a given curvature. At the same time the resistance to torsion is increased with increasing pretwist.

The equilibrium equations for the particular problems of pretwisted cantilever beam subjected either to tip load or uniformly distributed load are obtained by Carnegie (5). For the derivation of these equations, the variational method of applying Euler characteristic equations to the integral expression for potential energy is used. This method fulfills the requirement for stationary value of potential energy and hence for the equilibrium. However, the second variation deciding the stability or otherwise of the equilibrium conditions is not considered, the stability being assumed. The coupling between the deflections along the two principal axes of cross-section, produced by pretwist, is clearly indicated by the equations. The effects of inclination of the longitudinal fibres due to initial twisting are not considered in the derivation. However, these effects are taken into account in a latter paper (6). For a pretwisted cantilever of rectangular cross-section sufficient agreement is shown to exist between the calculated and the measured values of deflections.

In the case of rotating beams, the additional bending moments caused by the centrifugal forces are functions of displacements and the resulting equations do not permit an



easy analytical solution, especially when the cross-section is not uniform. Apart from the classical approximate methods such as the Collocation method, the Rayleigh method, the Galerkin's method, etc., various other numerical methods appeared around 1945 for the bending analysis of rotor blades. A comparative study of these earlier approximate methods has been done by Flax (7) in 1947.

A matrix method for the calculation of deflections and moments of a pretwisted blade is given by Plunket (8). In this analysis the blade is considered as being made of several masses joined by rigid rods, the elasticity being concentrated at the mass stations. From the given loading the bending moment at each station is calculated and resolved along the principal axes of inertia of the cross-section. The deflections at each station are calculated by assuming that a bending moment  $M$  acting at a station would cause an abrupt change of slope of magnitude  $M\ell/EI$  at that station ( $\ell$  = length of the beam segment). The calculated deflections are along the principal axes which vary along the length of the beam due to pretwisting and are transformed to common axes. For rotating blades a method of successive approximations is suggested. It is pointed out that the successive substitution process results in continually oscillating values. An averaging technique, whereby the new value to

be used is the average of the previous value and the corrected value, is recommended to overcome this difficulty.

## 2.2 Vibration of Nonrotating Blades Without Pretwist

For vibration analysis, blades are generally treated as cantilever rods. An untwisted rod can vibrate in four distinct types of modes - longitudinal, torsional and bending along each of the principal axes of inertia of the cross-section. In each type there can exist the fundamental as well as the higher tones. The longitudinal frequencies are not generally of great practical importance in blade analysis. The most important, from practical considerations, are the first three flapwise bending modes, the first chordwise bending mode and the first two torsional modes. If the cross-section of a blade is such that its shear centre and the centroid do not coincide, coupling between bending and torsional vibrations takes place. The uncoupled bending and torsion are first discussed, followed by the methods for locating the shear centre and the analysis of coupled vibrations.

### 2.2.1 Bending Vibrations

For cantilever beams of uniform cross-section the natural frequencies can be determined by classical methods, and are given by

$$\omega_n = \frac{a_n^2}{L^2} \sqrt{EI/\gamma} \quad (2.1)$$

where  $EI$  is the flexural rigidity,  $\gamma$  the mass per unit length and  $L$  the length of the beam. The values of  $a$  for the first four modes are 1.875, 4.694, 7.855 and 10.996.

For tapered beams it is more convenient to use numerical methods. The tabular method of Myklestad (9) is, probably, the most widely used. In this method the beam mass is lumped at a number of discrete stations along the beam. A certain value of natural frequency is assumed and starting from one end, the shear, moment, slope and deflection at each successive station are calculated from the values at the previous station, till the other end is reached. As in the Holzer method, at the correct frequency the shaking force must vanish. A discussion of different methods available for forming the lumped parameter systems is given by Minhinnick (10).

When a continuous system is represented by a lumped mass system, obviously, a large number of stations must be used to get reliable results. The extent of error involved in this method of solving a continuous system has been studied by Duncan (11), in relation to a uniform cantilever beam. He has suggested an extrapolation formula by which accurate values can be predicted from the values obtained for a few mass stations. Further study of the effect of lumped parameters has been done by Leckie



and Lindberg (12) who have indicated a method for deriving the dynamic stiffness matrix by considering the actual mass distribution. The derivation consists of assuming a cubic expression for the deflection within an element and applying the principle of consistency of virtual work done by distributed and edge inertia loading. An extensive review of the various approximate methods, for determining the natural frequencies and the mode shapes, is carried out by Siddall and Isakson (13). A comparative study of various methods is made by carrying out computations for a tapered cantilever beam.

### 2.2.2 Torsional Vibrations

The classical method for the analysis of torsional vibrations of circular section rods results in a differential equation of motion of the second order, similar to the one for the longitudinal vibrations. For cantilever rods the substitution of the boundary conditions of zero twist at the fixed end and zero torque at the free end yields the expression for torsional frequencies in the form

$$\omega_n = \frac{n\pi}{2L} \sqrt{Cg/I_{c.g.}} \quad (n = 1, 3, 5 \dots) \quad (2.2)$$

where  $C$  is the torsional rigidity,  $L$  the length and  $I_{c.g.}$  the polar moment of inertia per unit length of the rod. Sometimes this expression is also used to give approximate

frequencies for non-circular rods by using the value of  $C$  given by the Saint Venant's theory of torsion.

For an aerofoil section the torsional rigidity cannot be calculated easily and recourse is generally made to experimental and empirical methods. Jaswon and Ponter (14) have suggested a method for calculating the torsional rigidity of any arbitrary cross-section. In this method the classical torsion problem of Saint Venant is formulated mathematically as a Neumann boundary value problem for the warping function, which can be found numerically on the boundary by means of an integral equation method. Several cross-sections have been analyzed in the paper and it is indicated that the torsional rigidity to an accuracy of 1 percent can be obtained.

A more accurate analysis of the torsional vibrations, taking into account warping of the cross-section, yields a fourth order differential equation given by Gere (15). The equation of motion, with a slight change of notation is

$$C \frac{\partial^2 \phi}{\partial x^2} - EC_{\omega} \frac{\partial^4 \phi}{\partial x^4} = I_{c.g.} / g \frac{\partial^2 \phi}{\partial t^2} \quad (2.3)$$

where  $E$  is the Young's Modulus,  $C_{\omega}$  the warping constant for the section and  $\phi$  the twist at a distance  $x$  along the beam at time  $t$ . If the warping is zero, as in a circular section, this equation reduces to the classical equation of the second order. The boundary conditions at the built-in end are

$\phi = 0$  and  $\frac{\partial \phi}{\partial x} = 0$  and at the free end  $\frac{\partial^2 \phi}{\partial x^2} = 0$  and  $\frac{C}{EC} \omega \frac{\partial \phi}{\partial x} - \frac{\partial^3 \phi}{\partial x^3} = 0$ . These boundary conditions ensure complete warping restraint at the fixed end and the vanishing of  $\sigma_x$  at the free end, in addition to zero twist at the fixed end and zero torque at the free end. Computations of the natural frequencies for these and the other boundary conditions are given in the paper (15).

Carnegie (16,17) has also derived a similar fourth order equation for the torsional vibrations of a cantilever beam of narrow rectangular cross-section by considering the bending of longitudinal fibres produced by torsion. Variational principle is used for the derivation. For a narrow section with breadth  $b$  and thickness  $t$ , the corrected formula for the natural frequencies is shown to be

$$\omega_n = \frac{n\pi}{2L} \sqrt{\frac{Cg}{I_{c.g.}}} \sqrt{1 + \frac{n^2 \pi^2 E t^3 b^3}{576 CL^2}} \quad (n = 1, 3 \dots) \quad (2.4)$$

The problem of torsional vibrations of a cantilever beam of thin-walled open section has also been studied by Hanawa and Koshide (18) by using trial functions in the direct application of variational calculus. The results compare well with those of Gere (15).

### 2.2.3 Shear Centre

When an untapered cantilever beam is loaded at its tip by surface tractions, their resultant would act through a



point S on the tip cross-section perpendicular to the axis of the beam. If this force does not cause any twist at the centroid of the cross-section, then the point S is called the 'Shear Centre' of the section. Many other names e.g. 'flexural centre', 'centre of flexure', 'elastic centrum' etc. are also commonly used for the same point. A different point on the cross-section, generally known as 'centre of least strain', has been sometimes called the shear centre. This is a point S' on the cross-section such that when the resultant of surface forces at the free end of the cantilever acts at that point, the aggregate work done by the torsional surface traction is zero. These two points S and S' coincide only if Poisson's ratio of the material is zero. Washizu (19) has claimed that with S' as the definition for centre of shear, the extension to a naturally curved and twisted slender bar is straight-forward.

For cross-sections having one axis of symmetry, different formulae for the location of the shear centre have been proposed in the past. Most of these earlier methods are reviewed by Duncan (20) in 1953. In the same paper an expression in terms of Prandtl torsion function, is also given for locating the shear centre of sections with one axis of symmetry. For any arbitrary section, Jacobs (21) has developed expressions for the coordinates of the shear centre in terms of torsion function. These expressions

are used in the paper to calculate the shear centre location of a particular aerofoil section. The torsion problem for the section is first solved by relaxation methods. For a section bounded by two circular arcs, the torsion function is well known in analytical form. Whitehead and McQuillin (22) have used this torsion function to find the shear centre of such a cross-section, when the inner arc has its centre on the circumference of the circle of which the outer arc forms a part. By varying the angle subtended by the arcs at the centre of the inner arc, the effect of camber and the thickness variation on the location of shear centre are investigated.

A computer programme based on the method of solving the torsion problems given by Jaswon and Ponter (14), has been developed by Cowper (23) to calculate the shear centre of any arbitrary cross-section.

#### 2.2.4 Coupled Bending-Torsion Vibrations

When the shear centre of the cross-section does not coincide with its centroid, the bending and the torsional vibrations are coupled and must be considered together. Myklestad (24) has extended his earlier tabular method (9) to the case of coupled bending-torsion vibrations. Here the variables at each station are taken to be shear, bending moment, slope, deflection, twist and torque. Myklestad's method has been somewhat modified by Targoff (25). In this



approach, after relating the variables of two consecutive stations by a matrix relation, successive matrix multiplication is carried out. Thus the quantities at one end of the beam are related directly to those at the other end of the beam. The correct frequency is obtained as in the Holzer approach.

Differential equations of motion for the coupled bending-torsion vibrations, resulting from the eccentricity of shear centre, are derived by Gere and Lin (26). In general there are three coupled fourth order equations for the deflections along each principal axis and the twist. A variable separation method for the solution of these partial differential equations is suggested. This reduces them to ordinary differential equations which are then combined into a single 12th order differential equation. The method is very laborious especially if the edges are not simply supported. The Rayleigh-Ritz method is used for determining the fundamental frequency. The analysis is directed mainly towards thin-walled open sections.

Gere's equations of motion (26) do not take into account the effects of deformation due to shear strain. Tso (27) has obtained the equation taking into account the shear strain effects. This higher order theory is derived using the variational formulation, and treating the thin-walled

beam as a special case of thin prismatic shell. Comparison of this higher order theory with Gere's theory is carried out on the basis of the natural frequencies obtained for a beam of circular split ring type cross-section. It is concluded that for long beams both theories give the same results. For medium length beams the non-inclusion of shear effects does not appreciably affect the frequencies of torsion-predominant modes but the natural frequencies of bending-predominant modes are over estimated. For very short beams, however, it is pointed out that even the higher order theory is not satisfactory and shell type analysis is called for.

### 2.3 Vibration of Nonrotating Pretwisted Blades

Figure (1) shows the end view of a pretwisted blade looking from the tip towards the root. For convenience the section has been shown as rectangular instead of aerofoil. The x-axis is along the length of the beam joining the centroids, while the y and the z axes are in the direction of the principal axes of inertia at the root section. At any intermediate section the principal axes are taken in the  $\xi$  and  $\eta$  directions. The torsional stiffness of a blade of length L, breadth b, thickness t and having an initial twist  $\psi$  is denoted by  $C_\psi$ . This common nomenclature is used to

facilitate the discussion of various papers in this field.

When a beam is initially twisted about its longitudinal axis bending along the y and the z direction occur simultaneously. Torsion occurs independent of bending provided that the centroid and shear centre coincide. Thus if the pretwisted beam has a doubly symmetric cross-section, such as a rectangle, one is faced with the problem of coupled bending-bending vibrations and of torsional vibrations. However in a pretwisted beam of aerofoil section, coupled bending-bending-torsion problem is to be considered. The results presented in almost all the papers are for linear variation of pretwist along the length of the cantilever blade.

### 2.3.1 Coupled Bending-Bending Vibrations

The effect of pretwist on the bending frequencies of a cantilever beam of rectangular section has been investigated by Rosard (28). In this analysis the beam is divided into a number of segments; the mass as well as the elasticity are concentrated at the stations. The bending variables (shear, moment, slope, and deflection) of two consecutive stations are related, for each plane of bending; and by successive elimination the values of displacements at the fixed end are found in terms of those at the free end. The boundary conditions of fixed and free end necessitate



the determinant of a relating matrix to vanish, giving the natural frequencies. The equations used for relating the variables of two stations are not as refined as those of Myklestad. This is justified in the paper on the ground that the purpose of the investigation is to study only qualitatively the effect of pretwist on frequencies. Variation of the first three bending frequencies with pretwist is studied for the breadth to depth ratio of the beam varying from 4 to 12. It is shown that the fundamental frequency is not greatly affected by pretwist. Coupling between the second flapwise frequency and the first chordwise frequency is produced by pretwist. The lower of these two frequencies is further reduced by pretwist whereas the higher one is increased. Hence, if the  $b/t$  ratio is less than 6.36 (at this ratio the second flapwise frequency is equal to the first chordwise frequency in an uncoupled case) the chordwise frequency decreases with pretwist while the second flapwise frequency increases. However for a  $b/t$  ratio larger than 6.36, the effect is reversed.

The bending vibrations of a twisted beam lead to two fourth order differential equations. A method of solving these two coupled fourth order equations is given by Troesch et al. (29). By taking the solution for the deflection in the  $y$  and the  $z$  directions of the form  $Ae^{\lambda x}$  and  $Be^{\lambda x}$ , an



eighth order characteristic equation in  $\lambda$  is derived. The solution of the problem is obtained for a particular case when the flexural rigidity of the section in one of the principal directions is infinitely large (e.g. narrow rectangular cross-section) and the pretwist per unit length is constant. The variation of the first four bending frequencies for pretwist varying from  $0^\circ$  to  $1000^\circ$  is computed in the paper. It is shown that the fundamental frequency rises with pretwist whereas the higher bending frequencies decrease with pretwist. When the pretwist tends to infinity, the first and the second frequency tend to the same value and this corresponds to the fundamental frequency of an untwisted beam of flexural rigidity twice that of the given narrow rectangular section. A somewhat different approach has been given in a latter paper (30). DiPrima and Handleman (31) have given the differential equations of motion for pretwisted beams in vectorial notations and indicated a method of obtaining eigenvalues from variational principles. The method is too involved from computational point of view. In the paper, only the fundamental frequency has been computed.

An approximate method of calculating the effect of pretwist on the bending frequencies of a cantilever beam is given by Martin (32). The effect of twist is taken as a first order perturbation. The twist per unit length is

assumed constant ( $k = \psi/L$ ). The ratio of the natural frequency of a twisted beam to the corresponding frequency of an untwisted beam is assumed to be given by  $1 + P(kL)^2$ . The aim of the paper is to determine the correction factor  $P$ . As a further approximation certain expressions for deflections along the principal axes of inertia of cross-sections are assumed which contain the parameter  $k$  ( $\xi = \xi_0 + k^2 \xi_1$ , and  $\eta = k \eta_1$ ). By substituting these in the equations of motion and equating like powers of  $k$  the values of  $\xi_0, \xi_1, \eta_1$  etc., and the value of  $p$  are obtained. The values of  $p$  for the first four bending modes for various values of breadth to thickness ratio are tabulated in the paper. It is pointed out that if the breadth to thickness ratio of a slightly twisted beam is such that a chordwise frequency and a flapwise frequency are equal, then an excitation in the flapwise direction can produce resonance in the other direction. The analysis presented does not give full justification for the assumed expressions. It is well known that the first frequency is not greatly affected by twist and this fact is not fully borne out by the values of the derived correction factor.

Carnegie (16) has used the Rayleigh energy method to calculate the first natural frequency in bending of a pretwisted cantilever beam. In this type of analysis an assumption re-

garding the deflected shape of the beam is necessary. In the paper the static deflection curves obtained earlier (5) are used. It is shown that for a narrow rectangular section, a pretwist of  $90^\circ$  increases the fundamental frequency by about 3.5% and for a square section it is unaltered by twist. Experimental values of the frequencies for rectangular cantilever beams with pretwist ranging from  $0^\circ$  to  $90^\circ$  are also presented in the paper for a particular breadth to thickness ratio.

The Rayleigh method used by Carnegie (16) gives only the fundamental bending frequency. Dawson (33) has extended the method for calculating the higher bending frequencies by use of the Rayleigh-Ritz approach. The characteristic functions representing the normal modes of vibration of straight beams in simple flexure are used as approximating functions for the bending displacements. A discussion of the mode shapes is given in a later paper (34).

The effect of the depth taper and the width taper in a pretwisted cantilever beam has been investigated by Carnegie et al. in the first part of Reference (35). In this analysis the equations of motion are converted to a set of linear algebraic equations by finite difference technique. It has been shown that for a fixed value of pretwist, the coupling between the bending modes increases with an increase in the ratio of width taper and the depth



taper.

Isakson and Easley (36) have used Targoff-Myklestad type analysis for calculating bending frequencies of pre-twisted beams. Although the method is mainly devised for rotating blades, nonrotating blades have been treated as a special case. In this method the beam is divided into segments and the mass of each segment is lumped at its centre. The flexural rigidity in both the principal directions is assumed to remain constant between the adjacent masses. The total pretwist of a segment is assumed to occur at the mass station. The vectors  $\{\Delta\}$  of 8 bending variables (shear, moment, slope and deflection along each bending direction) of two adjacent masses  $n$  and  $(n + 1)$  are related to each other by the matrix relation  $\{\Delta\}_{n+1} = [R][E][F]\{\Delta\}_n$ . The matrices  $[F]$ ,  $[E]$  and  $[R]$  correspond to the variations involved in movement across the mass, the weightless rod and the concentrated pretwist, respectively, and are given explicitly in the paper. Successive matrix multiplication relates the vectors of the two ends of the beam. By substituting boundary conditions and trying various values of natural frequency the correct values are obtained.

For pretwisted beams the condition of orthogonality for the normal modes has been derived by White (37) using Green's functions. Slyper (38) has proved this condition using the Maxwell reciprocal theorem and has used it for the

determination of coupled bending frequencies by the Stodola process. In this analysis a certain deflection curve is assumed for the fundamental mode and the inertia loading for a unit angular frequency is calculated. This inertia loading is taken as the static loading to calculate a new deflection curve. Repeating the process would ultimately give the correct fundamental mode shape. The ratio of the initial and the new deflection of the beam, in the final iteration, gives the square of the angular frequency. To calculate higher modes, the condition of orthogonality is used to remove the traces of all the lower modes of vibration already determined. Due to bending-bending coupling produced by the pretwist, the deflection shape is taken as  $y + jz$ , the  $j$  notation indicating that the deflection in the  $z$ -direction is at right angles to that in the  $y$ -direction. The results of computations for cantilever blades with breadth to thickness ratio from 2 to 16 and for pretwists varying from  $0^\circ$  to  $180^\circ$  are presented in the paper. They are shown to be in agreement with those obtained experimentally by Carnegie (16) and Rosard (28).

Dokumaci et al. (39) have used the finite element technique with matrix displacement type analysis for the determination of the bending frequencies of a pretwisted cantilever beam. The beam is divided longitudinally into small elements. At each end of the element four degrees of

freedom are assigned (slope and deflection along each principal axis of inertia of the cross-section). Within an element the deflection along each of the two directions is assumed in the form  $\alpha_1 + \alpha_2 x + \alpha_3 x^2 + \alpha_4 x^3$ . Stiffness and mass matrices for each element are formed by calculating the energy expressions in terms of the displacements at the ends of each element and by the application of the Lagrange equations of motion. The explicit expressions for the mass and the stiffness matrices are given in the paper. Natural frequencies and mode shapes are obtained from the resulting eigenvalue problem. Computations are carried out for pretwist angles of  $30^\circ$ ,  $60^\circ$  and  $90^\circ$  and for breadth to thickness ratios varying from 2 to 16. An extrapolation formula is suggested, by which, knowing the natural frequencies for the subdivision into  $n$  and  $n + 1$  elements, accurate values of the frequencies may be estimated.

It may be worthwhile here to comment briefly on the different methods available for calculating the bending frequencies of a pretwisted beam of rectangular section. The analytical methods of Troesch et al. (29,30) and DiPrima et al. (31) aim at the solution of coupled differential equations. These methods can not be easily extended to general cases where taper may be present or pretwist per unit length may not be constant. Approximate methods are thus important from practical considerations. The correction



factor for twist given by Martin (32) is based on rather unproven approximations, and the results obtained do not coincide very well with those obtained later by other authors, especially for the fundamental frequency. The Rayleigh method used by Carnegie (16) gives only the fundamental frequency. The method used by Rosard (28) involves the lumping of both mass and elasticity and the equations relating the variables of the adjacent stations are not very refined. Better results can be expected if the elasticity of the beam is considered distributed as used by Isakon et al. (36). The Rayleigh-Ritz method (33), the finite difference transformation method (35), the Stodola method (38) and the finite element technique (39) give almost identical results. A comparison of the results obtained by various methods is given in Reference (33).

From the results obtained by various investigators, certain general conclusions can be drawn regarding the coupled bending frequencies of pretwisted cantilever beams of rectangular cross-section. The conclusions are valid for the magnitudes of pretwist usually encountered in turbomachinery blading. The fundamental frequency is affected very little by the pretwist. If a chordwise frequency and a flapwise frequency are very close to each other, the effect of pretwist is to separate them more. If the breadth to thickness ratio is very large (say more than 20) the second and the

third bending frequencies decrease with pretwist. The effect of twist on the natural frequencies is less in tapered beams than in the beams of uniform cross-section.

### 2.3.2 Torsional Vibrations

For a pretwisted blade of rectangular section the torsion and the bending deformations remain uncoupled. The torsional stiffness, however, is very much increased due to pretwist, resulting in an increase in the torsional frequencies. The main cause of the increase in the torsional stiffness, over and above that given by the Saint Venant theory is due to the inclination of the blade longitudinal fibres which become helical due to the initial twist. When elastic twisting takes place in an initially twisted beam, the force acting along the fibre has a component along the longitudinal axis of the beam as well as a lateral component in the plane of the cross-section. This lateral component of the fibre force has a moment about the centre of torsion, resulting in the increased torsional stiffness. An explicit expression for the torsional stiffness of a beam of narrow rectangular cross-section, with a small magnitude of pretwist, is given by Chen-Chu (40) and also by Carnegie (16) following somewhat different approaches. The expression is

$$C_{\psi} = C \left[ 1 + \frac{1}{6} \left( \frac{b\psi}{2L} \right)^2 \frac{b^2}{t^2} \right] \quad (2.5)$$

The first term is the Saint Venant torsional stiffness, while the second term is the additional stiffness due to the pretwist  $\psi$ . For thin blades this additional rigidity may even be the dominant term.

The problem of torsional vibrations of pretwisted rods has been investigated by Reissner and Washizu (41). The differential equation of motion is derived from shallow shell equations using variational principles. The torsion of a pretwisted rod causes a decrease in its length, resulting in a coupling between the torsional and the longitudinal vibrations. DiPrima (42) has considered this problem of coupled vibrations. It is shown that the longitudinal frequencies are not significantly affected by pretwist, but the torsional frequencies increase considerably. The percentage increase is higher for higher  $b/t$  ratio. An expression is derived for the effective torsional stiffness of a pretwisted rod in the form

$$C_{\psi} = C \left[ 1 + \frac{EI_2 \psi^2}{CL^2} - \frac{EI_0^2 \psi^2}{CL^2 A} \right] \quad (2.6)$$

where  $I_2 = \int_A r^4 dA$  and  $I_0 = \int_A r^2 dA$ ,  $r$  being the distance from the centroid to any point on the cross-section of area  $A$ . For a bar of very narrow rectangular cross-section this reduces to

$$C_{\psi} = C \left[ 1 + \frac{2(1+\mu)}{15} \left( \frac{b\psi}{2L} \right)^2 \frac{b^2}{t^2} \right] \quad (2.7)$$



where  $\mu$  is the Poisson's ratio.

A similar expression has also been obtained by Reissner and Washizu (41) by neglecting the coupling between the torsional and the longitudinal motions. The only difference being that instead of  $(1 + \mu)$  in the numerator they have obtained  $(1 - \mu)$  in the denominator.

### 2.3.3 Coupled Bending-Bending-Torsion Vibrations

In a blade of aerofoil cross-section, apart from the coupling between the bending modes produced by pretwist, the torsional vibrations are also coupled. Mendelson and Gendler (43) have suggested a method for obtaining the natural frequencies using the concept of station functions. In this approach, a continuous loading function for the blade is obtained from the displacements at a finite number of stations along its length. From this the method of deducing the frequency equation is presented. Dunham (44) has derived the equations of motion in a twisted coordinate system following the blade length and has used them for the determination of the first natural frequency. Certain coupling terms have not been included in these equations and are pointed out later in his discussion of Reference (16). Carnegie (16) has used Rayleigh method to find an expression for determining the fundamental frequency of pretwisted cantilevers of aerofoil section. Although his equations are for the coupled

case, in the calculations the coupling between torsion and bending is neglected. Static deflection curves are used as mode shapes for calculating the energy expressions. In his discussion of this paper Dawson has pointed out that the coupling between the torsion and the chordwise bending is significant and should not be overlooked. The equations of motion for a pretwisted blade of general aerofoil section are modified later by Carnegie (17,45) to include the additional effects due to torsion, shear and rotary inertia.

Belgaumkar et al. (46) have calculated the first four bending frequencies and the first three torsional frequencies of five typical blades. They, too, have neglected the coupling between the bending and the torsion and have used the methods discussed for the rectangular sections. Computations are carried out using several of these methods and the results are compared with experimentally observed natural frequencies. This provides a basis for investigating the relative accuracy that could be expected from these methods.

Isakson and Eislely (47) have extended their method (36) to take into account the coupling between the bending and the torsion. Although this paper deals mainly with the rotating blades, nonrotating blades are considered as a special case. The vector of station unknowns, in addition to shears, moments, slopes and deflections, also includes the torque and the twist as variables.

In the second part of Reference (35) Carnegie et al. have given a method for solving the coupled bending-bending torsion differential equations by the Runge-Kutta numerical procedure. This approach converts the differential equations to ten equations of the first order. The method of solution consists of assigning, in turn, a unit value to one of the unknowns at the fixed end keeping the others zero, and determining the values of these quantities at the free end. The values found at the free end are then combined linearly. All this work is carried out for each test value for the frequency. For satisfying the boundary conditions at the free end, the determinant of these equations must vanish at the correct frequency. Computations are carried out for a typical blade taking into account the pretwist and the eccentricity of the shear centre.

#### 2.4 Vibration of Rotating Blades Without Pretwist

A rotating blade is subjected to a distributed centrifugal force which increases from the root to the tip. The distributed centrifugal forces have a stiffening effect on the blade and hence the frequencies of the rotating blades are higher than the corresponding frequencies of the nonrotating blades. The centrifugal forces induce several additional coupling terms in the already complicated equations of motion. In this discussion, the angle subtended by the



minor principal axis of inertia of a section of the blade with the plane of rotation is called the 'setting angle' and is denoted by  $\theta$ . Since no pretwist is considered in this section,  $\theta$  is constant all along the length of the blade. Figure (2) shows the system under investigation and the notations used. A brief survey of the earlier methods for this type of analysis has been done by Billington (48) in 1948, and only the later developments are included here.

If a cantilever beam is considered executing uncoupled bending vibrations in a plane perpendicular to the plane of rotation ( $\theta = 0^\circ$ ), it is well known, that the natural frequency of the rotating beam ( $\omega_r$ ) is related to the corresponding frequency of the nonrotating beam ( $\omega$ ) by the relation

$$\omega_r^2 = \omega^2 + S\Omega^2 \quad (2.8)$$

Here  $\Omega$  is the angular speed of rotation and the factor  $S$  is generally called the Southwell Coefficient. The relation can be easily established by the application of the Rayleigh energy method of equating the total potential energy of the bending and the centrifugal forces at maximum displacement, to the maximum kinetic energy. For the application of the Rayleigh method an approximate mode shape, consistent with the displacement boundary conditions of the beam, is required. If the nonrotating mode shape is used for energy

evaluation,  $S$  is found to be independent of the speed of rotation. This, of course, is not strictly true as the mode shapes in the rotating and the nonrotating cases are not identical.

When the bending vibrations occur in a plane perpendicular to the plane of rotation, the centrifugal forces form a system of parallel forces. However, if the rotating blade undergoes bending oscillations in the plane of rotation ( $\theta=90^\circ$ ), the centrifugal forces, in general, are not parallel but act in the directions which are radial from the axis of rotation. The stiffening effect of these forces is thus smaller and hence the value of the Southwell Coefficient is expected to be lower than for the case of  $\theta = 0^\circ$ .

The effect of rotation on the bending frequencies has been considered by Sutherland (49) by using a Myklestad type tabular method of analysis. The equations relating the shears and the moments of two consecutive stations are suitably modified to take into account the effect of the centrifugal forces. Computations carried out for a wedge shaped cantilever for  $\theta = 0^\circ$  and  $\theta = 90^\circ$  have been presented in the paper. From the results of the computations it is shown that the value of  $S$  depends on the setting angle, the hub radius and the speed of rotation, although the theoretical nature of the dependence has not been established in the paper. In his discussion of the paper, Plunket (50) has

pointed out that the equations relating the shear forces of two consecutive stations, derived by Sutherland, can be used to obtain a general relation between the value of  $S$  for  $\theta = 0^\circ$  and  $\theta = 90^\circ$ . He has shown that

$$S_{(\theta = 90)} = S_{(\theta = 0)}^{-1} \quad (2.9)$$

The case of the bending vibrations in a plane which is inclined at any general angle  $\theta$  with the plane of rotation, has been investigated by Lo et al. (51). They have observed that the equations of motion contain a nonlinear term resulting from the Coriolis acceleration. This term vanishes only when  $\theta = 0^\circ$ . By neglecting this nonlinear term a periodic solution of the problem is obtained and it is shown that the variation of the Southwell Coefficient with  $\theta$  is given by

$$S_\theta = S_{(\theta = 0)} - \sin^2 \theta \quad (2.10)$$

The effect of the nonlinear term due to the Coriolis acceleration is investigated in a later paper (52) by considering a simplified model. The beam is considered as rigid in bending except at the root where a spiral spring is assumed to be present. The resulting equation is the same as that for a spring-mass system with a nonlinear viscous damping. The damping is of the dissipating energy type for positive deflections, but for negative deflections the damping is negative. An approximate solution in the phase-plane for the



nonlinear problem is given in the paper. It is shown that the important parameters affecting the nonlinear solution are  $\omega_r/\Omega, \theta$  and the amplitude of vibrations. It is pointed out that for the practical values of these parameters, the error induced by neglecting the Coriolis force would be less than 1%. The effect of the Coriolis acceleration on the bending vibrations has been further discussed by Marshall (53).

Bogdanoff (54) has pointed out that when the rate of change of the angular momentum, i.e. the gyroscopic action of the cross-section is included, certain additional secondary inertia terms appear in the equations of motion. These terms couple the lateral and the torsional motions of a rotating beam, even though the cross-section may be doubly symmetric. The equations decouple only for a particular case of zero setting angle. From the results of computation, it is concluded that the secondary inertia terms have negligible effect on the fundamental frequency. The variation of the fundamental bending and the fundamental torsional frequencies with the rotational speed, when coupling is neglected, are presented in the paper.

The effect of rotation on the fundamental frequency of bending vibration has also been investigated by Schilhansl (55). The differential equation of motion is derived and converted to an ordinary differential equation by imposing a periodic solution. The differential equation is of the type

$$\frac{d^4 w}{dx^4} = A_1 \frac{d^2 w}{dx^2} + B_1 \frac{dw}{dx} + C_1 w \quad (2.11)$$

in which the coefficients  $A_1$  and  $B_1$  are functions of  $x$ . An approximate method of finding the fundamental frequency is given in the paper. It consists of assuming a solution  $w_0(x)$  for the deflection, satisfying the boundary conditions of the fixed end. This is substituted in the right hand side of the equation and by integration of the resulting equation a new value of  $w(x)$  is obtained. For an exact solution  $w(x)$  must be equal to  $w_0(x)$ . The best agreement of  $w$  and  $w_0$  is obtained by the equation

$$\int_0^L w_0(x) dx = \int_0^L w(x) dx \quad (2.12)$$

This equation yields the fundamental frequency. The process is repeated by using  $w(x)$  as the starting function, until convergence is obtained. By starting with a simple function  $w_0(x)$  it is shown that the expression for the Southwell Coefficient for the fundamental frequency of a cantilever beam is given by

$$S = 1.184 + 1.564 \frac{r}{L} - \sin^2 \theta \quad (2.13)$$

In the derivation, it is assumed that the speed of rotation ( $\Omega$ ) is small compared to the fundamental bending frequency of the nonrotating beam.

The effect of rotational speed on the fundamental bending frequency is further investigated by Kissel (56). He has considered the fourth order differential equation in  $w$  as the Euler characteristic equation of a variational problem, and obtained the corresponding energy function. An arbitrary expression for  $w(x)$  is assumed which, apart from satisfying all the boundary conditions of the cantilever beam, has an additional free parameter. This free parameter is so chosen as to give a minimum for the energy function. The expression for the deflection  $w(x)$  thus obtained is taken as the correct solution and the Southwell Coefficient is obtained. It is shown that

$$S = 1.1935 + 1.5712 \frac{r}{L} - \sin^2 \theta + f\left(\frac{r}{L}, \frac{\omega r}{\Omega}\right) \quad (2.14)$$

The expression for the last term which depends on the rotational speed ( $\Omega$ ) is rather lengthy and is given in the paper.

By using the nonrotating modes as an approximation for the rotating mode shapes, Yntema (57) has applied the Rayleigh principle to obtain the first three bending frequencies, for vibrations perpendicular to the plane of rotation. Extensive computations have been carried out in this paper for both the fixed and the hinged root blades of constant as well as linearly varying mass and elasticity distribution. The case when the blade carries a tip mass is



also analysed. The results are presented in the form of charts for quick estimation of the first three bending frequencies. In this method, for calculating the frequency of the  $n$ th bending mode of a rotating cantilever, a knowledge of the first and the  $n$ th natural frequencies and the mode shapes of the corresponding nonrotating beam is prerequisite. The Southwell Coefficient is divided into two parts,  $S = S_0 + S_r$ , where  $S_r$  is proportional to the distance of the axis of rotation from the root section. It is pointed out that  $S_0$  is appreciably affected by the beam mass distribution and to a less extent by the beam elasticity distribution. A more accurate analysis is also presented in the paper whereby the rotating mode is taken as the combination of the first five modes of a nonrotating beam. By comparing the results with the five mode expansion results, it is shown that the Rayleigh approach gives reliable results. The maximum deviation is reported for the fundamental frequency and is 5%, at the highest rotating speed (six times the fundamental frequency) considered in the paper. The percentage increase of frequency due to rotation is found to be highest for the fundamental mode and decreases for the higher bending modes.

Equations of motion for a rotating cantilever blade using the Hamilton's principle are derived by Carnegie (58).

The upper and lower bounds to the fundamental frequency of a rotating cantilever beam are considered by Kundu (59) by using Rayleigh-Southwell approach. The case of a rotating cantilever beam, having a cross-section in which the centroid and the shear centre do not coincide, is considered by Vorb'ev (60). A system of six differential equations is derived using the Hamilton's principle. It is shown that the well-known uncoupled equations can be obtained from these equations as special cases.

Summarizing the discussion of the various methods available for calculating the natural frequencies of rotating untwisted blades, it can be noted that most of the investigations are based on establishing the Southwell Coefficient (S). This coefficient gives the correction factor for the effect of rotation. For the fundamental frequency the expression for S given by Schilhansl (55) and Kissel (56) is almost the same and the special cases of Sutherland (49), Plunket (50), Lo (51) etc. can be obtained from them. For higher bending modes the Rayleigh-Southwell approach used by Yntema (57) appears to be promising. The nonlinear effects due to the secondary inertia terms have little influence at least on the fundamental frequency, as shown in References (52-54).



## 2.5 Vibration of Rotating Pretwisted Blades

In the previous section, since the blade is assumed to be straight, the bending in one plane only is considered and the effect of inclination of this plane to the plane of rotation is discussed. When the blade is pretwisted the setting angle is no longer constant along the length. The effect of the centrifugal forces on the bending in the flapwise and the chordwise directions must, therefore, be considered simultaneously. In most of the investigations the twisted blade is replaced by a system of lumped masses joined by weightless, untwisted rods. The pretwist of each segment is taken to occur at the mass stations. In earlier investigations, the segments of the blade between the masses are considered rigid and their elasticity is assumed to be concentrated at the mass stations. However, in more recent investigations the elasticity has been taken to be distributed. The physical model thus formed is illustrated in Figure (3).

Turner and Duke (61) have analysed the problem of vibrations of rotating propellers by replacing the structure by an idealized system consisting of lumped masses joined by rigid rods. The matrix equations of motion are derived by calculating the potential and the kinetic energy of the resulting multidegree of freedom system and the application of the Lagrange equations. The effect of rotation is accounted



for by including in the potential energy, the energy due to the opposing action of the centrifugal forces. The stiffness matrix thus obtained is the sum of the usual stiffness matrix for the nonrotating beam and the centrifugal stiffness matrix whose terms are proportional to  $\Omega^2$ . A somewhat similar approach is also used by Plunket (62) who has also idealized the system by concentrating the mass and the elasticity of the blade at the discrete stations. The effect of the centrifugal forces, however, is included by computing the bending moments produced by them at different stations and including these in the equations for calculating the deflections. In both these References (61,62), the matrix equations are first formed for deflections along the principal axes of inertia at each section and then transformed to common axes. The resulting eigenvalue problem has been formulated in both the papers.

Jaret and Warner (63) have also idealized the rotating blade by a lumped mass system, but unlike References (61,62), the elasticity is considered to be distributed rather than concentrated at the mass stations. The differential equations of motion of a rotating pretwisted blade have been reformulated for application to a lumped mass system. These equations relate the bending variables of the adjacent stations in a manner similar to the Myklestad type approach. As a numerical example, the first three bending frequencies of a rotating blade of a low pressure steam turbine, with lashing wires, have

been obtained in the paper. The mass of the lashing wires is assumed concentrated at their junction with the blade.

Targoff (64) has also used lumped mass and distributed elasticity idealization for calculating the bending frequencies of pretwisted rotating blades. However, the computational scheme is somewhat different. After relating the bending variables of the adjacent stations by matrix equations, successive matrix multiplication is performed to relate directly the unknowns of the two ends of the blade. This method of computation has also been used by Isakson and Eisley (36) for calculating the bending frequencies of both the rotating and the nonrotating blades. From the numerous computations carried out by these authors for different values of pretwist, setting angle at root, offset of the root from the axis of rotation and the rotational speed, they have drawn several conclusions regarding the effect of these parameters on bending frequencies. Fundamental bending frequency of a rotating cantilever is found to depend primarily on the setting angle at the root and only secondarily on pretwist. It is observed that if the curves of rotational speed versus natural frequency, for the untwisted blade, cross each other, the effect of pretwist is to yield the curves which tend not to cross. At higher modes the frequency ratio (frequency of rotating blade/frequency of nonrotating blade) is not highly sensitive to twist or the



setting angle. The increase in the distance of the root from the axis of rotation, increases the frequency ratio. It is further pointed out that the Rayleigh-Southwell approach of finding the natural frequencies of rotating blades, by assuming the nonrotating mode shape as an approximation, gives poor results in the case of twisted blades. This is claimed to be especially true when the coupling produced by the pretwist is large and the speed of rotation is high.

The centrifugal forces not only affect the bending vibrations but also the torsional oscillations of a pretwisted beam. The effect on the torsional frequencies has been investigated by Bogdanoff and Horner (65). They have calculated the angular velocity of a triad formed by the principal axes and hence derived the expression for the angular momentum about the centroid of the section. The expression for the torsional couple about the longitudinal axis, derived in the earlier paper (54) has been simplified by omitting the less important secondary terms. Relating the angular momentum with the torsional couple, the basic differential equation of motion for torsional oscillations has been derived. Natural frequencies have been obtained by imposing a periodic solution on this equation. Computations have been carried out for the first three torsional frequencies of a rotating blade, for different values of pretwist and the blade setting angle at the root. The torsional frequencies are found to increase with the



rotational speed, the increase being larger for higher values of pretwist, especially for the first torsional mode. For higher torsional modes, the increase in the frequency due to rotation is virtually independent of the pretwist present in the blade. Brady and Targoff (66) have used an analysis similar to that used for the bending vibrations in the earlier paper (64), to calculate the uncoupled torsional vibrations of pretwisted blades.

When the general case of a rotating pretwisted blade of aerofoil cross-section is to be considered, the effect of centrifugal forces on the bending and the torsional frequencies cannot be considered separately, as these modes get coupled. The analytical treatment of this problem is carried out by Houbolt and Brooks (67). They have derived the differential equations for the coupled flapwise bending, chordwise bending and twisting of a rotating pretwisted blade. The derivation of the equations is based on "Engineering" beam theory and the secondary effects such as the deformation due to shear are not included. The expressions for the longitudinal strain, at any point on the cross-section, are first evaluated in terms of the displacements. This strain arises from four types of motion: pure displacement of the planes towards or away from each other, rotation of the planes associated with chordwise bending, rotation of the planes associated with flapwise bending and the rotation of the

the planes relative to one another about the elastic axis resulting in the twisting of the blade. With the aid of the strain equation, the internal elastic moments are derived about the principal axes of cross-section. The elastic moments are then transformed to a common axes system and the equations of equilibrium established, giving the final differential equations. The equations contain many coupling type terms associated with the centrifugal forces, which are not generally accounted for in the approximate analysis. A method of solving these equations, for a few simple problems, has been indicated.

For nonrotating blades the Runge-Kutta technique of solving the coupled bending-bending-torsion differential equation has been given by Carnegie (35). Montoya (68) has extended this method to the case of rotating blades of aerofoil section. Computations are carried out for an actual blade taking into account the pretwist and the eccentricity of the shear centre.

The inclusion of the torsional deformation complicates the effects of pretwist and rotation considerably. There may be a sizable steady-state or "pseudo-static" torsional deformation of the rotating blade in some cases. This is due to the centrifugal twisting moment which, in the case of negative pretwist and positive pitch, tends to twist the blade negatively, and also the twisting moment associated



with tensile stress in the longitudinal fibres, the so-called "centrifugal untwisting moment". These two effects oppose each other in the normal case, and the extent to which one or the other predominates depends primarily upon the amount of pretwist and the pitch setting of the blade. An analysis of this deformation is given by Brady and Targoff (66).

The torsional stiffness departs considerably from the value provided by the Saint Venant theory. The departure associated with the inclination of the longitudinal fibres with the elastic axis, whereby the normal stresses in the fibres have a component in the plane of cross-section, is already discussed for nonrotating blades. In addition, normal stresses associated with centrifugal forces also contribute to torsional stiffness. Some of these effects have been considered in References (65,66).

The effect of the Coriolis forces, or so-called "secondary inertia forces", on the vibrations of untwisted beam is discussed in the previous section. A study of this effect for the coupled bending-torsion vibrations is carried out by Isakson and Easley (47). They have analysed a simple model with a few degrees of freedom. The model consists of a rigid weightless rod on one end of which is mounted a mass and the other end of which is connected to a rotating shaft. The connection to the shaft is through a hinge with



an axis normal to the rod and set at an angle to the shaft. A spring, restraining the motion about this hinge, simulates the bending stiffness. In addition, the rod is free to rotate about its own axis against the action of a spring, which simulates the torsional stiffness. The mass is assumed to be distributed along a line normal to the rod, simulating the major principal axis of the blade cross-section, with its centre of gravity displaced from the rod, simulating an offset of the mass axis of the blade from the elastic axis. An analysis of this simplified model is shown to indicate that the presence of the Coriolis forces causes a phase difference between the bending and the torsional oscillations; whereas the natural frequencies are only slightly affected.

Krupka and Baumanis (69) have derived the field equations for coupled bending-torsion vibrations of a rotating blade using Carnegie's formulation of the Lagrange equations of motion. They have solved the field equations using the Holzer-Myklestad type approach. Numerical computations of the first two natural frequencies for a typical blade have been given in the paper. A method of including the effect of rotary inertia and shear deformation in the numerical approach has been indicated by them in their later paper (70).

## 2.6 Low Aspect Ratio Blades

In almost all the published work the turbomachinery blades have been treated as pretwisted beams. This beam type analysis, although good for long blades, cannot be expected to give accurate results for low aspect ratio blades. Such blades ought to be treated as pretwisted plates rather than as pretwisted beams.

The transition from a beam to a plate, with a resulting increase of flexural rigidity by a factor of  $1/(1-\mu^2)$ , where  $\mu$  is the Poisson's ratio, has been considered by Ashwell (71). He has based his conclusions on the consideration of the anti-clastic curvature that is produced when a bar of rectangular section is subjected to pure bending moment. It is shown that the important parameter to be considered is the value of  $b^2/Rt$ , where  $b$  and  $t$  are the breadth and the depth of the section and  $R$  is the radius of curvature of the neutral fibre. It is concluded that for  $b^2/Rt$  greater than about 100, plate type flexural rigidity ought to be used. In this analysis, shear effects are not included. The problem has been further considered by Gerard (72), who has pointed out that a plate or a beam type behaviour is not solely dependent on the geometrical parameters. He has shown that a structural element of given size behaves initially as a beam and the flexural rigidity may grow as the bending progresses.

A modified beam theory, taking into account the effects

of bending in the transverse direction, has been developed by Cowper (73,74). Such effects are important in beams of large width. The transverse curvature due to bending appears as one of the basic quantities in this theory, and the equations relating it to bending deflection, bending moment, etc., have been derived. The theory has been applied to a number of examples in order to test its accuracy. Deflections, natural frequencies and mode shapes of rectangular plates have been calculated using the extended beam theory and compared with the values based on the classical plate theory.

The differential equations for beams of thin-walled open section given by Gere (26) and Tso (27) do not take into account the deformation of the cross-section during bending. These theories, therefore, can not predict the modes of vibration with one or more pairs of nodal lines running approximately along the length of the beam. Hasan and Barr (75) have derived the equations of motion for thin-walled beams of circular arc section, taking into account the coupling between the ordinary bending motion and the cross-sectional distortion. In deriving the theory the cross-sectional deformation is assumed to take the form of the characteristic functions of a curved beam. For bars of thin-walled open section, such as blades, this type of analysis may be considered as a bridge between the beam theory of Tso (27) and the analysis based on shallow shell theory.



For torsional vibrations of cantilever bars, the Saint Venant theory does not take into account the warping restraint at the fixed end. If the blade is long these end effects, which extend only for a short distance from the fixed end, do not greatly affect the results. However, for low aspect ratio blades, these could have an appreciable influence.

If the pretwist of a low aspect ratio blade is neglected, it can be considered as a cantilever plate. The natural frequencies of cantilever plates, using the Ritz energy method, have been obtained by Young (76) and Barton (77). Their method and the results are given in many standard texts on the subject. The problem of vibrations of cantilever plates of uniform and variable thickness has been considered by Dawe (78,79) using the finite element technique. In this approach, the plate is divided into small rectangular elements. To each element 12 degrees of freedom are assigned consisting of deflection and two slopes at each of the four nodes (corners) of the element. A polynomial expression of the form

$$\begin{aligned}
 w = & \alpha_1 + \alpha_2 x + \alpha_3 y + \alpha_4 x^2 + \alpha_5 xy + \alpha_6 y^2 + \alpha_7 x^3 \\
 & + \alpha_8 x^2 y + \alpha_9 xy^2 + \alpha_{10} y^3 + \alpha_{11} xy^3 + \alpha_{12} x^3 y
 \end{aligned}
 \tag{2.15}$$

is assumed for the deflection within an element. The 12 arbitrary constants ( $\alpha_1$  to  $\alpha_{12}$ ) are evaluated in terms of the nodal displacements of the element. The calculation of strain energy and the application of Castigliano's

principle yields the stiffness matrix for the element. The determination of the inertia matrix for the element is based on the consistency of the virtual work done by the distributed inertia loading and the equivalent nodal inertia forces, during an arbitrary virtual displacement. The assembly of the matrices for all the elements and the deletion of the rows and the columns corresponding to the fixed end, gives the resulting eigenvalue problem for free vibrations of the plate.

Vibration analysis of a uniform cantilever plate, by the finite element technique using triangular elements, is carried out by Anderson et al. (80). Three degrees of freedom are assigned to each node and a cubic polynomial expression with nine arbitrary coefficients is used for representing the deflection within a triangular element. The method of deriving the mass and the stiffness matrices is similar to the one discussed above.

The static bending of pretwisted rectangular plates, subjected to pure bending couples, has been investigated by Maunder and Reissner (81). The pretwisted plate is considered as a shallow hyperbolic paraboloidal shell. The differential equations are expressed as two fourth order equations in the deflection and the Airy stress function, as is customary in thin shallow shell theory. The final expressions for the deflection and the Airy stress function are given, and it is



shown that these satisfy the differential equations and the boundary conditions for a plate with two opposite edges free and the other pair of edges acted upon by bending couples. The basis for obtaining the solution is not given in the paper. It is shown that the results obtained differ from the predictions of the elementary beam theory and also from the theory of transverse bending of flat plates. The physical cause of the difference is attributed to the interaction which occurs between the pretwist and the lateral contractions induced by bending.

The differential equations of motion for transverse vibrations of thin shallow shells have been given by Reissner (82). Nagadhi (83) has characterized the problem of thin shallow shells by an exact system of equations containing the axial displacement, the stress function and two particular integrals. When the nonlinear terms are neglected in these equations, the system is still exact within the framework of the classical theory of thin shallow shells. The linearized system reduces to that of Reissner (82) when the longitudinal inertia is neglected. These equations have been successfully used for the vibration analysis of shells of revolution.

Vibration analysis of pretwisted rectangular plates, using the linearized equations given by Nagadhi (83), has been carried out by Nordgren (84). The equation of the middle surface of a pretwisted plate is taken as  $z = kxy$ , where  $k$  is



the pretwist per unit length and the plate is bounded between  $x = \pm \frac{L}{2}$  and  $y = \pm \frac{b}{2}$ . The solution necessitates that the two opposite edges of the plate must be simply supported. The method of solution is similar to the well known Levy solution for flat plates. The condition of two opposite edges being simply supported makes it possible to obtain the solution in a variable separation form. It is shown that the fundamental torsional frequency differs considerably from that calculated by considering the structure as pretwisted beam, when the aspect ratio is small. For aspect ratio of 2 the difference is of the order of 5 percent in the fundamental torsional frequency. For aspect ratio of 5, almost complete agreement is observed.

Finite element technique has been used by Olson et al. (85) for calculating the natural frequencies of a curved fan blade. The blade is considered as a cylindrical shell of uniform thickness with one of the curved edges built-in and the other edges free. The shell is subdivided into cylindrical elements. Seven degrees of freedom are assigned to each node, namely,  $u$ ,  $v$ ,  $w$ ,  $\frac{\partial w}{\partial x}$ ,  $\frac{\partial w}{\partial y}$ ,  $\frac{\partial u}{\partial y}$ , and  $\frac{\partial v}{\partial y}$ . The x-axis is taken along the length, the y-axis along the circular edge and the z-axis is normal to the shell surface.  $u$ ,  $v$  and  $w$  are the displacements along the x,y and z directions, respectively.

## 2.7 Effects of Root Flexibility

Although in most of the theoretical investigations, the blade is assumed to be completely fixed at the root, in actual practice, however, the blade is rather loosely mounted on the rotor disc. The vibrations of the blade, therefore, continue to some extent into the mounting. This has an effect similar to that of increased blade length and results in a lower frequency than the one calculated on the fixed end assumption. The root flexibility, generally, makes the root a nondeflecting end, but not a nonrotating end. As a result, the slope at the root is not zero but is proportional to the moment acting at the root. The root flexibility varies with the speed of rotation, since the centrifugal forces tend to tighten the blade in the disc and increase the fixidity. Moreover, various types of root fixings are used in practice and, therefore, a general analytical treatment of this effect is rather difficult. Some investigations of this and the other related problems have, however, been carried out and are discussed here.

The case of flexural vibrations of a partially restrained beam of uniform cross-section is considered by Newmark and Veletos (86). They have assumed that both the ends are nondeflecting but offer resistance to rotation, such that the slope at the ends is proportional to the bending

moment. The constant of proportionality is considered different for each support. From the numerical computations they have suggested an empirical formula for calculating the natural frequencies for any given end stiffnesses. A similar problem of both ends partially restrained has also been considered by Amba Rao (87), when the beam carries masses.

The effect of root flexibility on the vibrations of a cantilever beam of uniform cross-section has been considered by Perkins (88). The energy approach is used with the eigenfunctions of a cantilever beam. The resulting solution is quite complicated involving sums and series of infinite products.

Traupel (89) has suggested an empirical method of taking into account the effect of root flexibility on the fundamental natural frequency in bending. He has proposed the relation

$$\omega_a = C_v \omega \quad (2.16)$$

where  $\omega$  is the frequency calculated on the fixed end assumption and  $\omega_a$  is the actual frequency. He has plotted the value of  $C_v$  against the ratio ( $\lambda$ ) of the blade length to the radius of gyration of the root section, which is considered as a measure for the flexibility of the root. Baur (90) has suggested that the value of  $C_v$  given by Traupel, may also be used for the second flexural mode. The variation of  $C_v$



with  $\lambda$  is as given in Figure (4). For torsional vibrations, Baur has proposed a similar relation, but has pointed out that the variation of the correction factor be plotted against the nondimensional blade flexibility  $I_p/C$ , where  $I_p$  and  $C$  are the polar moment of inertia and the torsional stiffness at the root, respectively. Some additional information on the effect of root flexibility has also been given by Chaplin (91).

Vibrations of turbine blades with loose hinge roots, in a centrifugal force field, are considered by Niordson (92). After establishing the equations of motion, the solution for the fundamental mode is obtained by a modified Stodola method. Oscillations have been shown to be a superposition of the pendulum and the bending modes. Several limiting sub-cases have been evaluated and the variation of the fundamental frequency with the rotational speed is investigated.

The problem of pin-fixed blades is considered in more detail by Goatham and Snails (93). The blade is considered mounted on the disc through a loosely fitting pin, with a clearance ( $q$ ). The pin tightens when the blade rotates, due to the centrifugal forces on the blade. The deflection at the tip is composed of two parts: due to bending of the blade and due to rolling occurring at the root. An expression is derived for the ratio of these two deflections and is shown to be directly proportional to the square of the rotational speed

and inversely proportional to the clearance ( $q$ ). Another expression for the moment necessary to cause unit rolling at the root is also derived in the paper. The natural frequencies of the pin-fixed blade are obtained by idealizing it as a system of lumped masses connected by elastic springs. The centrifugal forces are replaced by equivalent transverse forces, giving the same bending moment distribution. It is pointed out that for the torsional frequency calculations, especially for low aspect ratio blades, the torsional flexibility of a portion of a blade, of length equal to one-fifth of the root chord and having root cross-section, be deducted from the total torsional flexibility.

### 2.8 Effects of Disc Elasticity

If the disc on which the blades are mounted is considered absolutely rigid, the blade can be treated as a separate unit for vibration analysis, as has been done in all the references discussed so far. However, the disc has some elasticity, and hence the blades and the disc ought to be considered as an assembly. Energy from a blade can be transferred to the adjacent blades through the disc, which modifies the vibration characteristics of the blades. The existence of the rotor coupling is demonstrated by tests in which a vibration exciter is attached to a blade on a rotor, at standstill. Large vibratory amplitudes are observed on

blades far from the exciter and connected to it only through the rotor. The response of each blade depends not only on its own natural frequency, damping and excitation, but also on the characteristics of the other blades and the rotor.

Ellington and McCallion (94) have investigated the effect of elastic coupling through the rim of the disc, on the frequencies of vibration of the blades, by analysing a simplified model. In this model, the blades are replaced by uniform beams fixed to the rim at their roots and vibrating in a plane parallel to the plane of the disc. This means that the effect of twist, taper and obliquity is neglected. The rim is considered as a uniform elastic ring, permitting no radial displacement at the roots of the blades. The mass of the rim is either neglected or considered as being concentrated at the roots of the blades. For the analysis, three adjacent blades ( $n + 1$ ,  $n$  and  $n - 1$ ) are assumed to be parallel to each other and the portion of the rim joining them is taken as a straight continuous beam, as shown in Figure (5). The method of analysis used can be summarized as follows:

The differential equation for the cantilever blade ( $n$ ) is first solved with the boundary conditions of zero shear and moment at the free end with zero deflection and a bending moment  $M_n$  at the root. An expression for the slope ( $\theta_n$ ) at the root is thus obtained. The portion of rim between the three adjacent blades is next treated as a continuous



beam with zero deflections at the roots of the blades and acted upon by the bending couples  $M_{n-1}$ ,  $M_n$  and  $M_{n+1}$  at these points. A relation between the slopes  $\theta_{n-1}$ ,  $\theta_n$  and  $\theta_{n+1}$  is thus established for each of the successive blades. Noting that the  $(N + 1)^{\text{th}}$  blade is in fact the same as the blade numbered zero (as shown in Figure 5), and imposing periodic solution for the slopes at the roots, the natural frequencies are obtained.

The analysis has shown that if there are  $N$  identical blades mounted on an elastic rim, the system has  $N$  fundamental frequencies,  $N$  first overtones etc. However, if the stiffness of the rim is large compared to that of the blade, as is generally the case, these  $N$  frequencies are very near to the corresponding frequency of the individual blade. Thus instead of sharp natural frequencies, there are bands of frequencies - width of the band decreasing with the increasing stiffness of the disc. This explains the scatter in the natural frequencies usually observed in vibration tests. The coupling effects due to the blade ring, for the cases when either all blades have identical frequencies or alternate blades have identical frequencies, have been investigated by Söhngen (95).

Fillipov (96) has considered the problem of the tangential vibrations of the blades together with the torsional vibrations of the disc, when all the blades vibrate in phase. The effect of the rim is allowed for, by introducing masses

and moments at the blade roots. Satisfying the coupling conditions, a transcendental equation for finding the frequencies is derived. The effect of the centrifugal force is accounted for by introducing a longitudinal force at the end of each blade.

A simplified model for a row of blades mounted on a flexible disc is suggested by Wagner (97) and is illustrated in Figure (6). Each blade is represented by a single degree of freedom system which has the same natural frequency and damping factor as that of a particular mode of the blade. Each subsystem is attached to a common ring support, representing the disc periphery. This ring is assumed to have flexibility and is attached elastically to a fixed foundation representing the centre of the disc, where there is assumed to be no vibratory deflection. The equations of motion of each subsystem are derived. All the subsystems would contribute to the deflection of the flexible support at the point of attachment of any subsystem; hence the influence factors for the flexible ring are necessary. These factors have been derived in the paper using the analysis of curved beams on elastic foundations. It has been concluded from this analysis that multiple resonance peaks and a large variation in the peak vibratory stresses, can be produced by the differences in the natural frequencies among the blades and the coupling resulting from the flexibility of the disc.



Coupling is also shown to average out the damping present in different blades of the same row.

Consideration of the methods, to account for the coupling effects due to disc elasticity, indicates that in this type of analysis the blades have either been considered as single degree of freedom systems (97), or as untwisted, untapered, parallel beams (94). Also, all the possible modes of vibration of the disc are not included. Obviously, this type of analysis can, at most, be expected to give a qualitative nature of the behaviour and a considerable amount of further investigation is needed in this area.

## 2.9 Effects of Shrouding

Turbomachinery blades are often joined together, either at their tips or at some intermediate location, to reduce the resonant amplitude. A single shroud ring may join all the blades in a row or else a packet of blades may be joined together. The shrouding significantly alters the natural frequencies and the mode shapes and hence the packet of shrouded blades should be analysed as a unit for the tangential, axial or torsional vibrations. The shroud also causes a coupling between the axial flexural vibrations and the torsional vibrations.

The effect of shrouding on the tangential vibrations (vibrations in the plane of the disc) of a packet of blades is



investigated by Smith (98) using several simplifying assumptions. The  $n$  blades forming a packet are assumed to be of uniform cross-section and parallel to each other. The blades are considered fixed at the roots. The shrouding is also considered to be of uniform section and attached rigidly to each blade at its tip, maintaining a constant pitch between the successive tips during small flexural vibrations. The mass of the shroud is taken to be concentrated at the blade tips. Both the blades and the shroud have elasticity but are assumed to be inextensible. The blades are considered nonrotating.

The reactive forces at the junction of the blade tip and the shroud are taken to be a bending moment and a force transverse to the blade length. Bending of one pitch of the shroud is first considered. Since the shroud mass is concentrated at the tips, the force-deflection relationships at the ends of the shrouding pitch, during vibration, are the same as for static deflections. From this analysis the relations between the moments and the slopes at the blade tips are derived. The condition of constant pitch at the blade tips, makes the sum of the transverse reactive forces equal to the inertia force due to total shroud mass. The bending vibrations of the blades are then considered and noting that the moments and the slopes at the tips are identi-

cal for both the blade and the shroud, the frequency equation is derived. The analysis has shown that for a packet of  $n$  blades, the modes of vibration fall into groups as follows:

- (a) One fundamental mode with the blades of the packet in phase;
- (b) A band of  $(n - 1)$  modes with the blades not in phase. The frequencies of these modes are very near to each other;
- (c) One overtone with the blades in phase, etc.

The variation of the natural frequencies of a packet of six blades with the rigidity of shroud are shown in Figure (7), for different values of  $r_m$  - the ratio of the shroud and the blade mass. The natural frequencies of the packet are expressed as a frequency ratio by dividing them with the fundamental frequency of a single blade; whereas the rigidity of one pitch of the shroud is expressed as rigidity ratio by dividing it with the rigidity of one blade.

A method of analysing the tangential, the axial and the torsional vibrations of a banded group of blades is given by Prohl (99). In this analysis the blades are considered fixed at their roots and firmly attached to the shroud at the tips. The blades are assumed to be parallel to each other and may be tapered. The shear and the rotary inertia are disregarded and the shear centre and the centroid of the



cross-section are assumed coincident. The axial and the torsional vibrations are coupled through the shroud, whereas the tangential vibrations remain uncoupled. The blades are assumed inextensible but extension of shroud during tangential vibrations is taken into account. The mass and the torsional inertia about the blade axis, of one pitch of the band, is concentrated at the blade tip. The distributed mass and torsional inertia of each blade is concentrated at several discrete stations along its length. A modified Holzer-Myklestad type analysis is used for the frequency determination.

A method of finding the natural frequencies of a group of shrouded blades, using the perturbation procedure is given by Tuncel et al. (100). The method is applicable for weakly coupled blade and shroud subsystems. The subsystems are dealt with individually in the first step followed by a second step accounting for the weak coupling. Fugino (101) has considered the effect of shrouding by taking the vibration form of the blades as a linear combination of fixed-free, fixed-supported and fixed-fixed modes for the tangential vibrations. A similar conclusion of  $(n - 1)$  modes of nearly the same frequency, which coincide when the stiffness of the shroud is negligibly small, is arrived at.

The problem of two adjacent blades, connected at their tips by a shroud to form a continuous frame, has been analysed by Singh and Nandeeswaraiya (102). The blades are assumed to



be parallel to each other and have no pretwist or taper. The equations of motion have been derived both for the tangential and the axial vibrations and the fundamental frequency is obtained. For rotating blades, a Southwell type correction factor is also derived.

An investigation of the vibrations of a coupled disc-blade-shroud assembly is considered by Stargardter (103), by experiments on flexible silicon rubber models. It is observed that the disc vibrates as a plate, mainly with nodal diameters, and the shroud acts as a ring. If the shroud is absent and the disc vibrates with two nodal diameters, the blades are constrained to retain their orientation relative to the disc, at the rim. The blades at the nodes are displaced in pure twist while those at the antinodes are displaced in pure translation. The other blades undergo a combined pitching-translatory motion. It has been observed that, in general, the pattern rotates relative to the rotor, subjecting all the blades to bending and twisting. The shroud forces the tangential deflection of the blade to zero at the point of attachment. The axial deformation curve, however, is not significantly altered. The observations from the study of different sizes and the locations of the shroud, on tapered and straight bladed rotors, are reported in the paper. The case when the shroud joins only two adjacent blades is also presented. The results are of qualitative nature and provide an insight into the vibration of the complex system.

## 2.10 Damping

The principal sources of dissipation of energy from the blades are:

- (a) Friction at the blade root and the hub;
- (b) Internal damping due to inelasticity of the material; and
- (c) Damping due to the presence of surrounding gas (Aerodynamic Damping).

In addition, sometimes, special internal friction dampers are also included to dissipate energy.

The dissipation of energy at the root is due to the relative motion between the blade and the rotor in the mechanical attachments. At lower rotor speeds this energy dissipation may be appreciable; however, at very high rotor speeds the centrifugal force essentially tightens the blade sufficiently to eliminate the dissipation. Some analysis of this type of damping has been reported in References (104-106). Goodman and Klump (105) have pointed out that when two machine parts, such as a blade root and a hub, are joined in press fit, the energy is dissipated by the microscopic slip at the interfaces. By considering the press-fit structure in a state of plane stress, they have suggested a method of evaluating the energy dissipated per cycle, in a simplified model with uniform pressure at the joint. Existence



of an optimum contact pressure to get maximum slip damping is indicated, and the possibility of corrosion fretting accompanying slip damping is pointed out. An experimental determination of the damping at the locking joints, when the turbine blades are vibrating, has been carried out by Kozolov (106). In these experiments an impulse excitation of the blade of a rotating turbine is affected by firing a rifle. From experimental vibrograms the logarithmic decrement at various amplitudes of stress, centrifugal force levels and temperatures is obtained. By investigating the different types of locking joints, the important parameters affecting damping have been determined.

Although these investigations offer some understanding of the phenomenon of root damping, it is very much dependent on the type of root, manufacturing tolerances, speed of rotation etc. Hence, it is difficult to account for it in the analytical calculations.

The internal material damping is caused by inelasticity of the material. The stress-strain curve for loading and unloading are not generally identical but form a hysteresis loop. The area bounded by the loop is a measure of the energy dissipated in each cycle. A brief resume of the damping capacity of the materials is given by Lazan (107). He has pointed out that at engineering stress levels, static hysteresis can be caused either by magnetoelastic effects or by plastic strain. He has further suggested that these



effects are a function only of the hysteresis loop and not of the strain rate. The damping capacity of thin vibrating beams from this source should, therefore, be a function of maximum stress (or vibration amplitude) but not of frequency. He has also indicated that, for a given material, damping capacity is proportional to  $\sigma^p$ , where  $\sigma$  is the maximum stress during a cycle and the exponent  $p$  lies between 2 and 3. Some investigation of the effect of internal damping in rotating beams has been carried out by Morduchow (108).

An extensive study of the flexural and torsional vibrations of beams, with special reference to turbine blades, taking into account the internal damping, has been carried out by Pisarenko (109). The stress-strain relation utilized, characterizes the departure from the Hooke's Law and is different for loading and unloading. The basic relationships used are

$$\begin{aligned}\bar{\sigma} &= E \left[ \xi - \frac{\nu}{n} (\xi_0 + \xi)^n - 2^{n-1} \xi_0^n \right] \\ \bar{\sigma}^* &= E \left[ \xi + \frac{\nu}{n} (\xi_0 - \xi)^n - 2^{n-1} \xi_0^n \right]\end{aligned}\tag{2.17}$$

where  $E$  is the average modulus of elasticity for extension,  $\xi_0$  the amplitude of strain and  $\xi$  the strain at any instant.  $\bar{\sigma}$  and  $\bar{\sigma}^*$  are the corresponding stresses while loading and unloading, respectively.  $\nu$  and  $n$  are the geometric parameters of the hysteresis loop of the material and must be evaluated experimentally.

With these stress-strain relations, the differential equation for the bending of beams takes the form

$$EI \frac{\partial^2 w}{\partial x^2} + \epsilon \Phi \left( \frac{\partial^2 w}{\partial x^2} \right) = M \quad (2.18)$$

The second term in the equation is the contribution to the bending moment due to the departure from the elastic behaviour. The presence of the small parameter  $\epsilon$  indicates that the deviation from the elastic moment is small. The function  $\Phi$  for loading and unloading can be obtained from the assumed stress-strain relations.

The resulting nonlinear problem is solved using the theory of asymptotic expansion in nonlinear mechanics. This consists of assuming the frequency in the form

$$\omega^2 = \omega_c^2 + \epsilon \Delta_1 + \epsilon^2 \Delta_2 \quad (2.19)$$

where  $\omega_c$  is the frequency when the hysteresis effects are neglected and the subsequent terms give the deviations of the first and second order. The method of evaluating the first and the second approximations are illustrated and applied to several important problems of transverse vibrations of cantilever beams and the torsional vibrations of rods. The centrifugal effects and the beam taper are also included.

Baker et al. (110) have considered the vibrations of cantilever beams in surrounding air. The damping arising from the air drag as well as from the internal material hysteresis

have been taken into account. The equation of transverse vibrations is shown to take the form

$$EI \frac{\partial^4 w}{\partial x^4} + E_1 I \frac{\partial^5 w}{\partial t \partial x^4} + C_1 \rho A \frac{\partial^3 w}{\partial t^3} + \rho A \frac{\partial^2 w}{\partial t^2} + \frac{C_2}{L} \frac{\partial w}{\partial t} = 0 \quad (2.20)$$

where  $E_1$  and  $C_1$  are the viscoelastic material constants representing the hysteresis effects and  $C_2$  is the parameter of the drag forces due to the air damping. The expressions for these coefficients have been given in the paper. A method of solution has been suggested by a variable separation technique offering an implicit expression for the special case of  $C_1 = 0$ . Approximate solutions by energy techniques are indicated to obtain the logarithmic decrement.

The aerodynamic damping is caused by the fact that the velocity acquired by a vibrating blade changes the incidence of the air stream. If the cascade characteristics are such that an increase of incidence causes an increase in the lift force on the blade, damping takes place. However, if an increase of incidence causes a decrease in the lift, it results in flutter. Pearson (111) has pointed out that in the unstalled region, the damping present is almost wholly aerodynamic, even when the excitation itself is aerodynamic, e.g. from wakes, etc. He has derived an expression for the energy removed ( $e$ ) by the air stream from a vibrating blade per unit length in unit time. For compressor blades this



expression is approximately equal to

$$e = \pi^2 f^2 \rho_1 V c a^2 \frac{\partial C_F}{\partial \alpha} \quad (2.21)$$

where  $a$  and  $f$  are the amplitude and the frequency of vibration,  $c$  the blade chord,  $V$  the air velocity with respect to the blade at the inlet to the blade,  $C_F$  the blade lift coefficient at right angles to the chordline,  $\alpha$  the air angle measured from the axial direction and  $\rho_1$  the air density. In the derivation it is assumed that the blade is vibrating in a flexural mode and that the blade behaviour is independent of the frequency i.e. the blade will give a certain lift at a certain incidence, irrespective of the frequency of vibration. It is pointed out that at low values of frequency parameter  $\lambda_f = 2\pi fc/V$ , this is quite true, but for higher values ( $\lambda_f > 1$ ), substantial corrections may be expected.

The idea of the magnitude of aerodynamic damping is given by pointing out that for a blade of 2" chord, vibrating at 400 cycles/sec with an amplitude of 0.1 inch, in an air velocity of 600 ft/sec, the energy removed by the air stream is 12 ft-lb per inch of blade length per second.

### 2.11 Aerodynamic Excitations and Design Considerations

The discussion so far is confined to the methods for the calculation of natural frequencies and mode shapes. From strength considerations the knowledge of the amplitude of vibration is also essential. To be able to calculate the

amplitude of vibration, it is necessary to know the nature of the excitation forces and the amount of damping. The various sources of damping and their nature and magnitude have already been discussed in the previous section. In this section the aerodynamic exciting forces, the methods of calculating deflection amplitudes, stress levels, etc. are considered.

Due to the lack of adequate knowledge about the aerodynamics of compressors, especially the axial flow machine, the published work regarding the analytical treatment of this field is somewhat limited. Most of the uncertainties are handled empirically. The practical aspects of design and vibration analysis have been reviewed in several papers. The more important of these reviews are those by Shanon (112), Carter and Kilpatrick (113), Blackwell (114), Armstrong and Stevenson (115,116), Lewis Centre Staff (117), etc. These references describe, what may be called, the current state of art in this area, and a few important points dealt with in these reviews are considered briefly here.

#### 2.11.1 Wake Excitation

In the air flow annulus of the compressor, there are, generally, a number of fixed vanes which carry services to the rotor or support the bearings. The air flow over these vanes creates wakes of low air velocity, compared to the remainder

of the annulus. As the rotor blade passes through these zones, the aerodynamic force on the blade is reduced, the frequency of the pulses being equal to the number of reductions in the air velocity times the speed of rotation. If this frequency, or its harmonic, is equal to one of the natural frequencies of the rotor blade, a fairly large amplitude can be built up. A similar effect occurs in the case of the obstructions in the exit annulus of the compressor. In this case, the nose of the vane gives rise to an increase in the local static pressure which is propagated upstream and causes a variation of the force on the blade in a way similar to the downstream wake of a vane.

Pearson (111) has shown that if the wake is regarded as a sinusoidal variation of incidence ( $\alpha_\omega$ ) on the blade, then at resonance, the energy (e) imparted to the blade per unit length and unit time is given approximately by

$$e = \pi f \alpha_\omega \left( \frac{1}{2} \rho_1 V^2 \right) c a \frac{\partial C_F}{\partial \alpha} \quad (2.22)$$

where the notation is the same as explained in the previous section. The amplitude of vibration due to the wake excitation can be assessed by equating the aerodynamic excitation and the aerodynamic damping, other damping being negligible. The amplitude of vibration obtained from this consideration is shown to be

$$a = \frac{\alpha_\omega V}{2\pi f} \quad (2.23)$$



It is interesting to note that the value of the amplitude times the frequency ( $af$ ) does not depend on the material of the blade or the air density. This, in addition to other considerations discussed later, has made it an important design factor. Another point mentioned by Pearson (111) is that the wakes die out rapidly in a compressor and should not affect the blades after, at most, two stages from start of the wake.

### 2.11.2 Flutter

The mechanism of this type of vibration is one of self excitation and is due to the shape of the aerodynamic lift-incidence characteristic. If the variation of the aerodynamic force with a change in the incidence is such that the force increases for a reduction of incidence, then the vibration builds up. Suitable conditions for self excitation are in the region of blade stall or in the zone of incidence and Mach number where the cascade becomes choked. The typical lift curve of a compressor blade in cascade at a constant Mach number is shown in Figure (8). As mentioned earlier, the energy dissipated by a vibrating blade to the air stream is proportional to  $\frac{\partial C_F}{\partial \alpha}$ . If  $\frac{\partial C_F}{\partial \alpha}$  is negative, instead of aerodynamic damping taking place, the blade would receive energy from the air stream resulting in flutter.

As can be observed from Figure (8), this occurs near the stalling incidence. By assuming  $AC = CB = \alpha_v$  the amplitude of the bending vibration is given by

$$a = \frac{\alpha_v V}{2\pi f} \quad (2.24)$$

Pearson's analysis has been extended by Carter and Kilpatrick (113) by including the mechanical damping.

Armstrong and Stevenson (115) have pointed out that the vibration, which has been identified as flutter, has so far occurred either in the fundamental flexure or the fundamental torsion mode. The peak amplitudes of different blades usually occur at the same speed. Often there is a large scatter, greater than 4:1, in the amplitudes of the blades on the same disc. Fundamentally, the most important parameter, in determining whether a blade is likely to flutter, is its operating incidence. Therefore, the amplitude of vibration is highly responsive to the inlet guide vane (I.G.V.) setting. In making a compressor flutter-free by the I.G.V. setting, some loss of performance is inevitable. It is pointed out that a change in the rotor tip stagger also controls the vibration with less performance penalties. Figure (9) illustrates the effect of the I.G.V. setting and the tip twisting.



### 2.11.3 Rotating Stall Cell Excitation

During research testing of an experimental compressor, Armstrong and Stevenson (115) have observed the breaking of the air flow into a series of stalled and unstalled patches, at conditions below the stall conditions. They have further observed that the stalled zones rotated in the same direction as the rotor but at approximately half the speed.

Because the stalled zones consist of low velocity air, the aerodynamic force on the rotor blade is reduced, giving rise to a pulsating force, as the cells pass the rotor blade. This can result in the build up of large resonant vibrations. The factors which determine the presence of the cells and their speed of rotation are not isolated and hence the prediction of this type of excitation is difficult. The characteristics of a rotating stall fall into two broad categories - unsteady and steady stall patterns. A method of identifying the unsteady pattern by hot wire anemometers etc. is given in the paper (115). The amplitude of this type of vibration is dependent on the blade material - steel blades giving less amplitude than aluminum blades; the probable reason given is the increased mechanical damping and Young's Modulus. At a more positive I.G.V. setting, the speed at which the stall cells are eliminated is reduced significantly.



#### 2.11.4 Random Excitations

Sometimes moderately large fluctuating amplitudes are obtained which are not caused by any of the above mentioned excitations. It has been suggested (115) that they are due to random disturbances. The mechanical details of the root fixing and the material of the blades affect these amplitudes considerably.

#### 2.11.5 Design Considerations

The principal cause of failure of compressor blades and the lower temperature stages of turbines is fatigue. Armstrong and Stevenson (115) have pointed out that 90 percent of these failures can be attributed to the first or the second flapwise bending modes, the first torsional mode or the first chordwise mode. Therefore, the first step for designing the blades against vibration failure, is to calculate accurately the natural frequencies of the first four or five modes of vibrations, at various speeds of rotation.

Possible resonances at engine order excitations can be predicted from the Campbell diagram for each row. In this diagram the engine-order lines are superimposed upon a plot of the blade natural frequencies versus the engine speed, as indicated in Figure (10). All points of intersection on this diagram represent possible resonances, if the appropriate engine order excitations are present. The principal causes

of the integral engine order excitations are the wakes from instream obstructions, blow-off or gas-bleed ports, inlet flow nonuniformities potential-flow disturbances propagated upstream from obstructions, etc. It is pointed out in Reference (118), that  $n$  symmetrically arranged disturbances within the flow cause  $n, 2n, 3n \dots$  engine order vibrations. If the same disturbances are arranged asymmetrically, then all engine order excitations may be present. The amplitude of vibrations for well defined disturbances, such as from the fixed obstructions, can be estimated by Fourier analysis of the wakes, by calculating the component of the fluctuation having a frequency equal to the resonant frequency under consideration.

The severity of vibrations is generally specified in terms of the amplitude times frequency ( $af$ ). In the case of a uniform cantilever, vibrating in one of its normal flexural modes, it can be shown that the maximum stress at the root sections is given by

$$\sigma_{\max} = 2\pi \frac{Y}{K_r} \sqrt{E\rho} (af) \quad (2.25)$$

where  $E$  and  $\rho$  are the Young's modulus and the density of the material respectively,  $y$  is the distance from the neutral axis to the point of maximum stress and  $K_r$  is the radius of gyration of the root section. If the section is rectangular,  $y/K_r$  is independent of the shape of the rectangle. However, if the



section is a typical aerofoil,  $y/K_r$  is constant to an accuracy of  $\pm 15$  percent, as pointed out by Blackwell (114). From design considerations the amplitudes of vibration are generally considered serious when  $(af)$  exceeds 2.0 ft/sec, in case of aluminum or steel blading.

The important factor for checking against flutter is the frequency parameter given by  $\omega c/V$ , where  $\omega$  is circular frequency,  $c$  the blade chord and  $V$  the velocity of the gas relative to the blade at its tip. The blades are considered flutter-free if this frequency parameter is greater than 1.6 for the fundamental torsion, and greater than 0.3 for the fundamental bending, as suggested by Armstrong (116). Smith (119) has pointed out that these limits are somewhat on the conservative side, and has suggested that if they are too restrictive a more precise limit on the frequency parameter, for unstalled flutter, may be obtained from Reference (120).

Apart from the form failures of blades, the root fixing failures are also quite common. At present, the design of satisfactory fixings is based mainly on empirical rules which have been devised as a result of experience. Armstrong (116) has pointed out that, in a number of instances, the volume of metal in a fir-tree root required to withstand the alternating stresses, is three times that needed for the steady centrifugal stresses. A method of optimising the root web thickness, for the fundamental flexure mode, has been



suggested by Bury (121). Two basic equations for the blade are obtained. The first equation represents the energy exchange between the aerodynamic excitation and the aerodynamic, mechanical and material damping. The second equation gives the total stress at the root of the section. The basic model consisting of these two equations is related to the fatigue characteristics of the blade material by a modified Goodman diagram to find the optimum root web thickness.

## CHAPTER 3

### THEORY FOR NONROTATING LOW ASPECT RATIO BLADES

In a low aspect ratio blade the length and the chord are of the same order of magnitude and the thickness is considerably smaller than both of them. The blade can, therefore, be treated as variable thickness shell. For a structure of complicated geometry, such as a blade, the exact analysis based on classical shell theory would be too difficult. The finite element technique offers a powerful method for such an analysis.

The basic ideas for the application of this technique for the bending analysis of a shell, by treating it as an assembly of small flat elements are outlined in the text by Zienkiewicz and Cheung (122). They have also used the method for the analysis of arch dams, using rectangular elements (123). Most of the shells, which are not surfaces of revolution, cannot be subdivided into rectangular elements and, therefore, for such structures triangular elements must be used. The bending analysis of thin shells, using flat triangular elements, has recently been carried out by Clough and Johnson (124). As yet, the finite element technique has not been used sufficiently for the vibration analysis of shells and hence the extent of accuracy that can

be achieved and the size of subdivision necessary for convergence are not well known.

As pointed out by Zienkiewicz and Cheung (122), the progress in the application of the method to shell problems has been slow, mainly due to the lack of a good bending stiffness matrix for a triangular element. From practical considerations, a good stiffness matrix is not necessarily the one which exhibits a monotonic convergence. A more important criterion is that the deviation from the exact result should be small, even when the structure is subdivided rather coarsely. This is especially important for shell problems where both the bending and the in-plane degrees of freedom are assigned to each node and, therefore, the memory of the computer does not permit the use of as fine a mesh as can be used in the plate problems. In the present analysis a new bending stiffness matrix for triangular element is developed and used.

The middle surface of the blade is subdivided into triangular elements, such as  $ijk$ , as shown in Figure (11a). Each of these elements is assumed to be flat. As the number of elements becomes large, the surface built up of small, flat elements should adequately represent the behaviour of the actual continuously curved surface.

$x, y, z$  is the system of global coordinate axes;  
 $(x_i, y_i, z_i)$ ,  $(x_j, y_j, z_j)$  and  $(x_k, y_k, z_k)$  are the coordinates



of the vertices  $i$ ,  $j$  and  $k$ , respectively.  $x'$ ,  $y'$ ,  $z'$  is the local coordinate axes system for the element; such that the triangle  $ijk$  lies in the  $x'y'$  plane. The origin is chosen at the vertex  $i$  and  $y'$ -axis along the line  $ij$ , as shown in Figure (11b). Hence, the local coordinates of the nodes  $i$ ,  $j$  and  $k$  are  $(0,0,0)$ ,  $(0,y'_j,0)$  and  $(x'_k,y'_k,0)$ . The direction of  $x'$  axis is so chosen that  $x'_k$  is always positive. Both  $x,y,z$  and  $x',y',z'$  are right handed coordinate systems. It can be shown that,

$$\begin{aligned} y'_j &= \sqrt{a_1} \\ y'_k &= (a_3 + a_1 - a_2)/2 \sqrt{a_1} \end{aligned} \quad (3.1)$$

and

$$x'_k = \sqrt{a_3 - y'^2_k}$$

where  $a_1$ ,  $a_2$ ,  $a_3$  are the squares of the lengths of sides  $ij$ ,  $jk$  and  $ki$ , respectively.

### 3.1 Bending Stiffness Matrix for an Element

The derivation of bending stiffness matrix for a triangular plate element, using the displacement method, necessitates an assumed expression for deflection  $w'$  normal to the plane of the element. Various conforming and nonconforming expressions have been in use (125-133) and are constantly being added to. The nonconforming functions, although ensuring continuity of deflection along the common edges

between the adjacent elements, do not satisfy the transverse slope continuity. The conforming functions satisfy the slope continuity as well. The rate of convergence depends on the assumed deflection expression.

For plate problems, probably the fifth degree polynomial expression for deflection, recently introduced by Cowper et al. (133) shows the best convergence. However, this shape function requires six degrees of bending freedom (deflection, 2 first derivatives and 3 second derivatives) at each node. When the triangular element is considered as a part of a shell, it is necessary to assign in-plane degrees of freedom to each node, in addition to the bending degrees of freedom. Hence, using the bending stiffness matrix of Reference (133) for shell problems would involve a total of, at least, 9 degrees of freedom at each node. Obviously, in that case a much coarser mesh can only be used, giving a poorer physical representation of the shell. When the bending stiffness matrix of a triangular element is derived for subsequent use in the solution of shell problems, it is, therefore, preferable to assign only three degrees of bending freedom ( $w'$ ,  $\theta'_x$  and  $\theta'_y$ ) to each node.  $\theta'_x$  and  $\theta'_y$  are the rotations about  $x'$  and  $y'$  axis, respectively. A cubic polynomial expression for  $w'$  may, therefore, be used.

The complete cubic polynomial in  $x'$  and  $y'$  involves



ten arbitrary coefficients and since only nine degrees of bending freedom are assigned to each element (three to each node), certain assumptions must be made regarding one of the coefficients. Adini (125) has assumed the coefficient of term  $x'y'$  to be zero and Tocher (126) has suggested that the terms  $x'^2y'$  and  $x'y'^2$  be assigned the same coefficient. However, a better way would be to choose the extra coefficient in such a way as to satisfy the transverse slope continuity along one of the sides of the element and hence make the expression 'partially conforming'. This is achieved by satisfying two conditions; (i) choosing the local coordinate axes for the element in such a way that the equation of the line, along which the transverse slope continuity is to be satisfied, becomes  $x' = 0$  and (ii) making the coefficient of the term  $x'y'^2$  to be zero. Hence, the assumed expression for deflection within the element is taken as

$$w' = \alpha_1 + \alpha_2x' + \alpha_3y' + \alpha_4x'^2 + \alpha_5x'y' + \alpha_6y'^2 + \alpha_7x'^3 + \alpha_8x'^2y' + \alpha_9y'^3 \quad (3.2)$$

This gives for the transverse slope  $\partial w'/\partial x'$  along the line  $x' = 0$ , the expression  $\alpha_2 + \alpha_5y'$ . Since the value of the slope is specified at the two ends of this line, the expression for transverse slope is unique along the line  $x' = 0$ . Equation



(3.2) can be expressed in the matrix form as

$$w' = [C]\{\alpha\} \quad (3.3)$$

where

$$[C] = [1, x', y', x'^2, x'y', y'^2, x'^3, x'^2y', y'^3] \quad (3.4)$$

and  $\{\alpha\}$  is the column vector of coefficients  $\alpha_1$  to  $\alpha_9$ .

The nine bending displacements of the nodes and the corresponding nodal forces, expressed as vectors, are

$$\{\delta'_b\} = [w'_i, \theta'_{xi}, \theta'_{yi}, w'_j, \theta'_{xj}, \theta'_{yj}, w'_k, \theta'_{xk}, \theta'_{yk}]^T \quad (3.5)$$

$$\{F'_b\} = [F'_{zi}, M'_{xi}, M'_{yi}, F'_{zj}, M'_{xj}, M'_{yj}, F'_{zk}, M'_{xk}, M'_{yk}]^T$$

Substituting for  $w'$  from equation (3.2) and noting that

$$\theta'_{x'} = \partial w' / \partial y' \quad (3.6)$$

$$\theta'_{y'} = -\partial w' / \partial x'$$

the first of equation (3.5) can be written as

$$\{\delta'_b\} = [A]\{\alpha\} \quad (3.7)$$

where

$$[A] = \begin{bmatrix} 1 & 0 & 0 & 0 & 0 & 0 & 0 & 0 & 0 \\ 0 & 0 & 1 & 0 & 0 & 0 & 0 & 0 & 0 \\ 0 & -1 & 0 & 0 & 0 & 0 & 0 & 0 & 0 \\ 1 & 0 & y'_j & 0 & 0 & y'^2_j & 0 & 0 & y'^3_j \\ 0 & 0 & 1 & 0 & 0 & 2y'_j & 0 & 0 & 3y'^2_j \\ 0 & -1 & 0 & 0 & -y'_j & 0 & 0 & 0 & 0 \\ 1 & x'_k & y'_k & x'^2_k & x'_k y'_k & y'^2_k & x'^3_k & x'^2_k y'_k & y'^3_k \\ 0 & 0 & 1 & 0 & x'_k & 2y'_k & 0 & x'^2_k & 3y'^2_k \\ 0 & -1 & 0 & -2x'_k & -y'_k & 0 & -3x'^2_k & -2x'_k y'_k & 0 \end{bmatrix} \quad (3.8)$$

Elimination of  $\{\alpha\}$  from equations (3.3) and (3.7) gives

$$w' = [C][A^{-1}]\{\delta'_b\} \quad (3.9)$$

The curvatures can be written as

$$\{R\} = \begin{Bmatrix} \partial^2 w' / \partial x'^2 \\ \partial^2 w' / \partial y'^2 \\ 2\partial^2 w' / \partial x' \partial y' \end{Bmatrix} = [C_1][A^{-1}]\{\delta'_b\} \quad (3.10)$$

where

$$[C_1] = \begin{bmatrix} 0 & 0 & 0 & 2 & 0 & 0 & 6x' & 2y' & 0 \\ 0 & 0 & 0 & 0 & 0 & 2 & 0 & 0 & 6y' \\ 0 & 0 & 0 & 0 & 2 & 0 & 0 & 4x' & 0 \end{bmatrix} \quad (3.11)$$

Assuming the material to be isotropic of Young's Modulus  $E$  and Poisson's ratio  $\mu$ , the bending strain energy of the element can be expressed as

$$U = \frac{E}{24(1-\mu^2)} \iint t^3 \{R\}^T [D] \{R\} dx' dy' \quad (3.12)$$

where

$$[D] = \begin{bmatrix} 1 & \mu & 0 \\ \mu & 1 & 0 \\ 0 & 0 & \frac{1-\mu}{2} \end{bmatrix} \quad (3.13)$$

and  $t$  is the thickness of the element at point  $(x', y')$ .

The integral extends over the area of the triangular element.

Substituting for  $\{R\}$  from equation (3.10) into equation (3.12),

the expression for strain energy can be written as

$$U = \frac{E}{24(1-\mu^2)} \{\delta'_b\}^T [A^{-1}]^T \left[ \iiint t^3 [C_1]^T [D] [C_1] dx' dy' \right] [A^{-1}] \{\delta'_b\} \quad (3.14)$$

According to Castigliano's theorem, the partial derivative of  $U$  with respect to any component of  $\{\delta'_b\}$  gives the corresponding component of  $\{F'_b\}$ . Thus

$$\{F'_b\} = \frac{E}{12(1-\mu^2)} [A^{-1}]^T \left[ \iiint t^3 [C_1]^T [D] [C_1] dx' dy' \right] [A^{-1}] \{\delta'_b\} \quad (3.15)$$

Comparing with the definition of stiffness matrix

$$\{F'_b\} = [K'_b] \{\delta'_b\} \quad (3.16)$$

The bending stiffness matrix for the element is given by

$$[K'_b] = \frac{E}{12(1-\mu^2)} [A^{-1}]^T \left[ \iiint t^3 [C_1]^T [D] [C_1] dx' dy' \right] [A^{-1}] \quad (3.17)$$

Obviously, each term of the matrix  $[K'_b]$  is of the form

$\iint x'^m y'^n dx' dy'$ , with the integration extending over the area of the element. For ease of computation, the following identity is introduced

$$\iint x'^m y'^n dx' dy' = \frac{x'_k{}^{m+1} y'_j{}^n}{m+n+2} \int_0^1 (1-\xi)^m \{(1-\xi)y'_k + \xi y'_j\}^n d\xi \quad (3.18)$$

This can easily be evaluated using Gauss quadrature technique.

This identity is valid for the chosen system of coordinate axes  $(x', y')$  as shown in Figure (11b) and for  $(m+n) \neq -2$ . The proof follows directly from equation 11.69 of Reference (134), after the appropriate change of notations and the evaluation of the first integral.





and

$$\begin{aligned}
 C_{11} &= 1/2 x'_k y'_j \\
 C_{21} &= 1/6 x'_k y'^2_j \\
 C_{31} &= 1/12 x'^3_k y'_j \\
 C_{12} &= 1/6 x'_k y'_j (y'_j + y'_k) \\
 C_{13} &= 1/12 x'_k y'_j (y'^2_j + y'_j y'_k + y'^2_k) \\
 C_{22} &= 1/24 x'^2_k y'_j (y'_j + 2y'_k)
 \end{aligned} \tag{3.22}$$

### 3.2 Complete Stiffness Matrix for an Element

A shell element is, generally, subjected to bending as well as in-plane forces. For a flat element these forces cause independent deformations and, therefore, the in-plane stiffness matrix can be derived independent of the bending stiffness matrix.

At each node of the triangular element two in-plane degrees of freedom are assigned. These are the displacements  $u'$  and  $v'$  along the  $x'$  and  $y'$  axes. The in-plane nodal displacements and the forces, expressed as vectors, are

$$\begin{aligned}
 \{\delta'_p\} &= [u'_i, v'_i, u'_j, v'_j, u'_k, v'_k]^T \\
 \{F'_p\} &= [F'_{xi}, F'_{yi}, F'_{xj}, F'_{yj}, F'_{xk}, F'_{yk}]^T
 \end{aligned} \tag{3.23}$$

For the distribution of  $u'$  and  $v'$ , linear expressions are assumed, i.e.,

$$u' = \alpha_{10}x' + \alpha_{11}y' + \alpha_{12} \quad (3.24)$$

$$v' = \alpha_{13}x' + \alpha_{14}y' + \alpha_{15}$$

This gives, for the in-plane stiffness matrix  $[K'_p]$ , the expression

$$[K'_p] = \frac{EV_e}{1-\mu^2} [B_1]^T [D] [B_1] \quad (3.25)$$

where  $V_e$  is the volume of the element and

$$[B_1] = \frac{-1}{x'_k y'_j} \begin{bmatrix} y'_j - y'_k & 0 & y'_k & 0 & -y'_j & 0 \\ 0 & x'_k & 0 & -x'_k & 0 & 0 \\ x'_k & y'_j - y'_k & -x'_k & y'_k & 0 & -y'_j \end{bmatrix} \quad (3.26)$$

This follows directly from equations (3.10), (3.18) and (3.26) of Reference (122), after appropriate change in notations and using the local coordinate axes as shown in Figure (11b).

The next step is to combine  $[K'_b]$  and  $[K'_p]$  to obtain the complete stiffness matrix  $[K'_e]$  for the element. In doing so, it is to be noted that the displacements prescribed for in-plane forces do not affect the bending deformations and vice-versa; also that the rotation  $\theta'_z$  does not enter as a parameter into the definitions of deformation in either mode. However, when the transformation to global coordinates is carried out, it is necessary to have  $\theta_z$  as a parameter. Hence the term  $\theta'_z$  is introduced at this stage; a fictitious



couple  $M'_z$  is associated with it and the appropriate number of zeroes are inserted in the stiffness matrix. The stiffness matrix for the element is, thus, given by

$$[K'_e] = \begin{bmatrix} K_e^{11} & | & K_e^{12} & | & K_e^{13} \\ \hline K_e^{21} & | & K_e^{22} & | & K_e^{23} \\ \hline K_e^{31} & | & K_e^{32} & | & K_e^{33} \end{bmatrix} \quad (3.27)$$

where

$$[K_e^{rs}] = \begin{bmatrix} K_p^{rs} & | & 0 & 0 & 0 & | & 0 \\ \hline 0 & 0 & | & & & | & 0 \\ 0 & 0 & | & K_b^{rs} & & | & 0 \\ 0 & 0 & | & & & | & 0 \\ \hline 0 & 0 & | & 0 & 0 & 0 & | & 0 \end{bmatrix} \quad (3.28)$$

$[K_p^{rs}]$  and  $[K_b^{rs}]$  being  $(2 \times 2)$  and  $(3 \times 3)$  submatrices, respectively, obtained by partitioning the matrices  $[K'_p]$  and  $[K'_b]$  in the same manner as in equation (3.27). The order of nodal displacements would be

$$\{\delta'_e\} = [u'_i, v'_i, w'_i, \theta'_{xi}, \theta'_{yi}, \theta'_{zi}, u'_j, \dots, \theta'_{zk}]^T \quad (3.29)$$

Since each of the stiffness matrices  $[K'_e]$  refers to the local coordinate system of its element, it must be transformed to common global coordinate system  $x, y, z$ . The

vector of nodal displacements  $\{\delta'_e\}$  for an element in local coordinates is related to the corresponding vector  $\{\delta_e\}$  in global coordinates by the relation

$$\{\delta'_e\} = [T]\{\delta_e\} \quad (3.30)$$

and similarly, the vector of nodal forces. Here  $[T]$  is the  $18 \times 18$  transformation matrix of direction cosines given by

$$[T] = \begin{bmatrix} \lambda & 0 & 0 & 0 & 0 & 0 \\ 0 & \lambda & 0 & 0 & 0 & 0 \\ 0 & 0 & \lambda & 0 & 0 & 0 \\ 0 & 0 & 0 & \lambda & 0 & 0 \\ 0 & 0 & 0 & 0 & \lambda & 0 \\ 0 & 0 & 0 & 0 & 0 & \lambda \end{bmatrix} \quad (3.31)$$

where

$$[\lambda] = \begin{bmatrix} l_x & m_x & n_x \\ l_y & m_y & n_y \\ l_z & m_z & n_z \end{bmatrix} \quad (3.32)$$

$(l_x, m_x, n_x)$ ,  $(l_y, m_y, n_y)$  and  $(l_z, m_z, n_z)$  are the direction cosines of  $x'$ ,  $y'$  and  $z'$  axes, respectively, with the global  $x$ ,  $y$  and  $z$  axes (e.g.  $m_z$  is the cosine of the angle made by  $z'$  axis with  $y$ -axis). These direction cosines can be evaluated from the following equations,

$$\begin{aligned}
A &= y_{ji}z_{ki} - y_{ki}z_{ji} \\
B &= x_{ki}z_{ji} - x_{ji}z_{ki} \\
C &= x_{ji}y_{ki} - x_{ki}y_{ji} \\
F &= \sqrt{x_{ji}^2 + y_{ji}^2 + z_{ji}^2} \\
G &= -\sqrt{A^2 + B^2 + C^2} \\
l_z &= A/G, \quad m_z = B/G, \quad n_z = C/G \\
l_y &= x_{ji}/F, \quad m_y = y_{ji}/F, \quad n_y = z_{ji}/F \\
l_x &= m_y n_z - m_z n_y \\
m_x &= l_z n_y - n_z l_y \\
n_x &= l_y m_z - m_y l_z
\end{aligned} \tag{3.33}$$

where

$$y_{ji} = y_j - y_i \text{ etc.}$$

The complete stiffness matrix for the element, referred to the global axes, is, therefore, given by

$$[K_e] = [T]^T [K'_e] [T] \tag{3.34}$$

### 3.3 Equivalent Nodal Forces for Distributed Loads

Generally, the blade is subjected to distributed external loads. The distributed loads, acting on an element, must be converted to equivalent nodal forces. The principle of finding the equivalent forces is that the work done by the two systems of forces, during an arbitrary virtual displacement, must be equal.



At a point within the element, let the external forces along  $x'$ ,  $y'$  and  $z'$  axes be  $F'_x$ ,  $F'_y$  and  $F'_z$  and the external moments about the  $x'$  and  $y'$  axes be  $M'_x$  and  $M'_y$ . The external bending forces  $F'_z$ ,  $M'_x$  and  $M'_y$  can be converted to a vector of equivalent nodal forces  $\{F'_b\}_{eq}$  as follows:

If  $\{\delta^*_b\}$  denotes the virtual nodal displacement, the virtual displacements at any point within the element, from equations (3.4), (3.6) and (3.9) are

$$\begin{Bmatrix} W^* \\ \theta^*_x \\ \theta^*_y \end{Bmatrix} = [N_b][A^{-1}]\{\delta^*_b\} \quad (3.35)$$

where

$$[N_b] = \begin{bmatrix} 1 & x' & y' & x'^2 & x'y' & y'^2 & x'^3 & x'^2y' & y'^3 \\ 0 & 0 & 1 & 0 & x' & 2y' & 0 & x'^2 & 3y'^2 \\ 0 & -1 & 0 & -2x' & -y' & 0 & -3x'^2 & -2x'y' & 0 \end{bmatrix} \quad (3.36)$$

Equating the work done by the actual distributed forces and the equivalent nodal forces,

$$\{\delta^*_b\}^T \{F'_b\}_{eq} = \int \begin{Bmatrix} W^* \\ \theta^*_x \\ \theta^*_y \end{Bmatrix}^T \begin{Bmatrix} F'_z \\ M'_x \\ M'_y \end{Bmatrix} d(\text{vol}) \quad (3.37)$$

Elimination of  $W^*$ ,  $\theta^*_x$  and  $\theta^*_y$  from equations (3.35) and (3.37)

gives

$$\{\delta^*_b\}^T \{F'_b\}_{eq} = \{\delta^*_b\}^T [A^{-1}]^T [N_b]^T \begin{Bmatrix} F'_z \\ M'_x \\ M'_y \end{Bmatrix} d(\text{vol}) \quad (3.38)$$

Since the virtual displacement  $\{\delta_b^*\}$  is arbitrary, equation (3.38) reduces to

$$\{F_b'\}_{eq} = [A^{-1}]^T \iint t[N_b]{}^T \begin{Bmatrix} F'_z \\ M'_x \\ M'_y \end{Bmatrix} dx'dy' \quad (3.39)$$

Similarly the in-plane external loads yield equivalent nodal forces  $\{F_p'\}_{eq}$  given by

$$\{F_p'\}_{eq} = [Q^{-1}]^T \iint t[N_p]{}^T \begin{Bmatrix} F'_x \\ F'_y \end{Bmatrix} dx'dy' \quad (3.40)$$

where

$$[N_p] = \begin{bmatrix} 1 & x' & y' & 0 & 0 & 0 \\ 0 & 0 & 0 & 1 & x' & y' \end{bmatrix} \quad (3.41)$$

and

$$[Q] = \begin{bmatrix} 1 & 0 & 0 & 0 & 0 & 0 \\ 0 & 0 & 0 & 1 & 0 & 0 \\ 1 & 0 & y'_j & 0 & 0 & 0 \\ 0 & 0 & 0 & 1 & 0 & y'_j \\ 1 & x'_k & y'_k & 0 & 0 & 0 \\ 0 & 0 & 0 & 1 & x'_k & y'_k \end{bmatrix} \quad (3.42)$$

It can also be shown that

$$\begin{Bmatrix} u' \\ v' \end{Bmatrix} = [N_p][Q^{-1}]\{\delta_p'\} \quad (3.43)$$

This method of finding the equivalent nodal forces is known as the 'consistent' method. Another way of dealing with the distributed loads is to lump the forces at the nodes from simple tributary area considerations. It has been suggested in Reference (122) that the lumped load technique is preferable in the problems where the shell is treated as an assembly of flat elements. However, this is not necessarily true in all cases, as would be shown later in Section 5.1.2, by carrying out computations for a test problem of a uniformly loaded hyperbolic paraboloid shell, using the consistent as well as the lumped load technique. When the curved shell element is considered flat, the  $z$  coordinate of any point within the element is somewhat altered. If the distributed load happens to be a function of this  $z$  coordinate, it is better to lump the actual loads at the nodes, rather than apply the consistent method to a flat surface. For example, in a rotating blade the intensity of the centrifugal force depends on the coordinates of the point. Hence, for calculating the stresses and the deformations due to these centrifugal forces, lumped load technique is preferable.

### 3.4 Calculation of Displacements

Having calculated the stiffness matrices,  $[K_e]$  for the individual elements, the next step is to combine all these matrices, according to the sequence of node numbering



employed on the structure, to obtain the complete stiffness matrix. The method of assembling is illustrated in Figure (12).

When all the elements joining at a particular node are in one plane a difficulty arises. In global coordinates six equations that are singular are obtained. This is due to the fact that only five of the equations can then be independent, due to the omission of the rotation perpendicular to the plane. For such nodes the rotations about the local  $x'$  and  $y'$  axes must be retained for assembly. In the type of subdivision shown in Figure (12), this is, in fact, necessary for node number 30.

If the boundary conditions specify certain nodal displacements to be zero, the rows and the columns corresponding to such displacements must be deleted from the complete stiffness matrix to obtain the final stiffness matrix  $[K]$ . In the present analysis, the nodes along the clamped edge are numbered zero and the rows and the columns corresponding to these displacements are not assembled at all. Thus the final stiffness matrix is directly obtained, resulting in considerable saving of computer memory.

The vectors of the nodal forces for the elements, on assembly, give the total force vector  $\{F\}$ . The displacements  $\{\delta\}$  can then be obtained from the equation

$$[K]\{\delta\} = \{F\} \quad (3.44)$$

### 3.5 Bending Mass Matrix for an Element

In the case of free vibrations, the blade is acted upon by distributed inertia load. By the application of d'Alembert principle, the dynamic problem can be treated as the static one, subjected to forces equal to the negative of the inertia loads. Since the deflection in the  $z'$ -direction of any point within the triangular element is  $w'$ , the intensity of the distributed force  $F'_z$  is given by

$$F'_z = -\rho \ddot{w}' \quad (3.45)$$

where  $\ddot{w}'$  denotes the second derivative of  $w'$  with respect to time and  $\rho$  is the mass per unit volume of the blade.

Substitution for  $w'$  from equation (3.9) gives

$$F'_z = -\rho [C] [A^{-1}] \{\ddot{\delta}'_b\} \quad (3.46)$$

By use of equation (3.39) this distributed bending force can be converted to equivalent nodal forces given by

$$\{F'_b\}_{eq} = [A^{-1}]^T \iint t [N_b]^T \begin{Bmatrix} -\rho [C] [A^{-1}] \{\ddot{\delta}'_b\} \\ 0 \\ 0 \end{Bmatrix} dx' dy' \quad (3.47)$$

Since the first row of  $[N_b]$  is identical to  $[C]$  (Equations 3.4 and 3.36), the nodal forces can be expressed in the form

$$\{F'_b\}_{eq} = -[M'_b] \{\ddot{\delta}'_b\} \quad (3.48)$$

where, the bending mass matrix is given by

$$[M'_b] = \rho [A^{-1}]^T \left[ \iint t [C]^T [C] dx' dy' \right] [A^{-1}] \quad (3.49)$$

### 3.6 Complete Mass Matrix for an Element

In addition to the displacement in the  $z'$ -direction, a point within the element undergoes in-plane displacements  $u'$  and  $v'$ . The corresponding d'Alembert forces along the  $x'$  and  $y'$  axes are

$$\begin{Bmatrix} F'_x \\ F'_y \end{Bmatrix} = -\rho \begin{Bmatrix} \ddot{u}' \\ \ddot{v}' \end{Bmatrix} \quad (3.50)$$

Substitution for  $u'$  and  $v'$  from equation (3.43) gives

$$\begin{Bmatrix} F'_x \\ F'_y \end{Bmatrix} = -\rho [N_p] [Q^{-1}] \{\ddot{\delta}'_p\} \quad (3.51)$$

The equivalent nodal forces for these distributed in-plane forces, obtained by the use of equation (3.40), are

$$\{F'_p\}_{eq} = -[M'_p] \{\ddot{\delta}'_p\} \quad (3.52)$$

where

$$[M'_p] = \rho [Q^{-1}]^T \left( \iint t [N_p]^T [N_p] dx' dy' \right) [Q^{-1}] \quad (3.53)$$

If the thickness of the element is constant, the in-plane mass matrix reduces to

$$[M'_p] = \frac{\rho V e}{3} \begin{bmatrix} 1/2 & & & & & & \\ & 1/2 & & & & & \\ & & \text{symmetric} & & & & \\ & & & & & & \\ 1/4 & 0 & 1/2 & & & & \\ 0 & 1/4 & 0 & 1/2 & & & \\ 1/4 & 0 & 1/4 & 0 & 1/2 & & \\ 0 & 1/4 & 0 & 1/4 & 0 & 1/2 & \end{bmatrix} \quad (3.54)$$



Assuming that the in-plane forces do not cause any bending displacements and vice-versa, and also introducing the nodal displacement  $\theta'_z$  and corresponding fictitious moment  $M'_z$ , the complete mass matrix of the element is given by

$$[M'_e] = \begin{bmatrix} M_e^{11} & | & M_e^{12} & | & M_e^{13} \\ \hline M_e^{21} & | & M_e^{22} & | & M_e^{23} \\ \hline M_e^{31} & | & M_e^{32} & | & M_e^{33} \end{bmatrix} \quad (3.55)$$

where

$$[M_e^{rs}] = \begin{bmatrix} M_p^{rs} & | & 0 & 0 & 0 & | & 0 \\ \hline 0 & 0 & | & & & | & 0 \\ 0 & 0 & | & M_b^{rs} & & | & 0 \\ \hline 0 & 0 & | & & & | & 0 \\ 0 & 0 & | & 0 & 0 & 0 & | & 0 \end{bmatrix} \quad (3.56)$$

$[M_p^{rs}]$  and  $[M_b^{rs}]$  being  $(2 \times 2)$  and  $(3 \times 3)$  submatrices obtained by partitioning the matrices  $[M'_p]$  and  $[M'_b]$  in the same manner as in equation (3.55).

The element mass matrix  $[M'_e]$  in local coordinates is then transformed to global coordinates by the relation,

$$[M_e] = [T]^T [M'_e] [T] \quad (3.57)$$

### 3.7 Natural Frequencies and Mode Shapes

The mass matrices  $[M_e]$  of all the elements are assembled in exactly the same manner as the stiffness matrices, to obtain the final mass matrix  $[M]$  for the blade. The resulting equation of motion is

$$[K]\{\delta\} = - [M]\{\ddot{\delta}\} \quad (3.58)$$

Assuming harmonic vibrations of circular frequency  $\omega$ , the equation of motion becomes

$$\left( [K] - \omega^2 [M] \right) \{\delta\} = \{0\} \quad (3.59)$$

or

$$\left( [K^{-1}] [M] - \frac{1}{\omega^2} [I] \right) \{\delta\} = \{0\} \quad (3.60)$$

The eigenvalues and eigenvectors of the matrix  $[K^{-1}][M]$  give the values of  $1/\omega^2$  and the mode shapes. Since only the first few largest values of  $1/\omega^2$  (lowest natural frequencies) are of practical importance, it is preferable to convert equation (3.59) to the form of equation (3.60) and apply Power method for the determination of eigenvalues and eigenvectors.

A subroutine 'Power' is especially prepared for this purpose and is given in Appendix III. It returns the eigenvectors as the columns of the original matrix and is, therefore, very economical from computer memory considerations. Also, the multiplication of the matrices  $[K^{-1}]$  and  $[M]$

is carried out using the core storage. Thus for  $N$  degrees of freedom problem, the dimensioned arrays necessary are:

- (a) a matrix of size  $(N \times N)$ , and
- (b) two vectors of size  $(N)$ .



## CHAPTER 4

### THEORY FOR ROTATING LOW ASPECT RATIO BLADES

The natural frequencies of rotating turbomachinery blades are known to be significantly higher than those of the nonrotating blades. One of the important design considerations is to avoid resonances of the blades near the design speed, in the first few modes of vibration. Possible resonances at engine order excitations are predicted by drawing Campbell diagram (Figure 10) for each row of the blades. This diagram, essentially, is a plot of the variation of the first few natural frequencies of the blades with the speed of rotation, with engine order lines superimposed over it. The points of intersection on the diagram represent possible resonances. Obviously, the correct estimation of the natural frequencies of the blades, at different speeds of rotation, is important.

Various methods are available for the analysis of long blades idealized as rotating cantilever beams; as discussed in Sections 2.4 and 2.5. In this chapter, the finite element technique is extended to the vibration analysis of rotating low aspect ratio blades. Essentially, the method consists of evaluating the stresses and the 'pseudo-static deformation' of the blade due to centrifugal

forces. These stresses are then used to determine the increase in the stiffness of the elements; and the blade is considered to vibrate about the new deformed configuration. For the sake of convenience of formulation, the theory for rotating cantilever plates is first developed, followed by the method for the vibration analysis of rotating low aspect ratio blades. Another reason for developing the theory for the rotating cantilever plates is that the results for rotating beams are available in the literature and, therefore, the manner in which the beam results are approached, with the increase in the aspect ratio, can be studied.

#### 4.1 Vibration of Rotating Cantilever Plates

The cantilever plate is considered mounted on the periphery of a rotating disc of radius  $r$  in such a manner that the plane of the plate is inclined to the plane of rotation of the disc at an angle  $\theta$ , called the setting angle.  $x, y, z$  is the system of cartesian global coordinate axes with the origin at the mid point of the fixed edge of the plate. The  $x$  axis is along the length of the plate, the  $y$  axis along the breadth of the plate and the  $z$  axis normal to the plate surface, as shown in Figure (2). The coordinate axes  $x, y, z$  are attached to the rotating disc. The disc is assumed to be rigid. The in-plane vibrations of the plate are not considered, since the stiffness for the in-plane motion

is considerably greater than the stiffness for the bending motion.

If  $w$  is the deflection of an arbitrary point on the middle surface of the plate, its instantaneous coordinates during vibration can be taken as  $(x, y, w)$ . The components of the d'Alembert force per unit volume of the plate along the  $x$ ,  $y$  and  $z$  axes are given by

$$\begin{aligned} F_x &= \rho \Omega^2 (x + r) + 2 \rho \Omega \dot{w} \sin \theta \\ F_y &= \rho \Omega^2 (y \cos^2 \theta - w \sin \theta \cos \theta) \\ F_z &= \rho \Omega^2 (-y \sin \theta \cos \theta + w \sin^2 \theta) - \rho \ddot{w} \end{aligned} \quad (4.1)$$

The derivation of these equations is given in Appendix I.

#### 4.1.1 Middle Surface Stresses

The force  $F_z$  normal to the plate surface does not produce stresses in the middle plane of the plate. These stresses are solely due to the in-plane forces  $F_x$  and  $F_y$ . The expressions for these forces (equation 4.1) have two components, one dependent on the displacement  $w$  and the other independent of the displacement. If the vibrations are assumed to be of small amplitude, the component of the stresses dependent on  $w$  may be taken to be small as compared to the stresses produced by the forces independent of  $w$ . Thus, the stresses in the middle plane of the plate are those produced by the distributed forces



$$\begin{aligned} F_x &\approx \rho \Omega^2 (x + r) \\ F_y &\approx \rho \Omega^2 y \cos^2 \theta \end{aligned} \quad (4.2)$$

The plate is subdivided into small triangular elements and the local  $x'$ ,  $y'$ ,  $z'$  axes for an element are chosen as shown in Figure (13). It may be pointed out here that for calculating the middle surface stresses in the rotating cantilever plate, the use of local axes different from the global axes is not essential and, in fact, requires a little extra computational work. The reason for doing this is to maintain the similarity of formulation with the more complex case of rotating low aspect ratio blades, for which it is necessary to use different local and global axes.

The direction cosines of the local axes are obtained from equations (3.33). The global coordinates  $(x, y)$  of any point within the element are related to its local coordinates  $(x', y')$  by the relation

$$\begin{Bmatrix} x \\ y \end{Bmatrix} = [\lambda_p]^T \begin{Bmatrix} x' \\ y' \end{Bmatrix} + \begin{Bmatrix} x_i \\ y_i \end{Bmatrix} \quad (4.3)$$

where

$$[\lambda_p] = \begin{bmatrix} l_x & m_x \\ l_y & m_y \end{bmatrix} \quad (4.4)$$

and  $(x_i, y_i)$  are the global coordinates of the node  $i$ . Also, the components of the forces  $F_x$  and  $F_y$  along the local axes

are given by

$$\begin{Bmatrix} F'_x \\ F'_y \end{Bmatrix} = [\lambda_p] \begin{Bmatrix} F_x \\ F_y \end{Bmatrix} \quad (4.5)$$

Substituting for  $F_x$  and  $F_y$  from equation (4.2) and using the coordinate transformation relation (equation 4.3), the forces  $F'_x$  and  $F'_y$  can be expressed as

$$\begin{Bmatrix} F'_x \\ F'_y \end{Bmatrix} = \rho\Omega^2 [\lambda_p] \begin{bmatrix} 1 & 0 \\ 0 & \cos^2\theta \end{bmatrix} [\lambda_p]^T \begin{Bmatrix} x' \\ y' \end{Bmatrix} + \rho\Omega^2 [\lambda_p] \begin{Bmatrix} x_i + r \\ y_i \cos^2\theta \end{Bmatrix} \quad (4.6)$$

The equivalent nodal forces corresponding to these distributed forces, from equation (3.40) are

$$\begin{aligned} \{F'_p\}_{eq} &= \rho\Omega^2 [Q^{-1}]^T \iint t [N_p]^T [\lambda_p] \begin{bmatrix} 1 & 0 \\ 0 & \cos^2\theta \end{bmatrix} [\lambda_p]^T \begin{Bmatrix} x' \\ y' \end{Bmatrix} + \\ &\quad \begin{Bmatrix} x_i + r \\ y_i \cos^2\theta \end{Bmatrix} dx' dy' \quad (4.7) \end{aligned}$$

If the thickness of the element is constant, equation (4.7) after some simplification and evaluation of the double integral reduces to

$$\{F'_p\}_{eq} = \rho\Omega^2 t [Q^{-1}]^T \begin{Bmatrix} b_1 C_{21} + b_3 C_{12} + b_4 C_{11} \\ b_1 C_{31} + b_3 C_{22} + b_4 C_{21} \\ b_1 C_{22} + b_3 C_{13} + b_4 C_{12} \\ b_3 C_{21} + b_2 C_{12} + b_5 C_{11} \\ b_3 C_{31} + b_2 C_{22} + b_5 C_{21} \\ b_3 C_{22} + b_2 C_{13} + b_5 C_{12} \end{Bmatrix} \quad (4.8)$$

where  $C_{11}$ ,  $C_{12}$  etc. are defined in equation (3.22) and

$$\begin{aligned}
 b_1 &= 1 - m_x \sin^2 \theta \\
 b_2 &= 1 - m_y \sin^2 \theta \\
 b_3 &= -m_x m_y \sin^2 \theta \\
 b_4 &= l_x (x_i + r) + m_x y_i \cos^2 \theta \\
 b_5 &= l_y (x_i + r) + m_y y_i \cos^2 \theta
 \end{aligned} \tag{4.9}$$

The in-plane stiffness matrix  $[K'_p]$  for an element in the local coordinates is given by equation (3.25). The transformation to global axes is accomplished by the relation

$$[K_p] = [T_p]^T [K'_p] [T_p] \tag{4.10}$$

where

$$[T_p] = \begin{bmatrix} \lambda_p & 0 & 0 \\ 0 & \lambda_p & 0 \\ 0 & 0 & \lambda_p \end{bmatrix} \tag{4.11}$$

Similarly the vector of equivalent nodal forces in global axes is given by

$$\{F_p\}_{eq} = [T_p]^T \{F'_p\}_{eq} \tag{4.12}$$

The stiffness matrices  $[K_p]$  and the force vectors  $\{F_p\}_{eq}$  of all the elements are assembled together, the rows and the columns corresponding to the nodes along the fixed edge are deleted, to obtain the final stiffness matrix and the force vector. The solution of these equations gives the nodal displacements. If  $\{\delta_p\}$  is the vector of nodal displacements



for an element along the global axes, the stresses along the local axes are given by

$$\begin{pmatrix} \sigma'_x \\ \sigma'_y \\ \tau'_{xy} \end{pmatrix} = \frac{E}{1-\mu^2} [S] \{\delta_p\} \quad (4.13)$$

where

$$[S] = [D][B_1][T_p]. \quad (4.14)$$

The matrices  $[D]$ ,  $[B_1]$  and  $[T_p]$  are defined by equations (3.13), (3.26) and (4.11), respectively. Since the assumed expressions for the in-plane displacements are linear in  $x'$  and  $y'$ , the stresses  $\sigma'_x$ ,  $\sigma'_y$  and  $\tau'_{xy}$ , in the middle surface of the element come out to be constant.

#### 4.1.2 Centrifugal Stiffness Matrix

In the absence of the initial stresses in the plate, the bending stiffness matrix  $[K'_b]$  for a triangular element is given by equation (3.17).

Due to the presence of the in-plane stresses  $\sigma'_x$ ,  $\sigma'_y$  and  $\tau'_{xy}$  in the middle surface, the strain energy stored in the element is higher than the usual bending strain energy by the amount

$$U_1 = 1/2 \int \left[ \sigma'_x \left( \frac{\partial w'}{\partial x'} \right)^2 + \sigma'_y \left( \frac{\partial w'}{\partial y'} \right)^2 + 2 \tau'_{xy} \left( \frac{\partial w'}{\partial y'} \right) \left( \frac{\partial w'}{\partial x'} \right) \right] d(\text{vol}) \quad (4.15)$$

Equation (4.15) can be written as

$$U_1 = 1/2 \iint t \begin{Bmatrix} \frac{\partial w'}{\partial x'} \\ \frac{\partial w'}{\partial y'} \end{Bmatrix}^T \begin{bmatrix} \sigma'_x & \tau'_{xy} \\ \tau'_{xy} & \sigma'_y \end{bmatrix} \begin{Bmatrix} \frac{\partial w'}{\partial x'} \\ \frac{\partial w'}{\partial y'} \end{Bmatrix} dx' dy'. \quad (4.16)$$

This energy, due to the centrifugal forces, gives an increase in the bending stiffness matrix of the element by the amount

$$[K'_C] = \iint t [G]^T \begin{bmatrix} \sigma'_x & \tau'_{xy} \\ \tau'_{xy} & \sigma'_y \end{bmatrix} [G] dx' dy' \quad (4.17)$$

where  $[G]$  is defined by the relation

$$\begin{Bmatrix} \frac{\partial w'}{\partial x'} \\ \frac{\partial w'}{\partial y'} \end{Bmatrix} = [G] \{\delta'_b\}. \quad (4.18)$$

Since  $[K'_C]$  is produced by the centrifugal forces, it may be called the centrifugal stiffness matrix. The proof for equation (4.17) is given by Kapoor and Hartz (135) while dealing with the problem of stability analysis of plates. For the stability analysis, a more refined expression for  $[K'_C]$  is given by Przemieniecki (136), by starting with nonlinear strain displacement relations. In the stability analysis the plate is subjected to compressive in-plane stresses resulting in large deflections and hence the nonlinear strain displacement relations are called for. In the present problem, however, the centrifugal forces produce tensile stresses and hence the nonlinearity need not be considered.

By taking the partial derivatives of  $w'$  from equation (3.9) and using equation (3.4), the slopes can be expressed in the form

$$\begin{Bmatrix} \frac{\partial w'}{\partial x'} \\ \frac{\partial w'}{\partial y'} \end{Bmatrix} = [H] [A^{-1}] \{\delta'_b\} \quad (4.19)$$

where

$$[H] = \begin{bmatrix} 0 & 1 & 0 & 2x' & y' & 0 & 3x'^2 & 2x'y' & 0 \\ 0 & 0 & 1 & 0 & x' & 2y' & 0 & x'^2 & 3y'^2 \end{bmatrix} \quad (4.20)$$

Comparing equations (4.18) and (4.19)

$$[G] = [H] [A^{-1}] \quad (4.21)$$

Substitution for  $[G]$  from equation (4.21) into equation (4.17) gives

$$[K'_c] = [A^{-1}]^T \left( \iint t[Z] dx' dy' \right) [A^{-1}] \quad (4.22)$$

where

$$[Z] = [H]^T \begin{bmatrix} \sigma'_x & \tau'_{xy} \\ \tau'_{xy} & \sigma'_y \end{bmatrix} [H] \quad (4.23)$$

The total bending stiffness matrix for the element is, therefore, given by

$$[K'_t] = [K'_b] + [K'_c] \quad (4.24)$$

#### 4.1.3 Natural Frequencies and Mode Shapes

The plate is subjected to a distributed force of intensity  $F_z$ , given by equation (4.1), in the direction normal



to its plane. The component  $-\rho\Omega^2 y \sin\theta \cos\theta$  of this force does not depend on the displacement  $w$ . This component produces only a small initial deformation of the plate and does not affect the natural frequencies. For the vibration analysis, therefore, the component dependent on  $w$  need only be considered. The distributed force along the local  $z'$  axis, at any point within an element is, thus, given by

$$F'_z = \rho\Omega^2 w' \sin^2\theta - \rho\ddot{w}'$$

From equation (3.39), the equivalent nodal forces corresponding to this are

$$\{F'_b\}_{eq} = [A^{-1}]^T \iint t[N_b]^T \begin{Bmatrix} \rho\Omega^2 w' \sin^2\theta - \rho\ddot{w}' \\ 0 \\ 0 \end{Bmatrix} dx'dy' \quad (4.25)$$

Since the first row of  $[N_b]$  is identical to  $[C]$  (equations 3.4 and 3.36), equation (4.25) can be written as

$$\{F'_b\}_{eq} = \rho[A^{-1}]^T \iint t[C]^T (\Omega^2 w' \sin^2\theta - \ddot{w}') dx'dy' \quad (4.26)$$

Substituting for  $w'$  from equation (3.9)

$$\{F'_b\}_{eq} = [M'_b] \left( \Omega^2 \sin^2\theta \{\delta'_b\} - \{\ddot{\delta}'_b\} \right) \quad (4.27)$$

where  $[M'_b]$  is defined by equation (3.49). The stiffness matrix  $[K'_t]$  and the mass matrix  $[M'_b]$  are now transformed to global axes, by the relations

$$[K_t] = [T_b]^T [K'_t] [T_b] \quad (4.28)$$

$$[M_b] = [T_b]^T [M'_b] [T_b]$$

where

$$[T_b] = \begin{bmatrix} \lambda_b & 0 & 0 \\ 0 & \lambda_b & 0 \\ 0 & 0 & \lambda_b \end{bmatrix} \quad (4.29)$$

and

$$[\lambda_b] = \begin{bmatrix} n_z & 0 & 0 \\ 0 & l_x & m_x \\ 0 & l_y & m_y \end{bmatrix} \quad (4.30)$$

The value of  $n_z$  would be +1 or -1, depending on the direction of  $z'$ -axis for the particular element. As pointed out earlier in Chapter 3, the direction of the  $x'$  axis is so chosen that  $x'_k$  is always positive and  $x', y', z'$  axes form a right handed system. Equations (3.33), automatically, give the appropriate values of the direction cosines.

Carrying out the assembly of the element matrices and deleting the rows and columns corresponding to the nodes along the fixed edge, the final equation of motion is obtained in the form

$$[K] \{\delta\} = \Omega^2 \sin^2 \theta [M] \{\delta\} - [M] \{\ddot{\delta}\} \quad (4.31)$$

If  $\omega_r$  is the frequency of harmonic vibrations, equation (4.31) can be expressed as

$$\left( [K] - (\omega_r^2 + \Omega^2 \sin^2 \theta) [M] \right) \{\delta\} = \{0\} \quad (4.32)$$

The eigenvalues and the eigenvectors of the matrix  $[K^{-1}][M]$ , therefore, give the values of  $1/(\omega_r^2 + \Omega^2 \sin^2 \theta)$  and the mode shapes.

It may be mentioned here that the steady state centrifugal forces produce a small pseudo-static deformation of the plate and the vibratory motion takes place about this deformed configuration. For more accurate analysis, therefore, the stiffness and the inertial properties must be evaluated in the deformed configuration. However, the inclusion of this small deformation would necessitate a shell type of analysis. This would not only increase the computational work, but, since the shell would be nearly flat, the resulting matrices would be ill-conditioned. This may, probably, cause more loss of accuracy than would be gained by the inclusion of pseudo-static deformation. For the vibration analysis of the actual blades, in the next section, this effect has, however, been included.

#### 4.2 Vibration of Rotating Low Aspect Ratio Blades

The blade is considered to be rigidly attached to the periphery of a rotating disc of radius  $r$ . At the root of the blade, the chord makes an angle  $\theta$  with the tangential direction of the disc as shown in Figure (14). This angle  $\theta$  is referred to as the setting angle.  $x, y, z$  is the system



of cartesian coordinate axes attached to the rotating disc. The origin of this right handed coordinate system is at the centroid of the root cross-section of the blade. The x-axis is in the radial direction and the y-axis is parallel to the root chord.

If  $u$ ,  $v$  and  $w$  are the displacements, along the  $x$ ,  $y$  and  $z$  axes, of a point on the middle surface of the blade, its instantaneous coordinates during vibration are  $(x+u, y+v, z+w)$ . The components of the d'Alembert force per unit volume of the blade, along the  $x$ ,  $y$  and  $z$  axes are given by

$$\begin{aligned} F_x &= Fx_1 + Fx_2 + Fx_3 + Fx_4 \\ F_y &= Fy_1 + Fy_2 + Fy_3 + Fy_4 \\ F_z &= Fz_1 + Fz_2 + Fz_3 + Fz_4 \end{aligned} \quad (4.33)$$

where

$$\begin{aligned} Fx_1 &= \rho\Omega^2 (x+r) \\ Fy_1 &= \rho\Omega^2 (y \cos^2\theta - z \sin\theta\cos\theta) \\ Fz_1 &= \rho\Omega^2 (-y \sin\theta\cos\theta + z \sin^2\theta) \end{aligned} \quad (4.34)$$

$$\begin{aligned} Fx_2 &= \rho\Omega^2 u \\ Fy_2 &= \rho\Omega^2 (v \cos^2\theta - w \sin\theta\cos\theta) \\ Fz_2 &= \rho\Omega^2 (-v \sin\theta\cos\theta + w \sin^2\theta) \end{aligned} \quad (4.35)$$

$$\begin{aligned}
 Fx_3 &= -\rho\ddot{u} \\
 Fy_3 &= -\rho\ddot{v} \\
 Fz_3 &= -\rho\ddot{w}
 \end{aligned}
 \tag{4.36}$$

$$\begin{aligned}
 Fx_4 &= 2\rho\Omega(\dot{w} \sin\theta - \dot{v} \cos\theta) \\
 Fy_4 &= 2\rho\Omega\dot{u} \cos\theta \\
 Fz_4 &= -2\rho\Omega\dot{u} \sin\theta
 \end{aligned}
 \tag{4.37}$$

The derivation of these equations is given in Appendix I.

#### 4.2.1 Pseudo-Static Deformation

In the steady state, the blade is subjected to distributed forces  $Fx_1$ ,  $Fy_1$  and  $Fz_1$  along the x, y and z axes. These forces cause a certain pseudo-static deformation of the blade and, also, produce some initial stresses. To calculate these, the blade is subdivided into small flat triangular elements. The stiffness matrices for all the elements are calculated and grouped together, to get the final stiffness matrix, as explained in Chapter 3.

The distributed forces at any point are seen to be functions of the z coordinate of the point (equation 4.34). For the reasons outlined in the last paragraph of Section 3.3, the distributed forces  $Fx_1$ ,  $Fy_1$  and  $Fz_1$  are lumped at the nodes instead of finding the consistent nodal loading. Thus, the total force acting on the area bounded by the dotted lines, in Figure (15), is concentrated at the node

within that area.

Once the nodal forces and the stiffness matrix, are obtained, the pseudo-static deformation can be calculated. The nodal displacements  $\{\delta_e\}$ , along the global axes, for each element are transformed back to the local axes; and the vector of in-plane nodal displacements  $\{\delta'_p\}$  is obtained. The stresses in the middle plane of the element are given by

$$\begin{pmatrix} \sigma'_x \\ \sigma'_y \\ \tau'_{xy} \end{pmatrix} = \frac{E}{1-\mu^2} [D] [B_1] \{\delta'_p\} \quad (4.38)$$

where  $[D]$  and  $[B_1]$  are defined by equations (3.13) and (3.26), respectively.

#### 4.2.2 Stiffness Matrix in Deformed Configuration

The pseudo-static deformation is the deformation of the blade due to the steady state centrifugal forces  $Fx_1$ ,  $Fy_1$  and  $Fz_1$ . If initially the coordinates of a particular node  $j$  are  $(x_j, y_j, z_j)$  and the deformation at the node is  $(u_j, v_j, w_j)$ , its coordinates after deformation would be  $(x_j + u_j, y_j + v_j, z_j + w_j)$ . Since the vibratory motion occurs about this deformed configuration, the element properties are evaluated for this configuration.



The bending stiffness matrix  $[K'_b]$  and the in-plane stiffness matrix  $[K'_p]$  are obtained from equations (3.17) and (3.25), respectively. Substituting for the middle surface stresses from equation (4.38), the centrifugal stiffness matrix  $[K'_c]$  is obtained, using equation (4.22). The total bending stiffness matrix of the element is, therefore,  $[K'_b] + [K'_c]$ . The complete stiffness matrix for the element is obtained by combining the in-plane and the total bending stiffness matrices, as follows:

$$[K'_{et}] = \begin{bmatrix} K_{et}^{11} & | & K_{et}^{12} & | & K_{et}^{13} \\ \hline K_{et}^{21} & | & K_{et}^{22} & | & K_{et}^{23} \\ \hline K_{et}^{31} & | & K_{et}^{32} & | & K_{et}^{33} \end{bmatrix} \quad (4.39)$$

where

$$[K'_{et}] = \begin{bmatrix} K_p^{rs} & | & 0 & 0 & 0 & | & 0 \\ \hline 0 & 0 & | & 0 & 0 & 0 & | & 0 \\ \hline 0 & 0 & | & K_b^{rs} + K_c^{rs} & & & | & 0 \\ \hline 0 & 0 & | & & & & | & 0 \\ \hline 0 & 0 & | & 0 & 0 & 0 & | & 0 \end{bmatrix} \quad (4.40)$$

$[K_p^{rs}]$ ,  $[K_b^{rs}]$  and  $[K_c^{rs}]$  are the submatrices obtained by partitioning the stiffness matrices  $[K'_p]$ ,  $[K'_b]$  and  $[K'_c]$  respectively, in the same manner as in equation (4.39).

### 4.2.3 Centrifugal Mass Matrix

The centrifugal mass matrix results from the distributed forces  $F_{x_2}$ ,  $F_{y_2}$  and  $F_{z_2}$ , given by equation (4.35). These forces can be written as

$$\begin{Bmatrix} F_x \\ F_y \\ F_z \end{Bmatrix}_2 = \rho \Omega^2 [\theta_1] \begin{Bmatrix} u \\ v \\ w \end{Bmatrix} \quad (4.41)$$

where

$$[\theta_1] = \begin{bmatrix} 1 & 0 & 0 \\ 0 & \cos^2 \theta & -\sin \theta \cos \theta \\ 0 & -\sin \theta \cos \theta & \sin^2 \theta \end{bmatrix} \quad (4.42)$$

Transformation of the forces and the displacements in equation (4.41) to the local axes gives

$$\begin{Bmatrix} F'_x \\ F'_y \\ F'_z \end{Bmatrix}_2 = \rho \Omega^2 [\theta_2] \begin{Bmatrix} u' \\ v' \\ w' \end{Bmatrix} \quad (4.43)$$

where

$$[\theta_2] = [\lambda] [\theta_1] [\lambda]^T \quad (4.44)$$

and the matrix  $[\lambda]$  is defined by equation (3.32). These distributed forces must be converted to equivalent nodal forces  $\{F'_e\}_2$ . Since in this case the forces are functions of, both, the in-plane and the bending displacements, the equations

for equivalent forces derived in section (3.3) are not convenient to apply directly.

With some rearrangement, equations (3.9) and (3.43) can be combined and written as

$$\begin{Bmatrix} u' \\ v' \\ w' \end{Bmatrix} = [N] [P_1^{-1}] \{\delta'_{15}\} \quad (4.45)$$

where

$$[N] = \begin{bmatrix} N_p & 0 \\ 0 & C \end{bmatrix} \quad (4.46)$$

$$\{\delta'_{15}\} = [u'_i, v'_i, w'_i, \theta'_{xi}, \theta'_{yi}, u'_j, v'_j, \dots, \theta'_{yk}]^T \quad (4.47)$$

and

$$[P_1] = \begin{bmatrix} \begin{bmatrix} N_p & 0 \\ 0 & N_b \end{bmatrix}_{\substack{x'=0 \\ y'=0}} \\ \begin{bmatrix} N_p & 0 \\ 0 & N_b \end{bmatrix}_{\substack{x'=0 \\ y'=y'_j}} \\ \begin{bmatrix} N_p & 0 \\ 0 & N_b \end{bmatrix}_{\substack{x'=x'_k \\ y'=y'_k}} \end{bmatrix} \quad (4.48)$$



The matrices  $[N_p]$ ,  $[N_b]$  and  $[C]$  are defined by equations (3.41), (3.36) and (3.4), respectively. Let the distributed forces given by equation (4.43) be equivalent to a vector of 15 nodal forces  $\{F'_{15}\}$  corresponding to the displacement vector  $\{\delta'_{15}\}$ . If  $\{\delta^*_{15}\}$  denotes the vector of virtual nodal displacements, the corresponding virtual displacements at a point within the element, from equation (4.45), would be

$$\begin{Bmatrix} u^* \\ v^* \\ w^* \end{Bmatrix} = [N][P_1^{-1}]\{\delta^*_{15}\} \quad (4.49)$$

Equating the work done by the two systems of forces, the following equation is obtained

$$\{\delta^*_{15}\}^T \{F'_{15}\} = \int \begin{Bmatrix} u^* \\ v^* \\ w^* \end{Bmatrix}^T \begin{Bmatrix} F'_x \\ F'_y \\ F'_z \end{Bmatrix}_2 d(\text{vol}) \quad (4.50)$$

Elimination of the virtual displacements from equations (4.49) and (4.50) gives

$$\{F'_{15}\} = [P_1^{-1}]^T \iiint t[N]^T \begin{Bmatrix} F'_x \\ F'_y \\ F'_z \end{Bmatrix}_2 dx'dy' \quad (4.51)$$

Substituting for the force vector from equation (4.43) and for the displacement vector from equation (4.45), the following expression for  $\{F'_{15}\}$  is obtained

$$\{F'_{15}\} = [P_2]\{\delta'_{15}\} \quad (4.52)$$

where

$$[P_2] = \rho \Omega^2 [P_1^{-1}]^T \left( \iint t [N]^T [\theta_2] [N] dx' dy' \right) [P_1^{-1}] \quad (4.53)$$

Introducing the rotational displacements  $\theta'_z$  and the corresponding fictitious moments  $M'_z$  at each node, the vector of 18 nodal forces is given by

$$\{F'_e\}_2 = [M'_{ec}] \{\delta'_e\} \quad (4.54)$$

where

$$[M'_{ec}] = \begin{bmatrix} M_{ec}^{11} & | & M_{ec}^{12} & | & M_{ec}^{13} \\ \hline M_{ec}^{21} & | & M_{ec}^{22} & | & M_{ec}^{23} \\ \hline M_{ec}^{31} & | & M_{ec}^{32} & | & M_{ec}^{33} \end{bmatrix} \quad (4.55)$$

and

$$[M_{ec}^{rs}] = \begin{bmatrix} & & & & & | & 0 \\ & & & & & | & 0 \\ & & P_2^{rs} & & & | & 0 \\ & & & & & | & 0 \\ & & & & & | & 0 \\ & & & & & | & 0 \\ \hline 0 & 0 & 0 & 0 & 0 & | & 0 \end{bmatrix} \quad (4.56)$$

$[P_2^{rs}]$  are the  $5 \times 5$  submatrices obtained by partitioning the matrix  $[P_2]$  of equation (4.53). Since the matrix  $[M'_{ec}]$  is due to the centrifugal forces, it is defined as Centrifugal Mass Matrix of the element.

#### 4.2.4 Natural Frequencies and Mode Shapes

Each of the distributed forces  $F_x$ ,  $F_y$  and  $F_z$ , acting on the blade, are composed of four components (Equation 4.33). The forces  $F_{x_1}$ ,  $F_{y_1}$  and  $F_{z_1}$  produce the deformed configuration and the centrifugal stiffness matrix. The components  $F_{x_2}$ ,  $F_{y_2}$  and  $F_{z_2}$  result in centrifugal mass matrix. The effect of the remaining two components is now studied.

The distributed forces  $F_{x_3}$ ,  $F_{y_3}$  and  $F_{z_3}$  are given by equation (4.36). Transformation to the local axes gives

$$\begin{Bmatrix} F'_x \\ F'_y \\ F'_z \end{Bmatrix}_3 = -\rho \begin{Bmatrix} \ddot{u}' \\ \ddot{v}' \\ \ddot{w}' \end{Bmatrix} \quad (4.57)$$

These forces are identical to the d'Alembert forces in the case of nonrotating blades. The equivalent nodal forces corresponding to these forces are, therefore, given by

$$\{F'_e\}_3 = - [M'_e] \{\ddot{\delta}'_e\} \quad (4.58)$$

where  $[M'_e]$  is the mass matrix for the element given by equation (3.55).

The forces  $F_{x_4}$ ,  $F_{y_4}$  and  $F_{z_4}$  given by equation (4.37) arise from the Coriolis acceleration and depend on the velocities  $\dot{u}$ ,  $\dot{v}$  and  $\dot{w}$ . The displacement  $u$  is in the direction of the length of the blade, the displacement  $v$  is in the chordwise direction, and the displacement  $w$  is in the flapwise direction (Figure 14).



Although the equations of motion along the  $x, y$  and the  $z$  direction are coupled, the blade is much more stiff in the longitudinal direction than in the flapwise or the chordwise directions. In the first few modes of vibration, therefore, the displacement  $u$  is expected to be considerably smaller than the displacements  $w$  and  $v$ . The force  $Fz_4$  can, therefore, be neglected in comparison to the forces  $Fz_2$  and  $Fz_3$ . Similarly the force  $Fy_4$  is small in comparison to forces  $Fy_2$  and  $Fy_3$ .

Further, since the frequencies corresponding to the longitudinal vibrations are very large, the lower frequencies corresponding, mainly, to the motion in the  $y$  and the  $z$  directions would be, practically, insensitive to the changes in the damping type force in the longitudinal direction. Hence, the force  $Fx_4$  would not affect, appreciably, the first few natural frequencies of the blade.

For the reasons outlined above, the Coriolis forces are neglected in the present analysis. It may be mentioned here that this assumption is made in almost all the investigations for the vibration analysis of long rotating cantilevers and blades (References 49-51, 55-58, 62-64). Some studies of the effect of including the Coriolis forces have been reported in the literature and the conclusions reached are given below.

Lo (52) has shown that the percentage error in the first bending frequency due to the omission of Coriolis forces increases with the increase in parameter  $\bar{A}$ , defined as

$$\bar{A} = \frac{2 \sin \theta}{\sqrt{\frac{1}{\bar{\Omega}^2} + \cos^2 \theta}} \times \frac{\text{Amplitude}}{\text{Length}} \quad (4.59)$$

Even for  $\bar{A}$  as high as 0.4, the error introduced is less than 0.7%.

Analysing a simplified model representing a twisted blade, Isakson and Easley (47) have observed that the Coriolis forces produce large phase differences between the bending and the torsional vibrations but the natural frequencies are only slightly affected. This phase difference would, of course, be expected since the forces are velocity dependent.

The formulation of the problem, including the Coriolis forces, is given in Appendix II for any further extension of the present work.

The stiffness and the mass matrices of the elements are transformed to the common global axes, by the relations

$$\begin{aligned} [K_{et}] &= [T]^T [K'_{et}] [T] \\ [M_{ec}] &= [T]^T [M'_{ec}] [T] \\ [M_e] &= [T]^T [M'_e] [T] \end{aligned} \quad (4.60)$$

The transformation matrix  $[T]$  is defined by equation (3.31).

These matrices are grouped together, the rows and the columns corresponding to the nodes along the fixed edge are deleted, to give the final equation of motion in the form

$$[K]\{\delta\} = [M_c]\{\delta\} - [M]\{\ddot{\delta}\} \quad (4.61)$$

The matrices  $[K]$ ,  $[M_c]$  and  $[M]$  are the assembled matrices corresponding to the element matrices  $[K_{et}]$ ,  $[M_{ec}]$  and  $[M_e]$ , respectively. Assuming harmonic vibrations of circular frequency  $\omega_r$

$$\left[ \left( [K] - [M_c] \right) - \omega_r^2 [M] \right] \{\delta\} = \{0\} \quad (4.62)$$

which gives the natural frequencies and the mode shapes of the rotating blade. Since in the final equation the matrix  $[M_c]$  is to be deducted from the matrix  $[K]$ , these matrices need not be assembled separately; the subtraction could be carried out at the element level.



## CHAPTER 5

### CONVERGENCE AND ACCURACY OF THE METHOD

The finite element idealization introduces two fundamental approximations into the analysis. First, the set of flat triangular elements provides only an approximation to the smoothly curved surface of the blade. Thus the structure that is analysed differs slightly from the actual blade. Second, the stiffness properties of the individual elements are derived on the basis of an assumed set of displacement patterns within the elements; thus constraints are imposed on the manner of deformation of the blade. The chosen displacement functions, although satisfying the continuity of displacements along the interfaces between the adjacent elements, violate the transverse slope continuity along these interfaces.

Intuitively, as the size of the subdivision decreases, the errors due to both of these approximations would tend to vanish and the convergence to accurate results must occur. However, the finite element technique has not, as yet, been used sufficiently for the solution of practical shell vibration problems. It is, therefore, necessary to verify that the convergence does, in fact, occur in the present

type of problems. Further, a good rate of convergence, by itself, is not sufficient. It should, also, be verified that the convergence to the correct solution takes place. For this purpose, the solution to some problems, for which the analytical or experimental results are available, must be obtained for comparison.

In the present analysis, a new bending stiffness matrix for a triangular plate element is used. It is, therefore, necessary to demonstrate that this stiffness matrix is somewhat superior to the other existing matrices for triangular elements, with the same number of degrees of freedom per node.

In the presentation of the results the expression 'Mesh' is commonly used. If the length and the breadth of the shell are divided into  $m$  and  $n$  equal parts respectively, and the triangular elements are formed by dividing the small rectangles along a diagonal, such type of subdivision is termed as  $(m \times n)$  mesh. Also, unless mentioned otherwise, the value of Poisson's ratio is taken as 0.3 in all the computations.

The computer programmes (Appendices III and IV) are written in terms of nondimensional input and output parameters. The natural frequency is expressed as a non-dimensional quantity  $\beta$ , defined as

$$\beta = \omega L^2 \sqrt{\rho t_{\max} / D} \quad (5.1)$$

where  $L$  is the length and  $t_{\max}$  is the maximum thickness of the shell.  $D$  is the maximum flexural rigidity given by

$$D = Et_{\max}^3 / 12(1 - \mu^2) \quad (5.2)$$

The deflections are also expressed as nondimensional parameters. Thus the deflection ( $w$ ) in the  $z$  direction is expressed as  $\alpha_z$ , defined by

$$\alpha_z = wD / WL^2 \quad (5.3)$$

where  $W$  is the total applied load. The computations in terms of the actual dimensions are carried out only where it is necessary for the sake of comparison.

## 5.1 Bending Analysis

The convergence and the accuracy of the method are first tested for the deflection analysis of plates and shells. Three different problems are investigated, namely, a simply supported plate with central load, a clamped hyperbolic paraboloid shell carrying uniformly distributed load and a pretwisted cantilever plate subject to tip loads.

### 5.1.1 Simply Supported Plate

In order to compare the convergence characteristics of the present bending stiffness matrix with those of the other existing stiffness matrices for a triangular plate element, computations are carried out for a test problem of a square simply supported plate. The plate carries a central point



load  $W$ . The length and the breadth of the plate are divided into  $m$  equal parts. Due to symmetry only one quarter of the plate is considered. Triangular elements are formed by dividing each square into two parts along the diagonal which is parallel to the portion of the diagonal of the plate in that quarter, as shown in Figure (16).  $m$  is varied from 2 to 16 and the results obtained for the deflection at the point of application of the load are shown by the solid curve in Figure (17). The curves marked A, T, and Z are those for the nonconforming models described in References (125), (126) and (127), respectively. The curve marked HCT is for the conforming triangle of Reference (128). In all these models the same three degrees of freedom are assigned to each node, as in the present analysis.

It can be observed from Figure (17) that the deviation from the exact solution in the case of the present model is much less than for the other models, with the same number of degrees of freedom per element.

#### 5.1.2 Clamped Hyperbolic Paraboloid Shell

To verify that the method converges to the exact results in the problems of bending of shells, computations are carried out for a square hyperbolic paraboloid shell. This shape closely resembles a pretwisted plate when the angle of pretwist is small. The shell carries a uniformly distributed load in the  $z$  direction over its entire surface and is clamped

all along the boundary. The shell and the method of subdivision used are shown in Figure (18). The dimensions considered are  $L = b = 12.92"$ ,  $h = 1.304"$  and the thickness =  $0.25"$ .  $E$  and  $\mu$  are taken as  $5 \times 10^5$  psi and  $0.39$ , respectively, and the intensity of loading is taken as  $1$  psi. The equation of the middle surface of the shell is  $z = 4hxy/Lb$ . For this shell the analytical solution based on Bongard's shallow shell equations has been given in Reference (137). The shell is divided both lengthwise and breadthwise into  $m$  equal parts and computations carried out for  $m = 4, 6, 8$  and  $10$ . The values of the calculated central deflection of the shell are given in Table (1), along with the deviation from the exact value. It can be observed from this table that the method does tend to converge to the exact value.

As pointed out in the last paragraph of Section 3.3, the uniformly distributed load can be converted to nodal loads either by lumping or by consistency of virtual work. It has been mentioned in Reference (122) that for the shell problems lumping gives better results. The computations for the hyperbolic paraboloid shell are carried out both for the lumped and the consistent loads. As can be observed from Table (1), the consistent loads give somewhat better results. This is because the shell considered is sufficiently shallow and the arguments put forward in Reference (122) are valid mainly for shells with large rise.

TABLE 1

Central Deflection of Hyperbolic Paraboloid Shell

Exact value =  $8.708 \times 10^{-3}$  inches

Mesh	No. of Nodes (using symmetry along diagonals)	Lumped loading ( $w_1$ ) $\times 10^3$	Consistent Loading ( $w_2$ ) $\times 10^3$	Deviation of $w_2$ from exact value
4 × 4	4	10.233	10.025	15.20%
6 × 6	9	9.628	9.449	8.51%
8 × 8	16	9.330	9.160	5.19%
10 × 10	25	9.190	9.024	3.63%



To illustrate further the extent of the accuracy achieved, the exact deflection of the shell all along the x-axis, is compared with the values obtained by the present method, using  $(10 \times 10)$  mesh. A fairly good agreement between the two sets of deflections is observed from Figure (19).

### 5.1.3 Pretwisted Cantilever Plate

The problem of a square cantilever plate, pretwisted about the central longitudinal axis, is next considered. The pretwist varies uniformly over the length of the plate from zero at the fixed edge to a value  $\psi$  at the free edge. The computations are carried out for  $\psi$  varying from  $0^\circ$  to  $60^\circ$  in steps of  $20^\circ$ . The ratio of the length to the thickness of the plate is taken as 48. The plate carries two concentrated loads, each of magnitude  $W/2$ , at the two free corners C and D as shown in Figure (20). The method of subdivision used is also shown in the figure.

The deflections are calculated using  $(m \times m)$  mesh, with  $m$  increasing from 2 to 6. This corresponds to an increase in the number of nodal points from 6 to 42. The deflection in the z direction of point D for the different meshes is given in Table (2). It may be pointed out that similar convergence is obtained for the displacements in the x,y and the z directions of all the nodes. As is apparent from this table, the method gives a good rate of convergence, the change in the

TABLE 2

Nondimensional Deflection ( $\alpha_z$ ) of Point D ( $\alpha_z = wD/WL^2$ )

$\psi$ \ Nodes	6 (2 × 2)	12 (3 × 3)	20 (4 × 4)	30 (5 × 5)	42 (6 × 6)
0°	0.3710	0.3649	0.3619	0.3602	0.3592
20°	0.3753	0.3634	0.3569	0.3538	0.3522
40°	0.3747	0.3565	0.3476	0.3433	0.3411
60°	0.3726	0.3479	0.3372	0.3321	0.3293

value of the deflection being 1.53% when the number of nodes is increased from 20 to 30, and 0.84% when it is increased from 30 to 42, for a pretwist of  $60^\circ$ . For lower values of pretwist the convergence is still faster.

## 5.2 Vibration Analysis

Having verified that the present method of analysis gives a good rate of convergence and accuracy for the static problems, the next step is to carry out similar verification for the vibration problems. Several cases of twisted and untwisted cantilever plates, with and without taper, are studied. The rate of convergence in the case of rotating pretwisted plates is also investigated.

### 5.2.1 Nonrotating Cantilever Plates

For cantilever plates of constant thickness, the natural frequencies, using the Ritz energy method, have been obtained by Barton (77). The finite element solution for this problem, using triangular elements, has been given by Anderson et al. (80) and Jagannath (138). The former have used the nonconforming displacement function (Z) described in Reference (127); while the conforming function (HCT) of Reference (128) is used by the latter. The solution of this problem would not only test the accuracy of the present method but would also provide a comparison for the different



bending stiffness matrices for the triangular elements. Computations are carried out for plates having aspect ratios of 1 and 2 and the results are given in Table (3) along with the results of References (77,80 and 138). It may be emphasized that the present results and the results of References (80 and 138) are for identical mesh sizes.

The values obtained by the Ritz energy method provide an upper bound for the natural frequencies. A good bending stiffness matrix, therefore, should not give the natural frequencies higher than the corresponding values obtained by the Ritz method. A total of 10 natural frequencies, provided by the Ritz method, are considered in Table (3). It is observed that the results of HCT model are higher than the Ritz method values in 7 cases, the maximum overshoot being 3.35%. In the case of Z model, the frequencies exceed the Ritz values in 2 cases and the maximum overshoot is 1.13%. For the present model the Ritz value is exceeded in one case and even there the overshoot is only 0.18%. Further, if the maximum deviation (positive or negative) from the Ritz values is compared, for HCT model it is 3.37%, for Z model it is 2.86%, and for the present model it is 1.97%.

Computations are also carried out for three variable thickness cantilever plates. In the first case the plate is tapered in longitudinal direction; in the second case the cross-section of the plate is a trapezoid and in the third

TABLE 3

Nondimensional Frequencies ( $\beta$ ) of Cantilever Plates

(a) Aspect Ratio = 1

Mode Number	Ref.77 Ritz Method	Ref.80 Model (Z) (5×5)	Ref.138 Model (HCT) (5×5)	Present Method (5×5)
1	3.49	3.469	3.436	3.445
2	8.55	8.535	8.640*	8.516
3	21.44	21.450*	21.779*	21.181
4	27.46	27.059	28.147*	26.919
5	31.17	-	32.216*	31.052

(b) Aspect Ratio = 2

Mode Number	Ref.77 Ritz Method	Ref.80 Model (Z) (8×4)	Ref.138 Model (HCT) (8×4)	Present Method (8×4)
1	3.47	3.44	3.353	3.419
2	14.93	14.77	15.102*	14.831
3	21.26	21.50*	21.133	21.285*
4	48.71	48.19	49.974*	48.318
5	-	60.54	-	59.711
6	94.49	91.79	96.220*	92.929

\*The value is higher than that obtained by Ritz method.

TABLE 4

Nondimensional Frequencies ( $\beta$ ) of Tapered Cantilever Plates

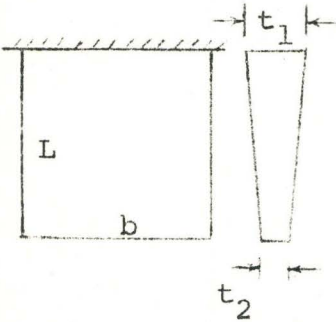
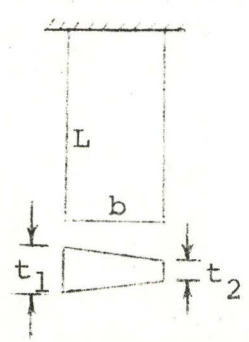
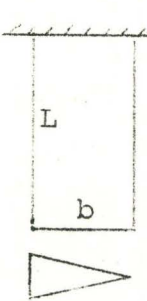
Problem	Mode Number	Calculated Frequency ( $\beta_c$ )	Experimental Frequency ( $\beta_e$ )	% Difference $\frac{100(\beta_c - \beta_e)}{\beta_c}$
 <p><math>L/b=1, t_2/t_1=0.259</math></p>		Mesh (5×5)	Ref. (79)	
	1	4.062	4.069	-0.17
	2	6.920	7.127	-2.99
	3	15.006	15.19	-1.23
	4	16.206	16.39	-1.13
 <p><math>L/b=2, t_2/t_1=0.307</math></p>		Mesh (8×4)	Ref. (79)	
	1	2.506	2.536	-1.20
	2	10.811	10.80	+0.10
	3	15.327	15.50	-1.13
	4	32.105	31.92	+0.58
 <p><math>L/b=2</math></p>		Mesh (8×4)	Ref. (139)	
	1	2.379	2.47	-3.83
	2	11.387	10.6	+6.91
	3	14.621	14.5	+0.83
	4	29.894	28.7	+3.99
	5	34.866	34.4	+1.34



plate the cross-section is an isosceles triangle. The experimental values of the natural frequencies have been obtained by Dawe (79) for the first two cases, and by Plunket (139) for the third case. The computed frequencies, along with the experimental results are given in Table (4). The two sets of results show reasonable agreement. The maximum difference (6.91%) between the calculated and the experimental frequency occurs in the second mode (torsional mode) for the plate with the triangular cross-section.

#### 5.2.2 Nonrotating Pretwisted Cantilever Plates

The convergence and the accuracy of the method are now tested for the problems of free vibrations of pretwisted cantilever plates, as this shape closely resembles a turbo-machinery blade. For testing the convergence, the first five natural frequencies of a square cantilever plate with a total pretwist ( $\psi$ ) of  $0^\circ$ ,  $40^\circ$  and  $80^\circ$  are calculated. In all the three cases the computations are carried out for mesh sizes  $(3 \times 3)$ ,  $(4 \times 4)$  and  $(5 \times 5)$ , i.e. for 12, 20 and 30 nodes, respectively. The results of computation are given in Table (5). A good rate of convergence is observed to exist for all the pretwist values considered. The largest difference between the frequencies obtained for mesh sizes  $(4 \times 4)$  and  $(5 \times 5)$  is 3.5% and occurs in mode three for pretwist of  $80^\circ$ . At lower values of pretwist, the deviation is considerably less.

TABLE 5

Nondimensional Frequencies ( $\beta$ ) of Pretwisted  
Cantilever Plates

$L/b=1.0$  ,  $b/t=16.0$

Pretwist ( $\psi$ )	Mode Number	Mesh (3×3) (12 nodes)	Mesh (4×4) (20 nodes)	Mesh (5×5) (30 nodes)
0°	1	3.418	3.435	3.445
	2	8.621	8.546	8.516
	3	21.500	21.264	21.181
	4	26.713	26.857	26.919
	5	31.699	31.262	31.052
40°	1	3.262	3.296	3.314
	2	16.524	16.669	16.676
	3	18.426	18.027	17.983
	4	28.092	28.528	28.151
	5	35.415	36.644	36.675
80°	1	2.967	3.011	3.034
	2	11.392	11.512	11.530
	3	24.785	25.885	25.016
	4	28.805	30.440	29.775
	5	34.363	37.801	38.684

To investigate the accuracy of the results, computations are carried out for a pretwisted cantilever plate of length 6 inches, breadth 1 inch and thickness 0.068 inches. For plate of these dimensions, the bending frequencies have been experimentally determined by Carnegie (16) for seven different values of pretwist angle ranging from  $0^\circ$  to  $90^\circ$ . Since the plate is sufficiently long, a mesh size of  $(10 \times 2)$  is employed. The variation of first three flexural frequencies with pretwist is shown in Figure (21), along with the experimental values. The material constants used in the calculations are those given by Carnegie and are mentioned in the figure.

The difference between the calculated and the experimental values for the first three bending frequencies is observed to be less than 5 percent for all the seven pretwist values. The experimental values are observed to be lower than the calculated values. This could be attributed to the fact that it is very difficult, in practice, to obtain a completely clamped edge and this would result in lower experimental values for the frequencies.

To investigate further the accuracy of the method, the natural frequencies are calculated for a tapered pretwisted cantilever plate. The cross-section of the plate is a narrow isosceles triangle with an apex angle of  $3.7^\circ$  as shown in Figure (22). The plate has an aspect ratio of 2 and is pretwisted about the central longitudinal line. The



pretwist varies uniformly from zero at the fixed edge of the plate to a value  $\psi$  at the free edge. For the plate of these dimensions, the natural frequencies have been experimentally determined by Plunket (139), for four different values of  $\psi$  ( $0^\circ$ ,  $11.6^\circ$ ,  $26^\circ$  and  $34.2^\circ$ ). The variation of the first six natural frequencies with pretwist is shown in Figure (22), along with the experimental results of Plunket. A mesh size of  $(7 \times 3)$  is used in the computations.

An examination of Figure (22) suggests that for lower values of pretwist the sixth natural frequency and for the higher values of pretwist the fifth natural frequency has been missed in the experimental investigation. It may be mentioned here that the possibility of having missed some of the frequencies is indicated in Reference (139). At lower values of pretwist, the sixth mode corresponds to the bending of the plate in the stiff direction. With the excitation in the direction normal to the plate surface, it is possible to miss this mode of vibration.

The largest difference (14.2%) between the experimental and the calculated value of frequency occurs in the third mode (fundamental torsion) for a pretwist of  $34.2^\circ$ . In all the other frequencies the difference is considerably smaller.

The possible reasons for the difference between the calculated and the experimental results are: (a) it is not possible, in practice, to have a completely clamped edge,

(b) the actual plate could not possibly have zero thickness along one edge, (c) the pretwist per unit length may not be constant along the length of the plate, (d) the triangular cross-section plate may not have the initial twist about the central longitudinal line and (e) the present method of analysis is only an approximate one and for more accurate results a finer mesh is necessary. Taking into account these possible sources of error, the experimental and the calculated frequencies compare reasonably well.

### 5.2.3 Rotating Cantilever Plates

In the preceding two sections, the convergence of the method has been tested for nonrotating plates. The major difference between the method used for the rotating plates and the one used for nonrotating plates is the inclusion of the additional stiffness due to the centrifugal effects. The centrifugal stiffness matrix depends on the in-plane stresses in the middle surface of the plate. In the actual case these stresses vary continuously over the plate. In the present analysis, however, linear expressions for in-plane displacements are used which yield constant stresses within each triangular element. When the number of elements increases, the stepped variation of the stresses is expected to correspond closely to the actual variation. A good rate of convergence can, therefore, be expected in the natural frequencies of the rotating plate as well.

In order to verify this, the first five natural frequencies of a square rotating cantilever plate are computed for mesh sizes (3×3), (4×4) and (5×5) at two different values of the rotational speed, the disc radius and the setting angle. The results are given in Table (6). Rotational speed and disc radius are expressed as nondimensional quantities  $\bar{\Omega}$  and  $\bar{r}$  respectively, defined as

$$\bar{\Omega} = \frac{\text{Speed of Rotation}}{\text{Fund.Freq.of the Nonrotating Plate}} \quad (5.4)$$

$$\bar{r} = \frac{\text{Radius of the Disc}}{\text{Length of the Plate}}$$

A good rate of convergence is observed to exist in both the cases. The maximum difference between the values of the natural frequencies obtained for (4×4) and (5×5) mesh is observed to be less than 1.6 percent.

#### 5.2.4 Rotating Pretwisted Cantilever Plates

The convergence of the method is also tested for a problem of rotating pretwisted cantilever plate. The aspect ratio of the plate is taken as 2 and the ratio of the breadth to the thickness is taken as 16. The pretwist varies uniformly from 0° at the root to 30° at the tip. The plate is mounted on a disc of radius equal to twice the length of the plate. The setting angle is taken as 90°, i.e. the breadth of the plate at the root is parallel to the axis of rotation of the disc. The natural frequencies are computed for mesh



TABLE 6

Nondimensional Frequencies ( $\beta_r$ ) of a Rotating  
Square Cantilever Plate

$\bar{\Omega}$	$\bar{r}$	$\theta$ (deg)	Mode No.	Mesh (3×3) (12 nodes)	Mesh (4×4) (20 nodes)	Mesh (5×5) (30 nodes)
1	0	0	1	5.091	5.094	5.097
			2	9.902	9.844	9.824
			3	23.182	23.016	22.913
			4	27.516	27.782	27.849
			5	33.133	32.847	32.735
2	1	45	1	10.826	10.790	10.771
			2	13.864	13.810	13.808
			3	29.247	29.212	29.127
			4	34.197	34.044	34.586
			5	38.127	41.495	41.228

TABLE 7

Nondimensional Frequencies ( $\beta_r$ ) of a Rotating Pretwisted  
Cantilever Plate

$$L/b=2.0, b/t=16.0, \psi=30^\circ, \bar{r}=2.0, \bar{\Omega}=1.0, \theta=90^\circ$$

Mode Number	Mesh (4×2) (12 nodes)	Mesh (5×3) (20 nodes)	Mesh (7×3) (28 nodes)
1	7.607	7.650	7.630
2	23.056	22.216	21.600
3	24.537	24.289	23.919
4	54.774	55.331	54.448
5	58.535	60.006	59.853

sizes (4×2), (5×3) and (7×3). For this pretwisted plate the fundamental frequency in the nonrotating case is

$$\omega_1 = \frac{3.383}{L^2} \sqrt{\frac{D}{\rho t}} \quad (5.5)$$

Computations are carried out for rotational speed equal to this fundamental frequency, i.e. for  $\bar{\Omega} = 1$ .

The results of computation are given in Table (7). A reasonably good convergence is obtained. The largest difference between the natural frequencies obtained for (5×3) and (7×3) meshes is 2.85%.

The results for all the different problems considered in this chapter indicate that the method converges to the correct solutions quite rapidly and reliable results are obtained when the number of nodes is greater than 25 and the number of triangular elements is about 40 or more. Further, for good results the triangular elements should not be long and narrow; i.e. the mesh size must be so chosen that the blade surface is divided, approximately, into squares.



## CHAPTER 6

### RESULTS AND DISCUSSION

The effect of different parameters, such as the amount of pretwist, the speed of rotation, the radius of the disc and the setting angle, on the natural frequencies and the mode shapes of a low aspect ratio blade are now investigated. The blade is idealized as a pretwisted cantilever plate of constant thickness. The pretwist increases uniformly along the length from zero at the root to a value  $\psi$  at the tip. In most of the cases the computations are carried out for aspect ratios of 1, 2 and 3. A study is made of the manner in which the known results for long blades, idealized as pretwisted cantilever beams, are approached with the increase in the aspect ratio. The results of the deformation of a pretwisted cantilever plate due to tip loading are also included; as this provides some insight into the deflected shape.

#### 6.1 Deflection of Pretwisted Cantilever Plate due to Tip Loading

The deflections are calculated for a square pretwisted cantilever plate subjected to two concentrated loads  $W/2$  as shown in Figure (20). The breadth to thickness ratio of the plate is taken as 48 and a (6×6) mesh is used.

Computations are carried out for values of  $\psi$  from  $0^\circ$  to  $90^\circ$  in steps of  $10^\circ$ . The deflections at the points of application of the loads (points C and D) and at the mid point of the free edge (point A) are given in Table (8). Two values of deflection are given for each point; one is the deflection along the z-axis (direction of the loads) and the other is the total deflection  $\sqrt{u^2+v^2+w^2}$  of the point. It may be pointed out that the slight difference in the values of deflections of points C and D is, probably, due to the unsymmetrical shape of the subdivision used (Figure 20).

It can be observed from Table (8) that the total deflection at the midpoint of the free edge is only slightly affected by the pretwist. It increases initially with the increase in the pretwist till a maximum occurs at a pretwist of approximately  $45^\circ$ . It then decreases with further increase in the value of  $\psi$ . A more important information is obtained from the results of the total deflections of the points of application of the loads. The total deflection is observed to increase considerably with the increase in the value of  $\psi$ . This suggests that the bending stiffness of the plate decreases with the increase in the pretwist. Thus, the first few bending frequencies of a thin pretwisted plate can be expected to be lower than the corresponding frequencies of the untwisted plate.

The variation of the deflection ( $w$ ) in the z-direction



TABLE 8

Deflections of Pretwisted Cantilever Plate due to Tip Loads.

Pretwist $\psi$ (Degrees)	L/b=1.0		b/t=48.0		Mesh (6x6)	
	Deflection of Point C		Deflection of Point A		Deflection of Point D	
	$wD/WL^2$	$\sqrt{u^2+v^2+w^2} D/WL^2$	$wD/WL^2$	$\sqrt{u^2+v^2+w^2} D/WL^2$	$wD/WL^2$	$\sqrt{u^2+v^2+w^2} D/WL^2$
0	0.359	0.359	0.333	0.333	0.359	0.359
10	0.355	0.357	0.335	0.335	0.357	0.359
20	0.350	0.357	0.337	0.338	0.352	0.359
30	0.345	0.359	0.337	0.339	0.347	0.361
40	0.340	0.363	0.336	0.340	0.341	0.365
50	0.334	0.368	0.332	0.339	0.335	0.370
60	0.329	0.375	0.328	0.338	0.329	0.376
70	0.323	0.380	0.323	0.336	0.323	0.381
80	0.316	0.383	0.316	0.331	0.316	0.383
90	0.310	0.385	0.310	0.328	0.310	0.385



along the longitudinal line FD of the plate is shown in Figure (23). Figure (24) is the plot of the deflection  $w$  along the free edge CD for different pretwist angles; and shows the anticlastic curvature obtained.

## 6.2 Vibration of Nonrotating Pretwisted Cantilever Plates

To investigate the effect of variation in pretwist and aspect ratio on natural frequencies and mode shapes of cantilever plates, computations are carried out for plates having aspect ratios of 1, 2 and 3. The total pretwist in the plate is varied from  $0^\circ$  to  $90^\circ$  in steps of  $10^\circ$ . A linear variation of pretwist along the length of the plate is assumed. The ratio of the breadth to the thickness of the plate is taken as 16. For unity aspect ratio,  $5 \times 5$  mesh (30 nodes) is used; whereas for aspect ratios of 2 and 3 a mesh of  $7 \times 3$  (28 nodes) is employed. The variation of the first five natural frequencies with pretwist is shown in Figures (25), (26) and (27) for the three aspect ratios considered. Markings B and T on the curves indicate the bending and the torsional modes, respectively. The curve marked 2L in Figure (25) is for the vibration mode with two longitudinal nodal lines. The variation of the first and the second bending frequencies, for all the three aspect ratios, are shown on enlarged scale in Figure (28). Figure (29) shows the first five mode shapes, obtained for

unity aspect ratio, at different pretwist values. These modes appear in increasing order of frequency. The mode shapes are based on displacements in the z-direction alone. For convenience of drawing, the plate has been shown as if it was unfolded. For pretwist of  $40^\circ$ , the second and the third mode shapes may not be very accurate, as the corresponding frequencies are very near to each other (Figure 25) and the Power method cannot be expected to give the eigenvectors accurately under these circumstances. For the other two aspect ratios, the mode shapes resemble closely to those of pretwisted beams and are, therefore, not included.

#### 6.2.1 Mode with Two Longitudinal Nodal Lines

In the vibration analysis of beams, three types of vibration modes are considered - bending along the major and the minor principal axes of inertia and torsion. If a beam is pretwisted the two bending modes get coupled. Examination of the mode shapes, for unity aspect ratio (Figure 29), shows the presence of an additional mode, appearing fourth in order of increasing frequency for all values of pretwist considered. This mode has two nodal lines (no displacement in z-direction) almost parallel to the length of the plate. This mode cannot be predicted in a beam type analysis. The frequency associated with this mode increases with an increase in the value of pretwist. For the pretwisted



plate of aspect ratio 2, it appears as seventh mode. For an aspect ratio greater than 2, the frequency associated with this mode is considerably high and, therefore, is not of much practical importance.

### 6.2.2 Bending Frequencies

The variation of the fundamental bending frequency for the pretwisted cantilever plates of aspect ratios of 1, 2 and 3 is shown in Figure (28). The frequency of the plate having aspect ratio equal to 3 is virtually unaffected by pretwist; whereas for lower aspect ratios it decreases with an increase in the value of  $\psi$ . Pretwisting the plate by  $90^\circ$  decreases the fundamental frequency by 14% when the aspect ratio is 1 and by 3.4% when the aspect ratio is 2. For aspect ratio of 3 the frequency increases by 0.3%. Analysing the fundamental frequency of pretwisted cantilever beams by the Rayleigh-Ritz method, Dawson (33) has shown that for  $b/t=16$ , this frequency increases by 2% due to an increase of pretwist from  $0^\circ$  to  $90^\circ$ .

It is observed from Figure (28) that the fundamental frequency for  $\psi = 0^\circ$  is somewhat higher for the plate of aspect ratio of unity. However, as the pretwist increases, the frequency of this plate decreases rapidly and for  $\psi$  greater than  $25^\circ$  the value falls below the values for aspect ratios of 2 and 3.



The second bending frequency corresponds to the mode with one nodal line parallel to the fixed edge of the pretwisted plate. The variation of this frequency with the pretwist is shown in Figure (28), for all the three aspect ratios considered. The second bending frequency is observed to decrease considerably with an increase in the pretwist. Increasing the value of  $\psi$  from  $0^\circ$  to  $90^\circ$  decreases the second bending frequency by 51%, 46% and 45% for aspect ratios of 1, 2 and 3, respectively. For pretwisted cantilever beam of the same breadth to thickness ratio ( $b/t=16$ ), Dawson (33) has shown that this frequency decreases from  $6.36 \omega_0$  to  $3.53 \omega_0$  (44.5%), when the pretwist increases from  $0^\circ$  to  $90^\circ$ .  $\omega_0$  is defined as the fundamental frequency of the beam when  $\psi=0^\circ$ .

If an untwisted cantilever beam of breadth to thickness ratio of 16 is considered, the third bending mode would correspond to the fundamental bending in the stiff direction and would have a natural frequency of  $16 \omega_0$ . The fourth bending frequency would correspond to the third bending mode in the flexible direction (two nodal lines parallel to the fixed edge). The frequency of this mode would be  $17.53 \omega_0$ . Since these two frequencies are close to each other, strong coupling occurs between them, when the beam is considered pretwisted. The effect of pretwist on the bending vibrations of cantilever beams of  $b/t=16$  has been studied by Slyper (38) using the Stodola method and also by Dawson (33)

using the Rayleigh-Ritz method. It is shown that the third bending frequency decreases with pretwist, whereas the fourth bending frequency increases.

The variation of the third and the fourth bending frequencies for the pretwisted cantilever plates is shown in Figures (26) and (27), for aspect ratios of 2 and 3, respectively. As in the case of cantilever beams, the effect of pretwist is to separate the two frequencies farther apart. However, the separation between the two curves is observed to be more for the plate with  $L/b=3$  than for the plate with  $L/b=2$ . The ratio of the fourth to the third bending frequency at  $\psi=90^\circ$  is 1.88 in the case of  $L/b=2$  and 2.00 in the case of  $L/b=3$ . The corresponding value given by Dawson (33) for pretwisted cantilever beams is 1.98 ( $26.83 \omega_0 / 13.58 \omega_0$ ), which differs by only 1% from the value for the aspect ratio of 3. For the plate having  $L/b=1$ , the fourth bending frequency does not fall within the first six modes that are investigated.

A comment may be made here about the nature of the curve for the third bending frequency for the plate having  $L/b=1$  (Figure 25). The nature of this curve is observed to be different from that of the corresponding curves (3B) for the plates having  $L/b=2$  and 3 (Figures 26 and 27). A probable reason for this is that the bending in the stiff direction of such a wide plate is accompanied by a larger



deformation in the flexible direction. This results in a much lower value for the frequency. The pretwist tends to decrease the deformation in the flexible direction and thus increases the value of the frequency, till it becomes sufficiently high to produce coupling with the fourth bending frequency. Thereafter the behaviour is identical to the one exhibited by long plates. In Figures (25), (26) and (27), the curves for the third bending frequency are drawn dotted between the pretwist values of  $0^\circ$  and  $10^\circ$ . This is due to the fact that this frequency cannot be obtained in the calculations for the untwisted plate, because of the deletion of the in-plane degrees of freedom when  $\psi=0^\circ$ .

For pretwisted cantilever beams it is customary to express the natural frequencies as 'frequency ratios'. The frequency ratio ( $f_n$ ) for the  $n^{\text{th}}$  bending mode, at a particular value of pretwist is defined as

$$f_n = \frac{\text{Frequency of the } n^{\text{th}} \text{ bending mode}}{\text{Fundamental bending frequency for } \psi=0} \quad (6.1)$$

In Table (9) the frequency ratios are given for plates having aspect ratios of 1, 2 and 3 at  $\psi=60^\circ$ . The corresponding values for the pretwisted cantilever beam are also included for comparison. The manner in which the beam values are approached with an increase in the aspect ratio is clearly indicated by these results. All the frequency ratios are observed to decrease with a decrease in the aspect ratio of



TABLE 9

Bending Frequency Ratios of Pretwisted Cantilever Plates

$\psi=60^\circ$   $b/t=16.0$

Aspect Ratio	$\frac{\text{Freq. of Mode 1B}}{\text{Fund. Freq. for } \psi=0}$	$\frac{\text{Freq. of Mode 2B}}{\text{Fund. Freq. for } \psi=0}$	$\frac{\text{Freq. of Mode 3B}}{\text{Fund. Freq. for } \psi=0}$	$\frac{\text{Freq. of Mode 4B}}{\text{Fund. Freq. for } \psi=0}$
1	0.924	4.043	12.079	-
2	0.979	4.256	14.039	21.408
3	1.001	4.422	14.934	24.660
Beam*	1.01	4.43	14.99	26.61
Beam**	1.01	4.41	15.02	26.59

\* Reference (35)

\*\* Reference (33)

the plate. For  $L/b=1$ , the frequency ratios for the first and the second bending modes differ from the beam values by approximately 9.5%; whereas for the third bending mode the difference is about 24%. The frequency ratios for  $L/b=3$  are, more or less, the same as obtained for the beam, except for the fourth mode, where the values differ by approximately 8%.

It could, therefore, be concluded that the pretwisted cantilever plates having aspect ratio higher than three may be treated as pretwisted beams without any appreciable error in the first few bending frequencies.

### 6.2.3 Torsional Frequencies

The torsional frequencies increase rapidly with pretwist for all the aspect ratios considered; as can be seen from Figures (25), (26) and (27). Increasing the value of  $\psi$  from  $0^\circ$  to  $30^\circ$  increases the first torsional frequency by 69.5%, 51.7% and 35.6% for plates having aspect ratios of 1, 2 and 3, respectively. The corresponding increase in the second torsional frequency is considerably less. The increase in the torsional frequencies with pretwist is very sensitive to the breadth to thickness ratio of the plate and the values given here are for  $b/t=16$ .

In Figures (25), (26) and (27) the curves for the torsional frequencies are drawn so as to cross the bending

frequency curves. In the present analysis, the frequencies are obtained as eigenvalues of the matrix  $[K^{-1}][M]$  by the Power method. Obviously, the computations could not be carried out for the exact value of  $\psi$  at which the two frequencies are identical. However, computations are carried out for points very close to this value of pretwist on either side and natural frequencies differing by as little as 0.5% are obtained. Further, the nature of the mode shapes obtained on either side of the critical pretwist suggests that the two curves cross each other.

The crossing of the curves for the bending and the torsional modes indicates that the coupling between these modes is negligible. This would, of course, be expected; since the shear centre and the centroid coincide for a rectangular section. In the case of pretwisted beams of rectangular section, the equations of motion for the bending and the torsional vibrations are separate and uncoupled. For certain values of  $\psi$ , therefore, the beam possesses identical frequencies corresponding to these two modes. In the case of plates, there is only a single equation of motion involving the deflection normal to the plate surface. Even then, for cantilever plates, there exist identical frequencies for the bending and the torsional modes for certain values of  $L/b$ , when the plate is of uniform thickness. This has been shown by Plunket (139).



Gladwell (140) has shown that in the case of free vibration of a system with  $N$  degrees of freedom, there are always  $N$  mutually orthogonal principal modes, whether the natural frequencies are all different or not. In the present analysis, the finite element technique reduces the problem of the pretwisted plate to a multidegree freedom system. The modes would, therefore, be orthogonal; even when the two frequencies are identical.

In Figure (25) the curve for the first torsional frequency (1T), for a plate having  $L/b=1$ , is observed to flatten out at higher values of pretwist. This is attributed to the presence of the additional mode (2L) with two longitudinal nodal lines, in the neighbourhood of the torsional frequency. For higher aspect ratios the mode 2L does not occur in the vicinity of the first torsional mode and, therefore, no such flattening is observed in Figures (26) and (27). Thus for low aspect ratio plates ( $L/b < 2$ ), the torsional frequencies cannot be considered as completely uncoupled; even when the cross-section is rectangular. Even though there is no coupling with the regular bending modes, there is a possibility of coupling between a torsional mode (one longitudinal nodal line) and the additional mode with two longitudinal nodal lines. As  $b/t$  increases, the torsional frequency increases more rapidly with pretwist, resulting in a stronger coupling with the mode 2L.

In order to study further the coupling between the modes 1T and 2L, computations are carried out for a very thin square cantilever plate ( $b/t=48$ ). The variation of the frequencies with pretwist is shown in Figure (30) and the corresponding mode shapes in Figure (31). As in the previous case (Figure 29), the mode shapes are based on the deflection in the  $z$  direction and the plate is drawn as if it was untwisted. Since in this case  $b/t$  is large, the third bending mode corresponds to two nodal lines parallel to the fixed edge. The curves for the torsional modes are observed to cross those for the regular bending modes (2B and 3B). The strong coupling between the modes 1T and 2L is evident from the fact that the two curves do not cross each other. Initially the frequency of mode 1T increases and the frequency of mode 3B decreases with an increase in pretwist. This trend continues till the two frequencies are close to the value of the frequency for the mode 2L. At this point the trend of the frequency curves is observed to change rather abruptly. The curve for the mode 3B becomes the curve for the first torsional mode and vice-versa. In this case the coupling occurs approximately at  $\psi=45^\circ$ , and in that region the mode shapes are too complex to recognize.

### 6.3 Vibration of Rotating Cantilever Plates

The natural frequencies and the mode shapes are computed for plates of three different aspect ratios (1,2



and 3), for various values of the nondimensional speed of rotation ( $\bar{\Omega}$  from 0 to 3), and the nondimensional radius of the disc ( $\bar{r}$  from 0 to 5) and the setting angle ( $\theta$  from  $0^\circ$  to  $90^\circ$ ). The nondimensional quantities  $\bar{\Omega}$  and  $\bar{r}$  are defined by equation (5.4). The mesh sizes used for the plates having aspect ratios of 1, 2 and 3 are  $(5 \times 5)$ ,  $(8 \times 4)$  and  $(10 \times 3)$ , respectively. The variation of the first five natural frequencies with the speed of rotation is shown in Figures (32), (33) and (34) for the three different aspect ratios, both for  $0^\circ$  and  $45^\circ$  setting angle. The variation of the natural frequencies with the radius of the disc is shown in Figures (35), (36) and (37). The markings B and T on the curves indicate the bending and the torsional modes of vibration respectively, while the marking 2L is for the mode with two longitudinal nodal lines. The mode shapes for the plate of unity aspect ratio, at different speeds of rotation, are shown in Figure (38).

All the natural frequencies are observed to increase with the speed of rotation and with the increasing radius of the disc. An increase in the setting angle causes a decrease in the natural frequencies. In Figure (34) the curves for the bending frequencies are observed to cross the curves for the torsional frequencies without any appreciable change in their nature. This suggests that the rotating speed does not produce any significant coupling between the bending and



the torsional modes of vibration. An examination of the mode shapes for the plate of unity aspect ratio (Figure 38) shows that the mode shape corresponding to the second bending frequency (2B) and the one with two longitudinal nodal lines (2L) are considerably affected by the rotating speed. As can be observed from Figure (32), the nature of the curves corresponding to these two modes of vibration is also appreciably affected when the two frequencies are close to each other. This indicates that the rotational speed produces significant coupling between these two modes of vibration. At higher values of aspect ratio the frequency associated with the mode 2L is too high and, hence, is not of much practical importance.

### 6.3.1 Southwell Coefficients

The natural frequency of a rotating cantilever beam ( $\omega_r$ ) is generally expressed as a function of the corresponding frequency of the nonrotating beam ( $\omega$ ) and the speed of rotation, in the form

$$\omega_r^2 = \omega^2 + S\Omega^2 = \omega^2 + (S_0 + S_r + S_\theta)\Omega^2 \quad (6.2)$$

The component  $S_r$  of the Southwell coefficient ( $S$ ) depends only on the radius of the disc and vanishes for  $r=0$ .

Similarly the component  $S_\theta$  is a function of the setting angle only, vanishing at  $\theta=0$ . The component  $S_0$  is independent of  $r$  and  $\theta$ . For rotating beams the approximate expressions for the Southwell coefficients, for different modes of

vibration, are available in the literature (References 55-58, 65). These expressions are very useful for the rapid estimation of the natural frequencies of rotating beams.

In the present analysis the natural frequencies of rotating plates are computed for numerous values of  $\Omega$ ,  $r$  and  $\theta$  for aspect ratios of 1, 2 and 3. It is worthwhile trying to fit these results of the computed frequencies in relations of the form of equation (6.2) and obtain the Southwell coefficients for different aspect ratios. The results presented in this form should be more useful, from practical considerations, than a long table of natural frequencies, at various values of the parameters. Also the trend of these computed expressions for  $S$  to approach the known values for the cantilever beam, when the aspect ratio is high, should provide a good test for the reliability of the method of analysis and the results.

Briefly, the method used for determining the expressions for  $S$  is as follows: The values of  $r$  and  $\theta$  are first taken as zero and the natural frequencies are computed for various values of  $\Omega$ . The value of  $S_0$  is determined by the direct search method in such a manner that the maximum percentage difference between the actual computed value of  $\omega_r$  and the value obtained by using equation (6.2), for any of the values of  $\Omega$ , should be as small as possible. For determining  $S_r$ , the natural frequencies at different values



of  $r$  are calculated keeping  $\theta=0$  and  $\Omega$  at a fixed value. Similarly for finding  $S_\theta$ ,  $r$  and  $\Omega$  are kept constant and frequencies computed at different values of  $\theta$ .

The expressions for  $S_0$ ,  $S_r$  and  $S_\theta$  for plates of different aspect ratios are given in Tables (10), (11), (12), (13) and (14) for modes 1B, 2B, 3B, 1T and 2T, respectively. The corresponding known expressions for a cantilever beam are also included in the tables, to illustrate the manner in which the beam values are approached with an increase in the aspect ratio. The mode (2L) with two longitudinal nodal lines is within the first five modes of vibration only for aspect ratio of unity. The Southwell coefficient for this case comes out to be

$$S = 3.985 + 1.544 \bar{r} + 0.729 \bar{r}^2 - 3.839 \sin^2 \theta \quad (6.3)$$

(Mode 2L for  $L/b=1$ )

For the bending modes of rotating cantilever beams, the values of  $S_0$  are given as constants, not depending on the speed of rotation (References 55 and 58). In the present analysis for rotating cantilever plates, this is observed to be the case for the second and the third bending frequencies, i.e the modes with one and two nodal lines parallel to the fixed edge of the plate. However, for the fundamental bending mode, it is observed that the value of  $S_0$  decreases somewhat with the speed of rotation. For this mode, a better fit is obtained by including a small



TABLE 10

Southwell Coefficient for Fundamental Bending Mode

Aspect Ratio	$S_0$	$S_r$	$S_\theta$
1	$1.190 - 0.0069\bar{\Omega}^2$	$1.571\bar{r} - 0.0045\bar{r}^2$	$-1.0008 \sin^2 \theta$
2	$1.187 - 0.0066\bar{\Omega}^2$	$1.560\bar{r} - 0.0045\bar{r}^2$	$-1.0001 \sin^2 \theta$
3	$1.186 - 0.0066\bar{\Omega}^2$	$1.558\bar{r} - 0.0048\bar{r}^2$	$-1.0000 \sin^2 \theta$
Beam* (Ref.55)	1.184	$1.564\bar{r}$	$-\sin^2 \theta$
Beam** (Ref.58)	1.175	$1.556\bar{r}$	$-\sin^2 \theta$

\*  $\bar{\Omega}$  is assumed to be small in Reference (55)

\*\* Equation (35) of Reference (58) can be modified to this form

TABLE 11

Southwell Coefficient for Second Bending Mode

Aspect Ratio	$S_0$	$S_r$	$S_\theta$
1	6.61	$8.74\bar{r} - 0.754\bar{r}^2$	$-1.273 \sin^2 \theta$
2	6.50	$8.73\bar{r} - 0.027\bar{r}^2$	$-1.004 \sin^2 \theta$
3	6.50	$8.65\bar{r} - 0.018\bar{r}^2$	$-1.002 \sin^2 \theta$
Beam (Ref.57)	6.5 (approx)*	$8.2\bar{r}$ (approx)**	$-\sin^2 \theta$

\* Obtained from Figure 18 of Reference (57)

\*\* Obtained from Figure 16 of Reference (57)

TABLE 12

## Southwell Coefficient for Third Bending Mode

Aspect Ratio	$S_0$	$S_r$	$S_\theta$
1	16.84	$25.27\bar{r} - 0.512\bar{r}^2$	$-1.065 \sin^2\theta$
2	17.11	$24.65\bar{r} - 0.261\bar{r}^2$	$-1.037 \sin^2\theta$
3	17.58	$24.61\bar{r} - 0.082\bar{r}^2$	$-1.021 \sin^2\theta$
Beam (Ref.57)	18 (approx)*	$22.3\bar{r}$ (approx)**	$-\sin^2\theta$

\*Obtained from Figure 18 of Reference (57)

\*\*Obtained from Figure 16 of Reference (57)

TABLE 13

## Southwell Coefficient for First Torsional Mode

Aspect Ratio	$S_0$	$S_r$	$S_\theta$
1	2.003	$1.468\bar{r}$	$-1.979 \sin^2\theta$
2	2.001	$1.504\bar{r}$	$-1.995 \sin^2\theta$
3	1.967	$1.515\bar{r}$	$-1.997 \sin^2\theta$
Beam* (Ref 65)	$\frac{b^2-t^2}{b^2+t^2} + 1$	$1.562\bar{r}$	$-2\frac{b^2-t^2}{b^2+t^2} \sin^2\theta$

\*Equation (12) of Reference (65) can be expressed in this form for a beam of rectangular cross-section and having no initial twist.

TABLE 14

Southwell Coefficient for Second Torsional Frequency

Aspect Ratio	$S_0$	$S_r$	$S_\theta$
1	7.22	$8.35\bar{r}$	$-1.907 \sin^2 \theta$
2	7.82	$9.76\bar{r}$	$-1.958 \sin^2 \theta$
3	8.14	$10.89\bar{r}$	$-1.964 \sin^2 \theta$
Beam	Not Available	Not Available	Not Available



term proportional to  $\bar{\Omega}^2$  in the expression for  $S_0$ , as given in Table (10). It may be pointed out that in the analysis of rotating cantilever beams given in References (55 and 58),  $\bar{\Omega}$  is assumed to be small; the quadratic term  $\bar{\Omega}^2$ , therefore, does not appear in such analysis.

The expression for the component  $S_r$  of the Southwell coefficient is given as a linear function of  $\bar{r}$  in the analysis for rotating beams (References 55, 57, 58 and 65). For the bending modes of rotating cantilever plates, it is observed that a much better fit is obtained by taking the expression for  $S_r$  in the form  $S_1\bar{r} + S_2\bar{r}^2$ . The values of the constants  $S_1$  and  $S_2$  for the different modes are given in Tables (10), (11) and (12).

The value of  $S_\theta$  for the bending modes of a rotating cantilever beam is  $-\sin^2\theta$ . For the bending modes of rotating cantilever plates,  $S_\theta$  is given by  $-S_3\sin^2\theta$ . The value of  $S_3$  is observed to be somewhat higher than 1 and increases with a decrease in the  $L/b$  ratio (Tables 10, 11 and 12). For the torsional modes the value of  $S_3$  is observed to approach 2 with the increase in the value of  $L/b$  (Tables 13 and 14).

The values of  $S_0$  and  $S_\theta$  for the first torsional mode of a rotating cantilever beam depend on the  $b/t$  ratio of the beam (Table 13). As  $b/t$  ratio increases,  $S_0$  and  $S_\theta$  approach the values 2 and  $-2\sin^2\theta$ , respectively. In the present analysis for rotating cantilever plates, all the

results for the nondimensional frequencies and the Southwell coefficients are independent of the  $b/t$  ratio of the plate. It may be added that the quantity  $b/t$  has to be large to justify the plate type analysis.

In all cases the Southwell coefficients for the plates of aspect ratio of 3 are very close to the values for the cantilever beams. It can, therefore, be concluded that the rotating plates having aspect ratio greater than 3 may be treated as rotating beams without any appreciable error in the natural frequencies.

The Southwell coefficients given in Tables (10) to (14) along with equation (6.2) can be used for the rapid estimation of the natural frequencies of rotating cantilever plates, for any value of the radius of the disc, the setting angle and the speed of rotation. Within the range of these parameters considered in the present investigation, these approximate frequencies are observed to be within 2 percent of the actual computed frequencies. An exception must, however, be made for the modes 2B and 2L for the aspect ratio of unity. In this case when the values of  $r$ ,  $\Omega$  and  $\theta$  are such that the frequencies corresponding to these two modes are close to each other, the approximate values of frequencies obtained from equation (6.2) may show somewhat higher deviation from the actual frequencies. The range of the parameters  $r$ ,  $\Omega$  and  $\theta$  investigated here should normally cover all practical cases



encountered in the present day turbomachinery blading.

#### 6.4 Vibration of Rotating Pretwisted Cantilever Plates

In a rotating pretwisted plate, the centrifugal forces produce certain pseudo-static deformation and the vibrations of the plate occur about the deformed configuration. The method described in Section 4.2 is used to study the nature and the amount of the pseudo-static deformation and the effect of rotation on the natural frequencies of pretwisted cantilever plates. The computations are carried out for a plate having  $L/b=2$  and  $b/t=16$ . The radius of the disc is taken to be twice the length of the plate ( $\bar{r}=2$ ).

##### 6.4.1 Pseudo-Static Deformation

To investigate the effect of the pretwist ( $\psi$ ) and the setting angle at the root ( $\theta$ ) on the deformation produced by the centrifugal forces, computations are carried out for values of  $\psi$  from  $-45^\circ$  to  $+45^\circ$  and in each case the value of  $\theta$  is varied from  $45^\circ$  to  $90^\circ$ . A mesh size of  $(8 \times 4)$  is used.

The results for the pseudo-static deformation are obtained in the form of nodal displacements. Examination of these results reveals that the plate, in effect, undergoes a torsional deformation through an angle  $\phi$ , in addition to a



small longitudinal displacement. In the deformed configuration, therefore, the plate possesses a total twist of  $\psi + \phi$ . In the present analysis the positive directions for  $\psi, \theta$  and  $\phi$  are as shown in Figure (39). The variation of the pseudo-static torsional deformation ( $\phi$ ) with the amount of pretwist in the plate is shown in Figure (40), for different values of the setting angle. Although, the nature of the variation is observed to be quite complex, several conclusions can be drawn regarding the value of the torsional deformation.

Except for the case when the magnitude of the pretwist is very small (say less than  $10^\circ$ ),  $\phi$  is observed to be negative for the positive values of  $\psi$  and vice-versa; which means that the centrifugal forces tend to untwist the plate.

The values of  $\phi$  are identical for positive and negative values of pretwist only for  $\theta = 90^\circ$ . This would, of course, be expected since for  $\theta = 90^\circ$  a change in the sign of  $\psi$  does not alter the basic problem, for the case of rectangular cross-section plates. The same would also be true for  $\theta = 0^\circ$ . In the range of the values of  $\theta$  and  $\psi$  considered, the torsional deformation is observed to be larger when both  $\theta$  and  $\psi$  have the same sign, than in the case when they have opposite sign. Thus, for  $\theta = 45^\circ$  the value of  $\phi / \bar{\Omega}^2$  is approximately  $-4^\circ$  when  $\psi = 20^\circ$  and the corresponding value for  $\psi = -20^\circ$  is only about  $1.4^\circ$ .

In the case of positive pretwist, the torsional

deformation is found to increase when  $\theta$  is decreased from  $90^\circ$  to  $45^\circ$ ; also the value of  $\psi$  at which the maximum occurs is observed to decrease. For values of pretwist between  $-15^\circ$  and  $-45^\circ$  the torsional deformation is observed to be practically the same for values of  $\theta$  lying between  $45^\circ$  and  $75^\circ$ . This may be of some importance, since many of the turbomachinery blades have values of  $\theta$  and  $\psi$  in this region.

The present analysis indicates that under certain combinations of  $\psi$  and  $\theta$ , the pseudo-static torsional deformation can be significant and must be accounted for.

#### 6.4.2 Natural Frequencies

In order to study the effect of the pretwist and the speed of rotation on the natural frequencies, a cantilever plate of aspect ratio equal to 2 and  $b/t=16$  is analysed. The radius of the disc is taken as twice the length of the plate ( $\bar{r}=2$ ) and the setting angle is taken as  $90^\circ$ . In the computations, a mesh size of  $(7 \times 3)$  is used. The variation of the natural frequencies with the angle of pretwist, for a constant speed of rotation ( $\bar{\Omega}=1$ ), is shown in Figure (41). The effect of changing the speed of rotation on the natural frequencies is shown in Figure (42) for a plate having  $\psi=30^\circ$ . The natural frequencies for this plate are also computed neglecting the pseudo-static deformation, in order to investigate the effect of this deformation on the natural



frequencies.

An examination of Figure (41) shows that the torsional frequency curves cross the bending frequency curves as in the case of nonrotating pretwisted blades. Thus, the rotation does not produce any appreciable coupling between the torsional and the bending motions when the plate is of uniform thickness. This observation is already known to be valid for rotating pretwisted beams; where the analysis for the bending and the torsional vibrations is carried out separately (References 64 and 66).

In Table (15), the effect of pretwist on the natural frequencies of a rotating plate is compared with the corresponding effect on the frequencies of the nonrotating plate. In both the cases, the first two bending frequencies are observed to decrease with increasing pretwist; while the torsional frequencies increase with the pretwist. With an increase in the value of  $\psi$ , the fundamental frequency decreases faster in the rotating case than in the case of the nonrotating plate. The percentage decrease in the second bending frequency is observed to be practically the same in both the cases.

With increasing pretwist, the torsional frequencies for the rotating plate do not increase as rapidly as for the nonrotating plate. An increase in the value of  $\psi$  from  $0^\circ$  to  $40^\circ$  increases the first torsional frequency by 79.7% and



TABLE 15

Effect of Pretwist on Natural Frequencies of  
 Rotating and Nonrotating Plates  
 $L/b=2.0$  ,  $b/t=16.0$

Vibration Mode	Freq. for $\psi=40^\circ$ / Freq. for $\psi=0^\circ$	
	Nonrotating Plate	Rotating Plate ( $\bar{\Omega}=1, \bar{r}=2, \theta=90^\circ$ )
First Bending	0.985	0.950
Second Bending	0.807	0.817
First Torsional	1.797	1.621
Second Torsional	1.387	1.318

the second torsional frequency by 38.7% when the plate is not rotating. The corresponding values for the rotating plate ( $\bar{\Omega} = 1$ ,  $\bar{r} = 2$ ,  $\theta = 90^\circ$ ) are observed to be 62.1% and 31.8%, respectively.

In the case of a nonrotating cantilever plate of  $b/t=16$  and  $\psi=0^\circ$ , the third and the fourth bending frequencies are very close to each other. An increase in the pretwist, therefore, produces a strong coupling between these two modes (Figure 26). As the speed of rotation increases, the values of the frequencies corresponding to the modes 3B and 4B, at  $\psi=0^\circ$ , get farther apart. The coupling between these two modes, therefore, gets weaker. In the present case the speed of rotation considered has separated these two frequencies considerably at  $\psi=0^\circ$  (Figure 41). Hence, there is practically no coupling between the modes 3B and 4B with increase in the value of pretwist. The two frequencies increase slightly with increase in the value of  $\psi$ .

The effect of increase in the speed of rotation, on the natural frequencies of a pretwisted cantilever plate, is shown in Figure (42). The dotted curves correspond to the case when the pseudo-static deformation is not included. In such a case the plate vibrates about its initial configuration and all the frequencies are observed to increase with the speed of rotation.

For the values of the parameters considered ( $\psi=30^\circ$ ,

$\theta=90^\circ$  and  $\bar{r}=2$ ), the pseudo-static deformation tends to untwist the plate; as can be observed from Figure (40). The effect of including this deformation should therefore, be similar to that of decreasing the value of pretwist. Referring to Figure (41), it is observed that the frequencies for the modes 1T, 2T, 3B and 4B decrease with a decrease in the value of  $\psi$ . This is reflected in Figure (42) by the fact that the solid curves are below the dotted curves. For the same reason the solid curve for the mode 2B is above the dotted curve; while the two curves practically coincide for the mode 1B.

For the values of the parameters considered, the decrease in the torsional frequencies, produced by the pseudo-static deformation, is observed to be greater than the increase caused by the rotation. The net effect is that the torsional frequencies decrease slightly with increasing speed of rotation (Figure 42). In the case of mode 3B, the increasing effect of rotational speed dominates the decreasing effect of pseudo-static deformation for  $\bar{\Omega}$  less than 1.25; but at higher speeds the effect is opposite.

The low aspect ratio turbomachinery blades are, generally, very stiff and have a high value for the fundamental frequency. In practice, therefore, the value of  $\bar{\Omega}$  may not exceed 1.0. In such cases, the pseudo-static deformation does not affect the natural frequencies appreciably.



TABLE 16

Nondimensional Frequencies ( $\beta_r$ ) of Rotating Pretwisted  
Plate at Different Values of Disc Radius

$$L/b=2.0, b/t=16.0, \psi=30^\circ, \bar{\Omega}=1.0, \theta=90^\circ$$

Vibration Mode	$\bar{r}=0$	$\bar{r}=1$	$\bar{r}=2$
First Bending	3.632	6.429	7.630
Second Bending	19.845	21.619	23.919
Third Bending	53.055	53.884	54.447
Fourth Bending	63.133	63.550	64.560
First Torsional	22.500	22.337	21.599
Second Torsional	60.408	59.785	59.853

This is evident from Figure (42).

The natural frequencies of the rotating pretwisted plate at different values of the disc radius are given in Table (16). The first and the second bending frequencies are observed to increase substantially with the disc radius. The effect on the frequencies of the third and the fourth bending modes, as well as on the torsional frequencies is small.

The number of the physical variables, on which the natural frequencies of a rotating pretwisted cantilever plate depend, is quite large. In addition, the pseudo-static deformation introduces further complexities in the manner in which the frequencies depend on the physical variables. No attempt is, therefore, made to derive any empirical formulae for the natural frequencies of rotating pretwisted plates.

## CHAPTER 7

### CONCLUDING REMARKS

A method based on finite element technique is developed for calculating the first few natural frequencies and the corresponding mode shapes of rotating and nonrotating low aspect ratio turbomachinery blades. The blades are assumed to be fixed at the root and the elasticity of the disc is not considered. The blade is treated as an assembly of small flat triangular elements.

The accuracy of the method is tested by solving several bending and vibration problems of plates and shells, for which analytical or experimental results are available, including the problem of a pretwisted tapered cantilever plate. The method is observed to give a good rate of convergence. The first few frequencies can be obtained quite accurately, when the number of nodal points is approximately 25 and the number of the triangular elements is about 40 or more.

A new bending stiffness matrix for a triangular element is used, based on a partially conforming displacement function. This function satisfies transverse slope continuity along one of the sides of the element. The solution of a few test problems suggests that this stiffness matrix gives



somewhat better results than the other existing stiffness matrices with the same number of degrees of freedom for the element.

The effect of variation in the aspect ratio, the amount of pretwist, the speed of rotation, the disc radius and the setting angle on the natural frequencies and the mode shapes are investigated. For this study, the blade is idealized as a pretwisted cantilever plate.

The fundamental frequency of a nonrotating cantilever beam is known to increase slightly with pretwist. For lower values of aspect ratio ( $L/b < 3$ ), it is observed that this frequency decreases with an increase in the pretwist. The deflection analysis of a pretwisted cantilever plate due to tip loads shows that the total deflection at the points of application of the loads increases with an increase in the value of pretwist. Both these results suggest that the bending stiffness of a cantilever plate is decreased by pretwisting. The torsional stiffness, however, is considerably increased and results in a rapid increase of the torsional frequencies with pretwist.

The frequency ratio (frequency of the  $n^{\text{th}}$  mode/fundamental frequency of the untwisted plate), for all the bending modes of a pretwisted plate, is observed to be lower than the corresponding value for a twisted beam. The deviation from the beam value decreases as the aspect ratio

increases; and for  $L/b > 3$  the two values are almost identical.

In a beam type analysis of blades, the flapwise bending, the chordwise bending and the torsional vibration modes are considered. In the case of plates an additional bending mode, with two longitudinal nodal lines, is also present. The frequency corresponding to this mode is sufficiently low for  $L/b < 2$  and is, therefore, of practical importance.

For pretwisted cantilever beams of rectangular cross-section the torsional and the bending motions are uncoupled. This is also observed to be the case for pretwisted cantilever plates of uniform thickness. However, the torsional modes exhibit a strong coupling with the additional mode with two longitudinal nodal lines; when the values of  $b/t$ ,  $\psi$  and  $L/b$  are such that the two frequencies are close to each other.

The natural frequencies of rotating cantilever plates are observed to increase with the speed of rotation and with an increase in the radius of the disc. An increase in the setting angle causes a decrease in the natural frequencies. For cantilever beams it is customary to express the frequency of the rotating beam in terms of the corresponding frequency of the nonrotating beam, the speed of rotation and the Southwell coefficient. The expressions for the Southwell coefficients for cantilever beams are available in the literature. From the results of present computations, the expressions for these



coefficients are obtained for rotating cantilever plates. These expressions permit a rapid estimation of the natural frequencies at any speed of rotation, disc radius and the setting angle. Within the range of these parameters considered, the approximate values of the frequencies, thus obtained, do not differ from the actually computed values by more than two percent.

For rotating cantilever beams the Southwell coefficient increases linearly with the radius of the disc. In the case of the bending frequencies of rotating cantilever plates, the coefficient contains a quadratic term in the radius, in addition to the linear term. The bending frequencies of a rotating cantilever plate decrease somewhat more with an increase in the setting angle, as compared to a rotating cantilever beam. With an increase in the aspect ratio of the plate the Southwell coefficients are observed to approach the corresponding expressions for the beam. For  $L/b > 3$  the two expressions are practically identical.

The centrifugal forces produce pseudo-static deformation in a rotating pretwisted cantilever plate; and the vibration of the plate should be considered about the deformed configuration. For the parameters of the pretwisted plate considered ( $b/t=16$ ,  $L/b=2$  and  $r/L=2$ ), this deformation tends to untwist the plate when the initial pretwist is large ( $\psi > 15^\circ$ ). The pseudo-static deformation depends not only on



the magnitudes of the initial twist and the setting angle, but also on their directions relative to each other.

The effect of rotation on the natural frequencies of a pretwisted cantilever plate can be divided into two parts. The first is due to the increased stiffness caused by the centrifugal stresses, resulting in an increase in all the frequencies. The second effect is due to the change in the pretwist of the plate produced by the pseudo-static deformation. This may cause an increase or a decrease in the different frequencies, depending on the direction of the deformation and whether the frequency has the tendency to increase or decrease with pretwisting. When the speed of rotation is small ( $\bar{\Omega} < 1$ ), the pseudo-static deformation does not affect the natural frequencies appreciably. If the parameters of the plate are such that the centrifugal forces tend to untwist the plate, the decrease in the torsional frequencies due to the second effect may be more than the increase due to the first effect. As a result the torsional frequencies may even decrease with an increase in the speed of rotation.

From the survey of the analytical methods for the vibration analysis of turbomachinery blades, many areas, in which a considerable amount of further investigation is needed, can be identified. In addition, the present method of analysis can be extended to study several other aspects of the problem.

The new developments in the finite element technique could be incorporated to improve the present method and the results. Some of the areas for further research are indicated below:

- (i) The small elements, into which the middle surface of the blade is subdivided, are considered flat in the present study. Recently, curved shell elements have been developed for the finite element method of analysis. It would be worthwhile to try these elements to investigate the extent of improvement that can be obtained in the results.
- (ii) An actual blade is not rigidly attached to the disc. The boundary conditions in the present approach may be modified by including springs at the root of the blade so that the slope at the root is proportional to the value of the moment at the root. By changing the stiffness of the springs, the effect of root flexibility can be studied.
- (iii) Although the formulation of the problem of a rotating pretwisted blade, including the Coriolis acceleration is given in Appendix II; the present results are obtained by neglecting this acceleration. It would be of interest to study the effect of including the Coriolis forces on the natural frequencies and the mode shapes. Since the Coriolis forces result in a

damping type matrix, any viscous damping present in the system can also be included in the analysis.

- (iv) A method of reducing the degrees of freedom in the vibration problems is given by Anderson et al. (80). By applying the method for the vibration analysis of a cantilever plate, it is shown that the matrices can be considerably reduced in size without appreciably affecting the first few natural frequencies. The method may be tried for the vibration analysis of shells, where the need for this reduction is more acute.
- (v) Once the method of reducing the degrees of freedom, significantly, is established, the vibration analysis of blade-disc assembly can be carried out. The disc may be subdivided into elements by drawing concentric circles and radial lines. The properties of the elements, thus formed, are given by Olson et al. (141).



**FIGURES**

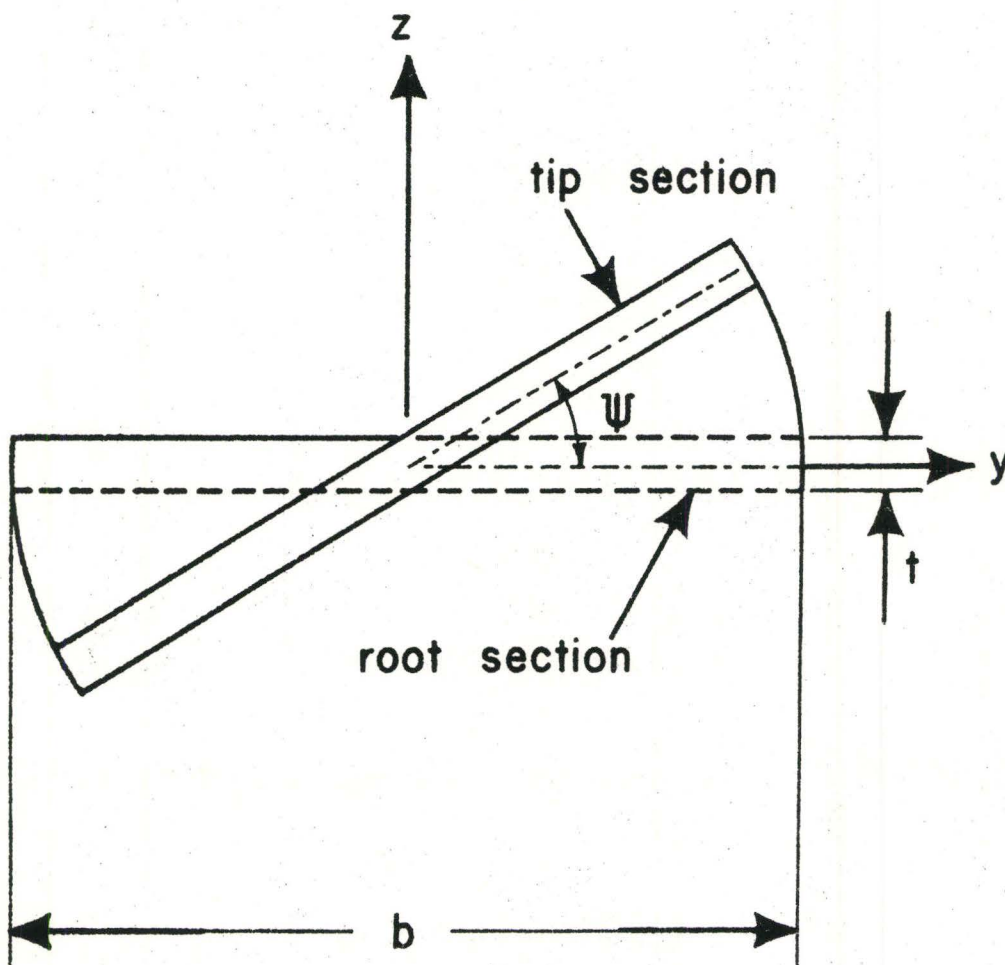


Figure 1

Side View of Pretwisted Blade of  
Rectangular Section Looking Towards  
Root Section

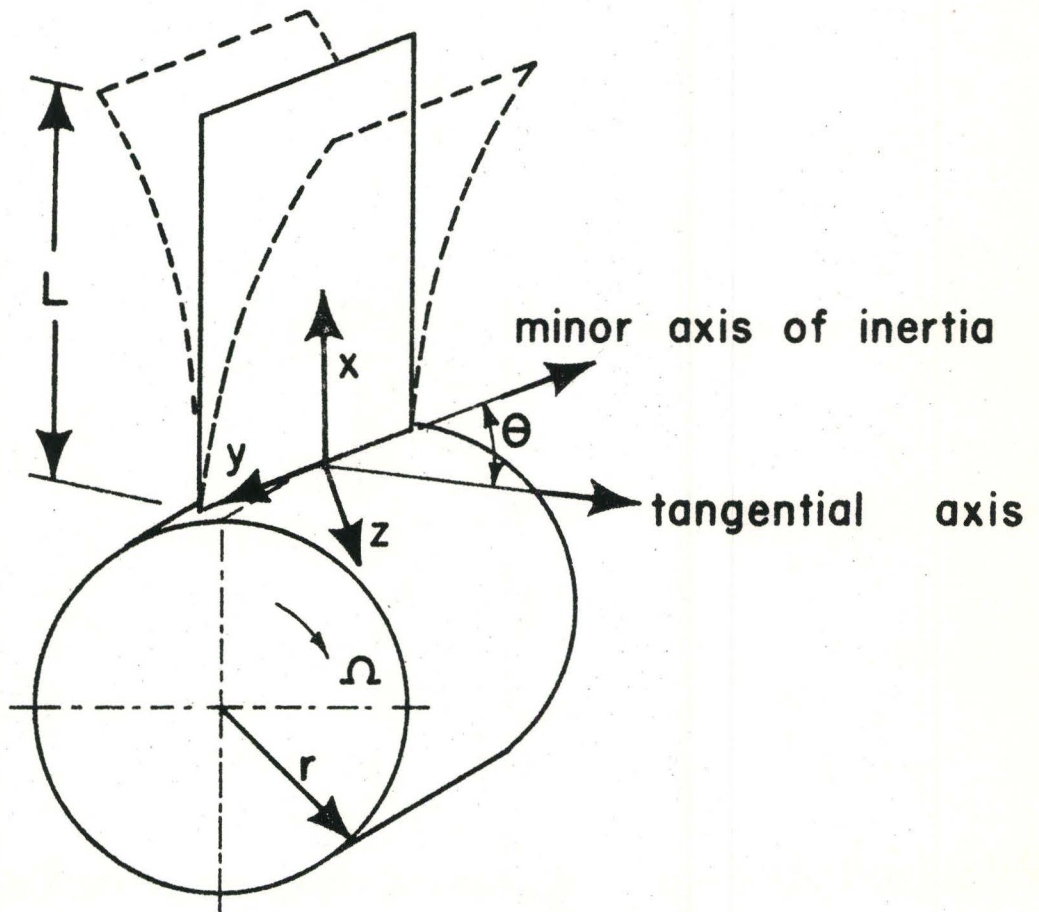


Figure 2

Sketch of a Blade Without Pretwist Mounted  
on Rotating Disc at Setting Angle  $\theta$



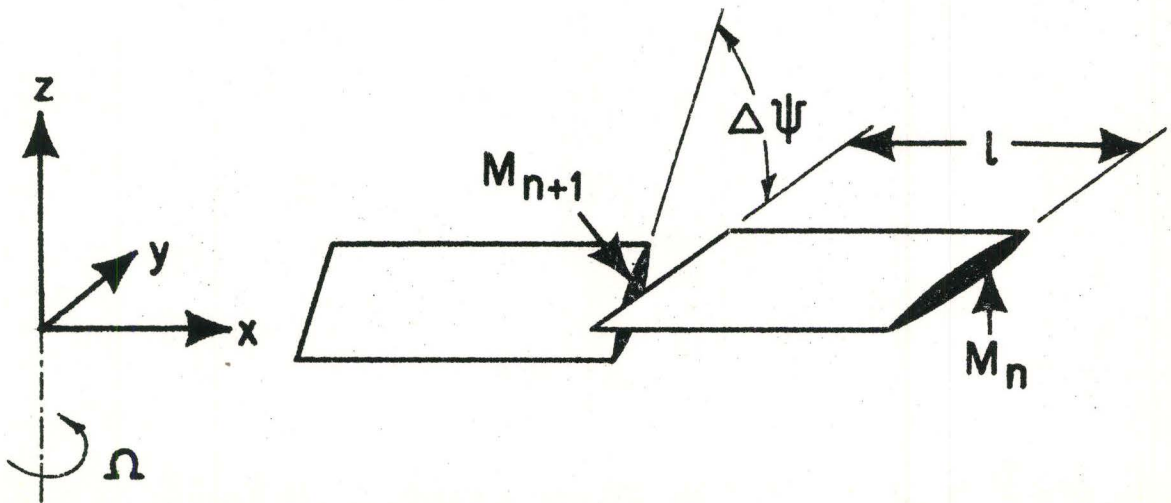


Figure 3

Lumped Mass Model of a Blade  
Showing Two Adjacent Segments

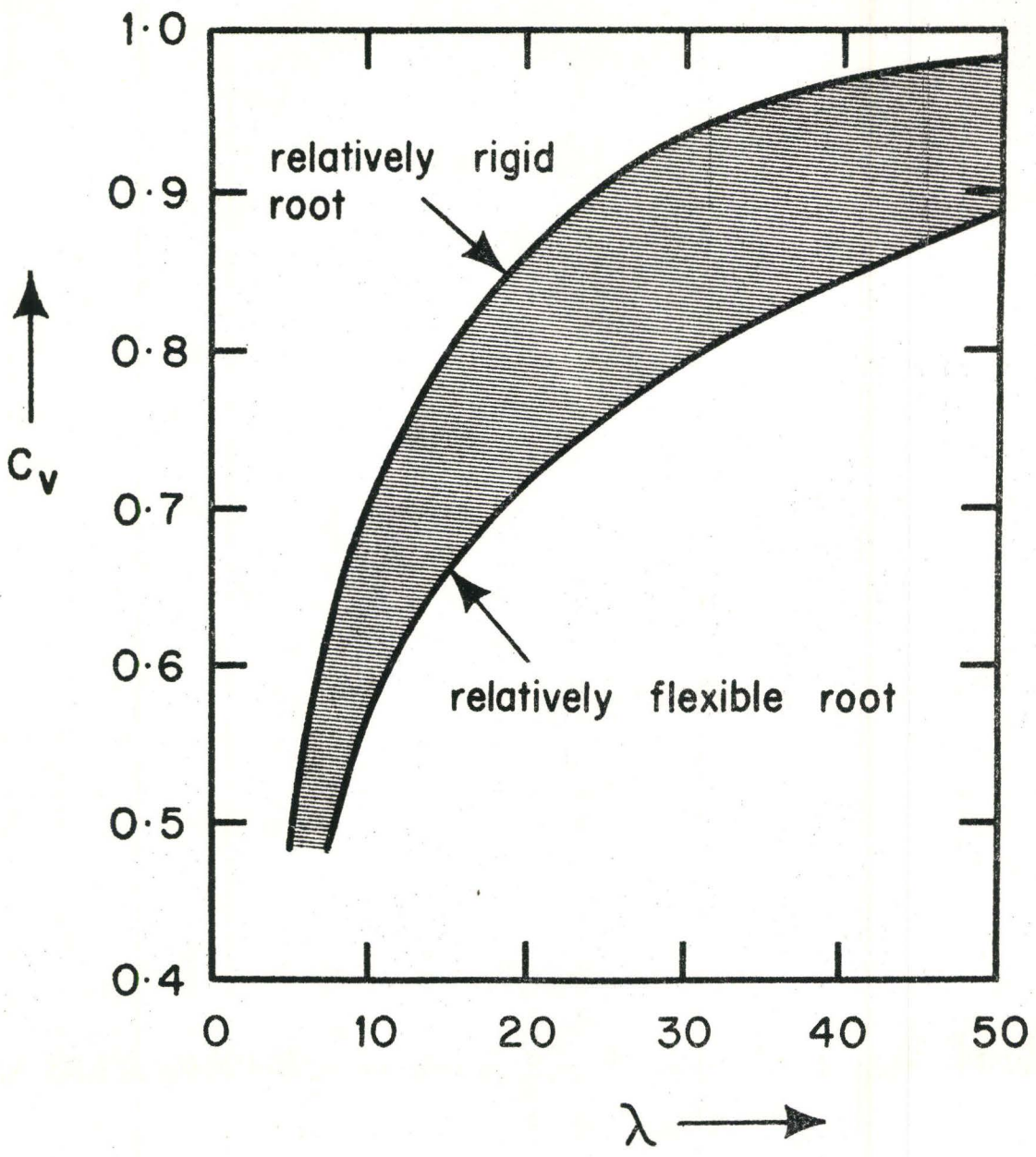


Figure 4

Effect of Root Flexibility on Flexural Frequency (Ref. 90).

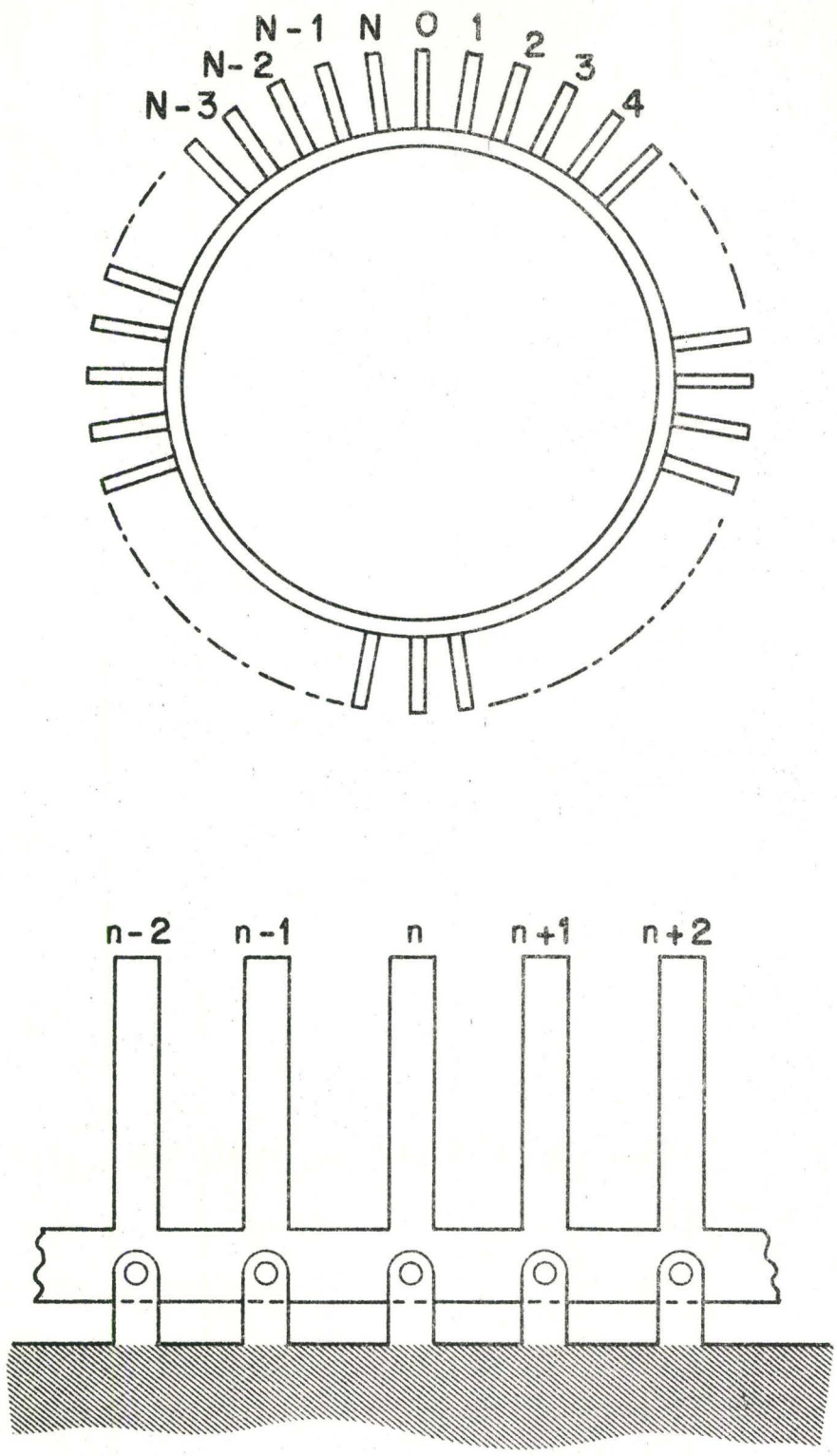


Figure 5

A Simplified Model for Blade-Disc Assembly  
Suggested by Ellington and McCallion (94).



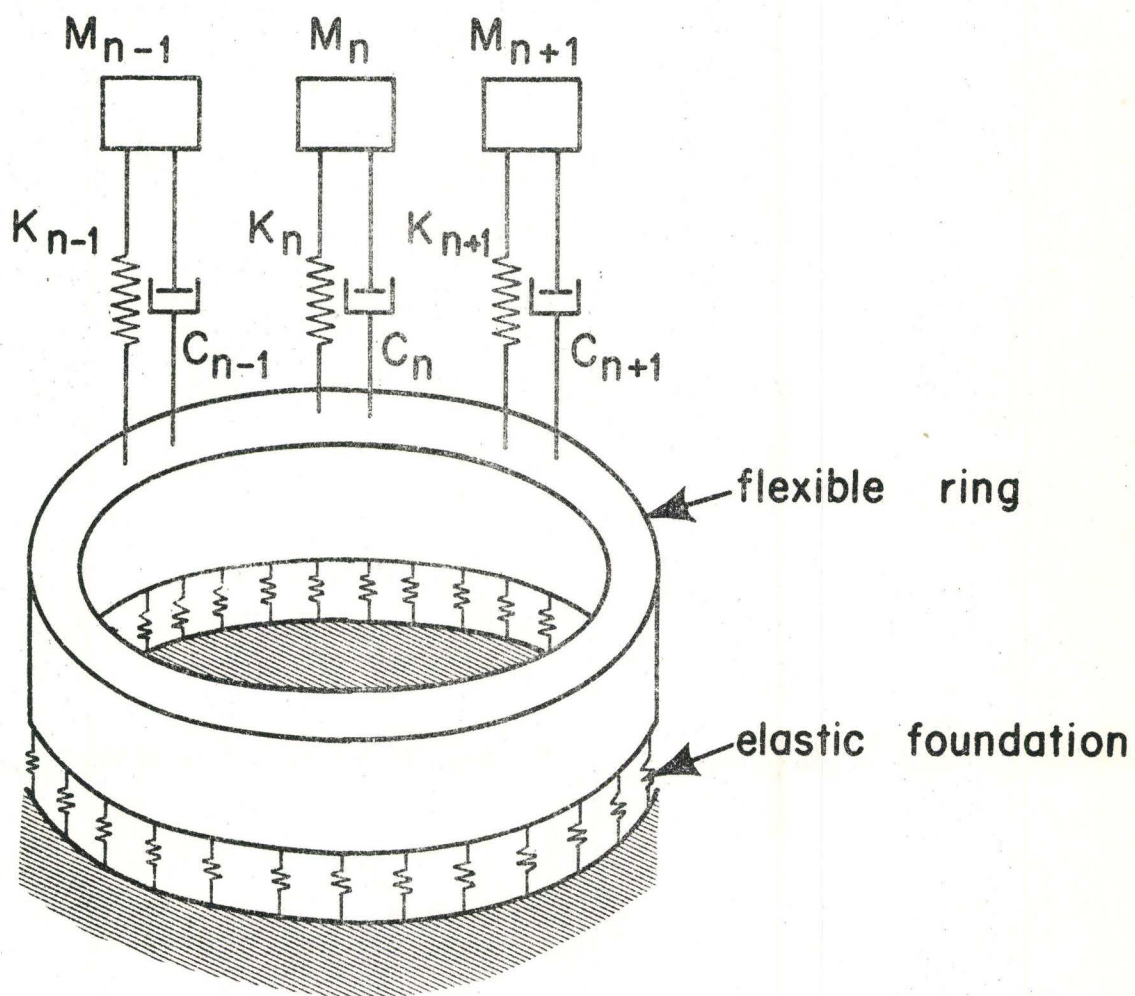


Figure 6

A Simplified Model for Blade-Disc Assembly Suggested by Wagner (97).

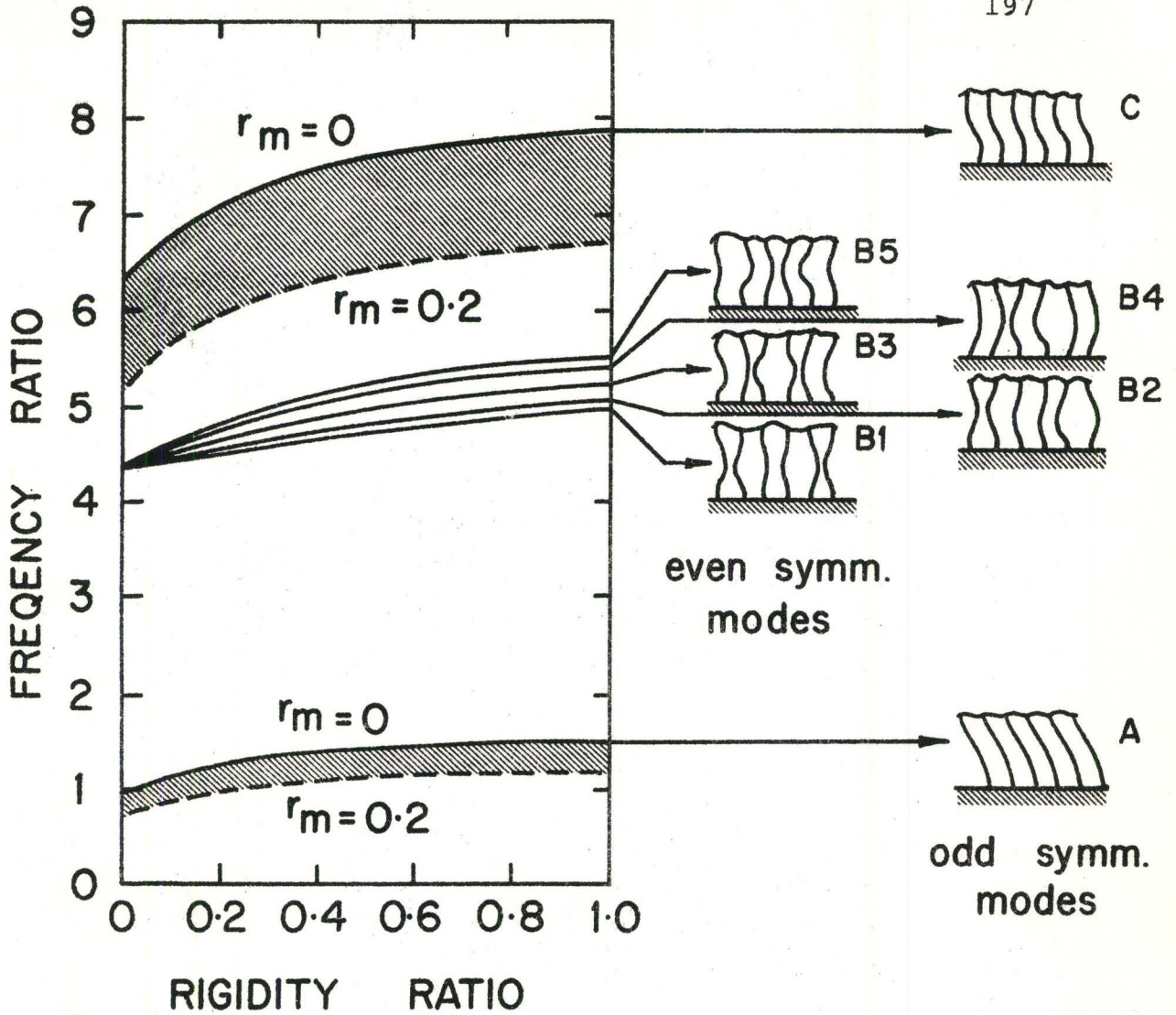


Figure 7

Natural Frequencies and Mode Shapes of a Packet of Six Shrouded Blades (Ref. 98)

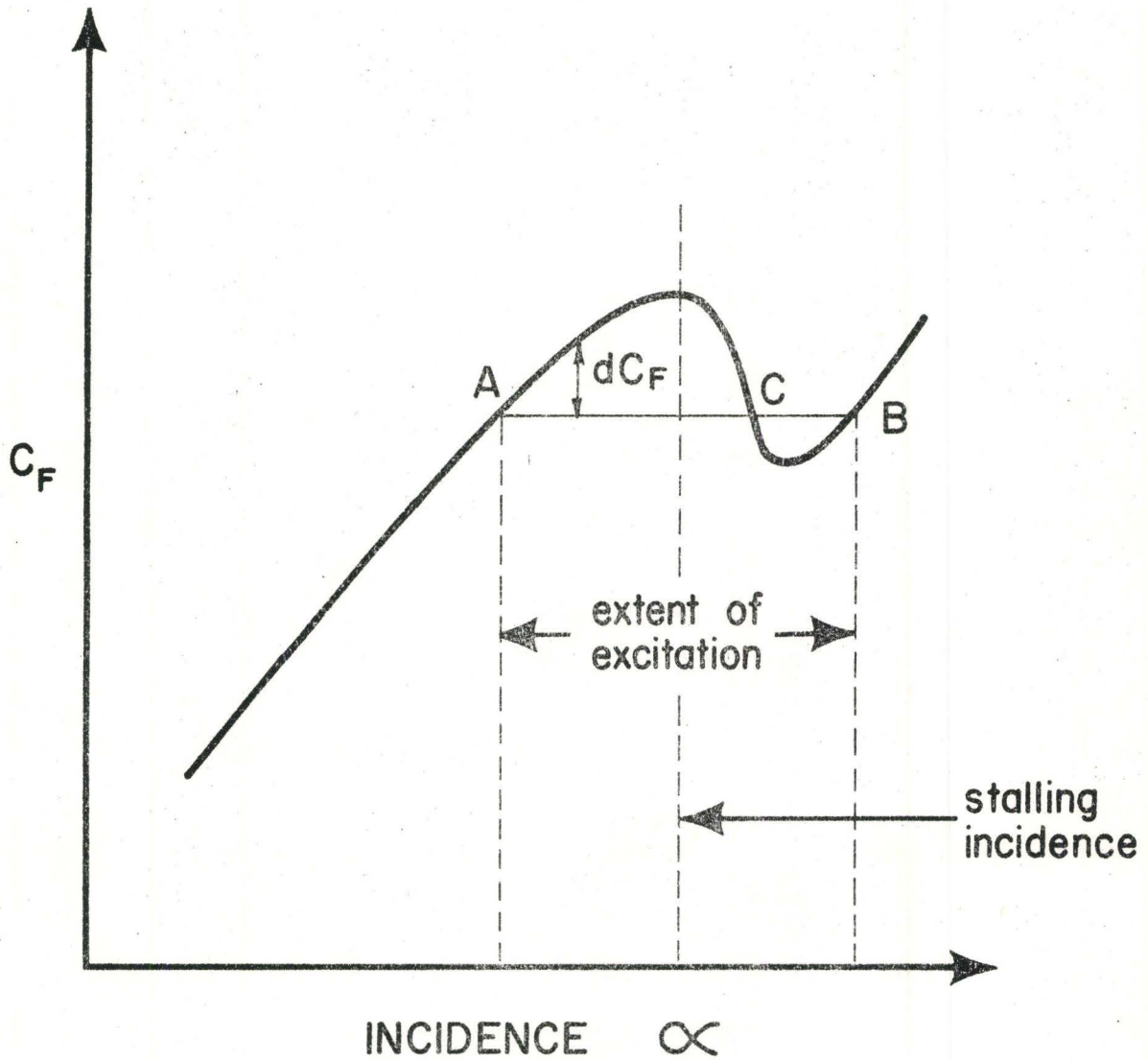


Figure 8

A Typical Lift Curve of Compressor Blade  
in Cascade at Constant Mach Number



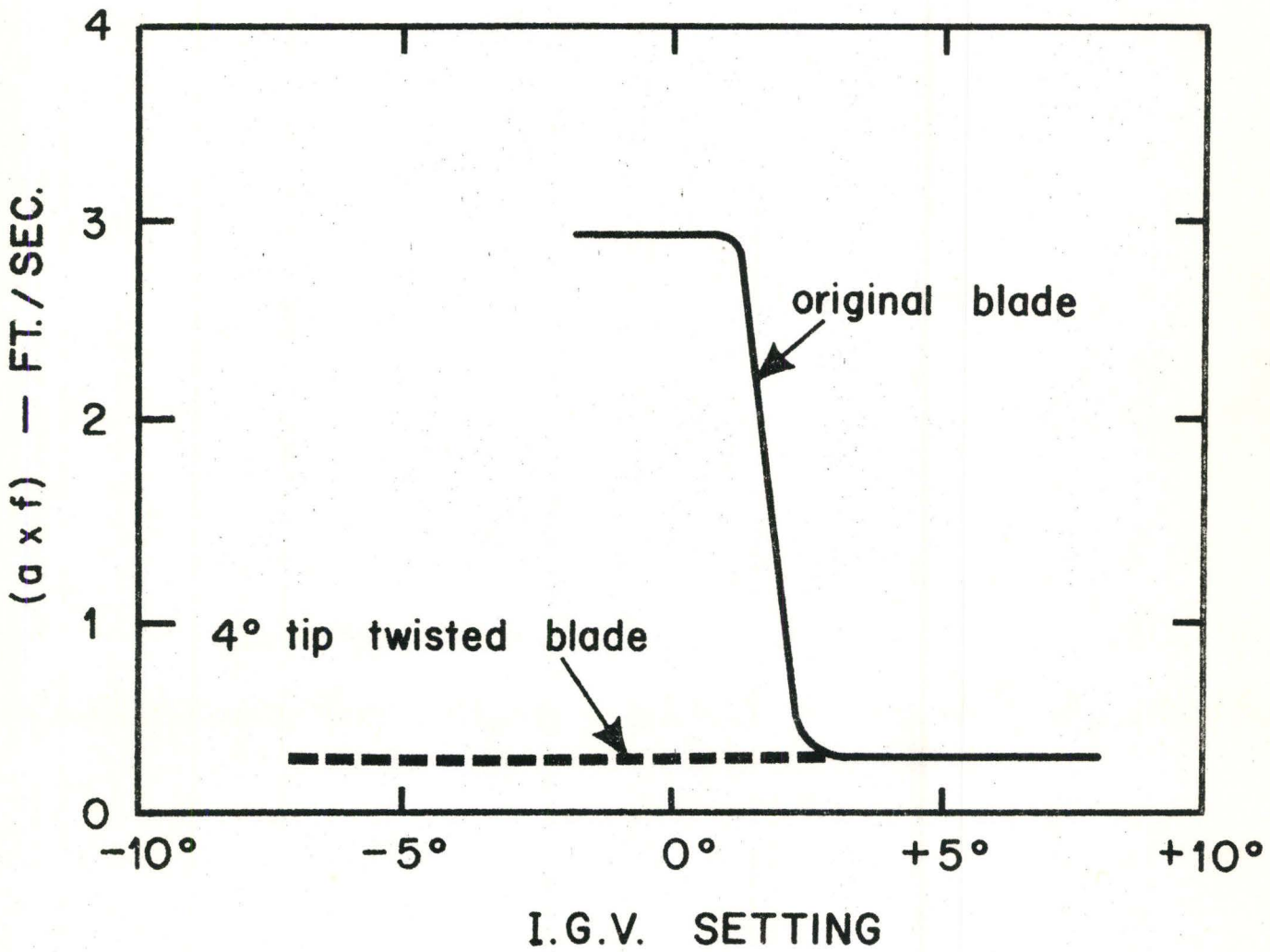


Figure 9

Effect of Inlet Guide Vane Setting Angle  
on Flutter Vibration Amplitude (Ref.115)

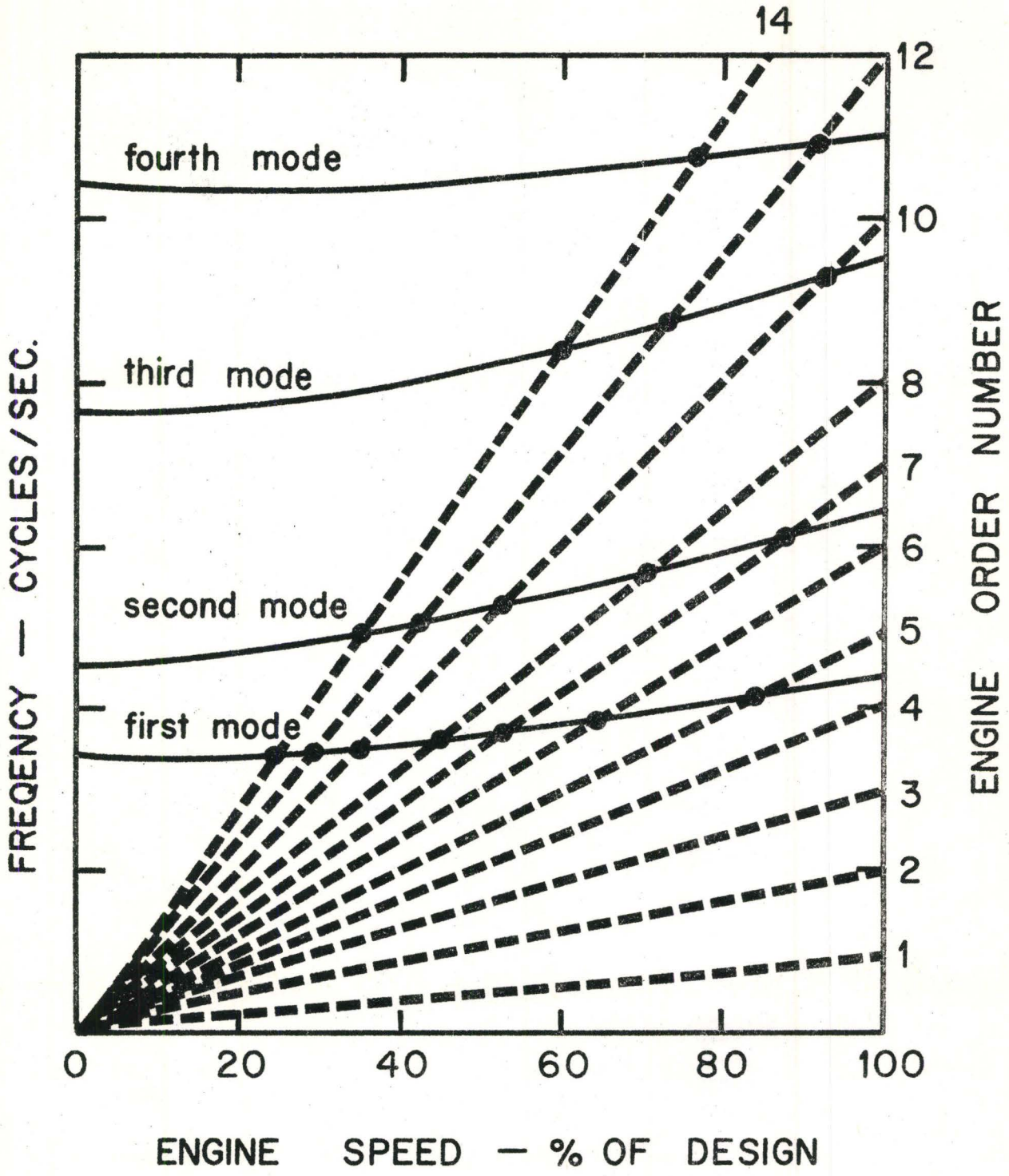
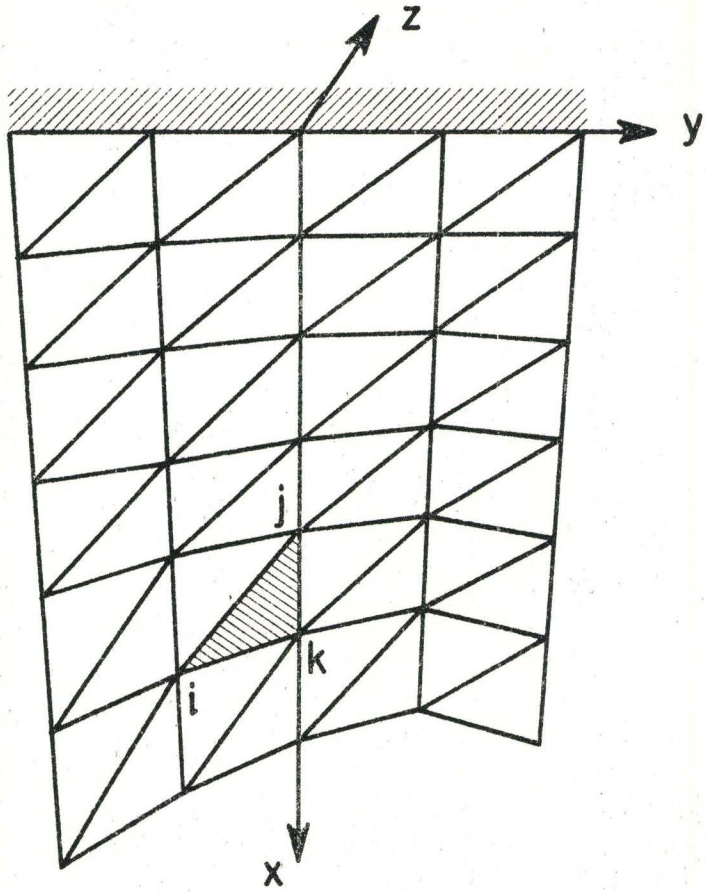
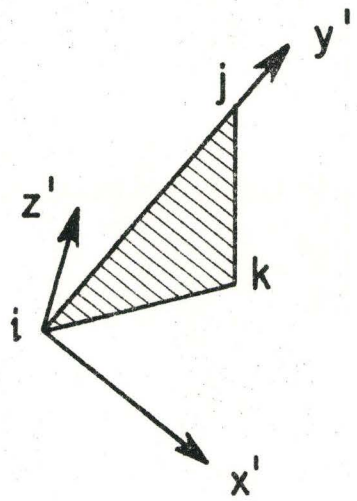


Figure 10

An Illustration of Campbell Diagram



(a)



(b)

Figure 11

- (a) Subdivision of a Blade Into Triangular Elements
- (b) Local Coordinate Axes for an Element



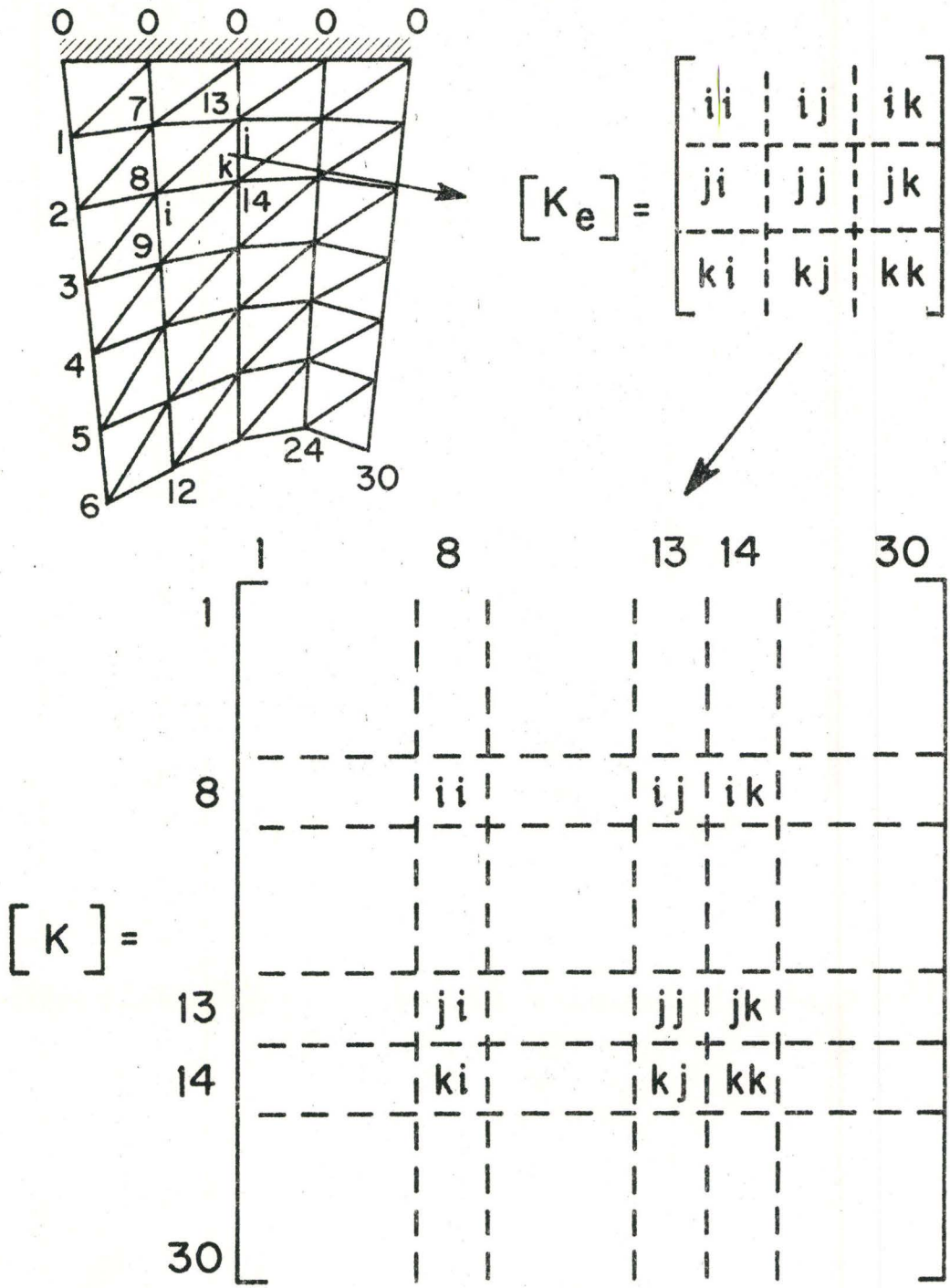
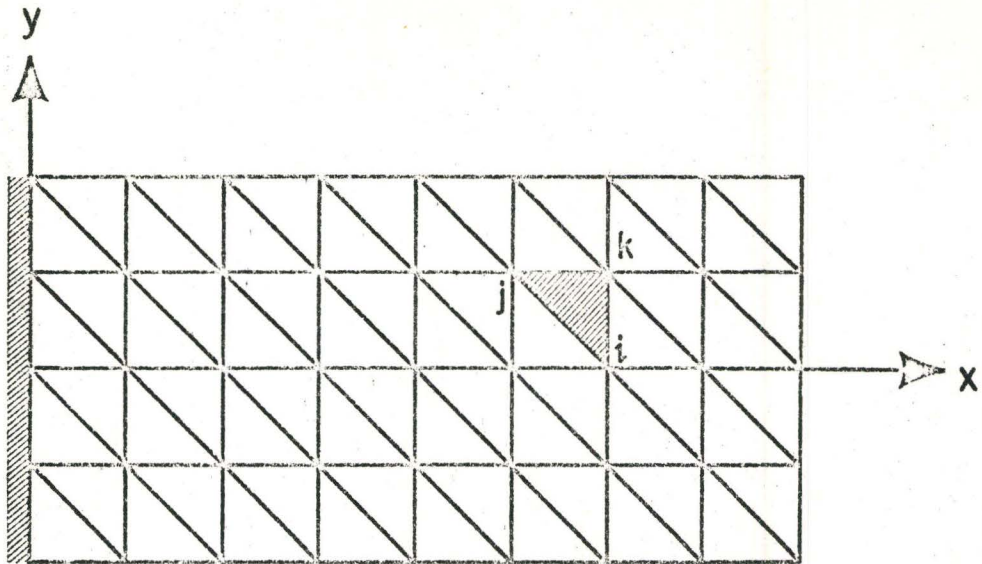
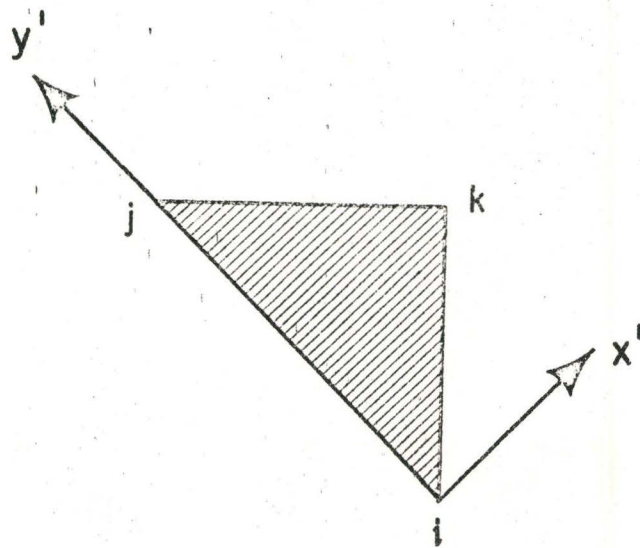


Figure 12

An Illustration of the Method of Assembling the Element Stiffness Matrices.



(a)



(b)

Figure 13

- (a) Subdivision of a Cantilever Plate Into Triangular Elements
- (b) Local Coordinate Axes for an Element.

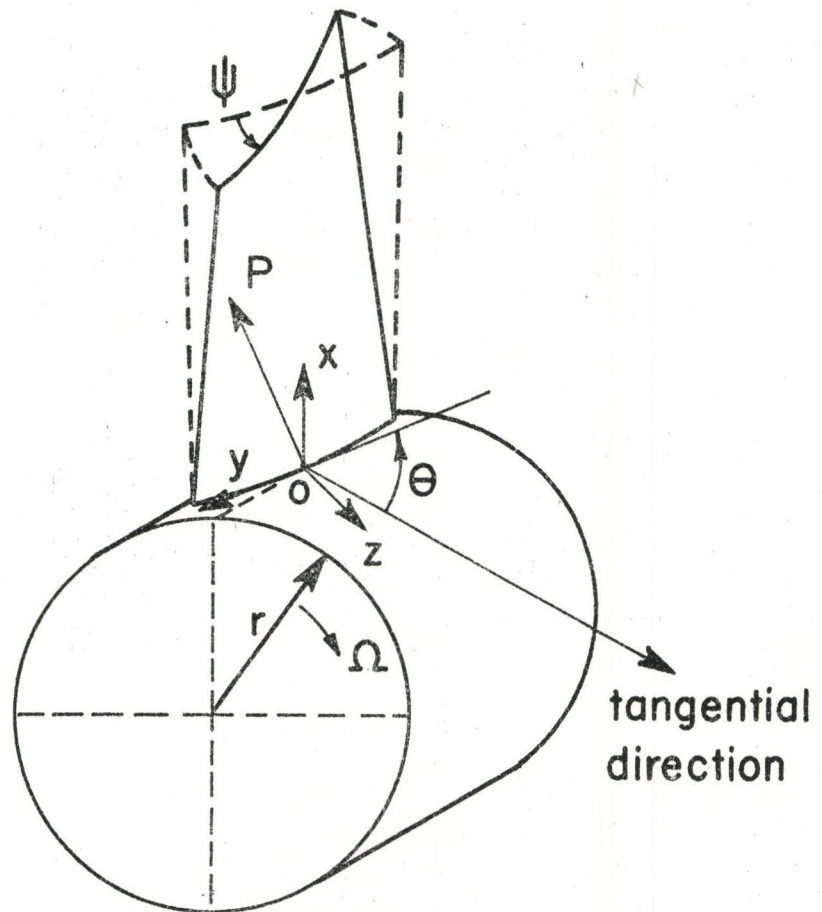
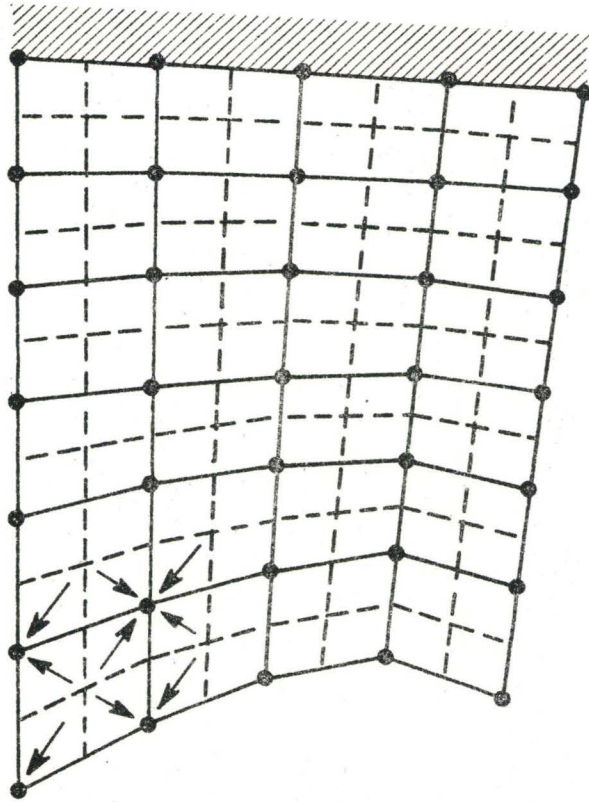


Figure 14

Sketch of a Blade Mounted on Rotating  
Disc at Setting Angle  $\theta$





• nodal points

Figure 15

An Illustration of the Method of Lumping  
the Centrifugal Forces at the Nodes

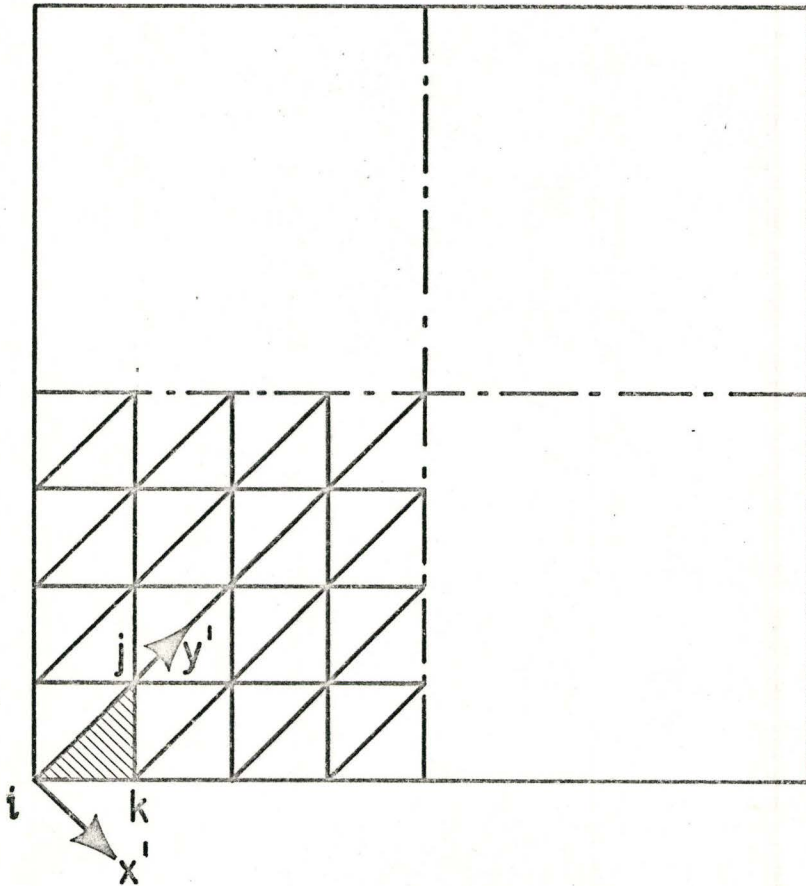


Figure 16

Subdivision of Simply Supported  
Plate Into Triangular Elements  
(Mesh 8×8)

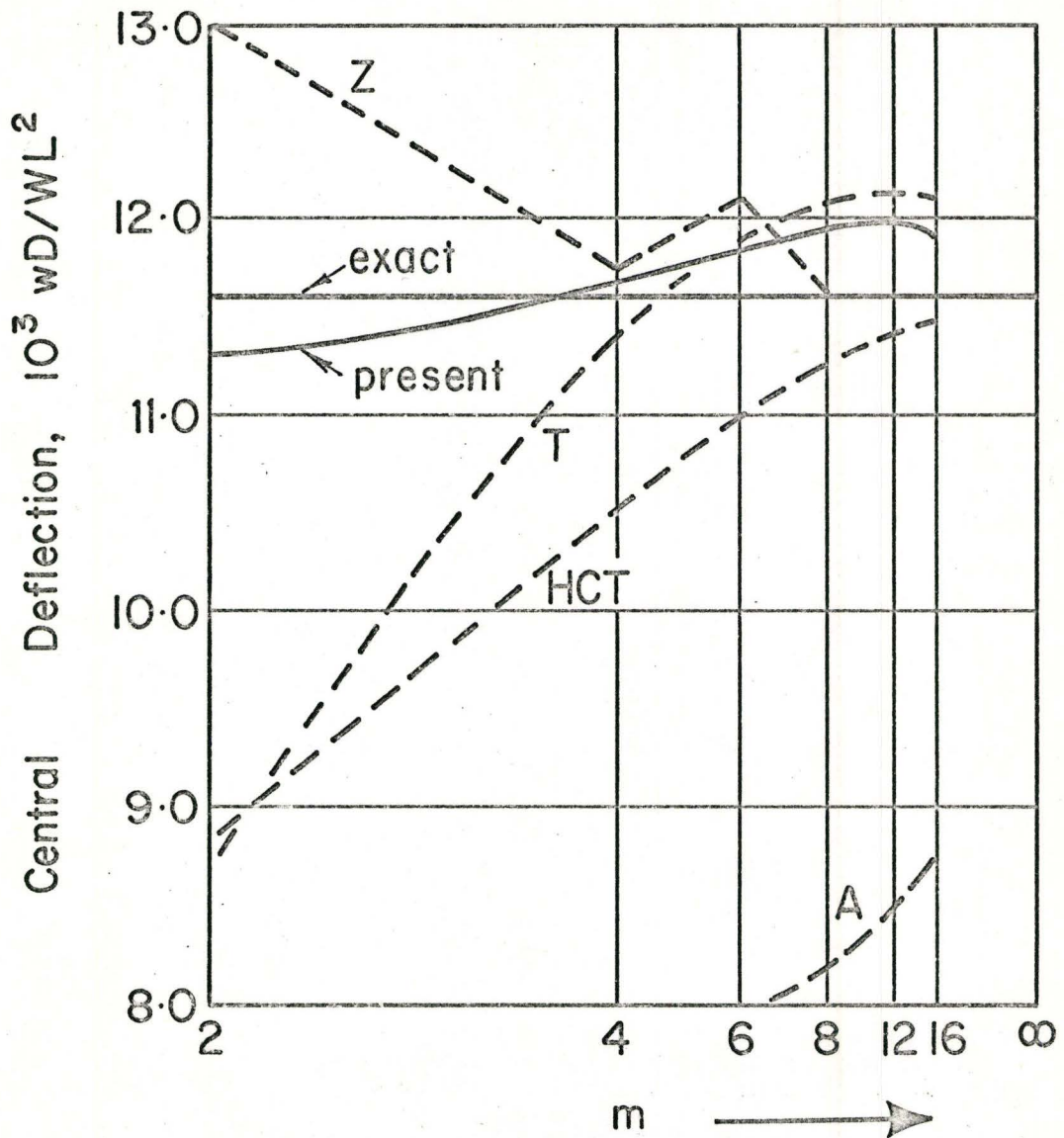


Figure 17

Central Deflection of Square Simply Supported Plate Under Central Point Load



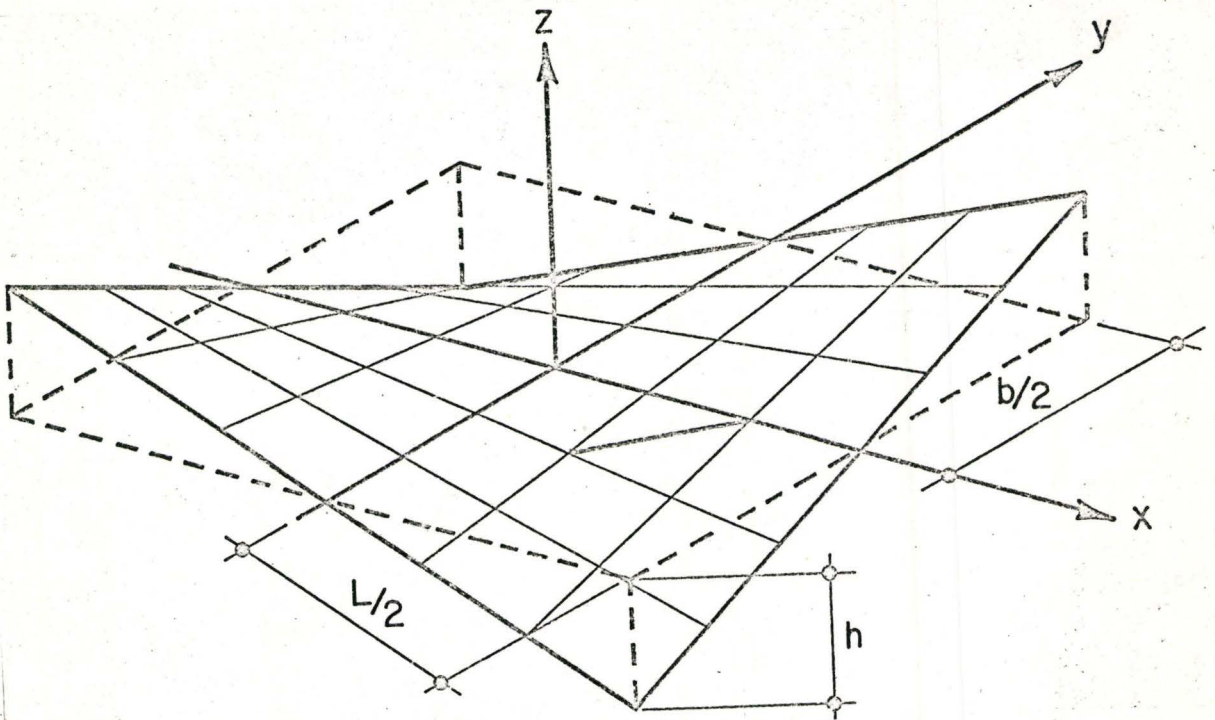


Figure 18  
The Geometry of the Hyperbolic  
Paraboloid Shell

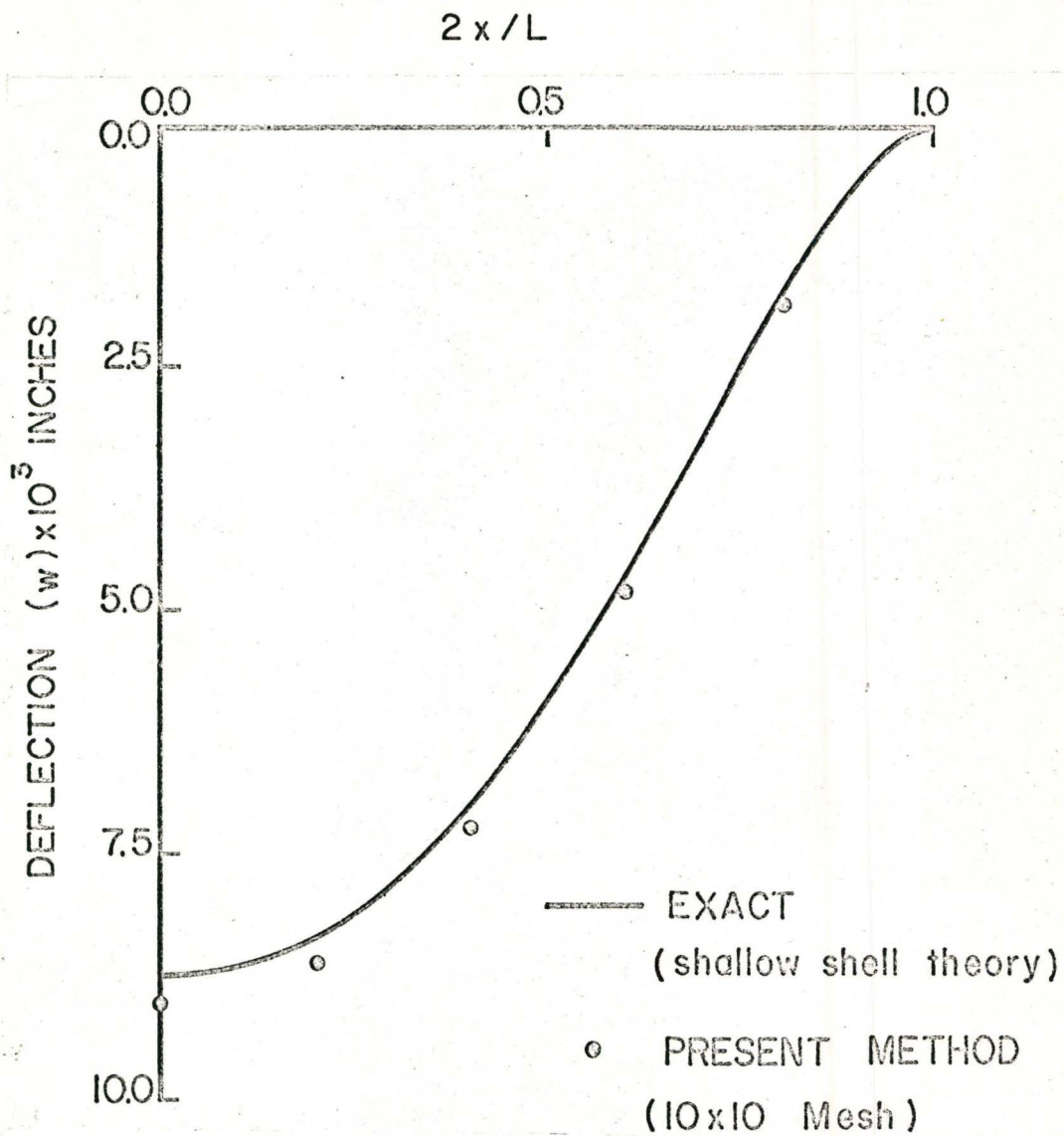
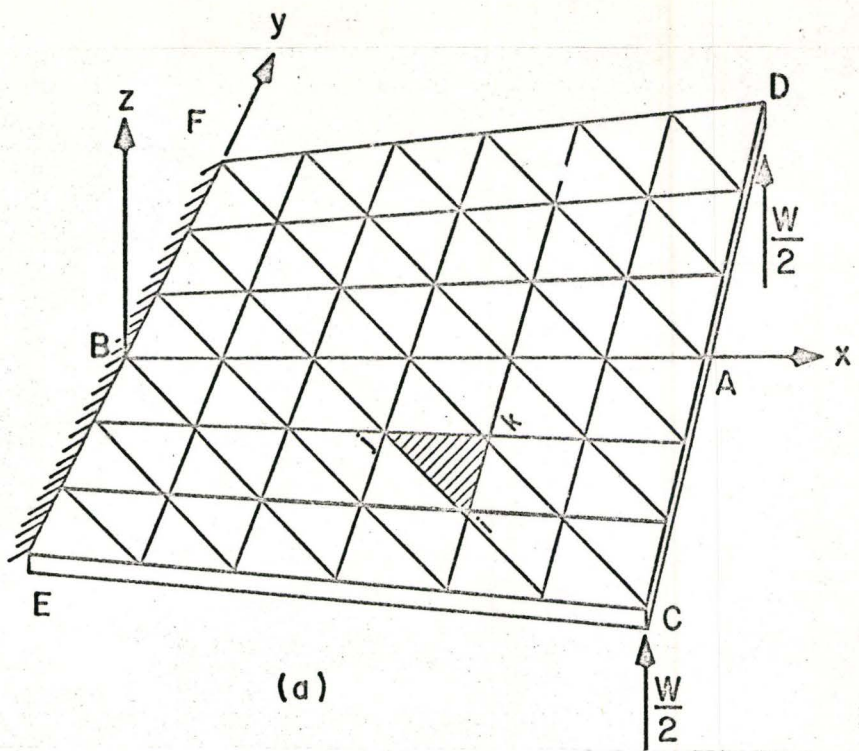
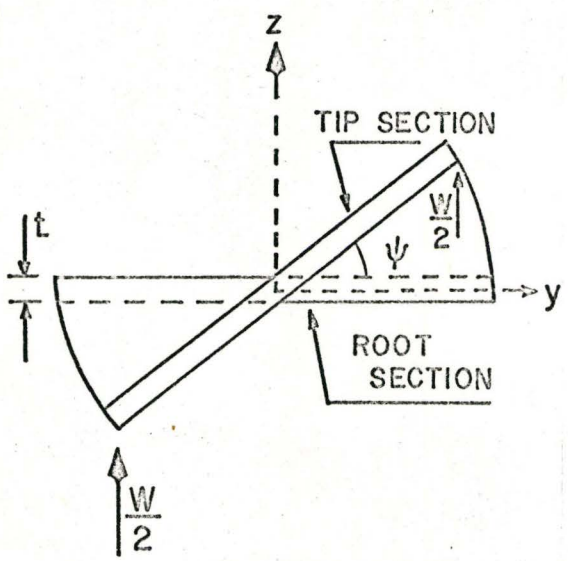


Figure 19

Deflection Along the Centre Line of  
Square Clamped Hyperbolic Paraboloid  
Shell Under Uniformly Distributed Load



(a)

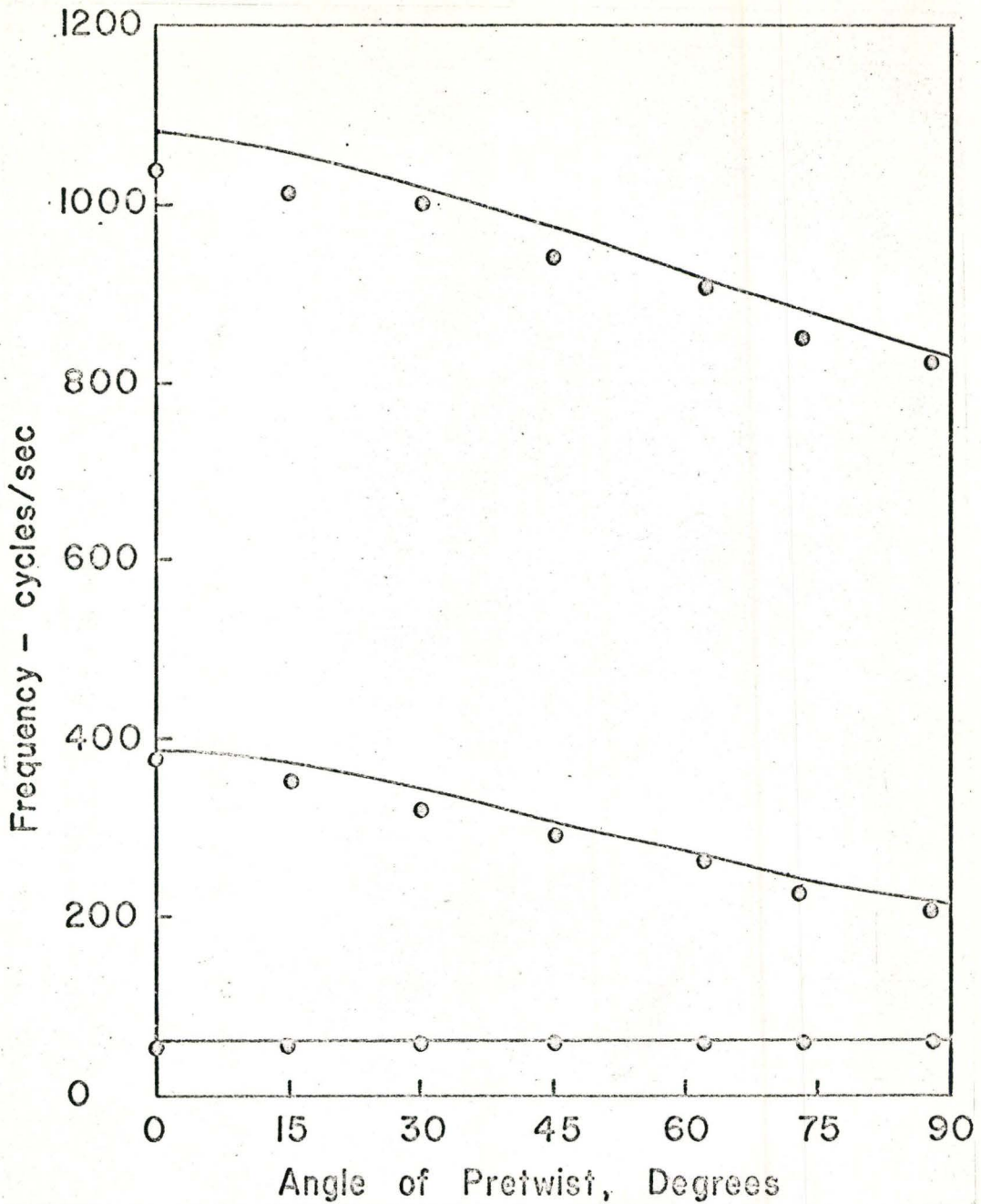


(b)

Figure 20

- (a) Pretwisted Cantilever Plate Loaded at Free Corners
- (b) Side View of the Pretwisted Plate Looking Towards Root Section

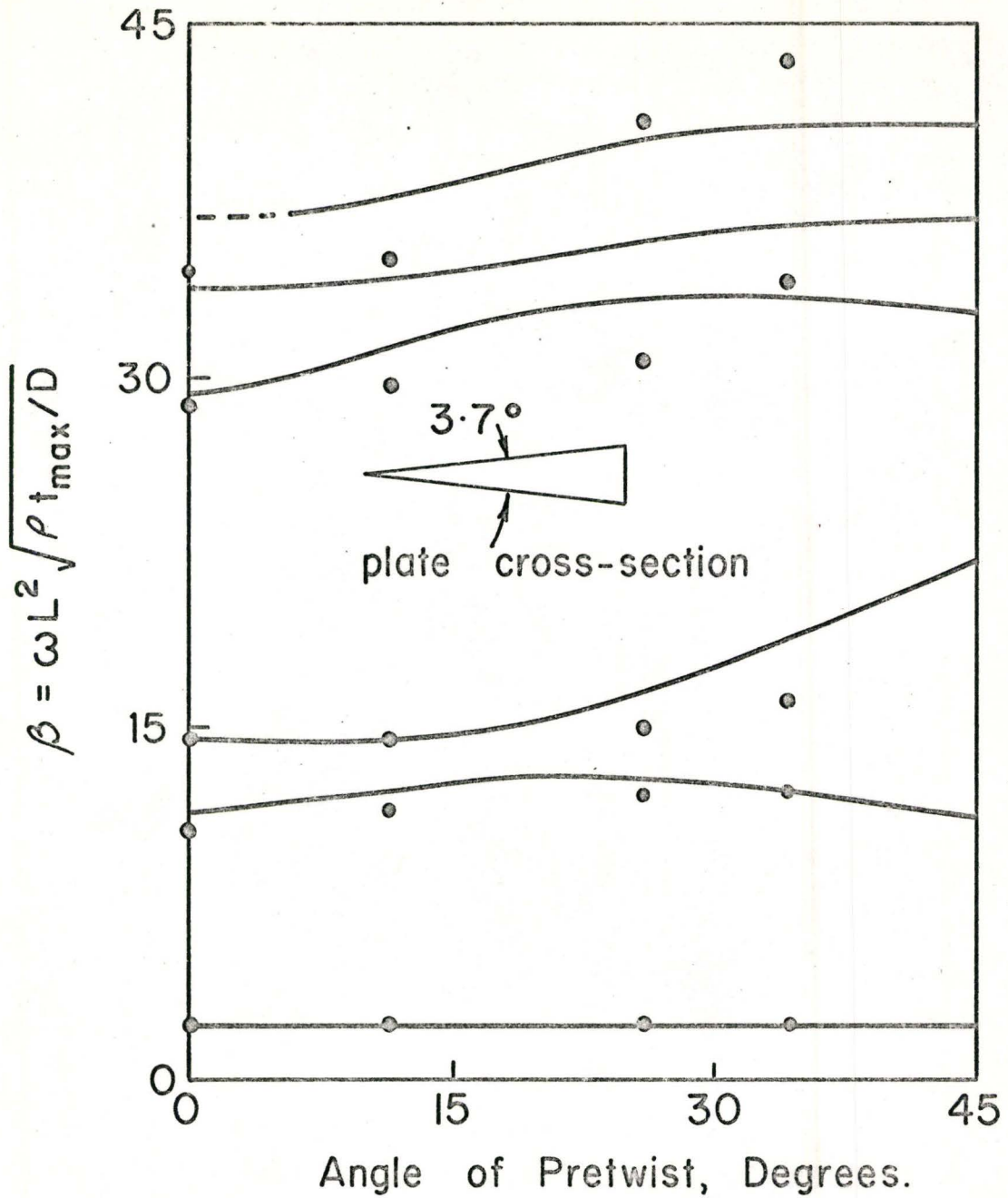




• Experimental Values (Ref. 16)

Figure 21

Bending Frequencies of a Pretwisted Cantilever Plate  
 $L = 6''$ ,  $b = 1''$ ,  $t = 0.068''$ ,  $E = 30 \times 10^6$  psi,  $\mu = 0.3$ ,  
 Density =  $0.284 \text{ lbs/in}^3$ , Mesh (10×2).



• Experimental Values (Ref. 139)

Figure 22

Natural Frequencies of a Tapered Pretwisted  
Cantilever Plate

$L/b=2$ , Mesh (7×3).

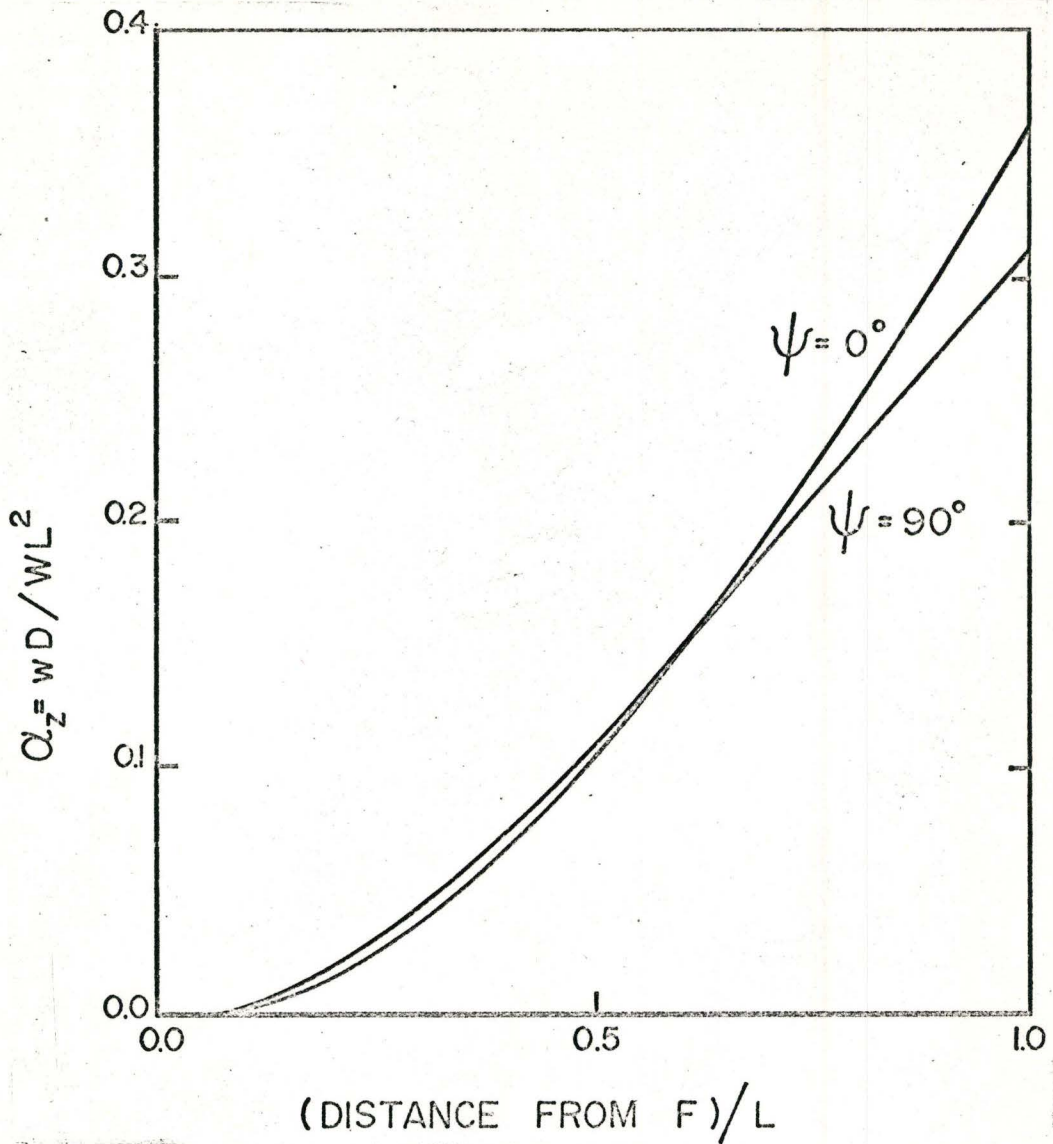


Figure 23

Deflection ( $w$ ) along the Line FD of  
Pretwisted Cantilever Plate Loaded at  
Free Corners

$L/b=1$ ,  $b/t=48$ , Mesh (6×6)



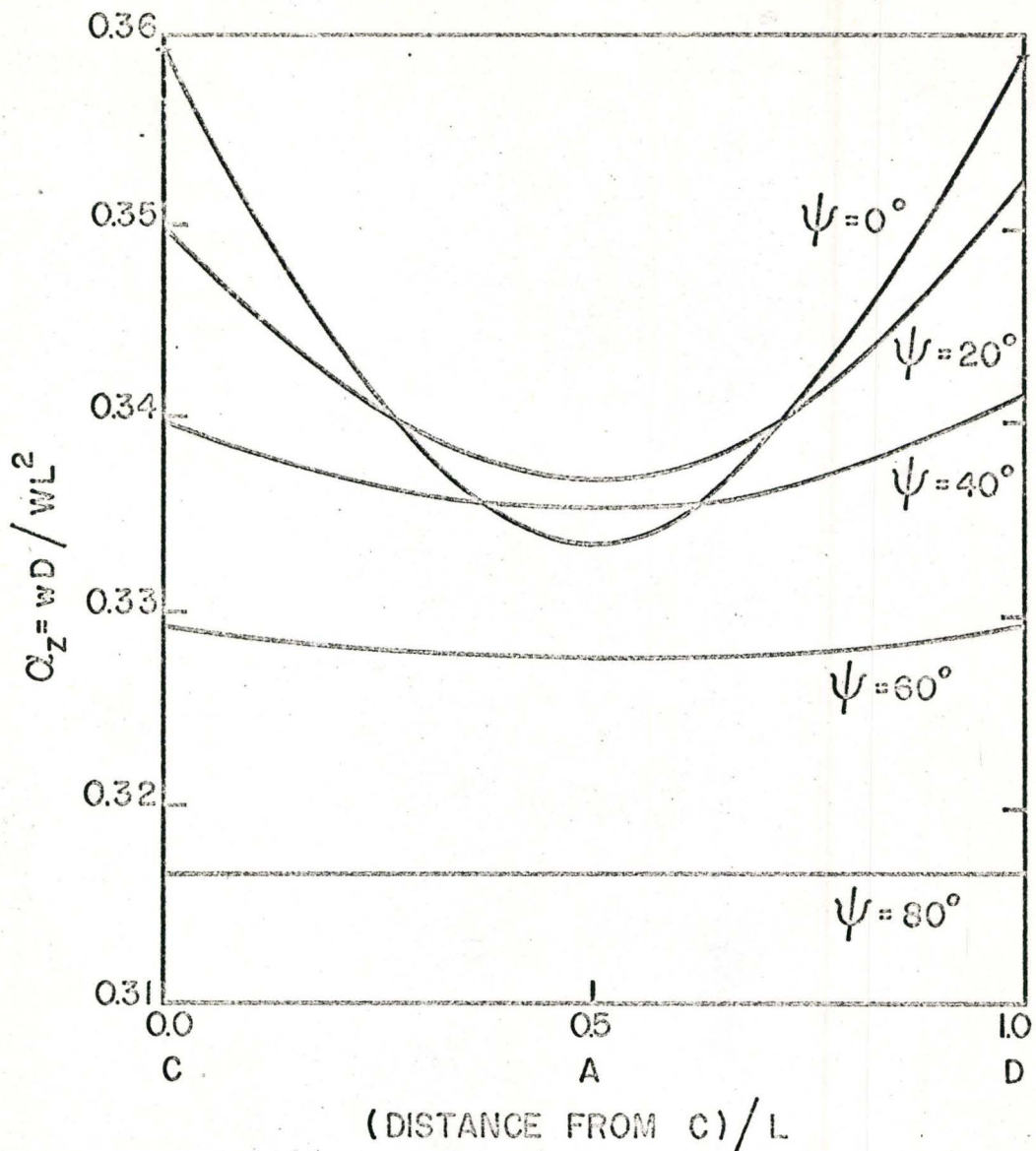
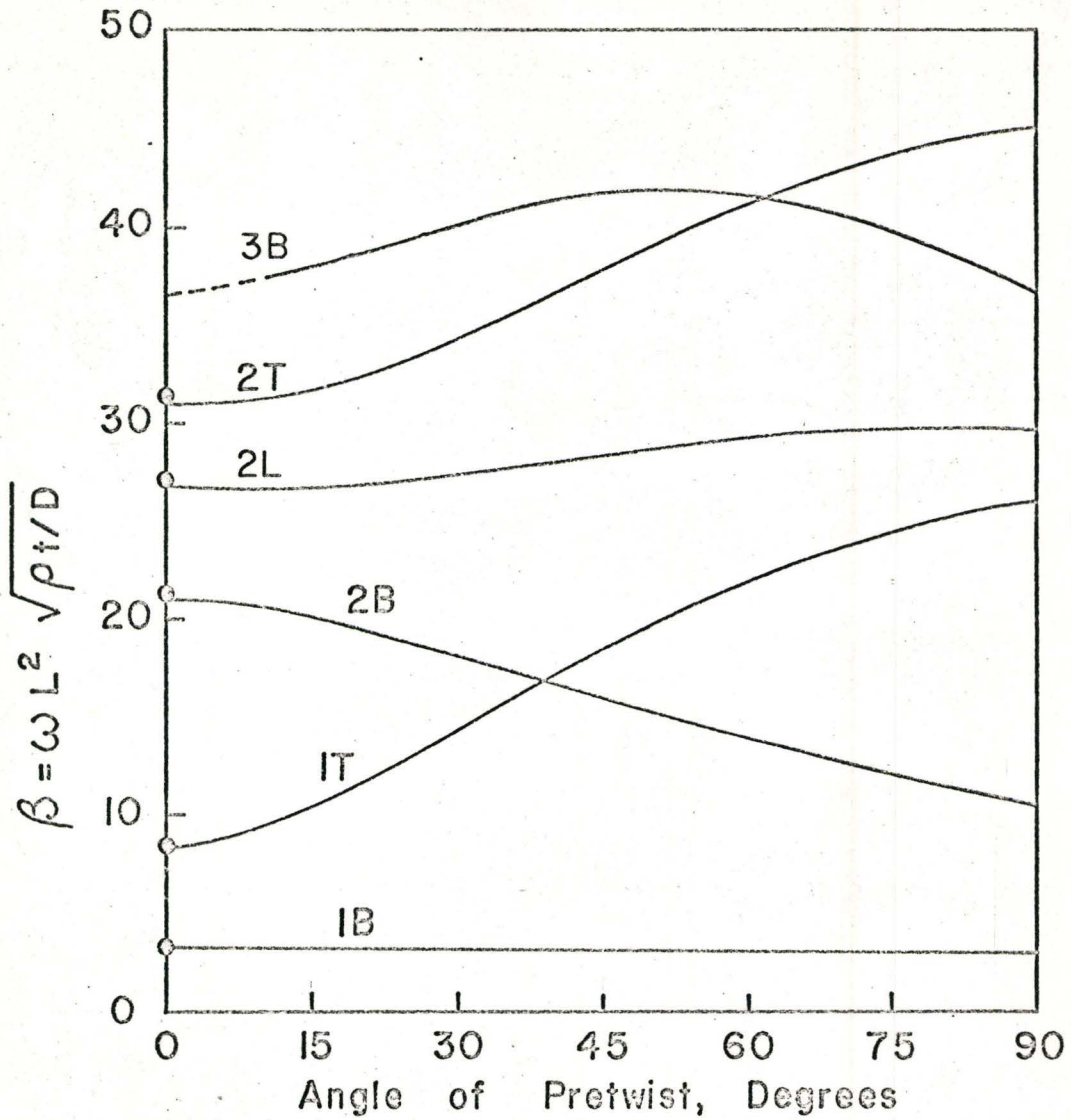


Figure 24

Deflection ( $w$ ) along the Line CD of  
Pretwisted Cantilever Plate Loaded at  
Free Corners

$L/b=1$ ,  $b/t=48$ , Mesh (6×6)

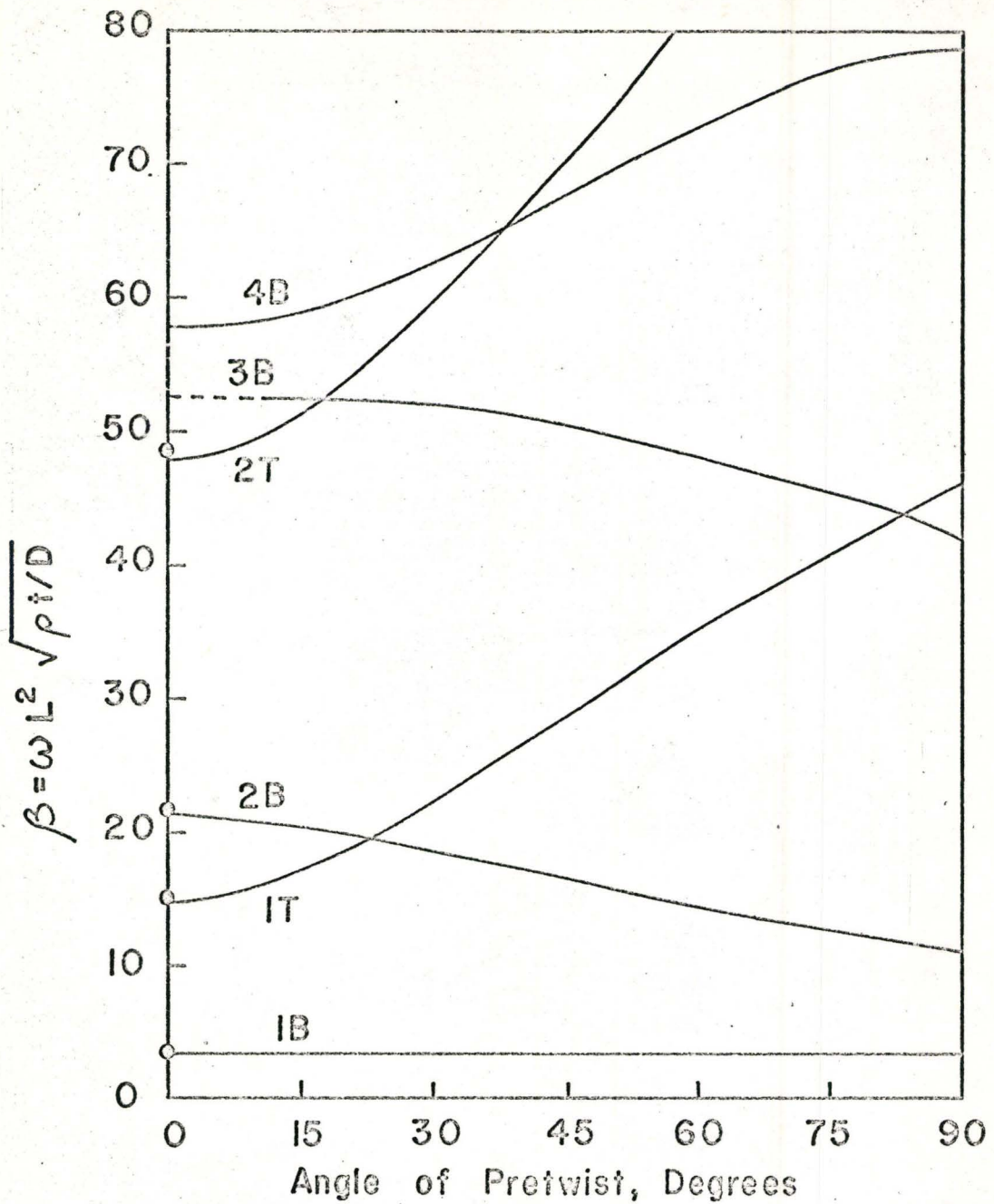


o Values by Ritz Method (Ref. 77)

Figure 25

Variation of Natural Frequencies with Pretwist for a Nonrotating Plate

$L/b=1$ ,  $b/t=16$ , Mesh (5×5)



○ Values by Ritz Method (Ref.77)

Figure 26

Variation of Natural Frequencies with Pretwist for Nonrotating Plate

$L/b=2, b/t=16, \text{Mesh } (7 \times 3)$



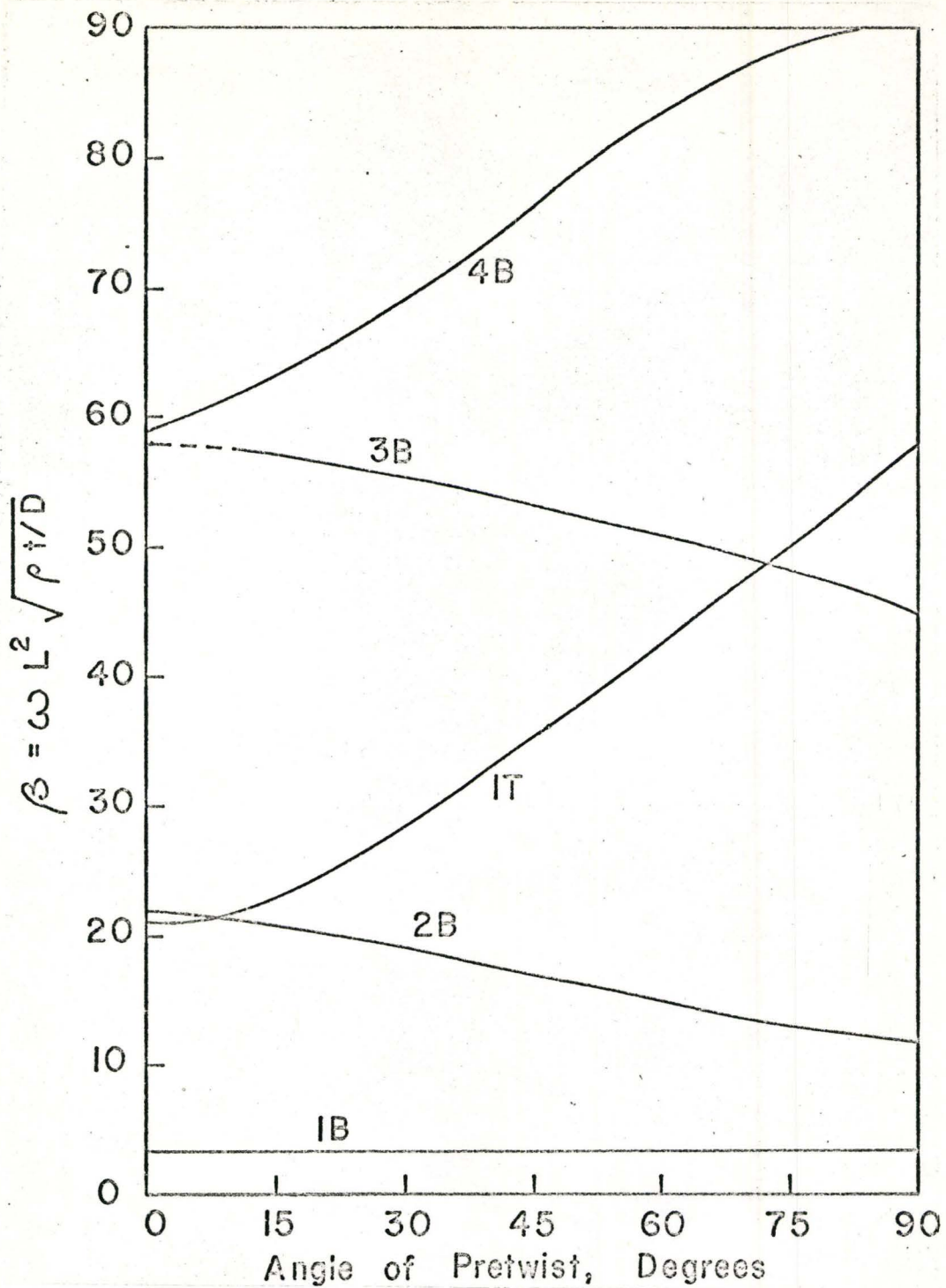
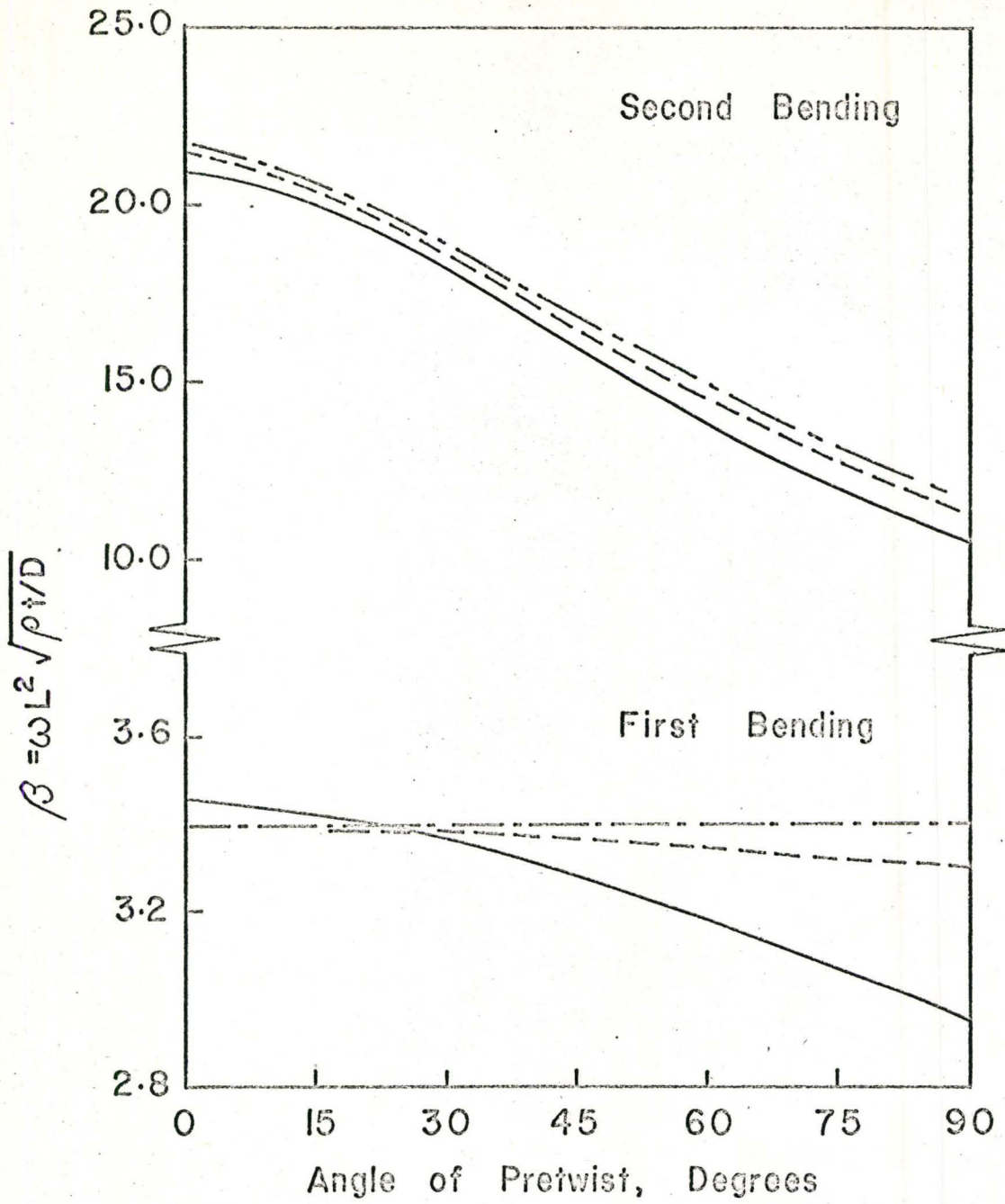


Figure 27

Variation of Natural Frequencies with Pretwist for a Nonrotating Plate

$L/b=3$ ,  $b/6=16$ , Mesh (7×3)



- $L/b = 1.0$
- - - - -  $L/b = 2.0$
- · - · -  $L/b = 3.0$

Figure 28

Variation of the First Two Bending Frequencies with Pretwist for Different Aspect Ratios

$b/t=16$

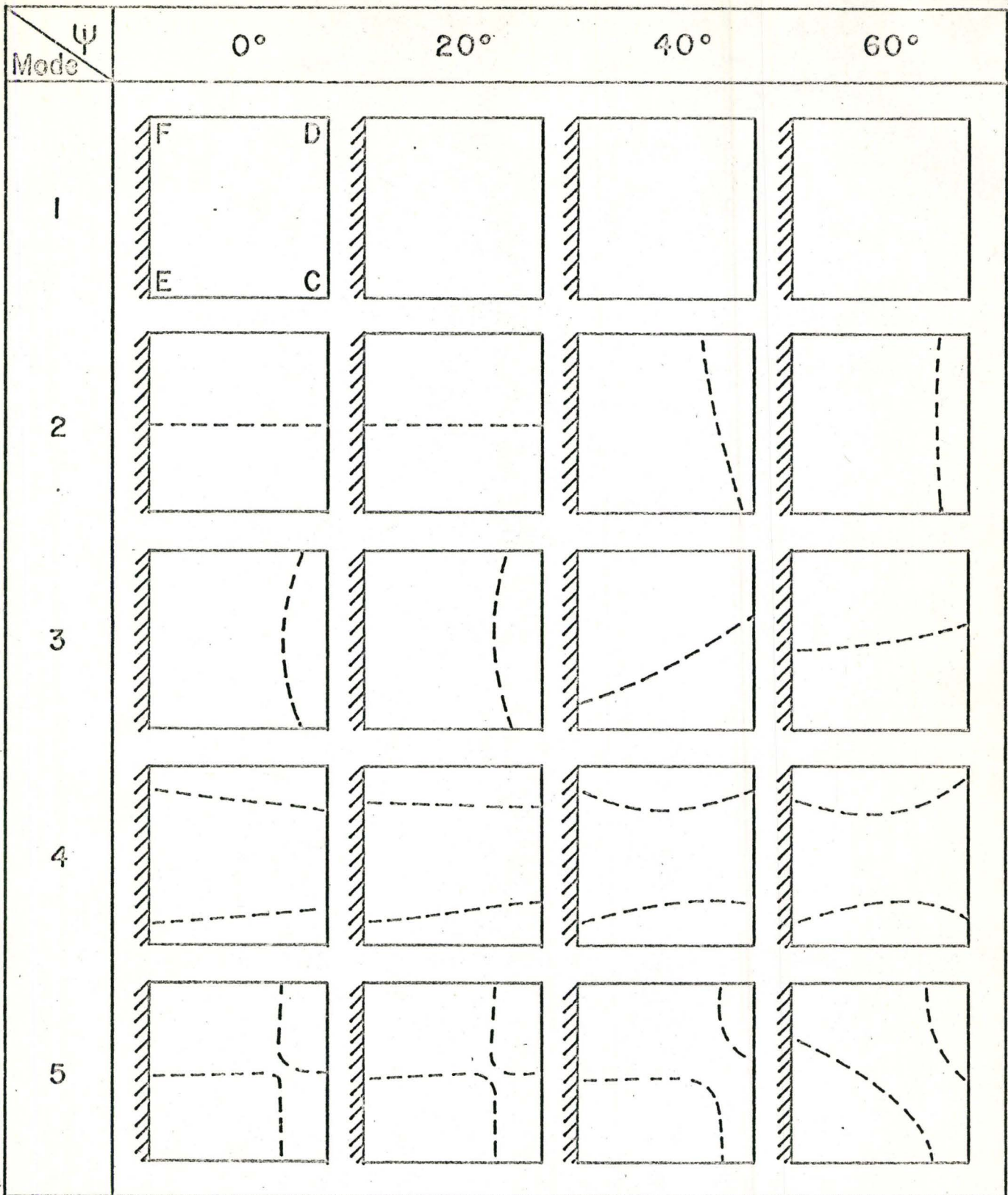
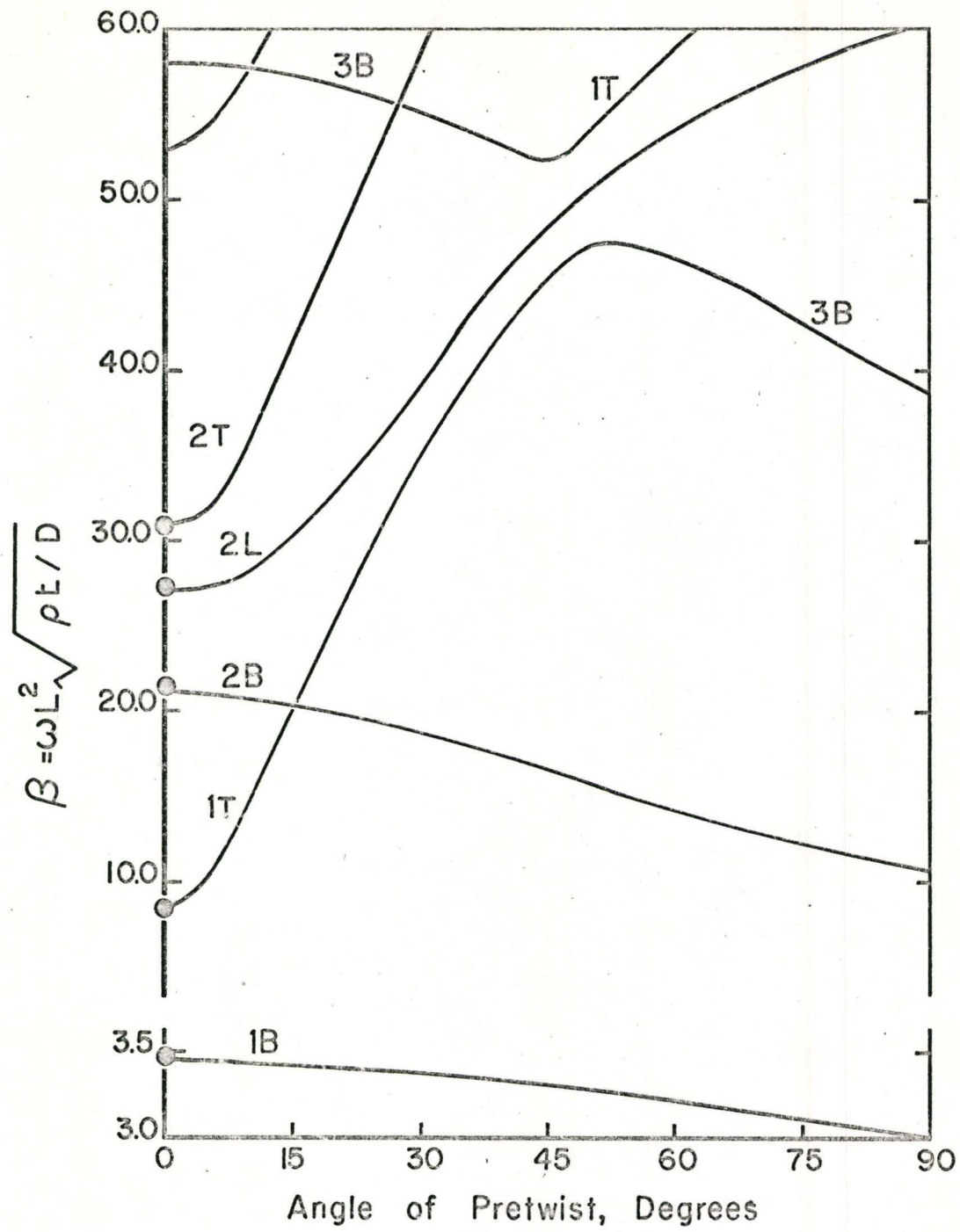


Figure 29

Mode Shapes of a Nonrotating Pretwisted Cantilever Plate  
 $L/b=1$ ,  $b/t=16$ , Mesh (5×5)





o Values by Ritz Method (Ref. 77)

Figure 30

Variation of Natural Frequencies with Pretwist for a Nonrotating Plate  
 $L/b=1, b/t=48, \text{ Mesh } (5 \times 5)$

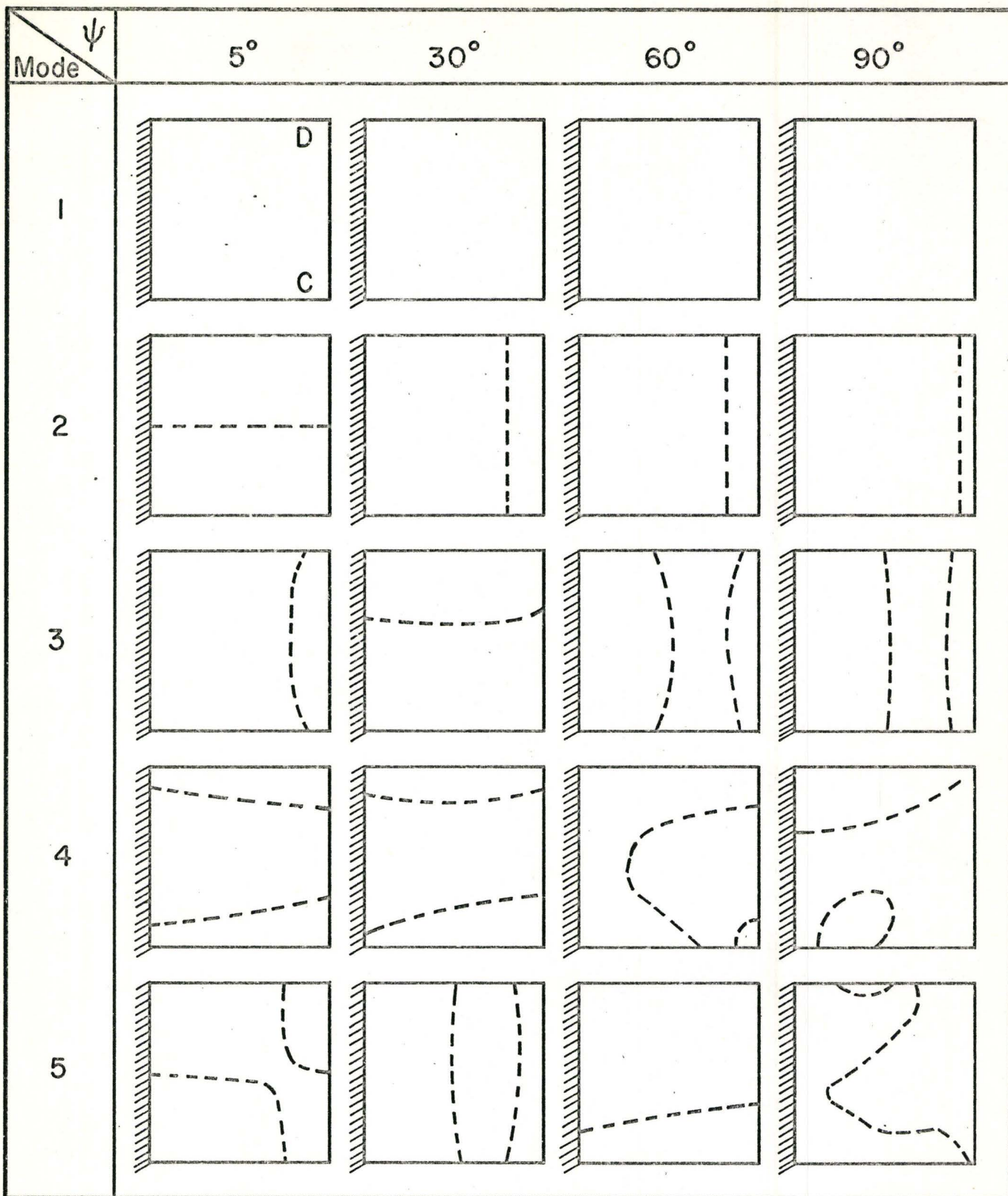


Figure 31

Mode Shapes of a Nonrotating Pretwisted Cantilever Plate  
 $L/b=1$ ,  $b/t=48$ , Mesh (5×5)

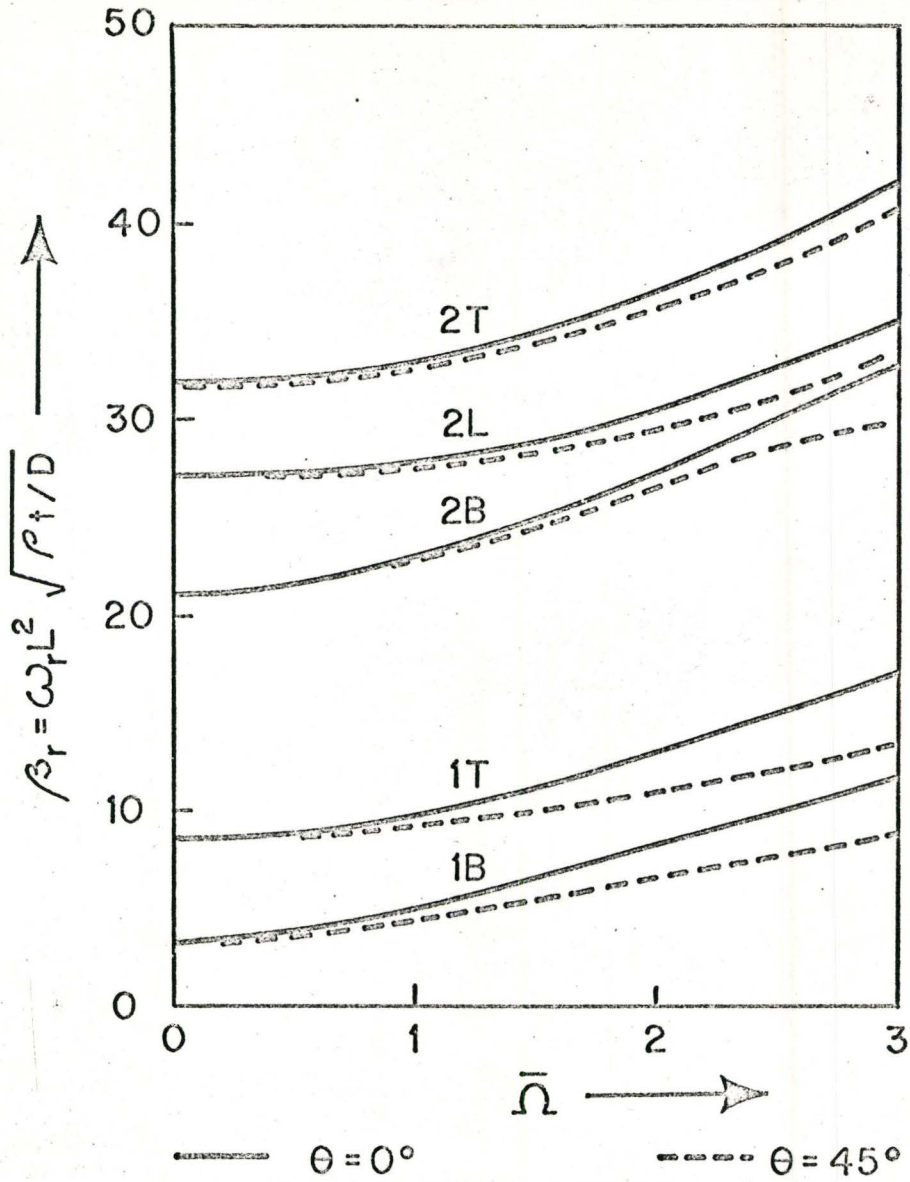


Figure 32

Variation of Natural Frequencies with Speed of Rotation for a Cantilever Plate

$L/b=1, \bar{r}=0, \text{Mesh } (5 \times 5)$



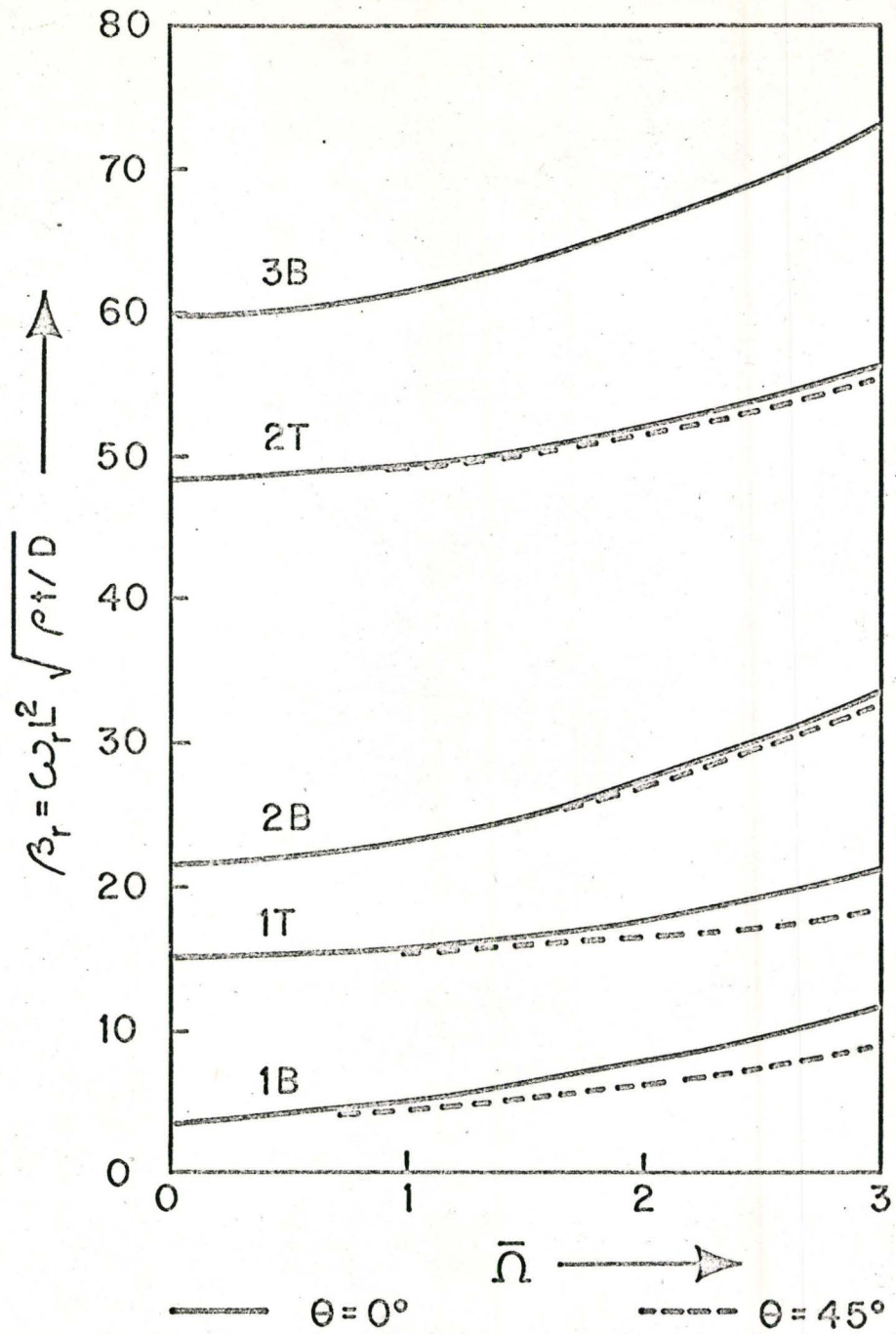


Figure 33

Variation of Natural Frequencies with  
Speed of Rotation for a Cantilever Plate

$L/b=2, \bar{r}=0, \text{mesh } (8 \times 4)$

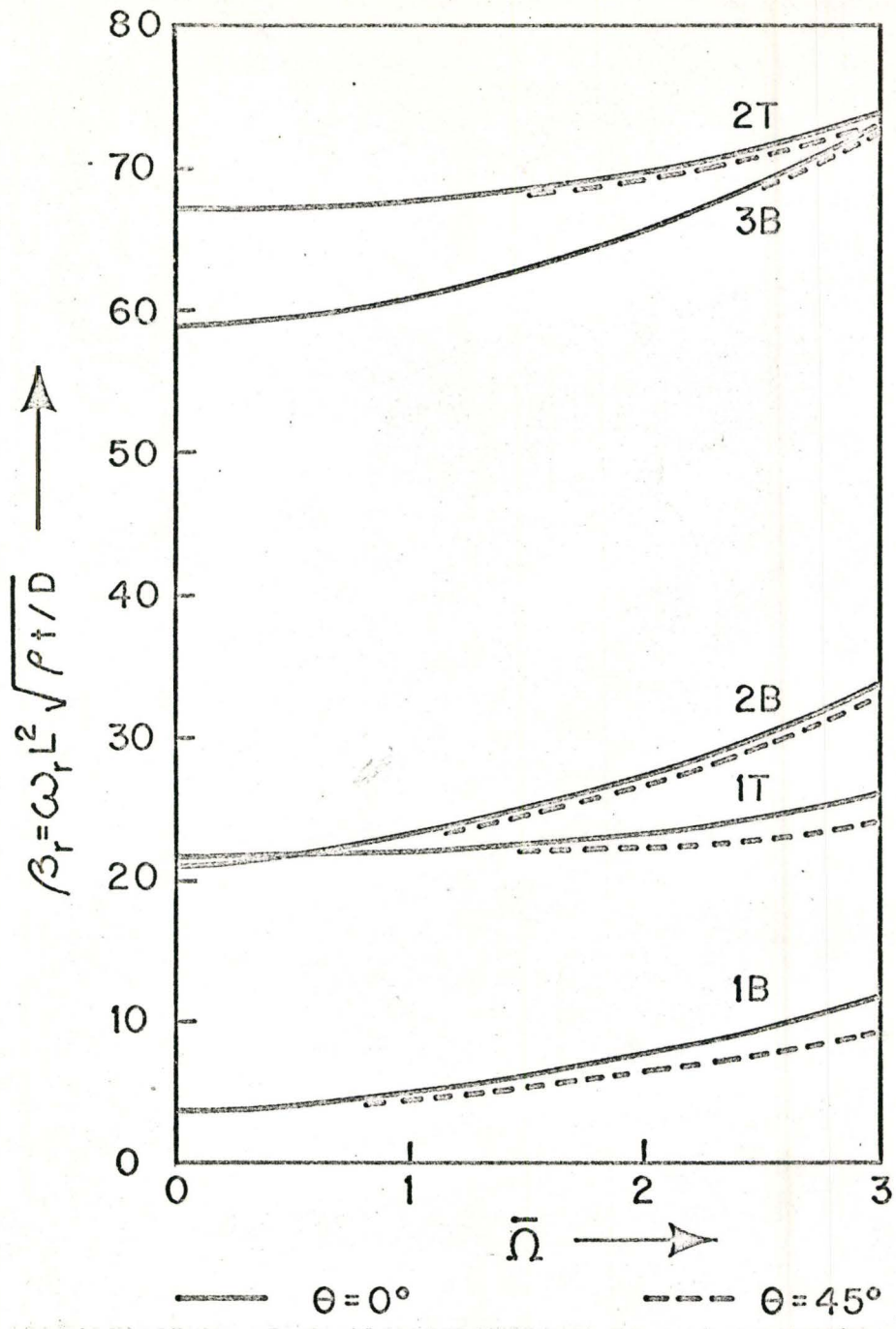


Figure 34

Variation of Natural Frequencies with  
 Speed of Rotation for a Cantilever Plate  
 $L/b=3, \bar{r}=0, \text{Mesh } (10 \times 3)$

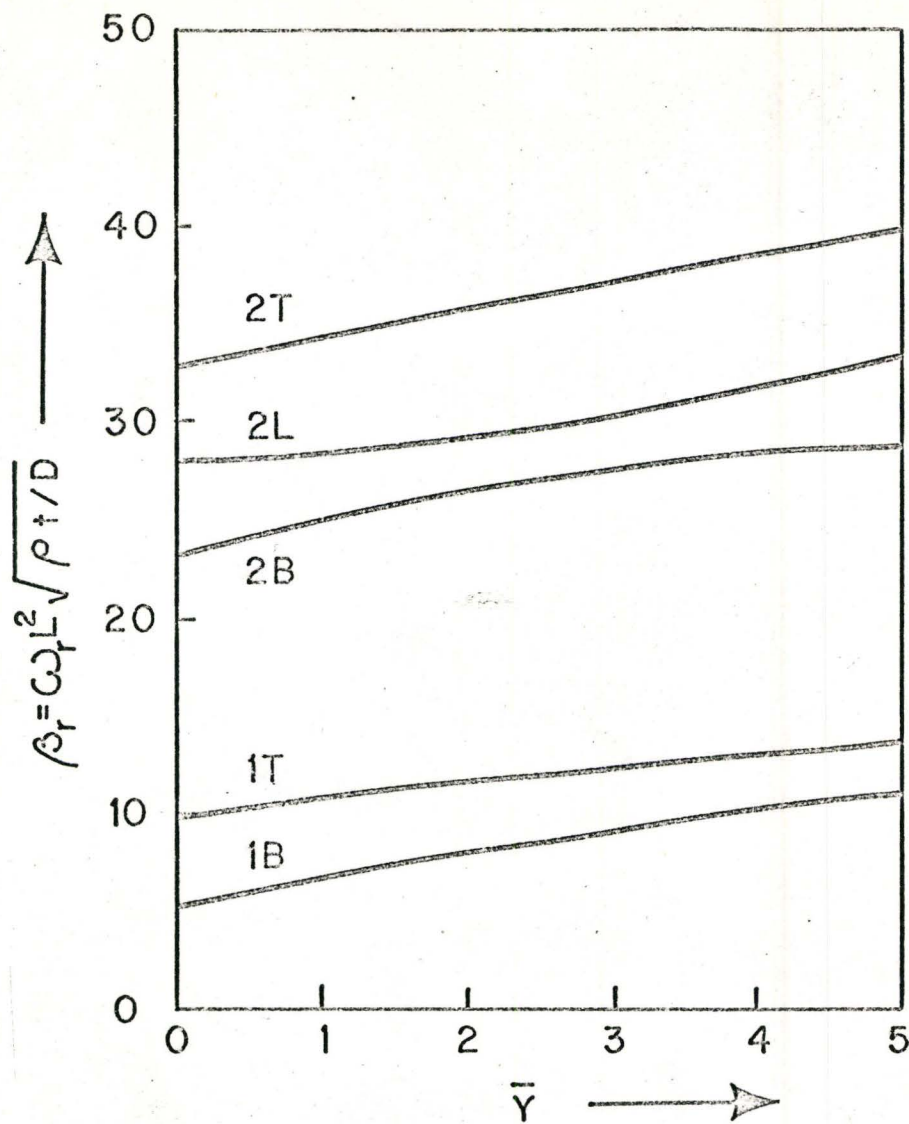


Figure 35

Variation of Natural Frequencies with Disc Radius for a Rotating Cantilever Plate

$L/b=1, \theta=0^\circ, \bar{\Omega}=1, \text{Mesh } (5 \times 5)$



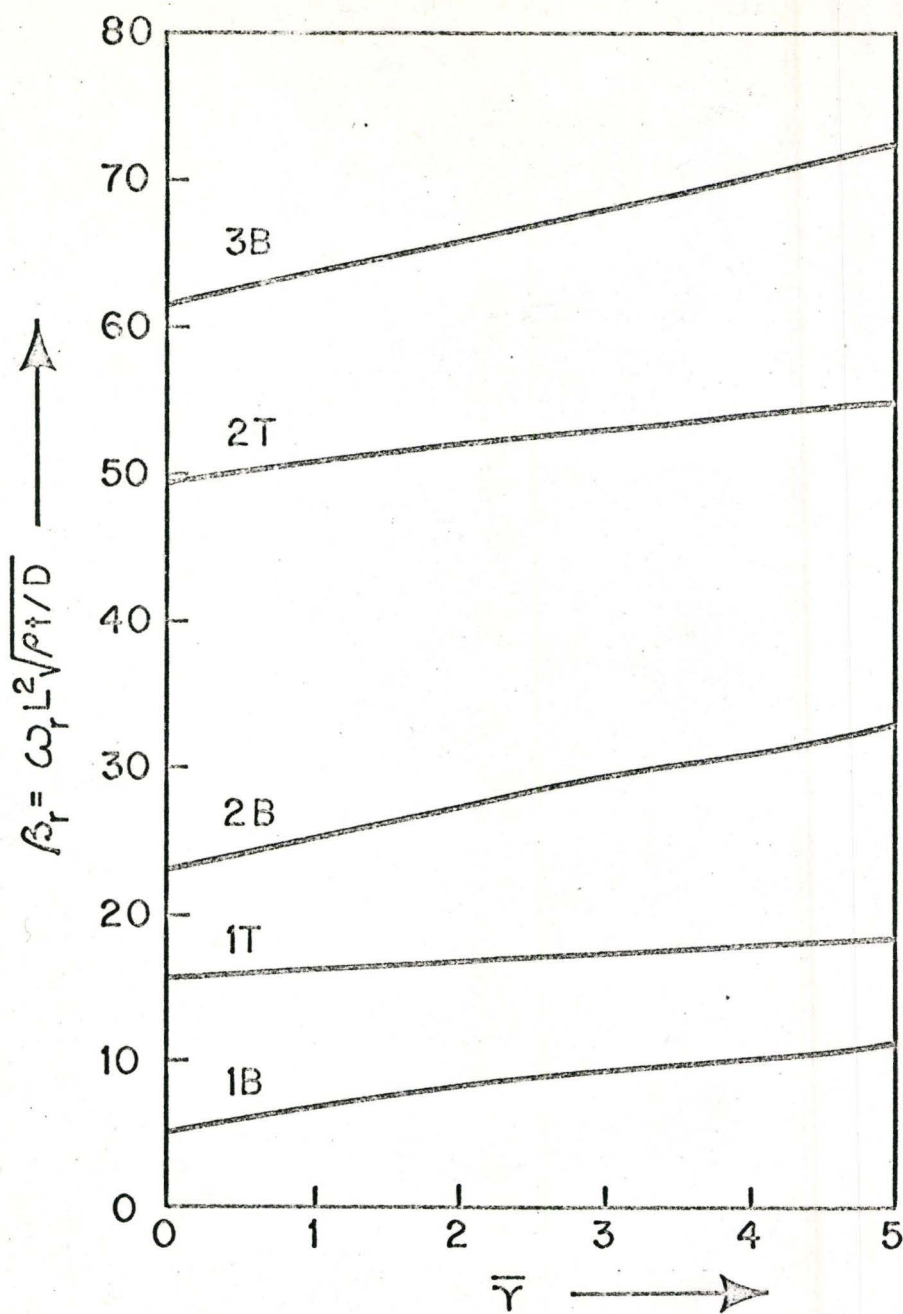


Figure 36

Variation of Natural Frequencies with  
Disc Radius for a Rotating Cantilever Plate

$L/b=2$ ,  $\theta=0^\circ$ ,  $\bar{\Omega}=1$ , Mesh (8×4)

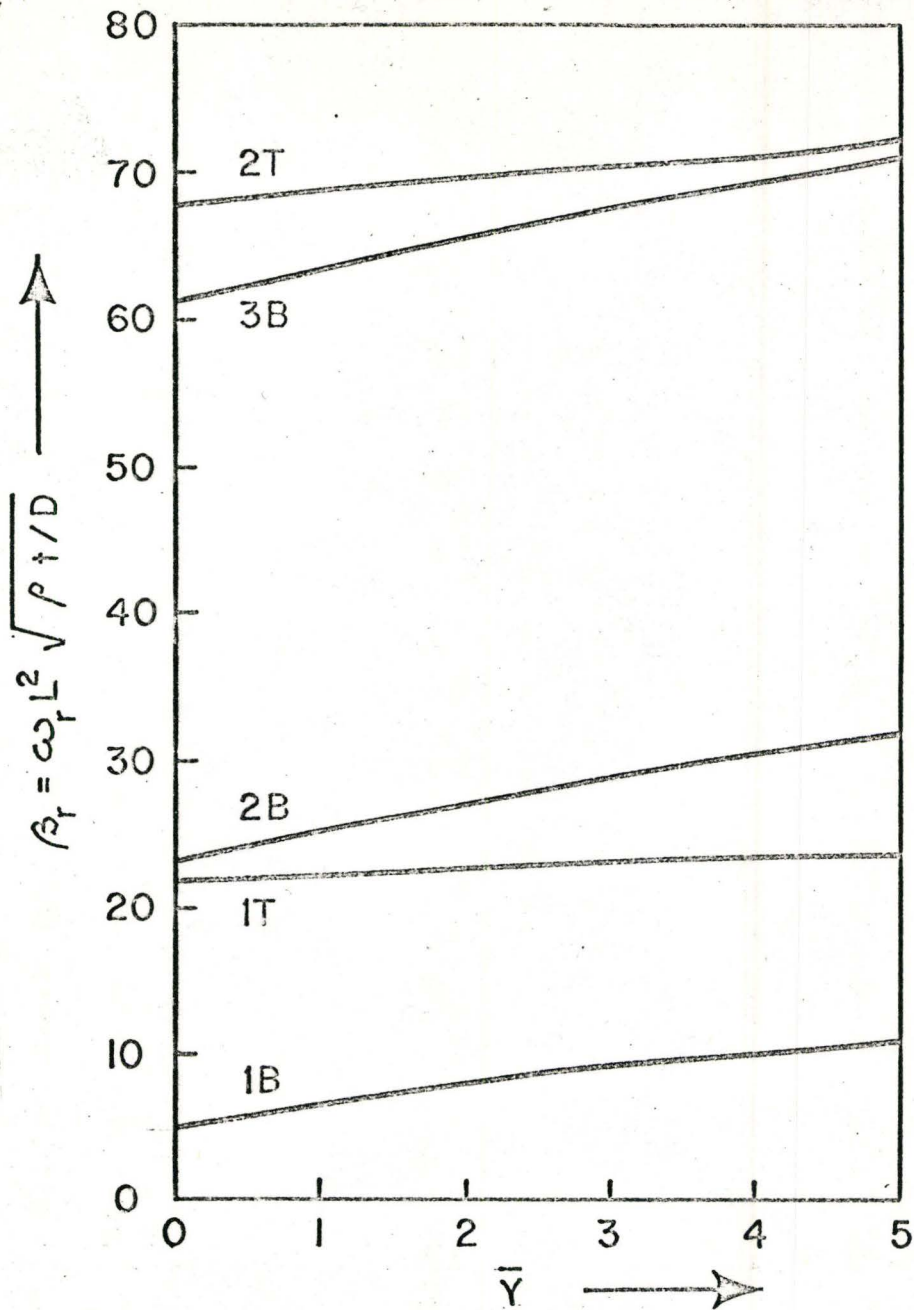


Figure 37

Variation of Natural Frequencies with  
Disc Radius for a Rotating Cantilever Plate

$L/b=3$ ,  $\theta=0^\circ$ ,  $\bar{\Omega}=1$ , Mesh (10×3)

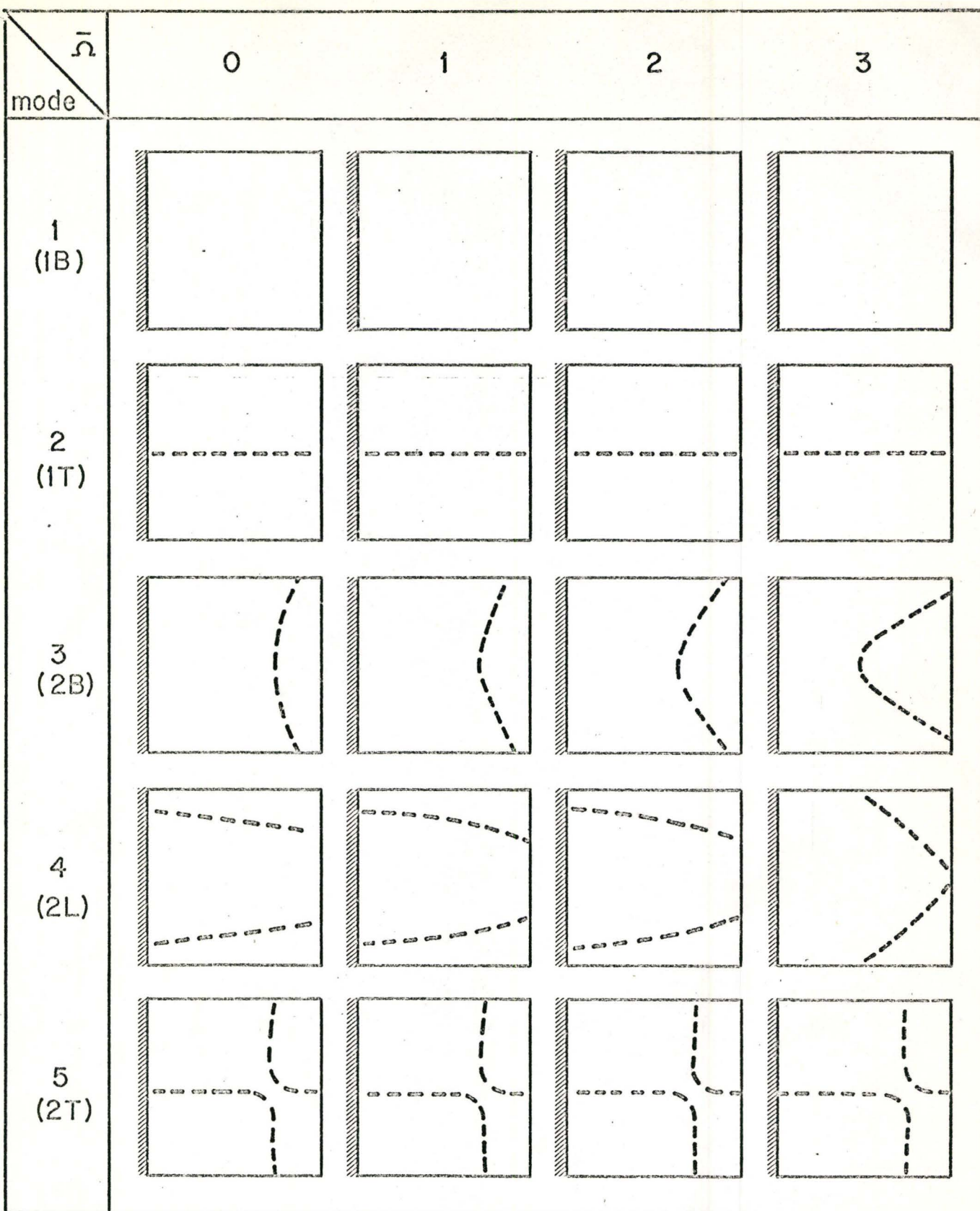


Figure 38

Mode Shapes of a Rotating Cantilever Plate  
 $L/b=1$ ,  $\bar{r}=0$ ,  $\theta=0^\circ$ , (Mesh  $5 \times 5$ )



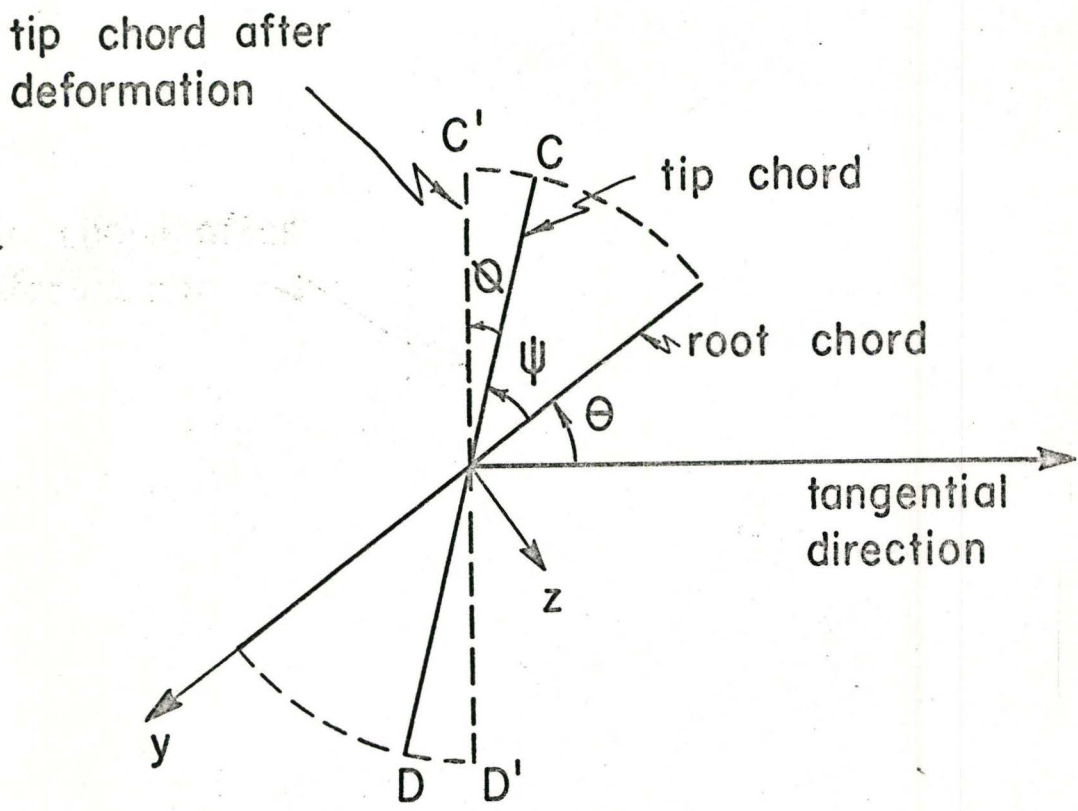


Figure 39

An Illustration for Positive Directions for  $\psi$ ,  $\theta$  and  $\phi$  in a rotating Pretwisted Cantilever Plate

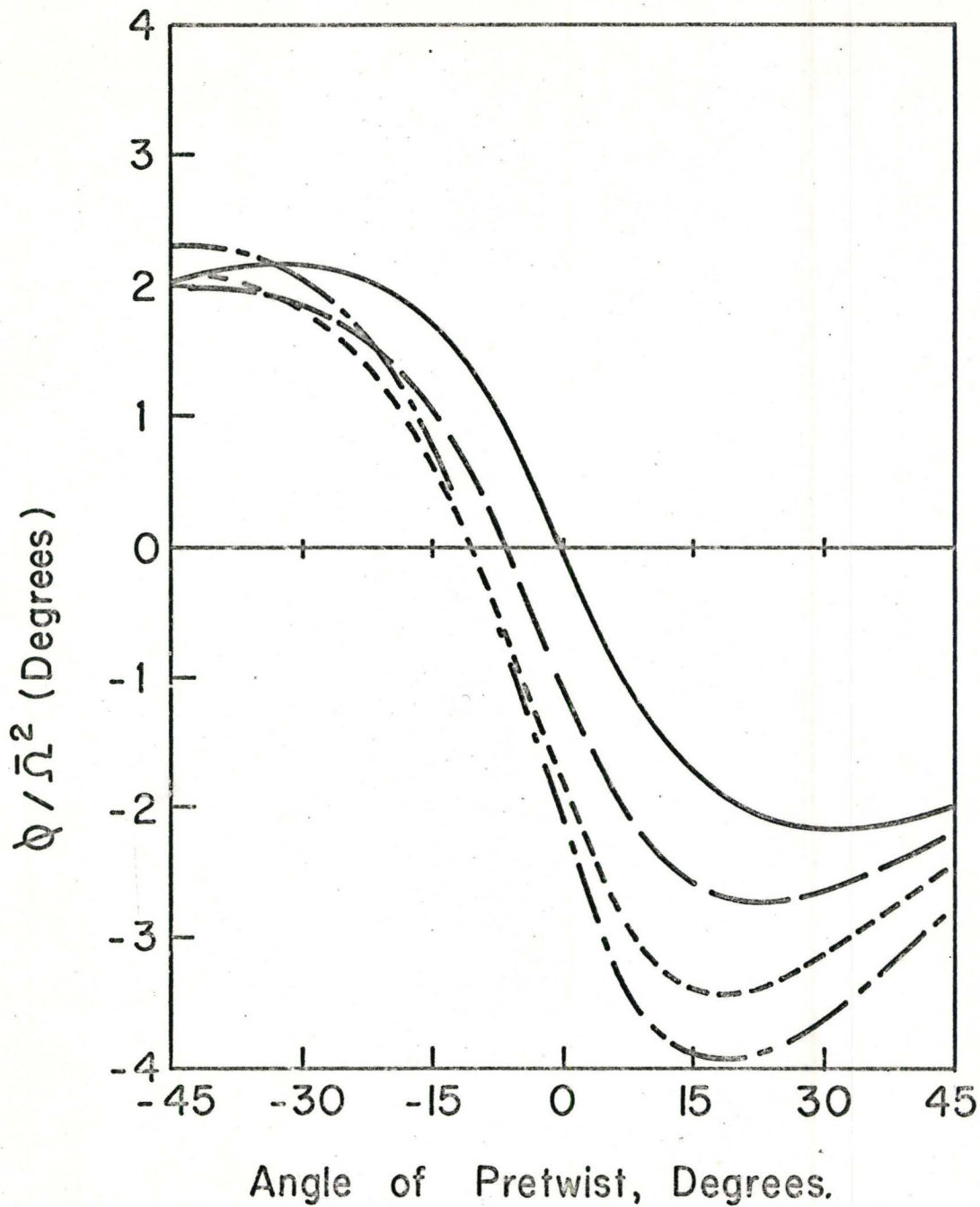


Figure 40

Pseudo-Static Deformation of a Rotating  
Pretwisted Cantilever Plate

$L/b=2, b/t=16, \bar{r}=2, \text{Mesh } (8 \times 4)$

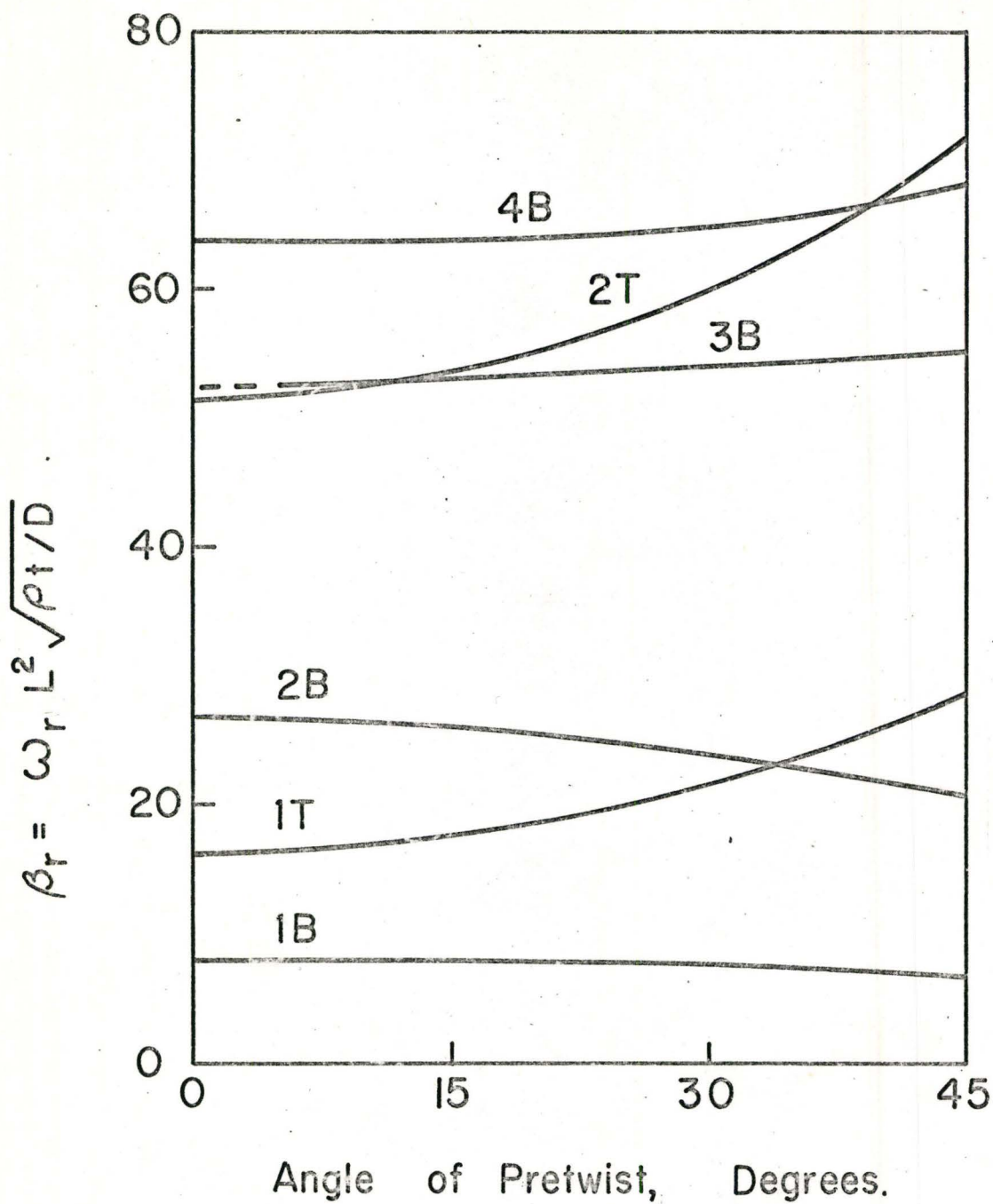
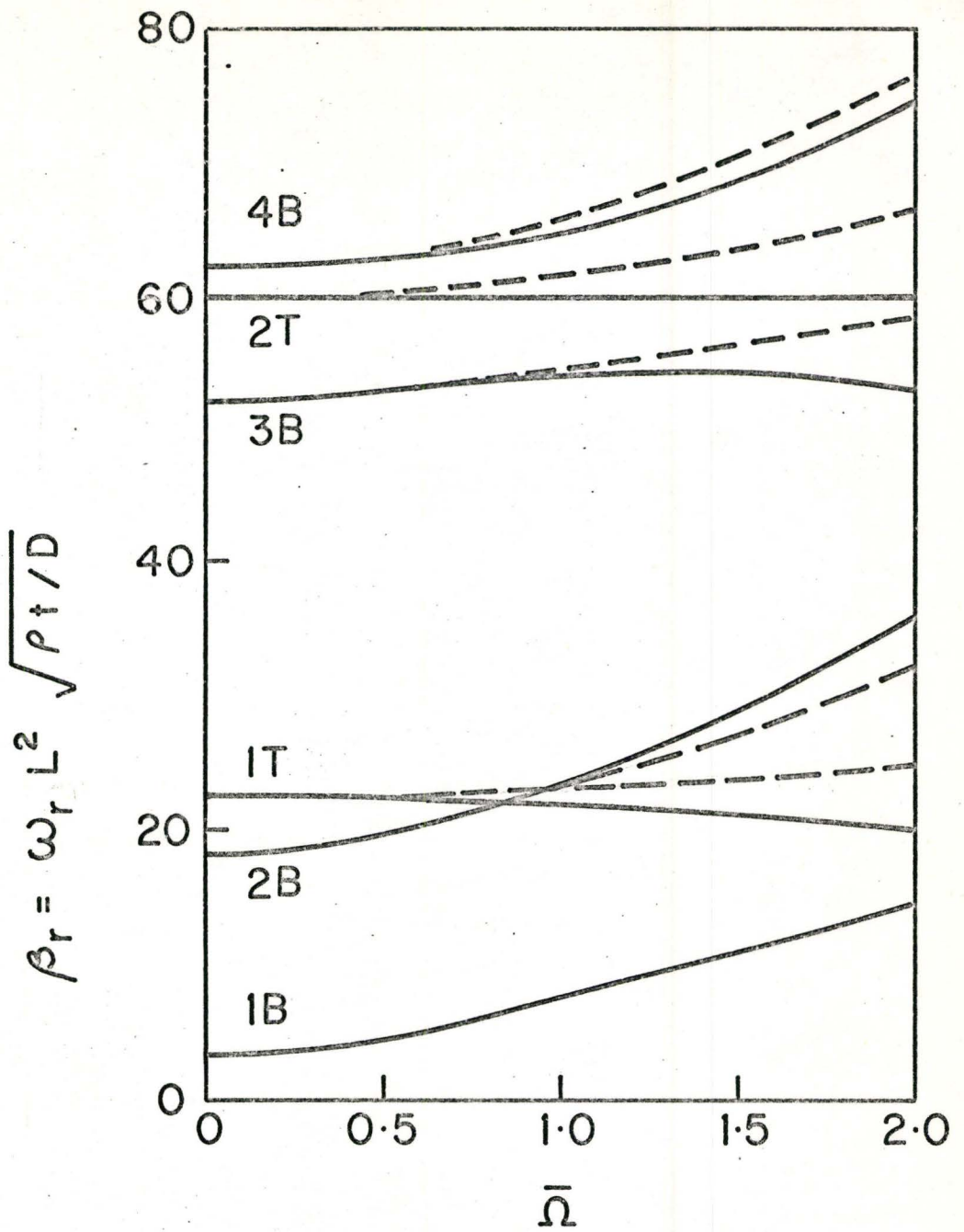


Figure 41

Variation of Natural Frequencies with Pretwist for a Rotating Cantilever Plate  
 $L/b=2$ ,  $b/t=16$ ,  $\bar{r}=2$ ,  $\theta=90^\circ$ ,  $\bar{\Omega}=1$ , Mesh (7×3)



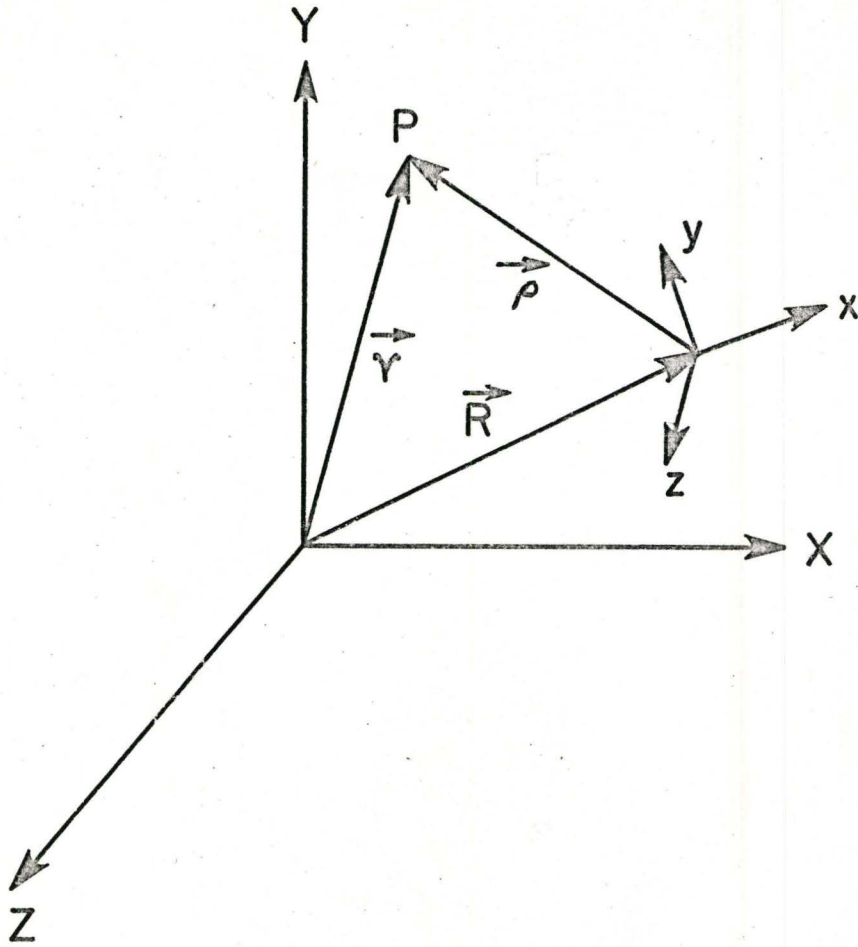


————— pseudo - static deformation included  
 - - - - - pseudo - static deformation neglected

Figure 42

Variation of Natural Frequencies with Speed of Rotation for a Pretwisted Cantilever Plate

$L/b=2, b/t=16, \bar{r}=2, \psi=30^\circ, \theta=90^\circ, \text{Mesh } (7 \times 3)$



XYZ fixed coordinate axes  
 xyz moving coordinate axes

Figure 43

Position Vectors of a Point on the  
 Blade Referred to Fixed and Moving  
 Coordinate Axes

## REFERENCES

1. Dokainish, M.A. and Jagannath, D.V., "Experimental Investigation of Gas Turbine Blade Vibration - A Review", ASME Paper No. 69-Vibr-59, 1969.
2. Zickel, J., "Bending of Pretwisted Beams", Journal of Applied Mechanics, Trans. ASME, Vol. 22, No. 3, Sept. 1955.
3. Zickel, J., "Pretwisted Beams and Columns", Journal of Applied Mechanics, Trans. ASME, Vol. 23, No. 2, June, 1956.
4. Den Hartog, J. P., "Advanced Strength of Materials", McGraw-Hill Book Company, Inc., New York, 1952.
5. Carnegie, W., "The Static Bending of Pretwisted Cantilever Blading", Proc. Instn. Mech. Engrs., Vol. 171, No. 32, 1957.
6. Carnegie, W., "Bending of Pretwisted Turbine Blades, Effect of Inclination of Longitudinal Fibres", Engineering, Vol. 185, No. 4809, May 9, 1958.
7. Flax, A. H., "Bending of Rotor Blades", Journal of the Aeronautical Sci. Vol. 14, No. 1, Jan. 1947.
8. Plunket, R., "Matrix Method of Calculating Propeller Blade Moments and Deflections", Journal of Applied Mechanics, Trans. ASME, Vol. 16, No. 4, Dec. 1949.
9. Myklestad, N.O., "A New Method of Calculating Natural Modes of Uncoupled Bending Vibration of Airplane Wings and Other Types of Beams", Journal of the Aeronautical Sci., Vol. 11, No. 4, April 1944.
10. Minhinnick, I.T., "The Theoretical Determination of Normal Modes and Frequencies of Vibration", AGARD Publications, Rep. 36, April 1956.
11. Duncan, W.J., "A Critical Examination of the Representation of Massive and Elastic Bodies by Systems of Rigid Masses Elastically Connected", The Quarterly Journal of Mechanics and Applied Maths., Vol. 5, 1952.
12. Leckie, F. A. and Lindberg, G.M., "The Effect of Lumped Parameters on Beam Frequencies", The Aeronautical Quarterly, Aug. 1963.



13. Siddall, J.N. and Isakson, G., "Approximate Analytical Methods for Determining Natural Modes and Frequencies of Vibration", MIT, Dept. Aero. Eng., Contract No. N5 ori-07833, ONR Project NR-035-259, Jan. 1951.
- ✓ 14. Jawson, M. J. and Ponter, A.R., "An Integral Equation Solution of the Torsional Problem", Proc. Royal Soc., Series A, Vol. 273, 1963.
- ✓ 15. Gere, J.M., "Torsional Vibrations of Beams of Thin-Walled Open Section", Journal of Applied Mechanics, Trans. ASME, Vol. 21, No. 4, Dec. 1954.
- ✓ 16. Carnegie, W., "Vibrations of Pretwisted Cantilever Blading", Proc. Instn. Mech. Engrs., Vol. 173, No. 12, 1959.
- ✓ 17. Carnegie, W., "Vibrations of Pretwisted Cantilever Blading: An Additional Effect Due to Torsion", Proc. Instn. Mech. Engrs., Vol. 176, No. 13, 1962.
18. Hanawa, T. and Koshide, S., "Numerical Examination of the Effects of Constraint on the Trial Function in Direct Application of Variational Calculus - Pure Torsional Vibration of a Cantilever Beam as an Example", Proc. Fourteenth Japan National Cong. of Applied Mechanics, 1964.
- ✓ 19. Washizu, K., "Some Consideration of the Centre of Shear", Trans. Japan Soc. Aero. Space Sci., Vol. 9, No. 15, 1966.
20. Duncan, W. J., "The Flexural Centre or Centre of Shear", Journal of the Royal Aeronautical Soc., Vol. 57, Sept. 1953.
- ✓ 21. Jacobs, J.A., "The Centre of Shear of Aerofoil Sections", Journal of the Royal Aeronautical Soc., Vol. 57, April, 1953.
22. Whitehead, L.G. and McQuillin, L.A., "The Centre of Shear for Sections Bounded by Two Circular Arcs", Journal of the Royal Aeronautical Soc., Vol. 58, Feb. 1954.
- ✓ 23. Cowper, G.R., "A Computer Programme for Calculating Shear Centres and Other Section Properties", Mem. No. ST-68, National Aeronautical Estab., Ottawa, Canada, March 1966.

- ✓ 24. Myklestad, N.O., "New Method of Calculating Natural Modes of Coupled Bending-Torsion Vibrations of Beams", Trans. ASME, Vol. 67, No. 1, Jan. 1945.
25. Targoff, W. P., "The Associated Matrices of Bending and Coupled Bending-Torsion Vibrations", Journal of the Aeronautical Sci., Vol. 14, No. 10, Oct. 1947.
- ✓ 26. Gere, J. M. and Lin, Y. K., "Coupled Vibrations of Thin-Walled Beams of Open Cross-section", Journal of Applied Mechanics, Trans. ASME, Vol. 25, No. 3, Sept. 1958.
27. Tso, W. K., "Coupled Vibrations of Thin-Walled Elastic Bars", Journal of Eng. Mechanics Div., Proc. ASCE, EM3, June 1965.
28. Rosard, D.D., "Natural Frequencies of Twisted Cantilever Beams", ASME Paper No. 52-A-15, 1952.
29. Troesch, A., Anliker, M. and Ziegler, H., "Lateral Vibrations of Twisted Rods", Quarterly Journal of Applied Maths., Vol. XII, No. 2, 1954.
30. Anliker, M. and Troesch, B.A., "Theory of Lateral Vibrations of Pretwisted Rods", Z.A.M.P., Vol. 14, 1963.
31. DiPrima, R. C. and Handelman, G. H., "Vibrations of Twisted Beams", Quarterly Journal of Applied Maths., Vol. XII, No. 3, 1954.
- ✓ 32. Martin, A.I., "Approximation for the Effect of Twist on the Vibration of a Turbine Blade", The Aeronautical Quarterly, Aug. 1957.
- ✓ 33. Dawson, B., "Coupled Bending-Bending Vibrations of Pretwisted Cantilever Blading Treated by the Rayleigh-Ritz Energy Method", Journal of Mech. Eng. Sci., Vol. 10, No. 5, 1968.
34. Dawson, B. and Carnegie, W., "Modal Curves of Pretwisted Beams of Rectangular Cross-Section", Journal of Mech. Eng. Sci., Vol. 11, No. 1, 1969.
- ✓ 35. Carnegie, W., Dawson, B. and Thomas, J., "Vibration Characteristics of Cantilever Blading", Applied Mechanics Convn., Proc. Instn. Mech. Engrs., Vol. 180 (Part 3I), 1965-66.



36. Isakson, G. and Eisley, J.G., "Natural Frequencies in Bending of Twisted Rotating Blades", NASA, TN. D-371, March 1960.
37. White, W. T., "An Integral Equation Approach to Problems of Vibrating Beams", Journal Franklin Inst., Vol. 245, 1948.
38. Slyper, H. A., "Coupled Bending Vibrations of Pretwisted Cantilever Beams", Journal of Mech. Eng. Sci., Vol. 4, No. 4, 1962.
39. Dokumaci, E., Thomas, J. and Carnegie, W., "Matrix Displacement Analysis of Coupled Bending-Bending Vibrations of Pretwisted Blading", Journal of Mech. Eng. Sci., Vol. 9, No. 4, 1967.
40. Chen Chu, "The Effect of Initial Twist on the Torsional Rigidity of Thin Prismatic Bars and Tubes", Proc. First U.S. National Cong. of Applied Mechanics, 1951.
41. Reissner, E. and Washizu, K., "On Torsional Vibrations of a Beam with a Small Amount of Pretwist", Journal Japan Soc. of Aeronautical Engrs., Vol. 5, 1957.
42. DiPrima, R.C., "Coupled Torsional and Longitudinal Vibrations of a Thin Bar", Journal of Applied Mechanics, Trans. ASME, Vol. 26, No. 4, Dec. 1959.
- ✓ 43. Mendelson, A. and Gendler, S., "Analytical and Experimental Investigation on Effects of Twist on Vibrations of Cantilever Beams", NACA, TN 2300, 1951.
44. Dunham, J., "The Lowest Natural Frequency of an Axial Compressor Blade", Journal of the Royal Aeronautical Soc., Vol. 62, Sept. 1958.
- ✓ 45. Carnegie, W., "Vibrations of Pretwisted Cantilever Blading Allowing for Rotary Inertia and Shear Deflection", Journal of Mech. Eng. Sci., Vol. 6, No. 2, 1964.
46. Belgaumkar, B.M., Lakshminarayana, K. and Nakra, B.C., "Vibration Characteristics of Axial Flow Compressor Blades", Journal Sci. Eng. Research, India, Vol. VI, Pt. 2, 1962.
- ✓ 47. Isakson, G. and Eisley, J.G., "Natural Frequencies in Coupled Bending and Torsion of Twisted Rotating and Nonrotating Blades", NASA, CR-65, 1964.



48. Billington, A.E., "The Vibrations of Stationary and Rotating Cantilever With Special Reference to Turbine Blades", Council Sci. Indus. Res. Div. Aero. Report No. SM-109-E-61, Jan. 1948.
49. Sutherland, R.L., "Bending Vibration of a Rotating Blade Vibrating in the Plane of Rotation", Journal of Applied Mechanics, Trans. ASME, Vol. 16, No. 4, Dec. 1949.
50. Plunket, R., "Bending Vibration of a Rotating Blade Vibrating in the Plane of Rotation", Journal of Applied Mechanics, Trans. ASME, Vol. 17, No. 2, June 1950.
51. Lo, Hsu and Renbarger, J. L., "Bending Vibrations of Rotating Beams", Proc. First U.S. National Cong. of Applied Mechanics, 1951.
52. Lo, Hsu, "A Nonlinear Problem in Bending Vibration of a Rotating Beam", Journal of Applied Mechanics, Trans. ASME, Vol. 19, No. 4, Dec. 1952.
53. Marshall, H.M., "The Effect of Coriolis Acceleration on the Bending Vibration of a Rotating Beam", Master of Science Thesis, School of Aeronautics, Perdue Univ., 1952.
54. Bogdanoff, J. L., "Influence of Secondary Inertia Terms on Natural Frequencies of Rotating Beams", Journal of Applied Mechanics, Trans. ASME, Vol. 22, No. 4, Dec. 1955.
55. Schilhansl, M. J., "Bending Frequency of a Rotating Cantilever Beam", Journal of Applied Mechanics, Trans. ASME, Vol. 25, No. 1, March 1958.
56. Kissel, W., "The Lowest Natural Bending Frequency of a Rotating Blade of Uniform Cross-Section", Escher Wyss News, Vol. 31, No. 3, 1958.
57. Yntema, R. T., "Simplified Procedures and Charts for the Rapid Estimation of Bending Frequencies of Rotating Beams", NACA, TN. 3459, 1955.
58. Carnegie, W., "Vibrations of Rotating Cantilever Blading: Theoretical Approaches to the Frequency Problem Based on Energy Methods", Journal of Mech. Eng. Sci., Vol. 1, No. 3, 1959.

59. Kundu, B.B., "Note on the Transverse Vibration of a Homogeneous Rotating Thin Rod in the Form of a Pyramid With Square Base", Indian Journal of Mechanics and Maths., Vol. 4, No. 1, 1966.
60. Vorob'ev, Yu. S., "Improved Equations of the Free Oscillations of Rotating Rods" (In Russian), Rabochie Protssesy V Turbomashinakh i Prochnust'ik Elementov, Kiev, Nauk-Dumka, 1965.
61. Turner, M.J. and Duke, J.B., "Propeller Flutter", Journal of the Aeronautical Sci., Vol. 16, No. 6, June 1949.
62. Plunket, R., "Free and Forced Vibrations of Rotating Blades", Journal of Aeronautical Sci., Vol. 18, No. 4, April 1951.
63. Jaret, G.W. and Warner, P.C., "The Vibration of Rotating, Tapered Twisted Beams", Journal of Applied Mechanics, Trans. ASME, Vol. 20, No. 3, Sept. 1953.
64. Targoff, W., "The Bending Vibrations of a Twisted Rotating Beam", Proc. Third Midwestern Conf. on Solid Mechanics, 1957.
65. Bogdanoff, J.L. and Horner, J.T., "Torsional Vibrations of Rotating Twisted Bars", Journal of the Aeronautical Sci., Vol. 23, No. 4, April 1956.
66. Brady, W.G. and Targoff, W.P., "Uncoupled Torsional Vibrations of a Thin, Twisted, Rotating Beam", WADC Tech. Report 56-501, 1957.
67. Houbolt, J.C. and Brooks, G.W., "Differential Equations of Motion for Combined Flapwise Bending, Chordwise Bending and Torsion of Twisted, Nonuniform Rotor Blades", NACA, Report 1346, 1958.
68. Montoya, J., "Coupled Bending and Torsional Vibrations in a Twisted Rotating Blade" Brown Boveri Review, Vol. 53, No. 3, March 1966.
69. Krupka, R.M. and Baumanis, A.M., "Bending-Torsion Mode of a Rotating Tapered Twisted Turbomachine Blade", ASME Paper No. 68-WA/GT-6, 1968.
70. Krupka, R.M. and Baumanis, A.M., "Bending-Bending Mode of a Rotating Tapered-Twisted Turbomachine Blade Including Rotary Inertia and Shear Deformation", ASME Paper No. 69-Vibr -50, 1969.



71. Ashwell, D.G., "The Anticlastic Curvature of Rectangular Beams and Plates", Journal of the Royal Aeronautical Soc., Vol. 52, Nov. 1948.
72. Gerard, G., "Note on Beams and Plates", Journal of the Aeronautical Sci., Vol. 19, No. 3, March 1952.
73. Cowper, G. R., "An Extension of Beam Theory to Include Transverse Curvature", Mem. No. ST-84, National Aeronautical Estab., Ottawa, Canada, Aug. 1967.
74. Cowper, G.R., "Some Applications of Extended Beam Theory to Flat Plates", Mem. No. ST-94, National Aeronautical Estab., Ottawa, Canada, June 1968.
75. Hasan, S.A. and Barr, A.D.S., "Cross-Section Deformation Effects in the Vibration of Thin-Walled Beams of Arc Section", Journal of Mech. Eng. Sci., Vol. 7, No. 3, 1965.
76. Young, D., "Vibration of Rectangular Plates by Ritz Method", Journal of Applied Mechanics, Trans. ASME, Vol. 17, No. 4, Dec. 1950.
77. Barton, M. V., "Vibration of Rectangular and Skew Cantilever Plates", Journal of Applied Mechanics, Trans. ASME, Vol. 18, No. 2, June 1951.
78. Dawe, D.J., "A Finite Element Approach to Plate Vibration Problems", Journal of Mech. Eng. Sci., Vol. 7, No. 1, 1965.
79. Dawe, D.J., "Vibration of Rectangular Plates of Variable Thickness", Journal of Mech. Eng. Sci., Vol. 8, No. 1, 1966.
80. Anderson, R.G., Irons, B.M. and Zienkiewicz, O.C., "Vibration and Stability of Plates Using Finite Elements", Int. Journal of Solids and Structures, Vol. 4, 1968.
81. Maunder, L. and Reissner, E., "Pure Bending of Pretwisted Rectangular Plates", Journal of Mechanics and Physics of Solids, Vol. 5, 1957.
82. Reissner, E., "On Transverse Vibrations of Thin Shallow Elastic Shells", Quarterly of Applied Maths., Vol. 13, 1955.



83. Nagadhi, P. M., "On the General Problem of Elastokinetics in the Theory of Shallow Shells", Proc. IUTAM Symposium on the Theory of Thin Elastic Shells, Delf., Netherlands, 1959.
84. Nordgren, R. P., "On Vibrations of Pretwisted Rectangular Plates", Journal of Applied Mechanics, Trans. ASME, Vol. 29, No. 1, March 1962.
85. Olson, M. V. and Lindberg, G.M., "A Finite Cylindrical Shell Element and the Vibrations of a Curved Fan Blade", Aeronautical Report LR-497, National Research Council of Canada, Feb. 1968.
86. Newmark, N. M. and Veletos, A. S., "A Simple Approximation for the Natural Frequencies of Partly Restrained Bars", Journal of Applied Mechanics, Trans. ASME, Vol. 19, No. 1, March, 1952.
87. Amba Rao, C. L., "Method of Calculation of Frequencies of Partially Fixed Beams Carrying Masses", Journal of Acoustical Soc. of America, Vol. 40, No. 2, 1966.
88. Perkins, K.A.R., "The Effect of Support Flexibility on The Natural Frequencies of a Uniform Cantilever", Journal of Sound and vibration, Vol. 4, No. 1, July 1966.
89. Traupel, W., "Thermische Turbomaschinen", Vol. 2, Springer, Berlin, 1960.
90. Baur, P., "Natural Frequencies of Unshrouded Cantilever Blades", The Engineer, Vol. 218, No. 5675, Oct. 30, 1964.
91. Chaplin, R., "Natural Frequencies of Vibration of Prismatic Blades with Particular Reference to a 12 Stage Turbine", Aeronautical Research Council, London, Curr. Paper 95, 1952.
92. Niordson, F., "Vibration of Turbine Blades with Loose Hinge Support", Acta Ployt., Mech. Eng. Series, Vol. 3, No. 3, 1954.
93. Goatham, J. I. and Smailes, G.T., "Some Vibration Characteristics of Pin-Fixed Compressor Blades", ASME Paper No. 66-WA/GT-4, 1966.

94. Ellington, J.P. and McCallion, H., "Blade Frequency of Turbines, Effect of Disc Elasticity", Engineering, Vol. 187, No. 4862, May 15, 1959.
95. Söhngen, H., "Vibrational Behaviour of Blade Ring in Vacuum", (In German), Dtsch. Versuchsanstalt Luftabart E.V. Report 1, Aug. 1955.
96. Fillipov, A.P., "Tangential Vibrations of Turbine Blades Taking into Account Vibrations of Disc in Its Plane", (In Ukranian), Prikl Mekh, Vol. 6, No. 3, 1960.
97. Wagner, J.T., "Coupling of Turbomachine Blade Vibrations Through the Rotor", ASME Paper No. 66-WA/GT-5, 1966.
98. Smith, D.M., "Vibrations of Turbine Blades in Packets", Proc. Seventh Int. Congress of Applied Mechanics, Vol. 3, 1948.
99. Prohí, M.A., "A Method for Calculating Vibration Frequency and Stress of a Banded Group of Turbine Buckets", ASME Paper No. 56-A-116, 1956.
100. Tuncel, Ö., Bueckner, H.F. and Koplik, B., "An Application of Diakoptics in the Determination of Turbine Bucket Frequencies by the Use of Perturbations", ASME Paper No. 69-Vibr-57, 1969.
101. Fujino, T., "A Theoretical Consideration on the Vibration of Turbine Blade System", Bult. Japan Soc. Mech. Eng., Vol. 1, No. 2, 1958.
102. Singh, B.R. and Nandeeswaraiya, N.S., "Vibration Analysis of Shrouded Turbine Blades", Journal Instn. Engrs., India, Vol. 40, No. 1, Pt. 2, Sept. 1959.
103. Stargardter, H., "Dynamic Models of Vibrating Rotor Stages", ASME Paper No. 66-WA/GT-8, 1966.
104. Hanson, M.P., "Effect of Blade-Root Fit and Lubrication on Vibration Characteristics of Ball Root Type Axial-Flow Compressor Blades", NACA, RM E50C17, 1950.
105. Goodman, L.E. and Klumpp, J.H., "Analysis of Slip Damping with Reference to Turbine Blade Vibration", Journal of Applied Mechanics, Trans. ASME, Vol. 23, No. 3, Sept. 1956.



106. Kozolov, I. A., "Structural Dissipation of Energy During Vibration of Turbine Blades", (In Russian), V.Sb., Rasseyanie Energii pri Kolebaniyakh Uprug. Sistem. Kiev. Nauk, USSR. 1963.
107. Lazan, B. J., "Energy Dissipation in Structures with Particular Reference to Material Damping in Structural Damping", (Editor J. E. Ruzicka), ASME, New York, Dec. 1959.
108. Morduchow, M., "On Internal Damping of Rotating Beams", NACA, TN. 1996, 1949.
109. Pisarenko, G.S., "Vibration of Elastic Systems Taking Account of Energy Dissipation in the Material: WADD TR. 60-582, Feb. 1962.
110. Baker, W. E., Woolam, W. E. and Young, D., "Air and Internal Damping of Thin Cantilever Beams", Int. Journal of Mech. Eng. Sci., Vol. 9, 1967.
111. Pearson, H., "The Aerodynamics of Compressor Blade Vibration", Proc. Fourth Anglo-American Aeronautical Conf., London, 1953.
112. Shannon, J. F., "Vibration Problems in Gas Turbine, Centrifugal and Axial Flow Compressors", Aeronautical Research Council, R and M 2226, March 1945.
113. Carter, A. D. S. and Kilpatrick, D. A., "Self Excited Vibration of Axial-Flow Compressor Blades", Proc. Instn. Mech. Engrs., Vol. 171, No. 7, 1957.
114. Blackwell, B.D., "Some Investigations in the Field of Blade Engineering", Journal of the Royal Aeronautical Soc., Vol. 62, Sept. 1958.
115. Armstrong, E. K. and Stevenson, R. E., "Some Practical Aspects of Compressor Blade Vibration", Journal of the Royal Aeronautical Soc., Vol. 64, March 1960.
116. Armstrong, E. K., "Recent Blade Vibration Techniques", ASME Paper No. 66-WA/GT-14, 1966.
117. Lewis Center Staff, "Factors That Affect Operational Reliability of Turbojet Engines", NASA, TR R-54, 1960.



118. "The Vibration of Blades in Axial Turbomachinery, Part I: Theory and Practice of Design and Development; Part II: Design and Development Handbook", Northern Research and Eng. Corp., Cambridge, Mass., Report No. 1088, 1965.
119. Smith, J.E., "The Vibration of Blades in Axial Turbomachinery", ASME Paper No. 66-WA/GT-12, 1966.
120. Whitehead, D. S., "Bending Flutter of Unstalled Cascade Blades at Finite Deflection", Aeronautical Research Council, England, Report No. 24059, 1962.
121. Bury, K. V., "A Method of Calculating and Designing for a Minimum Vibration of Turbomachinery Blades", ASME Paper No. 67-Vibr-49, 1967.
122. Zienkiewicz, O. C. and Cheung, Y. K., "The Finite Element Method in Structural and Continuum Mechanics", McGraw-Hill Publishing Co. Ltd., 1967.
123. Zienkiewicz, O. C. and Cheung, Y. K., "Finite Element Method of Analysis for Arch Dam Shells and Comparison with Finite Difference Procedures", Proc. of Symposium on Theory of Arch Dams, Southampton Univ., 1964, (Pergamon Press, 1965).
124. Clough, R. W. and Johnson, C. P., "A Finite Element Approximation for the Analysis of Thin Shells", Int. Journal of Solids and Structures, Vol. 4, 1968.
125. Adini, A., "Analysis of Shell Structures by Finite Element Method", Ph.D. Dissertation, Dept. of Civil Eng., Univ. of California, 1961.
126. Tocher, J. L., "Analysis of Plate Bending Using Triangular Elements", Ph.D. Dissertation, Dept. of Civil Eng., Univ. of California, 1962.
127. Bazeley, G. P., Cheung, Y. K., Irons, B.M. and Zienkiewicz, O. C., "Triangular Elements in Plate Bending - Conforming and Non-Conforming Solutions". Matrix Methods in Structural Mechanics, Wright-Patterson AFB, Ohio, AFFDL-TR-66-80, 1966.
128. Clough, R. W. and Tocher, J. L., "Finite Element Stiffness Matrices for Analysis of Plate Bending", Matrix Methods in Structural Mechanics, Wright-Patterson AFB, Ohio, AFFDL-TR-66-80, 1966.

129. Argyris, J. H., Fried, I. and Scharpf, D. W., "The TUBA Family of Plate Elements for the Matrix Displacement Method", The Aeronautical Journal, Royal Aeronautical Soc., Vol. 72, 1968.
130. Bosshard, W., "Ern Neues, Vollverträgliches Endliches Element für Plattenbiegung", Int. Assoc. for Bridge and Structural Eng., Bult. Vol. 28, 1968.
131. Shieh, W.Y.J., "Analysis of Plate Bending by Triangular Elements", Journal of Eng. Mechanics Div., Proc. ASCE, EM5, Oct. 1968.
132. Cowper, G.R., Kosko, E., Lindberg, G.M. and Olson, M.D., "Formulation of a New Triangular Plate Bending Element", Canadian Aeronautics and Space Inst. Trans., Vol. 1, No. 2, Sept. 1968.
133. Cowper, G.R., Kosko, E., Lindberg, G.M. and Olson, M.D., "A High Precision Triangular Plate-Bending Element", Aeronautical Report LR-514, National Research Council of Canada, Dec. 1968.
134. Przemieniecki, J.S., "Theory of Matrix Structural Analysis", McGraw Hill Book Co., N.Y., 1968.
135. Kapoor, K. K. and Hartz, B.J., "Stability of Plates Using the Finite Element Method", Journal of Eng. Mechanics Div., Proc. ASCE, EM2, April 1966.
136. Przemieniecki, J. S., "Discrete-Element Methods for Stability Analysis of Complex Structures", The Aeronautical Journal, Royal Aeronautical Soc., Vol. 72, Dec. 1968.
137. Chetty, S.M.K. and Tottenham, H., "An Investigation into the Bending Analysis of Hyperbolic Paraboloid Shells", Indian Concrete Journal, July 1964.
138. Jagannath, D.V., "Blade Vibration Measurement Techniques and Vibration Analysis of Plates", M. Eng. Thesis, Dept. of Mech. Eng., McMaster Univ., Hamilton.
139. Plunket, R., "Natural Frequencies of Uniform and Non-Uniform Rectangular Cantilever Plates", Journal of Mech. Eng. Sci., Vol. 5, No. 2, 1963.
140. Gladwell, G.M.L., "Vibrating Systems with Equal Natural Frequencies", Journal of Mech. Eng. Sci., Vol. 3, No. 2, 1961.



141. Olson, M.D., Lindberg, G.M. and Tulloch, H.A., "Finite Plate-Bending Elements in Polar Coordinates", Aeronautical Report LR-512, National Research Council of Canada, Oct. 1968.



## APPENDIX I

D'Alembert Forces for a Rotating Vibrating Blade

Referring to Figure (43), if XYZ is a system of fixed coordinate axes and xyz a system of moving coordinate axes, the absolute acceleration of a point P can be expressed as

$$\ddot{\vec{r}} = \ddot{\vec{R}} + \dot{\vec{\Omega}} \times (\vec{\Omega} \times \vec{\rho}) + \dot{\vec{\Omega}} \times \vec{\rho} + \ddot{\vec{\rho}}_r + 2\dot{\vec{\Omega}} \times \dot{\vec{\rho}}_r \quad (\text{I.1})$$

where

- $\ddot{\vec{r}}$  = Absolute acceleration of point P  
 $\ddot{\vec{R}}$  = Translational acceleration of xyz system  
 $\vec{\Omega}$  = Angular velocity of xyz system  
 $\dot{\vec{\Omega}}$  = Angular acceleration of xyz system  
 $\dot{\vec{\rho}}_r$  = Velocity of point P relative to xyz system  
 $\ddot{\vec{\rho}}_r$  = Acceleration of point P relative to xyz system.

The proof of equation (I.1) is given in the texts on elementary dynamics.

This equation can be used to determine the acceleration of point P (Figure 14) on the middle surface of the rotating and vibrating blade. If  $\vec{i}$ ,  $\vec{j}$  and  $\vec{k}$  are the unit vectors along the x, y and z axes, respectively, it can be seen that

$$\dot{\vec{\Omega}} = -\Omega(\sin\theta \vec{j} + \cos\theta \vec{k}) \quad (\text{I.2})$$

If  $u$ ,  $v$  and  $w$  are the displacements at point P along the  $x$ ,  $y$  and  $z$  axes, then

$$\vec{\rho} = (x+u)\vec{i} + (y+v)\vec{j} + (z+w)\vec{k} \quad (\text{I.3})$$

$$\dot{\vec{\rho}}_r = \dot{u}\vec{i} + \dot{v}\vec{j} + \dot{w}\vec{k} \quad (\text{I.4})$$

$$\ddot{\vec{\rho}}_r = \ddot{u}\vec{i} + \ddot{v}\vec{j} + \ddot{w}\vec{k} \quad (\text{I.5})$$

The translational acceleration of xyz system is the centripetal acceleration, given by

$$\ddot{\vec{R}} = -\Omega^2 r \vec{i} \quad (\text{I.6})$$

Since the disc is assumed to rotate at constant angular speed

$$\dot{\Omega} = 0 \quad (\text{I.7})$$

Substituting equations (I.2 to I.7) in equation (I.1)

$$\begin{aligned} \ddot{\vec{r}} = & -[\Omega^2(x+r+u) - \ddot{u} + 2\Omega(\dot{w} \sin\theta - \dot{v} \cos\theta)]\vec{i} \\ & -[\Omega^2\{(y+v)\cos^2\theta - (z+w)\sin\theta\cos\theta\} - \ddot{v} + 2\Omega\dot{u}\cos\theta]\vec{j} \quad (\text{I.8}) \\ & -[\Omega^2\{-(y+v)\sin\theta\cos\theta + (z+w)\sin^2\theta\} - \ddot{w} - 2\Omega\dot{u}\sin\theta]\vec{k} \end{aligned}$$

The d'Alembert force per unit volume of blade is  $-\rho\ddot{\vec{r}}$ .

Its components along  $x$ ,  $y$  and  $z$  axes, therefore, are

$$\begin{aligned} F_x & = \rho\Omega^2(x+r+u) - \rho\ddot{u} + 2\rho\Omega(\dot{w} \sin\theta - \dot{v} \cos\theta) \\ F_y & = \rho\Omega^2\{(y+v)\cos^2\theta - (z+w)\sin\theta\cos\theta\} - \rho\ddot{v} + 2\rho\Omega\dot{u}\cos\theta \quad (\text{I.9}) \\ F_z & = \rho\Omega^2\{-(y+v)\sin\theta\cos\theta + (z+w)\sin^2\theta\} - \rho\ddot{w} - 2\rho\Omega\dot{u}\sin\theta \end{aligned}$$

In the case of vibration analysis of a rotating cantilever plate the in-plane motion is not considered and, therefore,  $u=0$  and  $v=0$ . Also the middle surface of the plate

lies in the  $xy$  plane and hence  $z=0$ . Substituting in equations (I.9), the d'Alembert forces per unit volume of the rotating plate are

$$\begin{aligned}F_x &= \rho\Omega^2(x+r) + 2\rho\Omega\dot{w} \sin\theta \\F_y &= \rho\Omega^2\{y \cos^2\theta - w \sin\theta\cos\theta\} \\F_z &= \rho\Omega^2\{-y \sin\theta\cos\theta + w \sin^2\theta\} - \rho\ddot{w}\end{aligned}\tag{I.10}$$



## APPENDIX II

Formulation of the Problem of Rotating Blade  
Including the Coriolis Forces

When a rotating blade undergoes vibratory motion, the Coriolis forces in the x,y and the z direction (Figure 14) are given by equation (4.37). These can be expressed as

$$\begin{Bmatrix} F_x \\ F_y \\ F_z \end{Bmatrix}_4 = -2\rho\Omega [\theta_3] \begin{Bmatrix} \dot{u} \\ \dot{v} \\ \dot{w} \end{Bmatrix} \quad (\text{II.1})$$

where

$$[\theta_3] = \begin{bmatrix} 0 & \cos\theta & -\sin\theta \\ -\cos\theta & 0 & 0 \\ \sin\theta & 0 & 0 \end{bmatrix} \quad (\text{II.2})$$

Transformation of equation (II.1) to the local axes of the element gives

$$\begin{Bmatrix} F'_x \\ F'_y \\ F'_z \end{Bmatrix}_4 = -2\rho\Omega [\theta_4] \begin{Bmatrix} \dot{u}' \\ \dot{v}' \\ \dot{w}' \end{Bmatrix} \quad (\text{II.3})$$

where

$$[\theta_4] = [\lambda][\theta_3][\lambda]^T \quad (\text{II.4})$$

The equivalent nodal forces corresponding to these distributed forces can be obtained by changing the force vector

in Equation (4.51). This gives

$$\{F'_{15}\} = -2\rho\Omega [P_1^{-1}]^T \left( \int \int \int t[N]^T [\theta_4] \begin{Bmatrix} \dot{u}' \\ \dot{v}' \\ \dot{w}' \end{Bmatrix} dx' dy' \right) \quad (\text{II.5})$$

Substituting for the velocities from equation (4.45)

$$\{F'_{15}\} = -[P_3] \{\delta'_{15}\} \quad (\text{II.6})$$

where

$$[P_3] = 2\rho\Omega [P_1^{-1}]^T \left( \int \int \int t[N]^T [\theta_4] [N] dx' dy' \right) [P_1^{-1}] \quad (\text{II.7})$$

Introducing the rotational displacements  $\theta'_z$  and the corresponding fictitious couples  $M'_z$  at each node, the vector of 18 nodal forces, corresponding to the Coriolis forces, is given by

$$\{F'_e\}_4 = -[C'_{ed}] \{\delta'_e\} \quad (\text{II.8})$$

where

$$[C'_{ed}] = \begin{bmatrix} c_{ed}^{11} & | & c_{ed}^{12} & | & c_{ed}^{13} \\ \hline c_{ed}^{21} & | & c_{ed}^{22} & | & c_{ed}^{23} \\ \hline c_{ed}^{31} & | & c_{ed}^{32} & | & c_{ed}^{33} \end{bmatrix} \quad (\text{II.9})$$

and

$$[C^{rs}_{ed}] = \begin{bmatrix} & & & & & | & 0 \\ & & & & & | & 0 \\ & & & & & | & 0 \\ & & & & & | & 0 \\ & & & & & | & 0 \\ & & & & & | & 0 \\ \hline 0 & 0 & 0 & 0 & 0 & | & 0 \end{bmatrix} \quad (\text{II.10})$$

$[P_3^{rs}]$  are the  $5 \times 5$  submatrices obtained by partitioning the matrix  $[P_3]$  of equation (II.7). Since the matrix  $[C'_{ed}]$  is due to the Coriolis forces, it is defined as the 'Coriolis Matrix' for the element.

The transformation to the common global axes is accomplished by the relation,

$$[C_{ed}] = [T]^T [C'_{ed}] [T] \quad (\text{II.11})$$

where the matrix  $[T]$  is given by equation (3.31). The assembly for these element matrices is carried out in exactly the same manner as for the stiffness and the mass matrices. The final equation of motion would be

$$[M]\{\ddot{\delta}\} + [C_d]\{\dot{\delta}\} + ([K] - [M_c])\{\delta\} = \{0\} \quad (\text{II.12})$$

where  $[C_d]$  is the final assembled Coriolis matrix. The other matrices are the same as in equation (4.61).

This equation is of the standard form encountered in the multidegree damped vibration problems and, therefore, does not pose any basic problems for solution, except for the memory of the computer. In addition, if the actual viscous damping forces are also present in the blade, these could be added to the matrix  $[C_d]$ .



## APPENDIX III

COMPUTER PROGRAMME FOR VIBRATION ANALYSIS OF ROTATING  
CANTILEVER PLATE

A4176,CM124000,T2000.

RAWTANI S.

RUN(S)

LGO.

REWIND LGO.

RUN(S)

LGO.

```

'          6400 END OF RECORD
PROGRAM TST (INPUT,OUTPUT,TAPE5=INPUT,TAPE6=OUTPUT,
1 TAPE 1,TAPE 2,TAPE 3)

```

C

```

DIMENSION CK(14000),CKP(6000),P(166),DISP(166),TY(166,3)
DIMENSION X(3),Y(3),Z(3),XX(3),YY(3),ALMD(3,3),FP(6),
1 DP(6),EKP(6,6),STRESS(3),S(3,6),EKB(9,9),CFK(9,9),
2 A(9,9),DD(9,9),F(9)

```

C

C

C NOTATIONS

C

C	AR	ASPECT RATIO
C	V	POISSONS RATIO
C	TL	LENGTHWISE TAPER FACTOR. THICKNESS AT
C		(L,0,0)/THICKNESS AT (0,0,0)
C	TB	BREADTHWISE TAPER FACTOR. THICKNESS AT
C		(0,B/2,0)/THICKNESS AT (0,0,0)
C	ROTC	ROTATING SPEED/FUND. NONROTATING FREQ.
C	BETA1	FUND. NONROTATING FREQ. (NONDIMENSIONAL)
C	THETA	SETTING ANGLE (DEGREES)
C	ROVERL	RADIUS OF DISC/LENGTH OF PLATE
C	NL	LENGTHWISE SUBDIVISIONS
C	NB	BREADTHWISE SUBDIVISIONS
C	NEIGEN	NUMBER OF EIGENVALUES REQUIRED

C

C

```

-----
C DATA INPUT. IF THE PLATE IS NONROTATING, PUT ROTC,
C BETA1, THETA AND ROVERL AS ZERO.
C -----

```

C

```

READ(5,1)AR,TL,TB,V
READ(5,1)ROTC,BETA1,THETA,ROVERL
READ(5,2)NL,NB,NEIGEN
1 FORMAT(4F10.4)
2 FORMAT(3I2)

```

```

C -----
C ALL LINEAR DIMENSIONS ARE NORMALIZED BY TAKING THE
C BREADTH OF THE PLATE AS UNITY. THE NUMBER OF TRIANGULAR
C ELEMENTS(NTE), THE NUMBER OF IN-PLANE DEGREES OF
C FREEDOM(NRP), NUMBER OF BENDING DEGREES OF FREEDOM(NR),
C THE SIZES NWP AND NW OF THE SYMMETRIC IN-PLANE AND
C BENDING STIFFNESS MATRICES STORED AS COLUMN VECTORS
C ARE DETERMINED. THE MATRIX IS INITIALLY SET TO ZERO.
C -----

```

```

C
C RADIUS = ROVERL*AR
C NTE = NL*NB*2
C NRP = NL*(NB+1)*2
C NR = NL*(NB+1)*3
C NWP = NRP*(NRP+1)/2
C NW = NR*(NR+1)/2
C DO 3 I=1,NW
C CK(I) = 0.
C IF(I.LE.NWP)CKP(I) = 0.
C IF(I.LE.NRP)P(I) = 0.
3 CONTINUE

```

```

C -----
C THE GLOBAL COORDINATES (X,Y,Z) OF THE NODES AND THE
C NODE NUMBERS (I,J,K) ARE GENERATED. PROPERTIES IN THE
C LOCAL AXES ARE DETERMINED AND STORED ON TAPE 1.
C -----

```

```

C
C REWIND 1
C DO 5 N=1,2
C Y(1) = -0.5-1./NB
C KR = 0
C DO 5 L=1,NB
C Y(1) = Y(1)+1./NB
C Y(2) = Y(1)+1./NB
C Y(3) = Y(1)
C IF(N.EQ.2)Y(3) = Y(2)
C KR = KR+1
C LZ = (L-1)*(NL+1)-KR
C DO 5 M=1,NL
C X(1) = M*AR/NL
C X(2) = (M-1)*AR/NL
C X(3) = X(2)
C IF(N.EQ.2)X(3) = X(1)
C DO 4 I=1,3
C Z(I) = 0.
4 CONTINUE
C LZ = LZ+1
C I = LZ+1
C J = I+NL-1
C IF(M.EQ.1)J=0
C K = LZ
C IF(N.EQ.2)K=LZ+NL+1
C IF(M.EQ.1.AND.N.EQ.1)K=0

```

```

C
C THE DIRECTION COSINES OF THE LOCAL AXES(ALMD) AND THE
C LOCAL COORDINATES OF THE NODES (XX,YY) ARE DETERMINED.
C
A1 = (X(2)-X(1))**2+(Y(2)-Y(1))**2+(Z(2)-Z(1))**2
A2 = (X(3)-X(2))**2+(Y(3)-Y(2))**2+(Z(3)-Z(2))**2
A3 = (X(1)-X(3))**2+(Y(1)-Y(3))**2+(Z(1)-Z(3))**2
YY(2) = SQRT(A1)
YY(3) = (A3+A1-A2)/(2.0*YY(2))
XX(3) = SQRT(ABS(A3-YY(3)**2))
CALL LAMDA(X,Y,Z,ALMD)
C
C COEFFICIENTS C1,C2,C3(EQUATION 3.19) ARE DETERMINED.
C TRATIO = THICKNESS AT ORIGIN/MAXIMUM THICKNESS
C
TR = TB
IF(TR.LT.(2.-TB))TR = 2.-TB
IF(TR.LT.(TL+TB-1.))TR = TL+TB-1.
IF(TR.LT.(TL-TB+1.))TR = TL-TB+1.
TRATIO = 1./TR
C3 = ((TL-1.)*X(1)/AR+2.*(TB-1.)*Y(1)+1.)*TRATIO
C2 = (((TL-1.)*X(2)/AR+2.*(TB-1.)*Y(2)+1.)*TRATIO-C3)/
1 YY(2)
C1 = (((TL-1.)*X(3)/AR+2.*(TB-1.)*Y(3)+1.)*TRATIO-
1 C3-C2*YY(3))/XX(3)
C
C THE INVERSE OF MATRIX A (EQUATION 3.8) IS OBTAINED.
C
CALL AINVRS (XX,YY,A)
C
C THE MATRIX (DD) OF DOUBLE INTEGRALS IS OBTAINED.
C DD(M,N) IS THE VALUE OF INTEGRAL OF XX**(M-1)*YY**(N-1)
C
CALL DUBINT (XX,YY,DD)
C
C THE PROPERTIES OF ELEMENTS REQUIRED IN LATTER
C CALCULATIONS ARE STORED.
C
5 WRITE(1)X,Y,Z,I,J,K,XX,YY,ALMD,C1,C2,C3,A,DD
REWIND 1
C
C -----
C THE IN-PLANE STIFFNESS MATRIX FOR THE PLATE AND
C THE EQUIVALENT NODAL FORCES CORRESPONDING TO THE
C DISTRIBUTED IN-PLANE CENTRIFUGAL FORCES ARE DETERMINED.
C THE VECTOR OF NODAL IN-PLANE DISPLACEMENTS IS
C CALCULATED. THE ACTUAL DISPLACEMENT VECTOR IS THE
C VECTOR DISP OBTAINED HERE MULTIPLIED BY (MAXIMUM
C THICKNESS**2/12.)
C -----

```



```

REWIND 2
DO 6 L=1,NTE
READ(1)X,Y,Z,I,J,K,XX,YY,ALMD,C1,C2,C3,A,DD
SPD = (ROTC**2)*(BETA1**2)/(AR**4)
CALL EKPFP(X,Y,XX,YY,ALMD,C1,C2,C3,RADIUS,V,THETA,SPD,
1 DD,EKP,FP,S)
WRITE(2)I,J,K,XX,YY,C1,C2,C3,ALMD,A,DD,S
CALL GROUP(I,J,K,L,NTE,6,EKP,CKP,FP,P,0)
6 CONTINUE
CALL INVSYM (CKP,NRP,IERR)
IF(IERR.NE.0)WRITE(6,7)IERR
7 FORMAT(5X,5HIERR=,I3)
IF(IERR.NE.0)STOP
DO 8 I=1,NRP
DISP(I) = 0.
DO 8 K=1,NRP
IF(I.GE.K)L=I*(I-1)/2+K
IF(I.LT.K)L=K*(K-1)/2+I
8 DISP(I) = DISP(I)+CKP(L)*P(K)
REWIND 1
REWIND 2

C
C -----
C THE STRESSES IN THE MIDDLE SURFACE OF THE PLATE
C ARE CALCULATED. ACTUAL STRESSES ARE THOSE OBTAINED
C HERE MULTIPLIED BY FLEXURAL RIGIDITY/MAXIMUM THICKNESS
C -----
DO 14 L=1,NTE
READ(2)I,J,K,XX,YY,C1,C2,C3,ALMD,A,DD,S
DO 9 M=1,6
DP(M) = 0.
9 CONTINUE
IF(I.EQ.0)GO TO 10
DP(1) = DISP(2*I-1)
DP(2) = DISP(2*I)
10 IF(J.EQ.0)GO TO 11
DP(3) = DISP(2*J-1)
DP(4) = DISP(2*J)
11 IF(K.EQ.0)GO TO 12
DP(5) = DISP(2*K-1)
DP(6) = DISP(2*K)
12 DO 13 M=1,3
STRESS(M) = 0.
DO 13 N=1,6
STRESS(M) = STRESS(M)+S(M,N)*DP(N)
13 CONTINUE
14 WRITE(1)I,J,K,XX,YY,C1,C2,C3,ALMD,A,DD,STRESS
REWIND 1
REWIND 2

```

```

C -----
C THE BENDING STIFFNESS MATRIX, INCLUDING THE
C CENTRIFUGAL STIFFNESS MATRIX FOR THE COMPLETE PLATE
C IS CALCULATED. THE MATRIX IS DETERMINED AS COLUMN
C VECTOR. ACTUAL STIFFNESS MATRIX IS OBTAINED BY
C MULTIPLYING THE MATRIX CK BY FLEXURAL RIGIDITY.
C -----
DO 16 L=1,NTE
READ(1)I,J,K,XX,YY,C1,C2,C3,ALMD,A,DD,STRESS
CALL BENDK (C1,C2,C3,V,A,DD,EKB)
CALL CENTK(C1,C2,C3,STRESS,A,DD,CFK)
DO 15 M=1,9
DO 15 N=1,9
EKB(M,N) = EKB(M,N)+CFK(M,N)
15 CONTINUE
CALL TRNSFB(ALMD,EKB)
16 CALL GROUP(I,J,K,L,NTE,9,EKB,CK,F,P,1)
REWIND 1

C -----
C THE STIFFNESS MATRIX CK IS INVERTED USING LIBRARY
C SUBROUTINE INVSYM. IT IS STORED ON TAPE 2, THREE
C COLUMNS AT A TIME.
C -----
CALL INVSYM (CK,NR,IERR)
IF(IERR.NE.0)WRITE(6,7)IERR
IF(IERR.NE.0)STOP
IT = NR/3
DO 18 K=1,IT
M = 0
IK = K*3
IM = IK-2
DO 17 I=IM,IK
M = M+1
DO 17 J=1,NR
IF(I.GE.J)L=I*(I-1)/2+J
IF(I.LT.J)L=J*(J-1)/2+I
17 TY(J,M) = CK(L)
18 WRITE(2)((TY(M,N),N=1,3),M=1,NR)
REWIND 2

C -----
C THE MASS MATRIX FOR THE COMPLETE PLATE IS CALCULATED.
C THE MATRIX IS DETERMINED AS A COLUMN VECTOR CK.
C THE ACTUAL MASS MATRIX IS OBTAINED BY MULTIPLYING
C CK BY (DENSITY*MAXIMUM THICKNESS).
C -----

```

```

DO 19 I=1,NW
CK(I) = 0.
19 CONTINUE
DO 20 L=1,NTE
READ(1)I,J,K,XX,YY,C1,C2,C3,ALMD,A,DD,STRESS
CALL BENDM(C1,C2,C3,A,DD,EKB)
CALL TRNSFB(ALMD,EKB)
20 CALL GROUP (I,J,K,L,NTE,9,EKB,CK,F,P,1)
REWIND 1

```

C  
C  
C  
C  
C

-----  
THE MASS MATRIX IS STORED ON TAPE 1. THE FIRST PHASE  
OF THE PROGRAMME ENDS.  
-----

```

REWIND 3
DO 22 K=1,IT
M = 0
IK = K*3
IM = IK-2
DO 21 I=IM,IK
M = M+1
DO 21 J=1,NR
IF(I.GE.J)L=I*(I-1)/2+J
IF(I.LT.J)L=J*(J-1)/2+I
21 TY(J,M) = CK(L)
22 WRITE(1)((TY(M,N),N=1,3),M=1,NR)
WRITE(3)AR,V,BETA1,ROTC,ROVERL,TRIETA,TL,TB,NL,NB,
1 NR,NEIGEN
REWIND 1
REWIND 3
END
' 6400 END RECORD
DATA
' 6400 END RECORD

```

```

PROGRAM TST (INPUT,OUTPUT,TAPE5=INPUT,TAPE6=OUTPUT,
1 TAPE 1,TAPE 2,TAPE 3)

```

C  
C  
C  
C  
C  
C  
C  
C  
C  
C  
C

-----  
THE SECOND PHASE OF THE PROGRAMME STARTS WITH FRESH  
MEMORY. FROM THE FIRST PHASE THE FOLLOWING INFORMATION  
IS AVAILABLE ON THE TAPES.  
MASS MATRIX/(RHO\*TMAX) ON TAPE 1  
INVERSE OF STIFFNESS MATRIX\*FLEXURAL RIGIDITY ON TAPE 2  
PLATE DIMENSIONS ON TAPE 3.  
MATRICES ON TAPES 1 AND 2 ARE MULTIPLIED TO OBTAIN  
MATRIX CKM.  
-----



```

DIMENSION CKM(160,160),P(160),DISP(160),S(10)
READ(3)AR,V,BETA1,ROTC,ROVERL,THETA,TL,TB,NL,NB,
1 NR,NEIGEN
REWIND 3
IT = NR/3
DO 2 K=1,IT
LM=3
MR = NR-2
IF(K.LT.3)READ(1)((CKM(M,N),N=MR,NR),M=1,NR)
IF(K.GE.3)READ(1)((CKM(M,N),N=4,6),M=1,NR)
DO 1 J=1,IT
LN = 3
IF(J.EQ.1)REWIND 2
MR = NR-5
KR = NR-3
IF(K.LT.3)READ(2)((CKM(M,N),N=MR,KR),M=1,NR)
IF(K.GE.3)READ(2)((CKM(M,N),N=1,3),M=1,NR)
IK = (K-1)*3
DO 1 I=1,LM
IK=IK+1
IJ = (J-1)*3
DO 1 N=1,LN
IJ = IJ+1
CKM(IJ,IK) = 0.
DO 1 M=1,NR
IF(K.LT.3)CKM(IJ,IK) = CKM(IJ,IK)+CKM(M,MR-1+N)*CKM(M,
1 MR+2+I)
IF(K.GE.3)CKM(IJ,IK) = CKM(IJ,IK)+CKM(M,N)*CKM(M,3+I)
1 CONTINUE
IF(K.EQ.1)WRITE(3)((CKM(M,N),N=1,3),M=1,NR)
IF(K.EQ.2)WRITE(3)((CKM(M,N),N=4,6),M=1,NR)
2 CONTINUE
REWIND 3
READ(3)((CKM(M,N),N=1,3),M=1,NR)
READ(3)((CKM(M,N),N=4,6),M=1,NR)
C
C -----
C EIGENVALUES OF MATRIX CKM ARE DETERMINED AND EXPRESSED
C AS NONDIMENSIONAL QUANTITIES BETA. THE EIGENVALUES
C AND EIGENVECTORS ARE WRITTEN OUT.
C -----
C
CALL POWER (CKM,NR,NEIGEN,S,1.E-4,160,P,DISP)
SN = SIN(THETA*3.14/180.)
DO 3 J=1,NEIGEN
S(J) = (AR**4/S(J))-(BETA1*ROTC*SN)**2
3 S(J) = SQRT(S(J))
WRITE(6,4)AR,V,ROTC,BETA1,ROVERL,NL,NB,THETA,TL,TB
WRITE(6,5)NEIGEN
WRITE(6,6)(S(I),I=1,NEIGEN)

```

```

4   FORMAT(1H1,4X,*ASPECT RATIO=*,12X,F10.4,/,5X,
1   *POISSONS RATIO=*,10X,F10.4,/,5X,*ROT SPEED/FUND FREQ=*
2   ,5X,F10.4,/,5X,*NONDIMENSIONAL FUND FREQ=*,F10.4,/,
3   5X,*HUB RADIUS/PLATE LENGTH=*,1X,F10.4,/,5X,
4   *LENGTHWISE DIVISIONS=*,4X,I2,/,5X,
5   *BREADTHWISE DIVISIONS=*,3X,I2,/,5X,
6   *SETTING ANGLE (DEG)=*,F10.4,/,5X,*LENGTH TAPER FACTOR=*
7   ,5X,F10.4,/,5X,*BREADTH TAPER FACTOR=*,4X,F10.4)
5   FORMAT(/,10X,6HFIRST ,I2,17H EIGEN VALUES ARE,/)
6   FORMAT(50X,E15.6)
   WRITE(6,10)
   DO 8 I=1,NEIGEN
   WRITE(6,7) I
7   FORMAT(/,5X,16HEIGEN VECTOR NO.,1X,I2,1X,2HIS,/)
8   WRITE(6,9)(CKM(J,I),J=1,NR)
9   FORMAT(5(5X,3E16.6,/) )
10  FORMAT(12X,*W*,12X,*THETA X*,10X,*THETA Y*)
   STOP
   END
!     6400 END OF RECORD
!     6400 END FILE

```

```

SUBROUTINE LAMDA(X,Y,Z,ALMD)

```

```

-----
THIS SUBROUTINE FINDS THE DIRECTION COSINES OF THE
LOCAL COORDINATE AXES.
-----

```

```

DESCRIPTION OF PARAMETERS

```

```

X,Y,Z      GLOBAL COORDINATES OF NODES
ALMD       MATRIX OF DIRECTION COSINES DEFINED BY
           EQUATION 3.32

```

```

DIMENSION X(3),Y(3),Z(3),ALMD(3,3)

```

```

YJI = Y(2)-Y(1)

```

```

YMI = Y(3)-Y(1)

```

```

XJI = X(2)-X(1)

```

```

XMI = X(3)-X(1)

```

```

ZJI = Z(2)-Z(1)

```

```

ZMI = Z(3)-Z(1)

```

```

A = YJI*ZMI-YMI*ZJI

```

```

B = -XJI*ZMI+XMI*ZJI

```





```

A(9,4) = -2.*X(3)
A(6,5) = -Y(2)
A(7,5) = X(3)*Y(3)
A(8,5) = X(3)
A(9,5) = -Y(3)
A(4,6) = Y(2)**2
A(5,6) = 2.*Y(2)
A(7,6) = Y(3)**2
A(8,6) = 2.*Y(3)
A(7,7) = X(3)**3
A(9,7) = -3.*X(3)**2
A(7,8) = Y(3)*X(3)**2
A(8,8) = X(3)**2
A(9,8) = -2.*X(3)*Y(3)
A(4,9) = Y(2)**3
A(5,9) = 3.*Y(2)**2
A(7,9) = Y(3)**3
A(8,9) = 3.*Y(3)**2

```

C  
C  
C  
C

MATRIX A IS NOW INVERTED. IF THE INVERSION FAILS THE  
PROGRAMME STOPS.

```

CALL INVMAT(A,9,9,1.E-8,I,N)
IF(I.NE.0)WRITE(6,2)I
2  FORMAT(5X,5HIERR=,I3)
IF(I.NE.0)STOP
RETURN
END

```

SUBROUTINE DUBINT (XX,YY,DD)

C  
C  
C  
C  
C  
C  
C  
C  
C  
C  
C  
C  
C  
C  
C

-----  
THIS SUBROUTINE FINDS THE MATRIX OF DOUBLE INTEGRALS  
FOR A TRIANGULAR ELEMENT. GAUSS QUADRATURE FORMULA  
IS USED , WITH 16 ABSCISSA POINTS.  
-----

DESCRIPTION OF PARAMETERS

XX,YY LOCAL COORDINATES OF THE NODES  
DD MATRIX IN WHICH THE DOUBLE INTEGRALS ARE  
RETURNED. DD(M,N) CORRESPONDS TO THE  
INTEGRAL OF XX\*\*(M-1)\*YY\*\*(N-1)

DIMENSION XX(3),YY(3),DD(9,9),AX(16),A(16)

```

DO 1 I=1,9
DO 1 J=1,9
DD(I,J) = 0.
1 CONTINUE
C
C AX ARE THE 16 ABSCISSAE POINTS AND A ARE THE 16
C WEIGHT COEFFICIENTS OF THE GUASS QUADRATURE FORMULA
C
AX(1) = 0.989400934991650
AX(3) = 0.944575023073233
AX(5) = 0.865631202387832
AX(7) = 0.755404408355003
AX(9) = 0.617876244402644
AX(11) = 0.458016777657227
AX(13) = 0.281603550779259
AX(15) = 0.095012509837637
A(1) = 0.027152459411754
A(3) = 0.062253523938648
A(5) = 0.095158511682493
A(7) = 0.124628971255534
A(9) = 0.149595988816577
A(11) = 0.169156519395003
A(13) = 0.182603415044924
A(15) = 0.189450610455068
DO 2 I=2,16,2
2 AX(I) = -AX(I-1)
A(I) = A(I-1)
DO 4 I=1,9
DO 4 J=1,9
SUM = 0.0
DO 3 K=1,16
S = 0.5*AX(K)+0.5
F = (1.-S)**(I-1)*((1.-S)*YY(3)+S*YY(2))**(J-1)
3 SUM = SUM+A(K)*F*0.5
DD(I,J) = SUM*XX(3)**I*YY(2)/(I+J)
4 CONTINUE
RETURN
END

```

```

SUBROUTINE EKPFPS(X,Y,XX,YY,ALMD,C1,C2,C3,RADIUS,V,
1 THETA,SPD,DD,EKP,FP,S)

```

```

C
C -----
C THIS SUBROUTINE FINDS THE IN-PLANE STIFFNESS MATRIX
C AND THE EQUIVALENT NODAL FORCES CORRESPONDING TO THE
C DISTRIBUTED CENTRIFUGAL FORCES FOR AN ELEMENT.
C MATRIX S OF EQUATION 4.14 IS ALSO DETERMINED.
C -----
C

```

```

C      DESCRIPTION OF PARAMETERS
C
C      X,Y          GLOBAL COORDINATES OF NODES
C      XX,YY       LOCAL COORDINATES OF NODES
C      ALMD        MATRIX OF DIRECTION COSINES DEFINED BY
C                  EQUATION 3.32
C      C1,C2,C3    AS DEFINED BY EQUATION 3.19
C      RADIUS      RADIUS OF THE DISC
C      V          POISSONS RATIO
C      THETA       SETTING ANGLE (DEGREES)
C      SPD        (DENSITY)*(ROT.SPEED**2)*(MAX.THICKNESS**
C                  (FLEXURAL RIGIDITY), WHICH IS SAME AS
C                  (ROTC*BETA1)**2/AR**4
C      DD          MATRIX OF DOUBLE INTEGRALS.ELEMENT(I,J)
C                  OF THIS MATRIX IS THE VALUE OF INTEGRAL
C                  OF XX**(I-1)*YY**(J-1)
C      EKP        IN-PLANE STIFFNESS MATRIX IN GLOBAL AXES
C                  MULTIPLIED BY A FACTOR EQUAL TO 12.*
C                  (FLEXURAL RIGIDITY)/(MAXIMUM THICKNESS**2)
C      FP         VECTOR OF NODAL FORCES EQUIVALENT TO THE
C                  DISTRIBUTED CENTRIFUGAL FORCES/FLEXURAL
C                  RIGIDITY. THE NODAL FORCES ARE ALONG
C                  GLOBAL AXES.
C      S          AS DEFINED BY EQUATION 4.14

```

```

DIMENSION EKP(6,6),FP(6),S(3,6),Q(6,6),XX(3),YY(3),
1 N1(6),ALMD(3,3),X(3),Y(3),R(6),T(6,6),A(3,6),D(3,3),
2 D1(6,6),D2(6,3),DD(9,9)
DO 1 I=1,6
DO 1 J=1,6
Q(I,J) = 0.
T(I,J) = 0.
1 IF(I.LE.3)A(I,J) = 0.
DO 2 I=1,5,2
Q(I,1) = 1.
2 Q(I+1,4) = 1.
Q(5,2) = XX(3)
Q(3,3) = YY(2)
Q(5,3) = YY(3)
Q(6,5) = XX(3)
Q(4,6) = YY(2)
Q(6,6) = YY(3)
CALL INVMAT (Q,6,6,1.E-8,IERRR,N1)
IF(IERRR.NE.0)WRITE(6,3)IERRR
3 FORMAT(5X,5HIERR=,I3)
IF(IERRR.NE.0)STOP
ANGLE = THETA*3.14/180.
SN = SIN(ANGLE)**2
CS = COS(ANGLE)**2

```



```

A1 = 1.-ALMD(1,2)**2*SN
A2 = 1.-ALMD(2,2)**2*SN
A3 = -ALMD(1,2)*ALMD(2,2)*SN
A4 = ALMD(1,1)*(X(1)+RADIUS)+ALMD(1,2)*Y(1)*CS
A5 = ALMD(2,1)*(X(1)+RADIUS)+ALMD(2,2)*Y(1)*CS
R(1) = A4*C3*DD(1,1)+(A4*C1+A1*C3)*DD(2,1)+(A3*C3+A4*
1 C2)*DD(1,2)+A1*C1*DD(3,1)+(A3*C1+A1*C2)*DD(2,2)
2 +A3*C2*DD(1,3)
R(2) = A4*C3*DD(2,1)+(A1*C3+A4*C1)*DD(3,1)+(A3*C3+A4*
1 C2)*DD(2,2)+A1*C1*DD(4,1)+(A1*C2+A3*C1)*DD(3,2)
2 + A3*C2*DD(2,3)
R(3) = A4*C3*DD(1,2)+(A4*C1+A1*C3)*DD(2,2)+(A3*C3+A4*
1 C2)*DD(1,3)+A1*C1*DD(3,2)+(A3*C1+A1*C2)*DD(2,3)
2 +A3*C2*DD(1,4)
R(4) = A5*C3*DD(1,1)+(A5*C1+A3*C3)*DD(2,1)+(A2*C3+A5*
1 C2)*DD(1,2)+A3*C1*DD(3,1)+(A2*C1+A3*C2)*DD(2,2)
2 +A2*C2*DD(1,3)
R(5) = A5*C3*DD(2,1)+(A3*C3+A5*C1)*DD(3,1)+(A2*C3+A5*
1 C2)*DD(2,2)+A3*C1*DD(4,1)+(A2*C1+A3*C2)*DD(3,2)
2 +A2*C2*DD(2,3)
R(6) = A5*C3*DD(1,2)+(A5*C1+A3*C3)*DD(2,2)+(A2*C3+A5*
1 C2)*DD(1,3)+A3*C1*DD(3,2)+(A2*C1+A3*C2)*DD(2,3)
2 +A2*C2*DD(1,4)
DO 4 I=1,6
R(I) = R(I)*SPD
4 CONTINUE
DO 5 I=1,2
DO 5 J=1,2
T(I,J) = ALMD(I,J)
T(I+2,J+2) = T(I,J)
5 T(I+4,J+4) = T(I,J)
A(1,2) = 1.
A(2,6) = 1.
A(3,3) = 1.
A(3,5) = 1.
D(1,1) = 1.
D(1,2) = V
D(1,3) = 0.
D(2,1) = V
D(2,2) = 1.
D(2,3) = 0.
D(3,1) = 0.
D(3,2) = 0.
D(3,3) = (1.-V)/2.
DO 6 I=1,6
DO 6 J=1,6
D1(I,J) = 0.
DO 6 K=1,6
D1(I,J) = D1(I,J)+T(K,1)*Q(J,K)
6 CONTINUE

```

```

DO 7 I=1,6
FP(I) = 0.
DO 7 K=1,6
FP(I) = FP(I)+D1(I,K)*R(K)
7 CONTINUE
DO 8 I=1,6
DO 8 J=1,3
D2(I,J) = 0.
DO 8 K=1,6
D2(I,J) = D2(I,J)+D1(I,K)*A(J,K)
8 CONTINUE
DO 9 I=1,3
DO 9 J=1,6
S(I,J) = 0.
DO 9 K=1,3
S(I,J) = S(I,J)+D(I,K)*D2(J,K)
9 CONTINUE
DO 10 I=1,6
DO 10 J=1,6
EKP(I,J) = 0.
DO 10 K=1,3
EKP(I,J) = EKP(I,J) +D2(I,K)*S(K,J)
10 CONTINUE
DO 11 I=1,6
DO 11 J=1,6
EKP(I,J) = EKP(I,J)*(C1*DD(2,1)+C2*DD(1,2)+C3*DD(1,1))
11 CONTINUE
RETURN
END

```

SUBROUTINE TRNSFB(ALMD,EKB)

-----  
THIS SUBROUTINE TRANSFORMS THE BENDING MATRIX OF AN  
ELEMENT FROM LOCAL TO GLOBAL AXES.  
-----

DESCRIPTION OF PARAMETERS

ALMD            MATRIX OF DIRECTION COSINES DEFINED BY  
                 EQUATION 3.32.  
EKB             AS INPUT ELEMENT MATRIX IN LOCAL AXES  
                 AS OUTPUT ELEMENT MATRIX IN GLOBAL AXES.

```

DIMENSION ALMD(3,3),EKB(9,9),rH(9,9),S(9,9)
DO 1 I=1,9
DO 1 J=1,9
HH(I,J) = 0.
1 CONTINUE
HH(1,1) = ALMD(3,3)
DO 2 I=2,3
DO 2 J=2,3
HH(I,J) = ALMD(I-1,J-1)
2 CONTINUE
DO 3 I=1,3
DO 3 J=1,3
HH(I+3,J+3) = HH(I,J)
HH(I+6,J+6) = HH(I,J)
3 CONTINUE
CALL MULTP (EKB,HH,S,9,9,9,0,9,9,9)
CALL MULTP(HH,S,EKB,9,9,9,1,9,9,9)
RETURN
END

```

```

SUBROUTINE BENDK (C1,C2,C3,V,A,D,EKB)

```

```

C
C -----
C THIS SUBROUTINE FINDS THE BENDING STIFFNESS MATRIX
C OF AN ELEMENT. THE ACTUAL BENDING STIFFNESS MATRIX
C IS THE MATRIX LKB OBTAINED IN THIS SUBROUTINE,
C MULTIPLIED BY THE FLEXURAL RIGIDITY AS DEFINED BY
C EQUATION 5.2
C -----
C
C DESCRIPTION OF PARAMETERS
C
C C1,C2,C3 AS DEFINED BY EQUATION 3.19
C V POISSONS RATIO
C A INVERSE OF MATRIX A (EQUATION 3.8)
C D MATRIX OF DOUBLE INTEGRALS. D(I,J) IS THE
C VALUE OF INTEGRAL OF XX**(I-1)*YY**(J-1),
C WHERE (XX,YY) ARE THE LOCAL COORDINATES
C EKB BENDING STIFFNESS MATRIX/FLEXURAL RIGIDITY
C
C
C DIMENSION A(9,9),D(9,9),EKB(9,9),B(9,9),D1(9,9)
DO 1 I=1,9
DO 1 J=1,9
B(I,J) = 0.

```



```

      IF (I.LT.4.AND.J.LT.4) D1(I,J) = (C1**3)*D(I+3,J)+
1  (C2**3)*D(I,J+3)+(C3**3)*D(I,J)+(3.*C2*C1**2)*
2  D(I+2,J+1)+(3.*C1*C2**2)*D(I+1,J+2)+(3.*C3*C1**2)*
3  D(I+2,J)+(3.*C1*C3**2)*D(I+1,J)+(3.*C3*C2**2)*
4  D(I,J+2)+(3.*C2*C3**2)*D(I,J+1)+(6.*C1*C2*C3)*
5  D(I+1,J+1)
1  CONTINUE
      B(4,4) = 4.*D1(1,1)
      B(6,4) = 4.*V*D1(1,1)
      B(7,4) = 12.*D1(2,1)
      B(8,4) = 4.*D1(1,2)
      B(9,4) = 12.*V*D1(1,2)
      B(5,5) = 2.*(1.-V)*D1(1,1)
      B(8,5) = 4.*(1.-V)*D1(2,1)
      B(6,6) = 4.*D1(1,1)
      B(7,6) = 12.*V*D1(2,1)
      B(8,6) = 4.*V*D1(1,2)
      B(9,6) = 12.*D1(1,2)
      B(7,7) = 36.*D1(3,1)
      B(8,7) = 12.*D1(2,2)
      B(9,7) = 36.*V*D1(2,2)
      B(8,8) = 4.*D1(1,3)+8.*(1.-V)*D1(3,1)
      B(9,8) = 12.*V*D1(1,3)
      B(9,9) = 36.*D1(1,3)
      K=4
      DO 3 I=4,8
      K = K+1
      DO 3 J=K,9
3  B(I,J) = B(J,I)
      CALL MULTP (B,A,D1,9,9,9,0,9,9,9)
      CALL MULTP (A,D1,EKB,9,9,9,1,9,9,9)
      RETURN
      END

```

```

SUBROUTINE BENDM (C1,C2,C3,A,D,DD)

```

```

C
C -----
C THIS SUBROUTINE FINDS THE BENDING MASS MATRIX FOR
C AN ELEMENT.THE ACTUAL BENDING MASS MATRIX IS THE
C MATRIX DD OBTAINED FROM THIS SUBROUTINE MULTIPLIED
C BY A FACTOR EQUAL TO THE PRODUCT OF DENSITY AND
C MAXIMUM THICKNESS (RHO*TMAX)
C -----
C

```

```

C      DESCRIPTION OF PARAMETERS
C
C      C1,C2,C3      AS DEFINED BY EQUATION 3.19
C      A            INVERSE OF MATRIX A (EQUATION 3.8)
C      D            MATRIX OF DOUBLE INTEGRALS.ELEMENT(I,J)
C                  OF THIS MATRIX IS THE VALUE OF INTEGRAL
C                  OF  $XX^{*(I-1)}YY^{*(J-1)}$ 
C      DD           BENDING STIFFNESS OF  $7(\text{RHO}*\text{TMAX})$ 
C
C

```

```

DIMENSION A(9,9),D(9,9),DD(9,9),EKB(9,9)

```

```

DO 1 I=1,9

```

```

DO 1 J=1,9

```

```

IF(I.LE.8.AND.J.LE.8)EKB(I,J)=C3*D(I,J)+C2*D(I,J+1)

```

```

1 +C1*D(I+1,J)

```

```

1 CONTINUE

```

```

DD(1,1) = EKB(1,1)

```

```

DD(2,1) = EKB(2,1)

```

```

DD(3,1) = EKB(1,2)

```

```

DD(4,1) = EKB(3,1)

```

```

DD(5,1) = EKB(2,2)

```

```

DD(6,1) = EKB(1,3)

```

```

DD(7,1) = EKB(4,1)

```

```

DD(8,1) = EKB(3,2)

```

```

DD(9,1) = EKB(1,4)

```

```

DD(2,2) = EKB(3,1)

```

```

DD(3,2) = EKB(2,2)

```

```

DD(4,2) = EKB(4,1)

```

```

DD(5,2) = EKB(3,2)

```

```

DD(6,2) = EKB(2,3)

```

```

DD(7,2) = EKB(5,1)

```

```

DD(8,2) = EKB(4,2)

```

```

DD(9,2) = EKB(2,4)

```

```

DD(3,3) = EKB(1,3)

```

```

DD(4,3) = EKB(3,2)

```

```

DD(5,3) = EKB(2,3)

```

```

DD(6,3) = EKB(1,4)

```

```

DD(7,3) = EKB(4,2)

```

```

DD(8,3) = EKB(3,3)

```

```

DD(9,3) = EKB(1,5)

```

```

DD(4,4) = EKB(5,1)

```

```

DD(5,4) = EKB(4,2)

```

```

DD(6,4) = EKB(3,3)

```

```

DD(7,4) = EKB(6,1)

```

```

DD(8,4) = EKB(5,2)

```

```

DD(9,4) = EKB(4,4)

```

```

DD(5,5) = EKB(3,3)

```

```

DD(6,5) = EKB(2,4)

```

```

DD(7,5) = EKB(5,2)

```

```

DD(8,5) = EKB(4,3)
DD(9,5) = EKB(2,5)
DD(6,6) = EKB(1,5)
DD(7,6) = EKB(4,3)
DD(8,6) = EKB(3,4)
DD(9,6) = EKB(1,6)
DD(7,7) = EKB(7,1)
DD(8,7) = EKB(6,2)
DD(9,7) = EKB(3,4)
DD(8,8) = EKB(5,3)
DD(9,8) = EKB(3,5)
DD(9,9) = EKB(1,7)

```

```
K=1
```

```
DO 2 I=1,8
```

```
K = K+1
```

```
DO 2 J=K,9
```

```
2 DD(I,J) = DD(J,I)
```

```
CALL MULTP(DD,A,EKB,9,9,9,0,9,9,9)
```

```
CALL MULTP(A,EKB,DD,9,9,9,1,9,9,9)
```

```
RETURN
```

```
END
```

```
SUBROUTINE MULTP (A,B,C,I,J,K,IT,NA,NB,NC)
```

```
-----
THIS SUBROUTINE GIVES THE PRODUCT OF TWO MATRICES
-----
```

```
DESCRIPTION OF PARAMETERS
```

```

A,B      MATRICES TO BE MULTIPLIED. MATRIX A IS OF
          SIZE (I,K) IF IT=0. IF IT IS NONZERO, A IS OF
          SIZE (K,I), MATRIX B IS OF SIZE (K,J)

```

```

C        A*B (IF IT=0)
          A(TRANPOSE)*B (IF IT IS NONZERO)

```

```

NA,NB,NC FIRST DIMENSION OF MATRICES A,B,C IN THE
          DIMENSION STATEMENT

```

```
DIMENSION A(NA,1),B(NB,1),C(NC,1)
```

```
DO 1 M=1,I
```

```
DO 1 N=1,J
```

```
C(M,N) = 0.
```

```
DO 1 L=1,K
```

```
IF(IT.EQ.0)C(M,N) = C(M,N)+A(M,L)*B(L,N)
```

```
1 IF(IT.NE.0)C(M,N) = C(M,N)+A(L,M)*B(L,N)
```

```
RETURN
```

```
END
```



SUBROUTINE CENTK (C1,C2,C3,STRESS,A,D,HH)

-----  
 THIS SUBROUTINE FINDS THE CENTRIFUGAL STIFFNESS  
 MATRIX FOR AN ELEMENT. ACTUAL CENTRIFUGAL STIFFNESS  
 MATRIX IS THE MATRIX HH OBTAINED IN THIS SUBROUTINE  
 MULTIPLIED BY FLEXURAL RIGIDITY CORRESPONDING TO  
 MAXIMUM THICKNESS.  
 -----

DESCRIPTION OF PARAMETERS

C1,C2,C3 AS DEFINED BY EQUATION 3.19  
 STRESS (STRESSES IN THE MIDDLE SURFACE)\*(MAXIMUM  
 THICKNESS)/(FLEXURAL RIGIDITY). THE ORDER OF  
 STRESSES IS SIGMA X,SIGMA Y,TAU XY.  
 THE STRESSES ARE ALONG LOCAL AXES.  
 A INVERSE OF MATRIX A (EQUATION 3.8)  
 D MATRIX OF DOUBLE INTEGRALS.ELEMENT(I,J)  
 OF THIS MATRIX IS THE VALUE OF INTEGRAL  
 OF  $XX^{(I-1)}*YY^{(J-1)}$   
 HH CENTRIFUGAL STIFFNESS MATRIX/FLEXURAL  
 RIGIDITY

DIMENSION STRESS(3),A(9,9),D(9,9),EKC(9,9),DD(9,9),

1 HH(9,9)

SX = STRESS(1)

SY = STRESS(2)

TXY = STRESS(3)

DO 1 I=1,9

DO 1 J=1,9

HH(I,J) = 0.

1 IF(I.LT.6.AND.J.LT.6)DD(I,J) = (C1\*D(I+1,J)+C2\*D(I,J+1)  
 +C3\*D(I,J))

1 CONTINUE

HH(2,2) = SX\*DD(1,1)

HH(3,2) = TXY\*DD(1,1)

HH(4,2) = 2.\*SX\*DD(2,1)

HH(5,2) = SX\*DD(1,2)+TXY\*DD(2,1)

HH(6,2) = 2.\*TXY\*DD(1,2)

HH(7,2) = 3.\*SX\*DD(3,1)

HH(8,2) = 2.\*SX\*DD(2,2)+TXY\*DD(3,1)

HH(9,2) = 3.\*TXY\*DD(1,3)

HH(3,3) = SY\*DD(1,1)

HH(4,3) = 2.\*TXY\*DD(2,1)

HH(5,3) = TXY\*DD(1,2)+SY\*DD(2,1)

HH(6,3) = 2.\*SY\*DD(1,2)

```

HH(7,3) = 3.*TXY*DD(3,1)
HH(8,3) = 2.*TXY*DD(2,2)+SY*DD(3,1)
HH(9,3) = 3.*SY*DD(1,3)
HH(4,4) = 4.*SX*DD(3,1)
HH(5,4) = 2.*(SX*DD(2,2)+TXY*DD(3,1))
HH(6,4) = 4.*TXY*DD(2,2)
HH(7,4) = 6.*SX*DD(4,1)
HH(8,4) = 4.*SX*DD(3,2)+2.*TXY*DD(4,1)
HH(9,4) = 6.*TXY*DD(2,3)
HH(5,5) = SX*DD(1,3)+2.*TXY*DD(2,2)+SY*DD(3,1)
HH(6,5) = 2.*(TXY*DD(1,3)+SY*DD(2,2))
HH(7,5) = 3.*(SX*DD(3,2)+TXY*DD(4,1))
HH(8,5) = 2.*SX*DD(2,3)+3.*TXY*DD(3,2)+SY*DD(4,1)
HH(9,5) = 3.*(TXY*DD(1,4)+SY*DD(2,3))
HH(6,6) = 4.*SY*DD(1,3)
HH(7,6) = 6.*TXY*DD(3,2)
HH(8,6) = 4.*TXY*DD(2,3)+2.*SY*DD(3,2)
HH(9,6) = 6.*SY*DD(1,4)
HH(7,7) = 9.*SX*DD(5,1)
HH(8,7) = 6.*SX*DD(4,2)+3.*TXY*DD(5,1)
HH(9,7) = 9.*TXY*DD(3,3)
HH(8,8) = 4.*SX*DD(3,3)+SY*DD(5,1)+4.*TXY*DD(4,2)
HH(9,8) = 6.*TXY*DD(2,4)+3.*SY*DD(3,3)
HH(9,9) = 9.*SY*DD(1,5)
DO 2 I=1,9
DO 2 J=I,9
HH(1,J) = HH(J,I)
2 CONTINUE
CALL MULTP(HH,A,EKC,9,9,9,0,9,9,9)
CALL MULTP(A,EKC,HH,9,9,9,1,9,9,9)
RETURN
END

```

```

SUBROUTINE GROUP (I,J,K,L,NTE,IT,GK,CK,R,P,IVEC)

```

```

C -----
C THIS SUBROUTINE ASSEMBLES THE ELEMENT MATRICES TO
C GIVE THE COMPLETE MATRIX FOR THE PLATE. IF IVEC IS
C INPUT AS ZERO,THE VECTOR OF ELEMENT NODAL FORCES IS
C ALSO ASSEMBLED.
C -----

```

```

C
C DESCRIPTION OF PARAMETERS

```

```

C I,J,K          NODE NUMBERS.THE NODES ON THE FIXED EDGE
C                MUST BE NUMBERED ZERO

```

```

C      L          TRIANGULAR ELEMENT NUMBER
C      NTE        TOTAL NUMBER OF TRIANGLES
C      IT         NUMBER OF DEGREES OF FREEDOM PER ELEMENT
C      GK         THE ELEMENT MATRIX IN GLOBAL COORDINATES
C                TO BE ASSEMBLED
C      CK         THE ASSEMBLED MATRIX FOR THE PLATE. THIS
C                SYMMETRIC MATRIX IS RETURNED AS A COLUMN
C                VECTOR. THE ELEMENT (M,N) OF THE FULL MATRIX
C                IS THE ELEMENT M*(M-1)/2+N OF CK, WHERE N
C                IS LESS THAN M
C      R          VECTOR OF ELEMENT NODAL FORCES TO BE
C                ASSEMBLED
C      P          THE ASSEMBLED VECTOR OF NODAL FORCES
C      IVEC       IF NONZERO, ONLY THE MATRICES ARE TO BE
C                ASSEMBLED

```

```

DIMENSION CK(1),GK(IT,IT),R(IT),P(1)
I1 = (I-1)*IT/3+1
J1 = (J-1)*IT/3+1
K1 = (K-1)*IT/3+1
I2 = I*IT/3
J2 = J*IT/3
K2 = K*IT/3
IF(L.EQ.NTE.AND.IT.EQ.18)K2 = K2-1
M = 0
IF(I.EQ.0)GO TO 2
DO 1 II=I1,I2
CALL ASSEMB(I1,I2,J1,J2,K1,K2,II,M,IT,GK,CK,L,NTE)
1 IF(IVEC.EQ.0)P(II) = P(II)+R(M)
2 IF(I.EQ.0)M=M+IT/3
IF(J.EQ.0)GO TO 4
DO 3 II=J1,J2
CALL ASSEMB(I1,I2,J1,J2,K1,K2,II,M,IT,GK,CK,L,NTE)
3 IF(IVEC.EQ.0)P(II) = P(II)+R(M)
4 IF(J.EQ.0)M=M+IT/3
IF(K.EQ.0)GO TO 6
DO 5 II = K1,K2
CALL ASSEMB(I1,I2,J1,J2,K1,K2,II,M,IT,GK,CK,L,NTE)
5 IF(IVEC.EQ.0)P(II) = P(II)+R(M)
6 IF(K.EQ.0)M = M+IT/3
RETURN
END

```

```

SUBROUTINE ASSEMB (I1,I2,J1,J2,K1,K2,II,M,IT,GK,CK
1 ,LL,NTE)

```





```

C      DESCRIPTION OF PARAMETERS
C
C      CKM      MATRIX WHOSE EIGENVALUES ARE REQUIRED
C      NR      SIZE OF MATRIX CKM
C      NDIM     FIRST DIMENSION OF MATRIX CKM IN THE
C              DIMENSION STATEMENT
C      MR      NUMBER OF EIGENVALUES REQUIRED
C      ALPHA    VECTOR OF SIZE MR IN WHICH THE EIGENVALUES
C              ARE RETURNED
C      TOL     PERCENTAGE DIFFERENCE BETWEEN THE VALUES
C              FOR THE EIGENVALUE IN TWO SUCCESSIVE
C              ITERATIONS WHEN THE CONVERGENCE CAN BE
C              ASSUMED TO HAVE OCCURED
C      EY,EZ    DUMMY VECTORS

```

```

      DIMENSION CKM(NDIM,NDIM),EY(NDIM),EZ(NDIM),ALPHA(MR)
      NN=NR+1
      DO 12 L=1,MR
      NN=NN-1
      DO 1 I=1,NN
      EY(I) = 1.0
1     CONTINUE
      BETA = 1.0
2     DO 3 I=1,NN
      EZ(I) = 0.0
      DO 3 K=1,NN
      EZ(I) = EZ(I)+CKM(I,K)*EY(K)
3     CONTINUE
      ALPHA(L) = 0.0
      DO 4 I=1,NN
      IF (ABS(EZ(I)).GT.ALPHA(L)) ALPHA(L)=ABS(EZ(I))
4     CONTINUE
      ERROR = 100.*(ALPHA(L)-BETA)/BETA
      IF (ABS(ERROR).LT.ABS(TOL)) GO TO 6
      BETA = ALPHA(L)
      DO 5 I=1,NN
      EY(I) = EZ(I)/ALPHA(L)
5     CONTINUE
      GO TO 2
6     BETA = EY(1)
      DO 7 I=1,NN
      EY(I) = EY(I)/BETA
7     CONTINUE
      DO 8 J=1,NN
      EZ(J) = CKM(1,J)
8     CONTINUE
      DO 9 I=1,NN
      DO 9 J=1,NN
      K=NN+1-I

```

```

          CKM(K,J) = CKM(K,J)-EY(K)*CKM(1,J)
9      CONTINUE
        DO 10 I=2,NN
          DO 10 J=2,NN
            M=I-1
            N=J-1
10     CKM(M,N) = CKM(I,J)
          DO 11 J=2,NN
            I=J-1
11     CKM(NN,I) = EZ(J)
          DO 12 I=1,NN
            CKM(I,NN) = EY(I)
12     CONTINUE
C
C      IF ONLY THE EIGENVALUES ARE REQUIRED,THE SUBROUTINE
C      MAY BE TERMINATED HERE
C
        DO 22 M=1,MR
          N=MR-M
          MM=N+1
          L=NR-N
          DO 13 I=1,L
            EZ(I) = CKM(1,L)
13     CONTINUE
          IF(N.EQ.0) GO TO 18
14     L=NR-N
          LL=L+1
          C=0.
          NN = N+1
          DO 15 I=1,L
            C=C+EZ(I)*CKM(LL,I)
15     CONTINUE
          C=(ALPHA(MM)-ALPHA(N))/C
          DO 16 I=1,L
            EZ(I) = EZ(I)*C
16     CONTINUE
          DO 17 I=1,L
            J=L+2-I
            NN=J-1
17     EZ(J) = EZ(NN)+CKM(J,LL)
            EZ(1) = CKM(1,LL)
            N=N-1
            IF(N.GT.0) GO TO 14
18     C = ABS(EZ(1))
            DO 19 I=2,NR
              IF(ABS(EZ(I)).GT.C) C=ABS(EZ(I))
19     CONTINUE
            DO 20 I=1,NR
              EZ(I) = EZ(I)/C
20     CONTINUE

```



```
KJ = 2*MM-1
KK = 2*MM
KI = (NR+1)/2
KL = KI+1
DO 21 I=1,KI
CKM(I,KJ) = EZ(I)
21 CONTINUE
DO 22 I=KL,NR
CKM(I-KI,KK) = EZ(I)
22 CONTINUE
DO 24 MM=1,MR
KJ = 2*MM-1
KK = 2*MM
DO 23 I=1,KI
CKM(I,MM) = CKM(I,KJ)
23 CONTINUE
DO 24 I=KL,NR
CKM(I,MM) = CKM(I-KI,KK)
24 CONTINUE
RETURN
END
```

## NOTE

THIS PROGRAMME IS DESIGNED FOR TOTAL NUMBER OF NODES  
GREATER THAN 5.

## APPENDIX IV

COMPUTER PROGRAMME FOR VIBRATION ANALYSIS OF ROTATING  
PRETWISTED CANTILEVER PLATE

A4176,CM124000,T2000.

RAWTANI S.

RUN(S)

LGO.

REWIND LGO.

RUN(S)

LGO.

'

6400 END OF RECORD

PROGRAM TST (INPUT,OUTPUT,TAPE5=INPUT,TAPE6=OUTPUT,  
1 TAPE 1,TAPE 2,TAPE 3)

```

DIMENSION CK(15000),P(167),DISP(167),TY(167,6)
DIMENSION X(3),Y(3),Z(3),T(3),XX(3),YY(3),ALMD(3,3),
1 A(9,9),DD(9,9),FP(6),FB(9),EKB(9,9),EKP(6,6),F(18),
2 EK(18,18),STRSS(3),CFK(9,9),CFM(18,18),YU(3)

```

C

C

C NOTATIONS

C

C	AR	ASPECT RATIO
C	BOVERT	BREADTH/THICKNESS AT ORIGIN
C	TWIST	TOTAL PRETWIST (DEGREES)
C	V	POISSONS RATIO
C	TL	LENGTHWISE TAPER FACTOR. THICKNESS AT (L,0,0)/THICKNESS AT (0,0,0)
C	TB	BREADTHWISE TAPER FACTOR. THICKNESS AT (0,B/2,0)/THICKNESS AT (0,0,0)
C	ROTC	ROTATIONAL SPEED/FUND. NONROTATING FREQ.
C	BETA1	FUND. NONROTATING FREQ. (NONDIMENSIONAL)
C	THETA	SETTING ANGLE (DEGREES)
C	ROVERL	RADIUS OF DISC/LENGTH OF PLATE
C	NL	LENGTHWISE SUBDIVISIONS
C	NB	BREADTHWISE SUBDIVISIONS
C	NEIGEN	NUMBER OF EIGENVALUES REQUIRED

C

C

C -----

C DATA INPUT. IF THE PLATE IS NONROTATING, PUT ROTC,  
C BETA1, THETA AND ROVERL AS ZERO.

C

C

C -----

READ(5,1)AR,BOVERT,TWIST,TL,TB,V

READ(5,1)ROTC,BETA1,THETA,ROVERL

READ(5,2)NL,NB,NEIGEN

1 FORMAT(6F10.4)

2 FORMAT(3I2)

```

C -----
C ALL LINEAR DIMENSIONS ARE NORMALIZED BY TAKING THE
C BREADTH OF THE PLATE AS UNITY. THE NUMBER OF TRIANGULAR
C ELEMENTS(NTE), THE NUMBER OF DEGREES OF FREEDOM(NDF),
C AND THE SIZE(NW) OF THE SYMMETRIC STIFFNESS MATRIX
C (CK) STORED AS COLUMN VECTOR ARE DETERMINED. THE
C MATRIX IS INITIALLY SET TO ZERO.
C -----
RADIUS = ROVERL*AR
TORIGN = 1./BOVERT
NTE = NL*NB*2
NDF = NL*(NB+1)*6-1
NW = NDF*(NDF+1)/2
DO 3 L=1,NW
CK(L) = 0.
3 CONTINUE

C -----
C THE GLOBAL COORDINATES(X,Y,Z) OF THE NODES, THE NODE
C NUMBERS(I,J,K) AND THE THICKNESS AT THE NODES(T) ARE
C GENERATED FOR EACH ELEMENT. THESE ARE STORED ON TAPE
C NO.3. THE MAXIMUM THICKNESS(TMAX) OF THE PLATE IS
C ALSO DETERMINED.
C -----
REWIND 3
TMAX = 0.
DO 5 N=1,2
YU(1) = -0.5-1./NB
KR = 0
DO 5 L=1,NB
YU(1) = YU(1)+1./NB
YU(2) = YU(1)+1./NB
YU(3) = YU(1)
IF(N.EQ.2) YU(3) = YU(2)
KR = KR+1
LZ = (L-1)*(NL+1)-KR
DO 5 M=1,NL
X(1) = M*AR/NL
X(2) = (M-1)*AR/NL
X(3) = X(2)
IF(N.EQ.2) X(3) = X(1)
B1 = TORIGN*(TL-1.)/AR
B2 = 2.*TORIGN*(TB-1.)
B3 = TORIGN
DO 4 I=1,3
T(I) = B1*X(I)+B2*YU(I)+B3
IF(T(I).GT.TMAX) TMAX = T(I)
ANGLE = TWIST*X(I)*3.142/(180.*AR)
Z(I) = YU(I)*SIN(ANGLE)
4 Y(I) = YU(I)*COS(ANGLE)

```



```

LZ = LZ+1
I = LZ+1
J = I+NL-1
IF(M.EQ.1)J=0
K = LZ
IF(N.EQ.2)K=LZ+NL+1
IF(M.EQ.1.AND.N.EQ.1)K=0
5 WRITE(3)X,Y,Z,T,I,J,K
REWIND 3

C
C -----
C THE STIFFNESS MATRIX FOR THE PLATE IN THE INITIAL
C CONFIGURATION IS OBTAINED. ACTUAL STIFFNESS MATRIX
C IS THE MATRIX CK CALCULATED HERE MULTIPLIED BY THE
C FLEXURAL RIGIDITY OF THE PLATE.
C -----
C REWIND 1
C REWIND 2
C DO 6 L=1,NTE
C READ(3)X,Y,Z,T,I,J,K

C
C THE DIRECTION COSINES OF THE LOCAL AXES(ALMD) AND THE
C LOCAL COORDINATES OF THE NODES (XX,YY) ARE DETERMINED.
C
A1 = (X(2)-X(1))**2+(Y(2)-Y(1))**2+(Z(2)-Z(1))**2
A2 = (X(3)-X(2))**2+(Y(3)-Y(2))**2+(Z(3)-Z(2))**2
A3 = (X(1)-X(3))**2+(Y(1)-Y(3))**2+(Z(1)-Z(3))**2
YY(2) = SQRT(A1)
YY(3) = (A3+A1-A2)/(2.0*YY(2))
XX(3) = SQRT(ABS(A3-YY(3)**2))
CALL LAMDA(X,Y,Z,ALMD)

C
C COEFFICIENTS C1,C2,C3(EQUATION 3.19) ARE DETERMINED.
C
C3 = T(1)/TMAX
C2 = (T(2)/TMAX-C3)/YY(2)
C1 = (T(3)/TMAX-C3-C2*YY(3))/XX(3)

C
C THE INVERSE OF MATRIX A (EQUATION 3.8) IS OBTAINED.
C
CALL AINVR(X,YY,A)

C
C THE MATRIX (DD) OF DOUBLE INTEGRALS IS OBTAINED.
C DD(M,N) IS THE VALUE OF INTEGRAL OF XX**(M-1)*YY**(N-1)
C
CALL DUBINT(X,YY,DD)

C
C THE PROPERTIES OF ELEMENTS REQUIRED IN LATTER
C CALCULATIONS ARE STORED.

```

```

IF(ROTC.GL.1.E-8)WRITE(2)X,Y,Z,T,I,J,K,XX,YY,ALMD
IF(ROTC.LT.1.E-8)WRITE(1)I,J,K,XX,YY,C1,C2,C3,ALMD,A,DD

```

```

C
C THE IN-PLANE AND THE BENDING STIFFNESS MATRICES OF AN
C ELEMENT ARE DETERMINED AND COMBINED TO OBTAIN THE
C COMPLETE STIFFNESS MATRIX OF THE ELEMENT.
C

```

```

CALL PLANEK (XX,YY,TMAX,V,C1,C2,C3,EKP)
CALL BENDK (C1,C2,C3,V,A,DD,ERB)
CALL SHELL (EKP,ERB,EK,FP,FB,F,1)

```

```

C
C THE ELEMENT STIFFNESS MATRICES ARE TRANSFORMED TO
C GLOBAL AXES. FOR THE LAST NODE OF THE LAST TRIANGLE
C THE ROTATIONAL DEGREES OF FREEDOM ARE RETAINED
C ABOUT THE LOCAL AXES. THE ELEMENT MATRICES ARE GROUPED
C TO OBTAIN THE FINAL STIFFNESS MATRIX (CK) FOR THE PLATE.
C

```

```

CALL TRNSFR (ALMD,EK,F,1)
IF(L.EQ.NTE)CALL LAST (ALMD,EK,F,1)
6 CALL GROUP (I,J,K,L,NTE,18,EK,CK,F,P,1)
REWIND 1
REWIND 2
REWIND 3
IF(ROTC.LT.1.E-8)GO TO 19

```

```

C
C -----
C THE CENTRIFUGAL FORCES GIVEN BY EQUATION 4.37 ARE
C LUMPED AT THE NODES,THE STIFFNESS MATRIX CK IS
C INVERTED USING THE LIBRARY SUBROUTINE INVSYM, AND
C THE PSEUDO-STATIC DEFORMATION IS CALCULATED. IF THE
C INVERSION FAILS THE PROGRAMME STOPS.
C
C -----

```

```

SPD = (ROTC**2)*(BETA1**2)/(AR**4)
TR = TORIGN/TMAX
CALL LUMP(AR,TL,TB,TR,RADIUS,TWIST,THETA,NL,NB,SPD,P)
CALL INVSYM(CK,NDF,IERR)
IF(IERR.NE.0)WRITE(6,7)IERR
7 FORMAT(5X,5HIERR=,I3)
IF(IERR.NE.0)STOP
DO 8 I=1,NDF
DISP(I) = 0.
DO 8 K=1,NDF
IF(I.GE.K)L=I*(I-1)/2+K
IF(I.LT.K)L=K*(K-1)/2+I
8 DISP(I) = DISP(I)+CK(L)*P(K)

```

```

C
C -----
C THE STRESSES IN THE MIDDLE SURFACE AND THE COORDINATES
C OF THE NODES IN THE DEFORMED CONFIGURATION ARE
C DETERMINED. THESE ARE STORED ON TAPE 3
C
C -----

```

```

DO 14 L=1,NTE
READ(2)'X,Y,Z,T,I,J,K,XX,YY,ALMD
II = 6*(I-1)
JJ = 6*(J-1)
KK = 6*(K-1)
DO 9 N=1,9
FB(N) = 0.
9 CONTINUE
IF(1.EQ.0)GO TO 10
FB(1) = DISP(II+1)
FB(2) = DISP(II+2)
FB(3) = DISP(II+3)
10 IF(J.EQ.0)GO TO 11
FB(4) = DISP(JJ+1)
FB(5) = DISP(JJ+2)
FB(6) = DISP(JJ+3)
11 IF(K.EQ.0)GO TO 12
FB(7) = DISP(KK+1)
FB(8) = DISP(KK+2)
FB(9) = DISP(KK+3)
12 CALL STRESS (XX,YY,ALMD,V,FB,TMAX,STRSS)
DO 13 N=1,3
X(N) = X(N)+FB(3*N-2)
Y(N) = Y(N)+FB(3*N-1)
13 Z(N) = Z(N)+FB(3*N)
14 WRITE(3)X,Y,Z,T,I,J,K,STRSS
REWIND 2
REWIND 3

```

```

C
C -----
C THE STIFFNESS MATRIX,INCLUDING THE CENTRIFUGAL STIFF-
C NESS AND CENTRIFUGAL MASS MATRIX, IN THE DEFORMED
C CONFIGURATION ARE DETERMINED.ACTUAL STIFFNESS MATRIX
C IS THE MATRIX CK CALCULATED HERE MULTIPLIED BY THE
C FLEXURAL RIGIDITY OF THE PLATE.
C -----

```

```

DO 15 L=1,NW
CK(L) = 0.
15 CONTINUE
DO 18 L=1,NTE
READ(3)'X,Y,Z,T,I,J,K,STRSS

```

```

C
C THE DIRECTION COSINES OF THE LOCAL AXES(ALMD) AND THE
C LOCAL COORDINATES OF THE NODES (XX,YY) ARE DETERMINED.
C

```

```

A1 = (X(2)-X(1))**2+(Y(2)-Y(1))**2+(Z(2)-Z(1))**2
A2 = (X(3)-X(2))**2+(Y(3)-Y(2))**2+(Z(3)-Z(2))**2
A3 = (X(1)-X(3))**2+(Y(1)-Y(3))**2+(Z(1)-Z(3))**2
YY(2) = SQRT(A1)
YY(3) = (A3+A1-A2)/(2.0*YY(2))
XX(3) = SQRT(ABS(A3-YY(3)**2))
CALL LAMDA(X,Y,Z,ALMD)

```



```

C
C   COEFFICIENTS C1,C2,C3(EQUATION 3.19 )ARE DETERMINED.
C
C   C3 = T(1)/TMAX
C   C2 = (T(2)/TMAX-C3)/YY(2)
C   C1 = (T(3)/TMAX-C3-C2*YY(3))/XX(3)
C
C   THE INVERSE OF MATRIX A (EQUATION 3.8) IS OBTAINED.
C
C   CALL AINVRS (XX,YY,A)
C
C   THE MATRIX (DD) OF DOUBLE INTEGRALS IS OBTAINED.
C   DD(M,N) IS THE VALUE OF INTEGRAL OF XX**(M-1)*YY**(N-1)
C
C   CALL DUBINT (XX,YY,DD)
C
C   THE PROPERTIES OF ELEMENTS REQUIRED IN LATTER
C   CALCULATIONS ARE STORED.
C
C   WRITE(1) I,J,K,XX,YY,C1,C2,C3,ALMD,A,DD
C
C   THE BENDING AND THE CENTRIFUGAL STIFFNESS MATRICES
C   OF AN ELEMENT ARE OBTAINED AND ADDED.
C
C   CALL BENDK (C1,C2,C3,V,A,DD,EKB)
C   CALL CENTK(C1,C2,C3,STRSS,A,DD,CFK)
C   DO 16 M=1,9
C   DO 16 N=1,9
C   EKB(M,N) = EKB(M,N)+CFK(M,N)
16  CONTINUE
C
C   THE INPLANE STIFFNESS MATRIX OF AN ELEMENT IS
C   OBTAINED AND COMBINED WITH THE TOTAL BENDING STIFF-
C   NESS MATRIX TO GET THE COMPLETE STIFFNESS MATRIX
C   FOR AN ELEMENT.
C
C   CALL PLANEK (XX,YY,TMAX,V,C1,C2,C3,EKP)
C   CALL SHELL (EKP,EKB,EK,FP,FB,F,1)
C
C   THE CENTRIFUGAL MASS MATRIX OF AN ELEMENT IS OBTAINED
C   AND SUBTRACTED FROM THE STIFFNESS MATRIX.
C
C   CALL CENTM (C1,C2,C3,XX,YY,ALMD,THETA,SPD,DD,CFM)
C   DO 17 M=1,18
C   DO 17 N=1,18
C   EK(M,N) = EK(M,N)-CFM(M,N)
17  CONTINUE

```

```

C
C THE ELEMENT STIFFNESS MATRICES ARE TRANSFORMED TO
C GLOBAL AXES. FOR THE LAST NODE OF THE LAST TRIANGLE
C THE ROTATIONAL DEGREES OF FREEDOM ARE RETAINED
C ABOUT THE LOCAL AXES. THE ELEMENT MATRICES ARE GROUPED
C TO OBTAIN THE FINAL STIFFNESS MATRIX (CK) FOR THE PLATE.
C
CALL TRNSFR (ALMD,EK,F,1)
IF(L.EQ.NTE)CALL LAST (ALMD,EK,F,1)
18 CALL GROUP (I,J,K,L,NTE,18,EK,CK,F,P,1)
REWIND 1
REWIND 3

C
C -----
C THE MATRIX CK (STIFFNESS MATRIX - CENTRIFUGAL MASS
C MATRIX) IS INVERTED, USING LIBRARY SUBROUTINE INVSYM.
C IF THE INVERSION FAILS THE PROGRAMME STOPS. THE
C INVERTED MATRIX IS STORED ON TAPE 2, SIX COLUMNS
C AT A TIME.
C -----
19 CALL INVSYM(CK,NDF,IERR)
IF(IERR.NE.0)WRITE(6,7)IERR
IF(IERR.NE.0)STOP
IT = (NDF+1)/6
DO 21 K=1,IT
M = 0
IK = K*6
IM = IK-5
IF(K.EQ.IT)IK = IK-1
DO 20 I=IM,IK
M = M+1
DO 20 J=1,NDF
IF(I.GE.J)L=I*(I-1)/2+J
IF(I.LT.J)L=J*(J-1)/2+I
20 TY(J,M) = CK(L)
21 WRITE(2)((TY(M,N),N=1,6),M=1,NDF)
REWIND 2

C
C -----
C THE MASS MATRIX OF THE PLATE IS DETERMINED. THE
C ACTUAL MASS MATRIX IS THE MATRIX CK CALCULATED HERE
C MULTIPLIED BY (RHO*TMAX). RHO IS THE MASS PER UNIT
C VOLUME AND TMAX IS THE MAXIMUM THICKNESS.
C -----
DO 22 L=1,NW
CK(L) = 0.
22 CONTINUE
DO 23 L=1,NTE
READ (1)I,J,K,XX,YY,C1,C2,C3,ALMD,A,DD

```

```

C
C   THE IN-PLANE AND THE BENDING MASS MATRICES FOR AN
C   ELEMENT ARE DETERMINED. THESE ARE COMBINED TO GIVE
C   COMPLETE MASS MATRIX FOR AN ELEMENT.
C
CALL PLANEM (XX,YY,C1,C2,C3,DD,EKP)
CALL BENDM (C1,C2,C3,A,DD,EKB)
CALL SHELL (EKP,EKB,EK,FP,FB,F,1)

C
C   THE ELEMENT MASS MATRICES ARE TRANSFORMED TO GLOBAL
C   AXES. FOR THE LAST NODE OF THE LAST ELEMENT THE
C   ROTATIONAL DISPLACEMENTS ARE RETAINED ABOUT THE
C   LOCAL AXES. THE ELEMENT MATRICES ARE GROUPED TO
C   OBTAIN THE FINAL MASS MATRIX (CK) FOR THE PLATE.
C
CALL TRANSR (ALMD,EK,F,1)
IF(L.EQ.NTE)CALL LAST (ALMD,EK,F,1)
23 CALL GROUP (I,J,K,L,NTE,18,EK,CK,F,P,1)
REWIND 1

C
C   -----
C   THE MASS MATRIX (CK) IS STORED ON TAPE 1, SIX COLUMNS
C   AT A TIME.
C   -----
DO 25 K=1,IT
M = 0
IK = K*6
IM = IK-5
IF(K.EQ.IT)IK = IK-1
DO 24 I=IM,IK
M = M+1
DO 24 J=1,NDF
IF(I.GE.J)L=I*(I-1)/2+J
IF(I.LT.J)L=J*(J-1)/2+I
24 TY(J,M) = CK(L)
25 WRITE(1)((TY(M,N),N=1,6),M=1,NDF)
REWIND 1

C
C   -----
C   THE PLATE DIMENSIONS ARE STORED ON TAPE 3. THE
C   FIRST PHASE OF THE PROGRAMME ENDS.
C   -----
WRITE(3)AR,BOVERT,TWIST,ROVERL,THETA,ROTC,BETA1,NL,NB,
1 NDF,V,TL,TB,NEIGEN
REWIND 3
END
'   6400 END RECORD
'   DATA
'   6400 END OF RECORD

```



```

PROGRAM TST (INPUT,OUTPUT,TAPE5=INPUT,TAPE6=OUTPUT,
1 TAPE 1,TAPE 2,TAPE 3)
  DIMENSION CKM(167,167),P(167),DISP(167),S(16)

```

```

C
C -----
C THE SECOND PHASE OF THE PROGRAMME STARTS WITH FRESH
C MEMORY. FROM THE FIRST PHASE THE FOLLOWING INFORMATION
C IS AVAILABLE ON THE TAPES.
C MASS MATRIX/(RHO*TMAX) ON TAPE 1
C INVERSE OF STIFFNESS MATRIX*FLEXURAL RIGIDITY ON TAPE 2
C PLATE DIMENSIONS ON TAPE 3.
C MATRICES ON TAPES 1 AND 2 ARE MULTIPLIED TO OBTAIN
C MATRIX CKM.
C -----
  READ(3) AR,BOVERT,TWIST,ROVERL,THETA,ROTC,BETA1,NL,NB
1 ,NDF,V,TL,TB,NEIGEN
  REWIND 3
  IT = (NDF+1)/6
  DO 2 K=1,IT
    LM = 6
    IF(K.EQ.IT)LM=5
    MR = NDF-5
    IF(K.LT.3)READ(1)((CKM(M,N),N=MR,NDF),M=1,NDF)
    IF(K.GE.3)READ(1)((CKM(M,N),N=7,12),M=1,NDF)
    DO 1 J=1,IT
      LN = 6
      IF(J.EQ.IT)LN = 5
      IF(J.EQ.1)REWIND 2
      MR = NDF-11
      KR = NDF-6
      IF(K.LT.3)READ(2)((CKM(M,N),N=MR,KR),M=1,NDF)
      IF(K.GE.3)READ(2)((CKM(M,N),N=1,6),M=1,NDF)
      IK = (K-1)*6
      DO 1 I=1,LM
        IK = IK+1
        IJ = (J-1)*6
        DO 1 N=1,LN
          IJ = IJ+1
          CKM(IJ,IK) = 0.
          DO 1 M=1,NDF
            IF(K.LT.3)CKM(IJ,IK) = CKM(IJ,IK)+CKM(M,MR-1+N)*
1 CKM(M,MR+5+I)
            IF(K.GE.3)CKM(IJ,IK) = CKM(IJ,IK)+CKM(M,N)*CKM(M,6+I)
1 CONTINUE
            IF(K.EQ.1)WRITE(3)((CKM(M,N),N=1,6),M=1,NDF)
            IF(K.EQ.2)WRITE(3)((CKM(M,N),N=7,12),M=1,NDF)
2 CONTINUE
          REWIND 3
          READ(3)((CKM(M,N),N=1,6),M=1,NDF)
          READ(3)((CKM(M,N),N=7,12),M=1,NDF)

```

```

C -----
C EIGENVALUES OF MATRIX CKM ARE DETERMINED AND EXPRESSED
C AS NONDIMENSIONAL QUANTITIES BETA. THE EIGENVALUES
C AND EIGENVECTORS ARE WRITTEN OUT.
C -----
CALL POWER(CKM,NDF,NEIGEN,S,1.E-4,167,P,DISP)
DO 3 J=1,NEIGEN
  S(J) = AR**2/SQRT(S(J))
3 CONTINUE
  WRITE(6,4) AR,BOVERT,TWIST,V,ROVERL,THETA,ROTC,BETA1,
1 NL,NB,TL,TB
4 FORMAT(1H1,3X,*ASPECT RATIO=*,18X,F10.4,/,4X,
1*BREADTH/THICK.AT ORIGIN=*,8X,F10.4,/,4X,
2 *TOTAL PRETWIST(DEG)=*,11X,F10.4,/,4X,
3 *POISSONS RATIO=*,16X,F10.4,/,4X,*RADIUS/LENGTH=*,
4 17X,F10.4,/,4X,*SETTING ANGLE(DEG)=*,12X,F10.4,/,4X,
5 *ROT SPEED/FUND FREQ=*,11X,F10.4,/,4X,
6 *NONROTATING FUND FREQ(BETA1)=*,1X,F10.4,/,4X,
7 *LENGTHWISE SUBDIVISIONS=*,6X,12,/,4X,
8 *BREADTHWISE SUBDIVISIONS=*,6X,12,/,4X,
9 *LENGTHWISE TAPER FACTOR=*,7X,F10.4,/,4X,
X *BREADTHWISE TAPER FACTOR=*,6X,F10.4)
  WRITE(6,5)NEIGEN
5 FORMAT(/,10X,6HFIRST ,12,17H EIGEN VALUES ARE,/)
  WRITE(6,6)(S(I),I=1,NEIGEN)
6 FORMAT(50X,E15.6)
  DO 8 I=1,NEIGEN
  WRITE(6,7)I
7 FORMAT(/,5X,16HEIGEN VECTOR NO.,1X,12,1X,2HIS,/)
  WRITE(6,10)
8 WRITE(6,9)(CKM(J,I),J=1,NDF)
9 FORMAT(7(5X,6E16.6,/) )
10 FORMAT(12X,*U*,15X,*V*,15X,*W*,12X,*THETA X*,11X,
1 *THETA Y*,11X,*THETA Z*)
  STOP
  END
! 6400 END OF RECORD
! 6400 END FILE

```

```

SUBROUTINE PLANEK (XX,YY,TMAX,V,C1,C2,C3,EKP)

```

```

C -----
C THIS SUBROUTINE FINDS THE INPLANE STIFFNESS MATRIX
C OF AN ELEMENT. THE ACTUAL INPLANE STIFFNESS MATRIX
C IS THE MATRIX EKP OBTAINED IN THIS SUBROUTINE,
C MULTIPLIED BY THE FLEXURAL RIGIDITY AS DEFINED BY
C EQUATION 5.2
C -----

```

```

C      DESCRIPTION OF PARAMETERS
C
C      XX,YY      LOCAL COORDINATES OF THE NODES
C      TMAX      MAXIMUM THICKNESS OF THE PLATE
C      V         POISSONS RATIO
C      C1,C2,C3   AS DEFINED BY EQUATION 3.19
C      EKP       INPLANE STIFFNESS MATRIX/FLEXURAL RIGIDITY
C
C

```

```

DIMENSION BB(3,6),XX(3),YY(3),DA(3,3),HA(3,6),EKP(6,6)
DO 1 I=1,3
DO 1 J=1,6
1  BB(I,J) = 0.
   BB(1,1) = YY(2)-YY(3)
   BB(1,3) = YY(3)
   BB(1,5) = -YY(2)
   BB(2,2) = XX(3)
   BB(2,4) = -XX(3)
   BB(3,1) = XX(3)
   BB(3,2) = YY(2)-YY(3)
   BB(3,3) = -XX(3)
   BB(3,4) = YY(3)
   BB(3,6) = -YY(2)
DO 2 I=1,3
DO 2 J=1,6
2  BB(I,J) = -BB(I,J)/(XX(3)*YY(2))
   DA(1,1) = 1.0
   DA(1,2) = V
   DA(1,3) = 0.0
   DA(2,1) = V
   DA(2,2) = 1.0
   DA(2,3) = 0.0
   DA(3,1) = 0.0
   DA(3,2) = 0.0
   DA(3,3) = (1.0-V)/2.0
CALL MULTP (DA,BB,HA,3,6,3,0,3,3,3)
CALL MULTP (BB,HA,EKP,6,6,3,1,3,3,6)
C11 = XX(3)*YY(2)/2.
C12 = XX(3)*YY(2)*(YY(2)+YY(3))/6.
C21 = XX(3)*XX(3)*YY(2)/6.
A = 12.*(C1*C21+C2*C12+C3*C11)/(TMAX**2)
DO 3 I=1,6
DO 3 J=1,6
3  EKP(I,J) = EKP(I,J)*A
RETURN
END

```



```

SUBROUTINE LUMP(AR,TL,TB,TR,RADIUS,TWIST,THETA,NL,NB,
1 SPD,P)

```

```

-----
THIS SUBROUTINE FINDS THE VECTOR OF NODAL FORCES
CORRESPONDING TO THE DISTRIBUTED CENTRIFUGAL FORCES
GIVEN BY EQUATION 4.34, USING LUMPED LOAD METHOD AS
ILLUSTRATED IN FIGURE 15. THE ACTUAL VECTOR OF NODAL
FORCES IS THE VECTOR P OBTAINED IN THIS SUBROUTINE
MULTIPLIED BY FLEXURAL RIGIDITY CORRESPONDING TO
MAXIMUM THICKNESS.
-----

```

DESCRIPTION OF PARAMETERS

AR	ASPECT RATIO
TL	LENGTHWISE TAPER FACTOR. THICKNESS AT (L,0,0)/THICKNESS AT (0,0,0)
TB	BREADTHWISE TAPER FACTOR. THICKNESS AT (0,B/2,0)/THICKNESS AT (0,0,0)
TR	THICKNESS AT (0,0,0)/MAXIMUM THICKNESS
RADIUS	DISC RADIUS
TWIST	TOTAL PRETWIST (DEGREES)
THETA	SETTING ANGLE (DEGREES)
NL	LENGTHWISE SUBDIVISIONS
NB	BREADTHWISE SUBDIVISIONS
SPD	(DENSITY)*(ROT.SPEED**2)*(MAX.THICKNESS)/ (FLEXURAL RIGIDITY), WHICH IS SAME AS (ROTC*DETEAL)**2/AR**4
P	VECTOR OF NODAL FORCES/FLEXURAL RIGIDITY

```

DIMENSION P(1)

```

```

B1 = TR*(TL-1.)/AR

```

```

B2 = 2.*TR*(TB-1.)

```

```

B3 = TR

```

```

ANL = NL

```

```

ANB = NB

```

```

NN = NL*(NB+1)

```

```

II = NL*NB

```

```

T = NL*NB*4

```

```

NR = NL*(NB+1)*6-1

```

```

DO 1 I=1,NR

```

```

P(I) = 0.

```

```

CONTINUE

```

```

DO 6 I=1,NN

```

```

IF(I.LE.NL)AJ = I

```

```

IF(I.GT.II)AJ = I-II

```

```

IF(I.LE.NL)YU = -0.5
IF(I.GT.II)YU = 0.5
IF(NB.LT.2)GO TO 3
DO 2 K=2,NB
IF(I.GT.(K-1)*NL.AND.I.LE.K*NL)AJ = 1-(K-1)*NL
AK = K
2 IF(I.GT.(K-1)*NL.AND.I.LE.K*NL)YU = -0.5+(AK-1.)/ANB
3 X= AR*AJ/ANL
AM = AR*4.*(B1*X+B2*YU+B3)/T
IF(I.GT.II)AM = AR*2.*(B1*X+B2*(YU-0.25/ANB)+B3)/T
IF(I.EQ.NN)AM = AR*(B1*(X-0.25*AR/ANL)+B2*(YU-0.25/ANB)+B3)/T
IF(I.EQ.NL)AM = AR*(B1*(X-0.25*AR/ANL)+B2*(YU+0.25/ANB)+B3)/T
IF(I.LT.NL)AM = AR*2.*(B1*X+B2*(YU+0.25/ANL)+B3)/T
IF(NB.LT.2)GO TO 5
DO 4 K=2,NB
IF(I.EQ.K*NL)AM = AR*2.*(B1*(X-AR*0.25/ANL)+B2*YU+B3)/T
4 CONTINUE
5 ANGLE = TWIST*X*3.142/(AR*180.)
Y = YU*COS(ANGLE)
Z = YU*SIN(ANGLE)
SN = SIN(THETA*3.142/180.)
CS = COS(THETA*3.142/180.)
P(6*I-5) = AM*(X+RADIUS)
P(6*I-4) = AM*(Y*CS*CS-Z*SN*CS)
P(6*I-3) = AM*(-Y*SN*CS+Z*SN*SN)
6 CONTINUE
DO 7 I=1,NR
P(I) = P(I)*SPD
7 CONTINUE
RETURN
END

```

SUBROUTINE PLANEM (XX,YY,C1,C2,C3,DD,EKP)

```

C
C
C -----
C THIS SUBROUTINE FINDS THE IN-PLANE MASS MATRIX FOR
C AN ELEMENT.THE ACTUAL MASS MATRIX IS THE MATRIX EKP
C OBTAINED IN THIS SUBROUTINE MULTIPLIED BY FACTOR
C EQUAL TO THE PRODUCT OF DENSITY AND MAXIMUM THICKNESS
C (RHO*TMAX)
C -----

```

DESCRIPTION OF PARAMETERS

```

C
C XX,YY          LOCAL COORDINATES OF NODES
C C1,C2,C3       AS DEFINED BY EQUATION 3.19
C

```

```

C      DD      MATRIX OF DOUBLE INTEGRALS.ELEMENT(I,J)
C      OF THIS MATRIX IS THE VALUE OF INTEGRAL
C      OF XX**(I-1)*YY**(J-1)
C      EKP      IN-PLANE MASS MATRIX/(RHO*THICK)
C
C
C      DIMENSION XX(3),YY(3),DD(9,9),EKP(6,6),A(6,6),B(6,6),N1(6)
C      DO 1 I=1,6
C      DO 1 J=1,6
C      A(I,J) = 0.
C      EKP(I,J) = 0.
1     CONTINUE
C
C      DETERMINING MATRIX A CORRESPONDING TO MATRIX Q
C      DEFINED BY EQUATION 3.42 AND INVERTING IT
C
C      A(1,1) = 1.
C      A(2,4) = 1.
C      A(3,1) = 1.
C      A(4,4) = 1.
C      A(5,1) = 1.
C      A(6,4) = 1.
C      A(3,3) = YY(2)
C      A(4,6) = YY(2)
C      A(5,2) = XX(3)
C      A(6,5) = XX(3)
C      A(5,3) = YY(3)
C      A(6,6) = YY(3)
C      CALL INVMAT(A,6,6,1.E-8,IERR,N1)
C      IF(IERR.NE.0)WRITE(6,2)IERR
2     FORMAT(5X,5HIERR=,I3)
C      IF(IERR.NE.0)STOP
C
C      DETERMINING THE IN-PLANE MASS MATRIX
C
C      DO 3 I=1,3
C      DO 3 J=1,3
C      B(I,J) = C1*DD(I+1,J)+C2*DD(I,J+1)+C3*DD(I,J)
3     CONTINUE
C      EKP(1,1) = B(1,1)
C      EKP(1,2) = B(2,1)
C      EKP(1,3) = B(1,2)
C      EKP(2,1) = B(2,1)
C      EKP(2,2) = B(3,1)
C      EKP(2,3) = B(2,2)
C      EKP(3,1) = B(1,2)
C      EKP(3,2) = B(2,2)
C      EKP(3,3) = B(1,3)

```



```

DO 4 I=1,3
DO 4 J=1,3
EKP(I+3,J+3) = EKP(I,J)
4 CONTINUE
CALL MULTP(EKP,A,B,6,6,6,0,6,6,6)
CALL MULTP(A,B,EKP,6,6,6,1,6,6,6)
RETURN
END

```

```

SUBROUTINE SHELL (EKP,EKB,EK,FP,FB,F,IVEC)

```

```

-----
THIS SUBROUTINE COMBINES THE IN-PLANE AND THE BENDING
MATRICES TO GIVE THE COMPLETE MATRIX FOR THE ELEMENT.
IF THE FORCE VECTORS ARE ALSO TO BE COMBINED IVEC IS
INPUT AS ZERO.
-----

```

```

DESCRIPTION OF PARAMETERS

```

```

EKP      INPLANE MATRIX
EKB      BENDING MATRIX
EK       COMBINED MATRIX
FP       IN-PLANE FORCE VECTOR
FB       BENDING FORCE VECTOR
F        COMBINED FORCE VECTOR
IVEC     IF NONZERO, ONLY MATICES ARE TO BE COMBINED

```

```

DIMENSION EKP(6,6),EKB(9,9),EK(18,18),FP(6),FB(9),F(18)

```

```

DO 1 I=1,18
DO 1 J=1,18
EK(I,J) = 0.
1 IF(IVEC.EQ.0)F(J) = 0.
DO 2 I=1,2
DO 2 J=1,2
DO 2 K=1,3
M=(K-1)*6
N=(K-1)*2
DO 2 L=1,3
MM = (L-1)*6
NN = (L-1)*2
EK(I+M,J+MM) = EKP(I+N,J+NN)
2 IF(IVEC.EQ.0)F(J+MM) = FP(J+NN)
DO 3 I=1,3
DO 3 J=1,3
DO 3 K=1,3

```

```

M=(K-1)*6+2
N = (K-1)*3
DO 3 L=1,3
MM = (L-1)*6+2
NN = (L-1)*3
EK(I+M,J+MM) = EKB(I+N,J+NN)
3 IF(IVVEC.EQ.0)F(J+MM) = FB(J+NN)
RETURN
END

```

```

SUBROUTINE CENTM (C1,C2,C3,XX,YY,ALMD,THETA,SPD,D,P)

```

```

C
C
C -----
C THIS SUBROUTINE FINDS THE CENTRIFUGAL MASS MATRIX FOR
C AN ELEMENT.THE ACTUAL CENTRIFUGAL MASS MATRIX IS THE
C MATRIX P OBTAINED FROM THIS SUBROUTINE MULTIPLIED BY
C FLEXURAL RIGIDITY CORRESPONDING TO MAXIMUM THICKNESS
C -----
C
C
C DESCRIPTION OF PARAMETERS
C
C C1,C2,C3 AS DEFINED BY EQUATION 3.19
C XX,YY LOCAL COORDINATES OF NODES
C ALMD MATRIX LAMDA OF DIRECTION COSINES AS
C DEFINED BY EQUATION 3.32
C THETA SETTING ANGLE
C SPD (DENSITY)*(ROT.SPEED**2)*(MAX.THICKNESS)/
C (FLEXURAL RIGIDITY), WHICH IS SAME AS
C (ROTC*BETA1)**2/AR**4
C D MATRIX OF DOUBLE INTEGRALS.ELEMENT(I,J)
C OF THIS MATRIX IS THE VALUE OF INTEGRAL
C OF XX**(I-1)*YY**(J-1)
C P CENTRIFUGAL MASS MATRIX/FLEXURAL RIGIDITY
C
C
C DIMENSION XX(3),YY(3),ALMD(3,3),DD(9,9),P(18,18),
1 Q(15,15),N1(15),R(15,15),D(9,9)
C
C MATRIX Q CORRESPONDING TO MATRIX P1 OF EQUATION 4.48
C IS CALCULATED AND INVERTED. IF THE INVERSION FAILS
C THE PROGRAMME STOPS.
C
C DO 1 I=1,15
C DO 1 J=1,15
1 Q(I,J) = 0.
Q(1,1) = 1.

```

```

Q(2,4) = 1.
Q(3,7) = 1.
Q(4,9) = 1.
Q(5,8) = -1.
Q(6,1) = 1.
Q(6,3) = YY(2)
Q(7,4) = 1.
Q(7,6) = YY(2)
Q(8,7) = 1.
Q(8,9) = YY(2)
Q(8,12) = YY(2)**2
Q(8,15) = YY(2)**3
Q(9,9) = 1.
Q(9,12) = 2.*YY(2)
Q(9,15) = 3.*YY(2)**2
Q(10,8) = -1.
Q(10,11) = -YY(2)
Q(11,1) = 1.
Q(11,2) = XX(3)
Q(11,3) = YY(3)
Q(12,4) = 1.
Q(12,5) = XX(3)
Q(12,6) = YY(3)
Q(13,7) = 1.
Q(13,8) = XX(3)
Q(13,9) = YY(3)
Q(13,10) = XX(3)**2
Q(13,11) = XX(3)*YY(3)
Q(13,12) = YY(3)**2
Q(13,13) = XX(3)**3
Q(13,14) = XX(3)**2*YY(3)
Q(13,15) = YY(3)**3
Q(14,9) = 1.
Q(14,11) = XX(3)
Q(14,12) = 2.*YY(3)
Q(14,14) = XX(3)**2
Q(14,15) = 3.*YY(3)**2
Q(15,8) = -1.
Q(15,10) = -2.*XX(3)
Q(15,11) = -YY(3)
Q(15,13) = -3.*XX(3)**2
Q(15,14) = -2.*XX(3)*YY(3)
CALL INVMAT (Q,15,15,1.E-8,IERR,N1)
IF(IERR.NE.0)WRITE(6,2)IERR
2 FORMAT(5X,5HIERR=,I3)
IF(IERR.NE.0)STOP
C
C ELEMENTS OF THE MATRIX (THETA2) DEFINED BY EQUATION
C 4.44 ARE DETERMINED. SINCE THE MATRIX IS SYMMETRIC
C ONLY THE UPPER TRIANGULAR PART IS CALCULATED

```



```

ANGLE = THETA*3.14/180.
SN = SIN(ANGLE)
CS = COS(ANGLE)
A1 = ALMD(1,1)**2+ALMD(1,2)**2*CS**2+ALMD(1,3)**2*
1 SN**2-2.*ALMD(1,2)*ALMD(1,3)*SN*CS
A2 = ALMD(1,1)*ALMD(2,1)+ALMD(1,2)*ALMD(2,2)*CS**2+
2 ALMD(1,3)*ALMD(2,3)*SN**2-(ALMD(2,2)*ALMD(1,3)+
3 ALMD(2,3)*ALMD(1,2))*SN*CS
A3 = ALMD(1,1)*ALMD(3,1)+ALMD(1,2)*ALMD(3,2)*CS**2+
4 ALMD(1,3)*ALMD(3,3)*SN**2-(ALMD(1,2)*ALMD(3,3)+
5 ALMD(3,2)*ALMD(1,3))*SN*CS
A4 = ALMD(2,1)**2+ALMD(2,2)**2*CS**2+ALMD(2,3)**2*
6 SN**2-2.*ALMD(2,2)*ALMD(2,3)*SN*CS
A5 = ALMD(2,1)*ALMD(3,1)+ALMD(2,2)*ALMD(3,2)*CS**2+
7 ALMD(2,3)*ALMD(3,3)*SN**2-(ALMD(2,2)*ALMD(3,3)+
8 ALMD(3,2)*ALMD(2,3))*SN*CS
A6 = ALMD(3,1)**2+ALMD(3,2)**2*CS**2+ALMD(3,3)**2*
9 SN**2-2.*ALMD(3,2)*ALMD(3,3)*SN*CS

```

C  
C  
C  
C

MATRIX P CORRESPONDING TO MATRIX P2 OF EQUATION 4.53  
IS CALCULATED

```

DO 3 I=1,8
DO 3 J=1,8
3 DD(I,J) = C1*D(I+1,J)+C2*D(I,J+1)+C3*D(I,J)
DO 4 J=1,3
M = 0
N = 0
IF(J.EQ.2)M=1
IF(J.EQ.3)N=1
P(1,J) = A1*DD(1+M,1+N)
P(2,J) = A1*DD(2+M,1+N)
P(3,J) = A1*DD(1+M,2+N)
P(4,J) = A2*DD(1+M,1+N)
P(5,J) = A2*DD(2+M,1+N)
P(6,J) = A2*DD(1+M,2+N)
P(7,J) = A3*DD(1+M,1+N)
P(8,J) = A3*DD(2+M,1+N)
P(9,J) = A3*DD(1+M,2+N)
P(10,J) = A3*DD(3+M,1+N)
P(11,J) = A3*DD(2+M,2+N)
P(12,J) = A3*DD(1+M,3+N)
P(13,J) = A3*DD(4+M,1+N)
P(14,J) = A3*DD(3+M,2+N)
4 P(15,J) = A3*DD(1+M,4+N)
DO 5 J=4,6
M = 0
N = 0
IF(J.EQ.5)M=1
IF(J.EQ.6)N=1

```

```

P(4,J) = A4*DD(1+M,1+N)
P(5,J) = A4*DD(2+M,1+N)
P(6,J) = A4*DD(1+M,2+N)
P(7,J) = A5*DD(1+M,1+N)
P(8,J) = A5*DD(2+M,1+N)
P(9,J) = A5*DD(1+M,2+N)
P(10,J) = A5*DD(3+M,1+N)
P(11,J) = A5*DD(2+M,2+N)
P(12,J) = A5*DD(1+M,3+N)
P(13,J) = A5*DD(4+M,1+N)
P(14,J) = A5*DD(3+M,2+N)
5 P(15,J) = A5*DD(1+M,4+N)
DO 6 J=7,9
M=0
N=0
IF(J.EQ.8)M=1
IF(J.EQ.9)N=1
P(7,J) = A6*DD(1+M,1+N)
P(8,J) = A6*DD(2+M,1+N)
P(9,J) = A6*DD(1+M,2+N)
P(10,J) = A6*DD(3+M,1+N)
P(11,J) = A6*DD(2+M,2+N)
P(12,J) = A6*DD(1+M,3+N)
P(13,J) = A6*DD(4+M,1+N)
P(14,J) = A6*DD(3+M,2+N)
6 P(15,J) = A6*DD(1+M,4+N)
P(10,10) = A6*DD(5,1)
P(11,10) = A6*DD(4,2)
P(12,10) = A6*DD(3,3)
P(13,10) = A6*DD(6,1)
P(14,10) = A6*DD(5,2)
P(15,10) = A6*DD(3,4)
P(11,11) = A6*DD(3,3)
P(12,11) = A6*DD(2,4)
P(13,11) = A6*DD(5,2)
P(14,11) = A6*DD(4,3)
P(15,11) = A6*DD(2,5)
P(12,12) = A6*DD(1,5)
P(13,12) = A6*DD(4,3)
P(14,12) = A6*DD(3,4)
P(15,12) = A6*DD(1,6)
P(13,13) = A6*DD(7,1)
P(14,13) = A6*DD(6,2)
P(15,13) = A6*DD(4,4)
P(14,14) = A6*DD(5,3)
P(15,14) = A6*DD(3,5)
P(15,15) = A6*DD(1,7)
DO 7 I=1,15
DO 7 J=I,15
7 P(I,J) = P(J,I)

```

```

      DO 8 I=1,15
      DO 8 J=1,15
8     P(I,J) = P(I,J)*SPD
      CALL MULTP (P,Q,R,15,15,15,0,18,15,15)
      CALL MULTP (Q,R,P,15,15,15,1,15,15,16)
C
C     MATRIX P IS NOW MODIFIED ACCORDING TO EQUATIONS
C     4.55 AND 4.56 TO BECOME THE CENTRIFUGAL MASS MATRIX.
C
      DO 9 I=1,15
      P(I,18) = 0.
      DO 9 K=1,5
      J=18-K
9     P(I,J) = P(I,J-2)
      DO 10 I=1,15
      P(I,12) = 0.
      DO 10 K=1,5
      J=12-K
10    P(I,J) = P(I,J-1)
      DO 11 I=1,15
      P(I,6) = 0.
11    CONTINUE
      DO 12 J=1,18
      P(18,J) = 0.
      DO 12 K=1,5
      I=18-K
12    P(I,J) = P(I-2,J)
      DO 13 J=1,18
      P(12,J) = 0.
      DO 13 K=1,5
      I=12-K
13    P(I,J) = P(I-1,J)
      DO 14 J=1,18
      P(6,J) = 0.
14    CONTINUE
      RETURN
      END

```

```

SUBROUTINE STRESS (XX,YY,ALMD,V,Fb,TMAX,STRSS)

```

```

C
C     -----
C     THIS SUBROUTINE FINDS THE STRESSES IN THE MIDDLE
C     SURFACE OF AN ELEMENT DUE TO CENTRIFUGAL FORCES.
C     THE ACTUAL STRESSES ARE THE STRESSES OBTAINED IN THIS
C     SUBROUTINE MULTIPLIED BY THE FLEXURAL RIGIDITY
C     CORRESPONDING TO MAXIMUM THICKNESS.
C     -----
C

```



```

C      DESCRIPTION OF PARAMETERS
C
C      XX,YY      LOCAL COORDINATES OF THE NODES
C      ALMD      MATRIX LAMDA OF DIRECTION COSINES AS
C                DEFINED BY EQUATION 3.32
C      V          POISSONS RATIO
C      FB        VECTOR OF NINE NODAL DISPLACEMENTS-U,V,W
C                AT EACH NODE. THESE DISPLACEMENTS ARE
C                ALONG GLOBAL AXES
C      TMAX      MAXIMUM THICKNESS
C      STRSS     (STRESSES IN THE MIDDLE SURFACE)*TMAX/
C                FLEXURAL RIGIDITY.THE STRESSES ARE ALONG
C                THE LOCAL AXES. THE ORDER OF THE STRESSES
C                IS SIGMA X ,SIGMA Y  AND TAU XY.
C
C
C

```

```

1  DIMENSION XX(3),YY(3),ALMD(3,3),B1(3,6),D(3,3),
    Q(3,6),T(9,9),FB(9),F(9),STRSS(3)

```

```

C      MATRIX B1 GIVEN BY EQUATION 3.26 IS DETERMINED.
C

```

```

C      DO 1 I=1,3
C      DO 1 J=1,6
1  B1(I,J) = 0.
    B1(1,1) = YY(2)-YY(3)
    B1(1,3) = YY(3)
    B1(1,5) = -YY(2)
    B1(2,2) = XX(3)
    B1(2,4) = -XX(3)
    B1(3,1) = XX(3)
    B1(3,2) = YY(2)-YY(3)
    B1(3,3) = -XX(3)
    B1(3,4) = YY(3)
    B1(3,6) = -YY(2)
    DO 2 I=1,3
    DO 2 J=1,6
    B1(I,J) = -B1(I,J)/(XX(3)*YY(2))
2  CONTINUE

```

```

C      MATRIX D GIVEN BY EQUATION 3.13 IS DETERMINED.
C

```

```

C      D(1,1) = 1.
C      D(1, 2) = V
C      D(1,3) = 0.
C      D( 2,1) = V
C      D( 2, 2) = 1.
C      D( 2,3) = 0.
C      D(3,1) = 0.
C      D(3, 2) = 0.
C      D(3,3) = (1.-V)/ 2.

```

```

C
C VECTOR F CORRESPONDING TO THE VECTOR OF LOCAL INPLANE
C NODAL DISPLACEMENTS IS DETERMINED.
C
DO 3 I=1,9
DO 3 J=1,9
T(I,J) = 0.
3 CONTINUE
DO 4 I=1,3
DO 4 J=1,3
DO 4 K=1,3
N = (K-1)*3
4 T(I+N,J+N) = ALMD(I,J)
DO 5 I=1,9
F(I) = 0.
DO 5 K=1,9
F(I) = F(I)+T(I,K)*FB(K)
5 CONTINUE
F(3) = F(4)
F(4) = F(5)
F(5) = F(7)
F(6) = F(8)
C
C STRESSES ARE CALCULATED USING EQUATION 4.38
C
CALL MULTP (D,B1,0,3,6,3,0,3,3,3)
DO 6 I=1,3
STRSS(I) = 0.
DO 6 K=1,6
STRSS(I) = STRSS(I)+Q(I,K)*F(K)
6 CONTINUE
DO 7 I=1,3
STRSS(I) = STRSS(I)*12./TMAX**2
7 CONTINUE
RETURN
END

```

## NOTE

THE REMAINING SUBROUTINES ARE GIVEN IN APPENDIX III.  
 THIS PROGRAMME IS DESIGNED FOR TOTAL NUMBER OF NODES  
 GREATER THAN 5 AND FOR PRETWIST NOT EQUAL TO ZERO.